A TRANSDISCIPLINARY SYSTEMS APPROACH FOR DEFINING TORNADO CHARACTERISTICS AND DEBRIS IMPACT ANALYSIS

by

Bobby G. McPeak, M.E.

A Dissertation

In

MECHANICAL ENGINEERING

Submitted to the Graduate Faculty
of Texas Tech University in
Partial Fulfillment of
the Requirements for
the Degree of

DOCTOR OF PHILOSOPHY

Approved by

Atila Ertas
Chairperson of the Committee

Hong C. Zhang
Member

Timothy Maxwell
Member

Stephen Ekwaro-Osire
Member

Derrick Tate
Member

Fred Hartmeister
Dean of the Graduate School

December 2009

ACKNOWLEDGEMENTS

Many individuals have contributed to the successful completion of this work. Without these unselfish contributions from others, this would not have been possible. I am grateful beyond description for the opportunity that I have been given for being associated with such people. Countless hours have been sacrificed in my behalf, and rest assured that this commitment will never be forgotten.

I offer my most sincere thanks to my advisor and the chairman of my committee, Dr. Atila Ertas. I am always amazed at his patience, his knowledge, his commitment, and his ability to motivate. I regard his counsel as the greatest benefit of having gone through this program. By his exceptional example, my attitude toward learning, science, and perfection has been redefined. Any successes that I may enjoy for the remainder of my career will in part be a testament to his dedication and friendship.

I offer thanks to my committee members: Dr. Stephen Ekwaro-Osire, Dr. Tim Maxwell, Dr. Derrick Tate, and Dr. Hong-Chao Zhang. My association with these genuine professionals has been a great source of knowledge and motivation.

I also like to thank other individuals that have assisted me in many ways: Mr. W.R Bruchey for his invaluable insight into impact dynamics, Dr. Darryl James for his patience and support in conjunction with the Texas Tech the tornado simulator, Mr. Emrah Gumus and Ms. Melisa Otkur for their invaluable help with the finite element analyses, Dr. M.M. Tanik for his advice and continued motivation, and Mr. Russell Foster for illustrating what is possible when you never give up.

I also thank my family. My wife, Jan has been denied my time, my attention, and often my good humor because of her unconditional support of this process. She deserves accolades greater than those which I receive. Also, I give special thanks to my parents who have offered encouragement and assistance in any path that I have chosen to transverse. All of my childhood, I heard the mantra “stay in school” from them – Mom and Dad, be careful what you wish for. And I thank God for creating such a marvelous world that demonstrate grandeur on a daily basis.

TABLE OF CONTENTS

ABSTRACT

Throughout history tornadoes have represented a force of nature that is both admired and feared. Tornadoes tend to strike with minimal warning, without regard to season, and just as quickly they are gone. The aftermath is often devastating in terms of property damage and the human toll. Until recently, the rudimentary knowledge of tornado behavior escaped explanation. As our understanding of tornadoes advances, it is more evident than ever that tornadoes are not mystical entities. They are natural phenomena that follow the laws of physics, and as such are excellent subjects of intense research. Most of the research regarding the tornado is delegated to the atmospheric sciences, but this status is undergoing a change. With the introduction of engineering into the sphere of tornado research, a new paradigm is changing the way that the world looks at these natural spectacles.

At the same time, another paradigm of research is becoming more widespread: the transdisciplinary approach to complex problems. In this arena of study, disciplines disappear. There is a coalescence of knowledge and methodology that transcends the previous model for research, resulting in an alternative way to look at issues. The introduction of engineering into the tornado research community represents a small integration of this concept.

This study takes the subject of tornado/structure interaction into the realm of transdisciplinarity. By intertwining the knowledge base of the characteristics of tornadoes and their associated wind fields, and applying this knowledge to structural problems, recommendations are formulated to allow for homes to be made more tornado resistant.

Up to this time, the determination of tornado resistant home techniques has relied almost exclusively on laboratory testing. This has resulted in methods that indeed increase the resistance homes to the effects of extreme winds. However, these tests are expensive and subject to aberrations in results, mostly due to inconsistencies in the properties of standard building materials. This study introduces empirical equations that are applicable to many building/projectile interactions. These equations

are validated by a combination of comparisons with Texas Tech impact testing and a finite element analysis.

Also included in this study is a series of surveys of tornado damage to fortify the current knowledge of resistant reactions to extreme winds and associated debris impacts. One of the surveys is of a forensic nature by evaluating a tornado that occurred more than 60 years ago. The hope is that by extracting useful information about this event, other tornadoes of the past will be studied in a further attempt to uncover pertinent artifacts regarding tornado behavior and as a means to compare contemporary building techniques with those of the past.

Lastly, this thesis categorizes building techniques which mirror the Enhanced Fujita scale of tornado intensity. This introduces means for various levels of protection achievable in cases where "almost absolute protection" is cost prohibitive. Additionally, this study includes a conceptual model of a possible portable tornado shelter.

LIST OF TABLES

LIST OF FIGURES

LIST OF SYMBOLS

A_P	Presented area of a projectile
β	Shape factor derived from testing
D	Diameter of a penetrator
E1	An event, in terms of probability
E2	An event, in terms of probability
E_t	Characteristic stress or energy per unit volume of target
E_p	Characteristic stress or energy per unit volume of projectile
GCp_f	External pressure coefficient
GCp_i	Internal pressure coefficient
K_Z	Exposure velocity pressure (change of wind speed with height)
K_{ZT}	Topographical factor for winds speeding up over hills and escarpments
K_d	Directionality factor
L or l	Length of a penetrator
m	Mass, in English units wgt/g
P	Penetration depth
p	Design wind pressure for Main Wind Force Resisting Systems (MWFRS)
ρ	Standard air Density
ρ_a	Ambient pressure
ρ_{eq}	Equivalent density of composite wall
ρ_s	Stagnation pressure on a flat surface

ρ_p Density of a penetrator

ρ_T Density of a target

$P(T)$ Probability of an event

q_h Velocity pressure evaluated at a specific height

R_T Characteristic target strength (for this study the tensile strength)

T or ω Thickness of a target

U or u Penetration velocity

V Velocity

V_L Limit velocity (velocity at which penetration just occurs)

V_0 Velocity of projectile at impact

V_r Residual velocity (projectile velocity after penetration)

Y_P Characteristic strength of penetrator

γ $\frac{\rho_t}{2}$

γ_{eq} Characteristic $\frac{\rho_t}{2}$ for composite wall system

α $\frac{A_p}{m}$

CHAPTER 1

INTRODUCTION

Since humans first appeared on this planet, they have been very aware of their surroundings. The availability of adequate food, physical safety, and suitable shelter has always been a vital constituent of survival. As civilization progressed in terms of knowledge and experience, the methodologies adopted to supply these necessities also evolved. Hunters developed innovative stalking skills and weaponry to increase their success at obtaining meat. [1] Agriculture allowed the addition of non-animal foods to supplement the diet. Familiarity with inherent dangers in the environment afforded a greater degree of physical safety. The development of various types of materials and techniques resulted in shelters specifically tailored to the prevailing conditions. [2]

The one environmental characteristic that affected all of these survival challenges was the weather. Weather influenced hunting conditions, was the mainstay of agriculture, could certainly compromise safety, and defined the requirements of shelter. As the centuries pasted, the quest for food became less of a burden, owing to advances in farming, ranching, processing, storage, and distribution. Many of the concerns about physical safety have disappeared. Depending on the locale, threats still exist, but with a much more manageable presence. Construction and economic achievements provide diverse choices in regards to shelter. For the most part, the weather's contribution (or interference) with man's day-to-day activities has greatly diminished.

The previous statement that the effect of weather on humankind has diminished does not imply that it does not exist. On the contrary, there are still situations where the weather continues to play a major role. [3] Despite, contemporary irrigation practices and massive greenhouses, agriculture is still quite dependant on the weather. Snow and ice storms persist in leaving transportation (ground and air) in states of gridlock. [4] People and property continue to suffer various levels of devastation during severe weather events. It is the last example that provides the focus of this essay.

Extreme weather can have a very destructive effect on humanity. Floods, lightning, thunderstorm winds, hurricanes, and tornadoes all contribute to the mayhem that sometimes results when weather turns violent. Perhaps the best example of atmospheric phenomena at its worse is the tornado. Tornadoes can strike with minimal warning. Their behavior is often unpredictable. They can come and go quickly, or remain in contact with the surface for long periods. They can strike a rural area and leave little or no trace of their visit, or they can ravage densely populated urban neighborhoods and cities and leave incomprehensible damage and loss of life.

According to the National Climate Data Center from 1953 through 2005, there were 48,632 reported tornadoes in the United States, resulting in 4,388 deaths. [5] The most devastating tornado in recorded history took place on May 25, 1925. The path of this tornado (or possibly a family of tornadoes) extended through Missouri, Illinois, and Indiana. During the 219-mile track (at times 1200 yards wide and a forward speed of up to 72 miles per hour), 695 people were killed and 2027 injured. [6] Though tornadoes do not represent the greatest threat against life in the United States, they embody a particularly disturbing hazard.

The best defense against tornadoes is time and knowledge: time to seek adequate shelter and knowledge of what actions can increase the odds of survival. Meteorology researchers have done an excellent job in understanding tornado characteristics to the point of increasing average warning times from 5 minutes to around 13 minutes. [7]

Since real-time tornado measurements are impossible given the current state of technology, the majority of research must rely on derivative evidence: satellite photos, radar images, surface and upper level analyses, and damage surveys. As a result, the data available for research is limited. Even though tornadoes often make the headlines, they are relatively rare events; thus, bounding the opportunity for examination. A complete understanding of tornado formation and behavior is not likely to occur in the near future; however, this does not suggest that we are helpless against these phenomena. The best protection against tornado dangers is avoidance. Public warning systems have progressed astronomically in the past few decades,

allowing for a highly increased public awareness of tornado locations and projected paths. There are instances where tornadoes form rapidly without warning. Tornadoes can occur at night when public vigilance is minimal. In short, there are times when evacuation is not a possibility. This study focuses on the times when individuals must face the hazards of tornadoes within their homes.

Motivation

Beginning with the Lubbock, Texas tornado of 1970, there has been a growing collaboration between meteorologists and engineers. Both disciplines have similar objectives: save lives, protect property, increase the knowledge base in regards to tornado behavior and wind/structure interfaces. This partnership has benefited both communities of researchers and progress has been tremendous. [8] Engineering studies of tornado damage assist the meteorologists in their understanding of the wind speeds and wind directions in and near tornadoes (hereafter referred to as wind- fields), and provides engineers with a better dataset with which to base designs that can withstand extreme wind pressures. Meteorology research helps define the tornado structure and occurrence probabilities which aid the engineers in concentrating their analyses on areas that are the most beneficial for structure improvement. Though not specifically referred to as a transdisciplinary methodology of research, this alliance illustrates the viability of transdisciplinary cooperation between seemingly unrelated disciplines.

One of the consequences of the introduction of engineering into the study of tornado behavior is the development of procedures to make individual residences more tornado resistant. At one time tornados appeared to have wind speeds from 500 miles per hour to the speed of sound. [9] At wind pressures this high, hardening a home to be resistant was extremely cost prohibited. At the wind speeds now believed to occur around tornadoes, homes can be constructed or modified to offer more protection at costs that are not insurmountable.

The Federal Emergency Management Agency (FEMA) has a publication called *Taking Shelter Form the Storm.* [10] In this publication is an estimate of the costs of building a FEMA approved safe room during the construction phase of a new home.

As illustrated in Table 1, the least expensive option is $6,300 in 2008 dollars. It further states that this level of protection in an *existing* home results in a cost increase of 20%, or $7,560.

Table 1: Costs Associated with Home Improvement
[10]

Size	Safe Room Characteristic	Average Cost	Notes
8 foot x 8 foot x 8 foot	Concrete Masonry Unit (CMU) Walls	$ 8,200	Based on 2008 dollars
	Concrete Walls	$ 8,100	
	Wood-Frame with CMU Infill	$ 7,600	
	Wood-Frame with Plywood/Steel Sheathing	$ 6,300	
	Insulating Concrete Form (ICF)	$ 8,300	
	Reinforced Concrete Box	$ 7,000	

Due to the low probability of a tornado strike (even in areas most susceptible to tornadoes), this amount would not be feasible for many families. Furthermore, there are many obstacles to adding a safe room to an existing residence: location in floor plan, proximity to exterior walls, disruption to existing living space, etc. For these reasons, most individuals choose not to harden their homes at all. This provides the motivation for this research.

As evidenced by damage survey photographs and actual field surveys, it is apparent that many tornado fatalities and serious casualties averted if only minor home modifications occurred. Data does not exist which orchestrates varying levels of wind protection. All of the resources involved in storm room construction focus on the level of protection recommended by FEMA. While this level of protection represents the “gold standard” for tornado resistance, any additional hardening of a residence increases its safety to some extent.

Research Objective

There is a great need for a process that defines an incremental philosophy for the design and construction of tornado resistance for existing structures. Much of the data that currently exists is economical for new construction, but proves difficult to retrofit in an existing home. Due to the prohibited cost of modifications to existing homes, many homes live with the inferior protection from high winds that came with their home. Most builders do not consider tornado resistance a cost effective strategy; therefore, standard building practices just meet the local codes. Additionally, according to FEMA, in order to achieve adequate tornado resistance, the modifications must meet their guidelines. This is true if the goal is to attain protection from the most intense portion of the most intense tornadoes. While this represents the most superior form of protection, lesser levels of protection can also saves lives. This is analogous to claiming that the only protection from burglars is a monitored, electronic security system. There are less expensive alternatives that also provide a level of protection from intruders such as dead bolt locks, outside lighting, shatter proof windows, and neighborhood watch groups.

The final motivating factor concerns individual safety practices when exposure to tornadoes is imminent. Improved safety measures could have a substantial effect on the number of people who escape death or injury when subjected to tornadic winds. Collecting significant data on death and injury mechanisms allows for the development of superior preventive options. This is especially critical when situations occur where optimum shelter is absent.

There are numerous sources of research related to tornado/structure interactions. Tim Marshall (an engineer and meteorologist) has authored many papers associated with the affects of tornadic winds on residences, especially in regard to the structural damage characteristics of wind and structure interface. [11, 12, 13, 14, and 15] Texas Tech has also led the way in tornado wind research, including the comprehensive introduction of engineering into the meteorological realm, *The Tornado: An Engineering-Oriented Perspective.* [8]

Surveys of tornado damage sites have provided tremendous information relating the methodology by which high winds cause buildings to fail. Dr. T.T. Fujita was instrumental in developing processes for surveying tornado damage and relating the data to both tornado behavior and the associated structural failures. [16]

The vast majority of structural engineering research concentrates on the structural failure of buildings. Load path failures require examination with great detail, and many products and techniques exist to eliminate the "weak links" in terms of the structural load paths of homes. The American Society of Civil Engineers ASCE has published a book of guidelines for the design of buildings with respect to high wind loading. [17] Unfortunately, these design aids are more appropriate for new construction.

The area of study dealing with tornado debris impact is another facet of the tornado/human interface. While debris impacts are typically not the result of massive structural failure, many deaths and serious injuries are the result of flying debris. The majority of technical data regarding debris impact are the result of laboratory testing. Again, Texas Tech has been at the forefront of this type of testing. [18, 19, and 20] The information gained from this testing has helped define the characteristics of the "safe room". In this case, the goal is not to minimize damage to the structure of the home, but to provide protection for the inhabitants.

Debris testing has occurred at many locations; however, they all seem to suffer from the same deficiency: They are looking for a pass or fail situation. Various walls consist of different materials and combinations of materials, and projectiles of different materials impact against these walls at different speeds. The wall systems are well defined, the projectile masses and velocity before impact exist, but some parameters are not typically measured. This would include high speed camera recording of the entire event, determination of the velocity of the projectile after penetration, determination of target specific resistance to penetration, just to name a few. Data of these types would assist in the creation and validation of empirical equations related to low velocity, relatively soft projectile, and relatively soft target impacts. Most impact dynamic studies involve much higher velocities, much harder

projectiles, and more substantial target materials: as experienced in ordinance against armor studies. Many studies of this type exist, but due to the high velocities and metallic constituents, these are mostly not applicable to this study. [21, 22, and 23]

The objectives of this research are typical of a research study exercised within the scope of transdisciplinarity. In the spirit of transdisciplinarity, the research emphasis of this dissertation was multi-dimensional. Traditional gathering of data contributed in terms of an exhaustive literature survey; however, due to the nature of the project, the research requirements were unique. Thomas Kuhn expressed the challenges of research with the following statement: "Bringing a normal research problem to a conclusion is achieving the anticipated in a new way, and it requires the solution of all sorts of complex instrumental, conceptual, and mathematical puzzles". [24]

Tate defines two types of research: *idiographic* research, which includes the gathering of data of one event or phenomenon, and *nomothetic* research, which includes data from several events with the goal of finding patterns in the data. [25] Since the data concerning this study is in terms of multiple events, the type of research associated with this study is nomothetic. The research for this study required a diverse collection of artifacts. Papers and textbooks on the subjects of transdisciplinary studies, meteorology (specifically convective activity and associated damage), structural damage analyses, and an exhaust literature search from the field of impact dynamics. Notes from classes and classroom discussions proved invaluable, especially on the subjects related to transdisciplinarity. Interviews occurred with subject matter experts from the fields of transdisciplinary science, meteorology, engineering, impact and penetration dynamics, as well as tornado eyewitnesses and survivors. Documents in the form of death certificates, newspaper accounts, maps, and photographs allowed for further study and inclusion into the final analysis. Historical data from various databases, the national weather agencies, personal communications, and personal experience provided specific information regarding the case studies that were included. Figure 1 illustrates, via a concept map, the transdisciplinary contributions described.

The concept map tool is a very valuable tool for performing a very complex research project. It provides a general "mapping" of the flowdown of needed information accumulation required to complete a study such as this. This study concentrated on three major disciplines: Meteorology, Engineering, and Home Building. The concept map illustrates, in detail, the "roadmap" that must be followed in order to produce the data needed to finalize this study. By following the map flowdown, the task of transdisciplinary research becomes plausible. Without the concept map, the activities might become random and result in many missed opportunities.

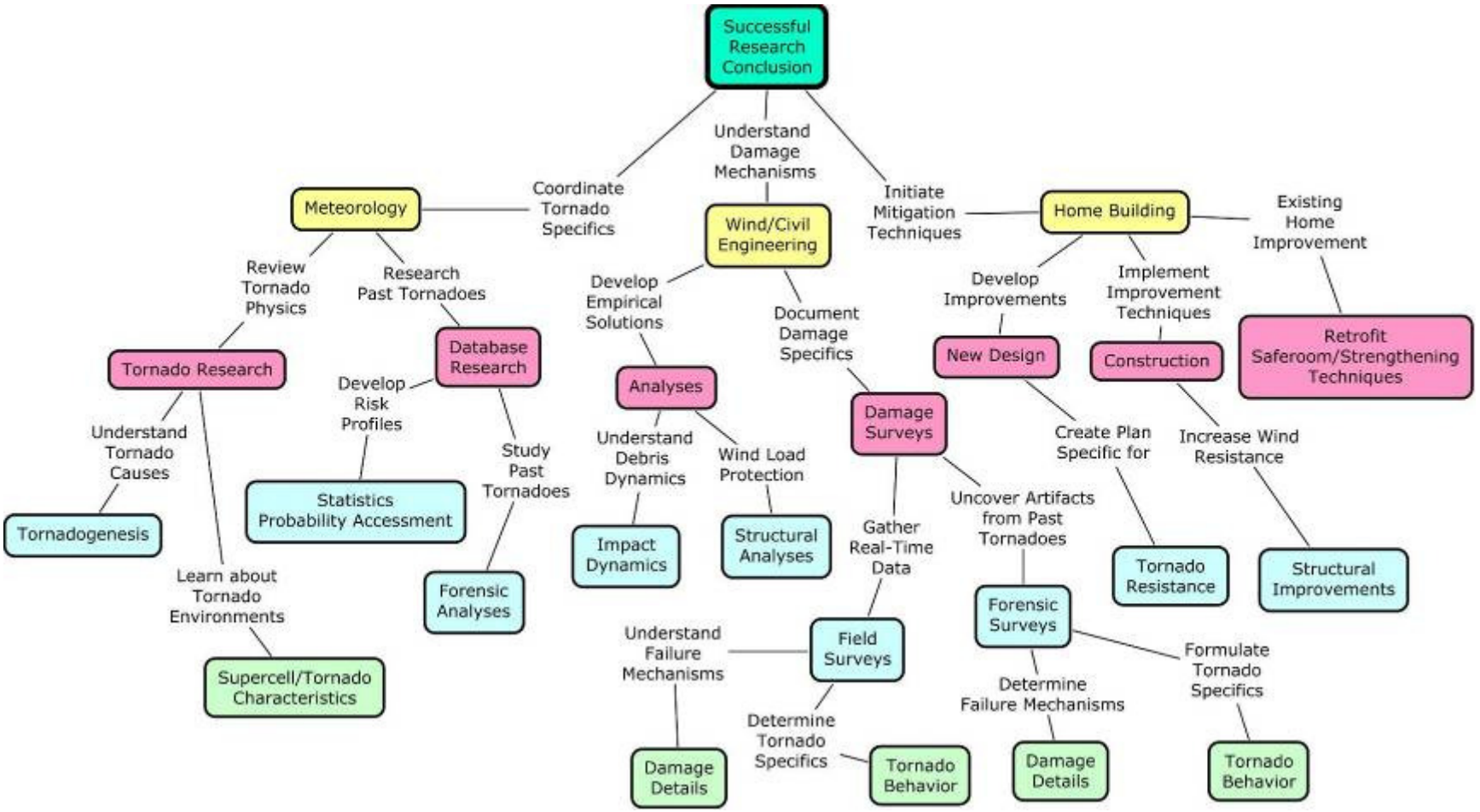

Figure 1: The Concept Map Provided a Systematic Scheme to Accumulate Needed Data

A statement from D.Q. McInerny defines the effectiveness or validity of the approach contained herein: "An argument is valid if its structure is sound, which means that its structure is such that true premises will ensure a true conclusion." [26] A case study included in this dissertation illustrates the effectiveness of the approach presented. As suggested by B.K. Bailey, this case study incorporates the suggested protocol [27]: (1) overview of the project; including objectives, issues, and references to relevant topics, (2) description of field procedures, (3) questions that the investigator hopes to answer, and (4) a guide for the study report.

Tom Grazulis states the challenges to tornado study realistically: "Tornadoes are very difficult to study...the thunderstorm protects the tornado from researchers with 100-mph straight winds, baseball-sized hail, 30,000,000-volt lightning discharges, and blinding rain." [28] For this reason, the study of after-the-fact tornado damage is the safest and most viable methodology for tornado/building interaction study.

The objective of this research is to develop a transdisciplinary framework for tornado research collaboration and establish a graduated scale of tornado impact protection techniques that corresponds to the Enhanced Fujita S scale of tornado intensity.

Dissertation Overview

This structure of this dissertation relates to the subject matter emphasis of each chapter.

Chapter 2 concentrates on the explanation and clarification of the transdisciplinary concept. Also included are the enumeration of the advantages and possible applications. Lastly, there is a description of the methodology for transdisciplinary research, and the applicability of these techniques as they relate to the subject matter of this dissertation.

Chapter 3 contains a primer on the subject of tornadoes and their associated damage characteristics. Included are the contemporary theories regarding the conditions necessary for the development of tornadoes and associated high-wind interaction. Since this is a subject somewhat unfamiliar to many, the explanations will range from the most basic to the current understanding of tornadic thunderstorms.

Chapter 4 concentrates on discussions of the interaction between tornadic winds and structures. Descriptions of damage surveys of the past are described, along with the data obtained through these activities. Also included are three damage surveys performed by this author: one survey of artifacts from a tornado 60 years ago, and two from resent tornado events.

Chapter 5 contains the specifics of impact dynamic studies and their relationship to this essay. Impact/penetration equations development provides a plausible venue for predicting the behavior of typical tornado debris impact to typical residential surfaces.

Chapter 6 is utilizes the equations highlighted in Chapter 5 to document impact predictions of projectiles into various wall geometries.

Chapter 7 includes the specifics of the finite element analysis derived from the LS-DYNA software package and the comparison of said analysis to the equations developed in chapter 5..

Chapter 8 contains suggestions, based on the research and associated data presented in the previous chapters for the hardening of both new homes and existing homes to resist tornadoes that fall into the different categories of intensity in the EF scale. Also, included are the contributions of this study.

CHAPTER 2

TRANSDISCIPLINARY APPROACH

Introduction

Contained in the "vision" statement of the Academy of Transdisciplinary Learning and Advanced Studies [29], the organization's "vision" states:

> "... [T]o be a catalyst for change, enabling the discovery of new approaches in education and research that lead to alternative solutions for the increasingly complex problems that face civilization".

The complexities of systems under development today are such that the current design processes are becoming ineffective. It is becoming progressively more difficult to make quality design decisions based on the tools that we now possess. Companies are now investing tremendously in processes such as Six Sigma, Common Process Architecture, Integrated Product Development Systems, and other similar techniques in an attempt to gain an advantage over complex systems through process controls. These practices and processes are very helpful and much success resulted from their introduction; however, they fall short of providing the "silver bullet" needed to comprehend the complex systems of the future. These concepts provide process "roadmaps" that encourage standard procedures for product design and analysis, but substantial shortcomings are apparent in their ability to achieve transdisciplinary thinking.

We have now entered an age that Thomas Kuhn would define as a time of Revolution: a time at which paradigms are likely to change in order for progress to continue in a particular discipline - In this case, the discipline of knowledge progression.

> "[L]ed by a new paradigm; scientists adopt new instruments and look in new places. Even more important, during revolutions scientists see new and different things when looking with familiar instruments in places they have looked before." [24]

Various disciplines can benefit, and many have already benefited, from the adoption of transdisciplinary research. Biological scientists have adopted a systems engineering approach, including statistical dynamics and network theory, to the study of various complex systems such as the human genome. [30]

In the past, the concept of disciplines has served mankind well. Tremendous success exists due to the depth of concentration in many disciplinary circles. As problems and systems further evolved into more complicated entities, this concept expanded to allow some level of cooperation across and between the specific disciplines. This represented the introduction of interdisciplinary and multidisciplinary approaches to problem solving. [31]

Both of these concepts have provided successful. They have allowed collaboration between disciplines, and the theories within disciplines, resulting in discoveries that would have been impossible without such cross-pollination. While these terms seem interchangeable, they represent distinct concepts. "Interdisciplinary approaches tend to share or combine methods between established disciplines while examining a broad set of topic areas. Multidisciplinary approaches tend to retain their disciplinary character while focusing on a common subject area." [32]

Transdisciplinary Science is quite different from the interdisciplinary and multidisciplinary concepts. The approach is mostly synthetic in terms of being not within or across boundaries, but without boundaries. Figure 2 illustrates the disparities between the approaches. Notice that the "hard boundaries" existing between the first two disciplinary examples are absent on the transdisciplinary example. The transdisciplinary approach demonstrates a higher level of collaboration, not possible when bounded by discipline-related constraints. [33]

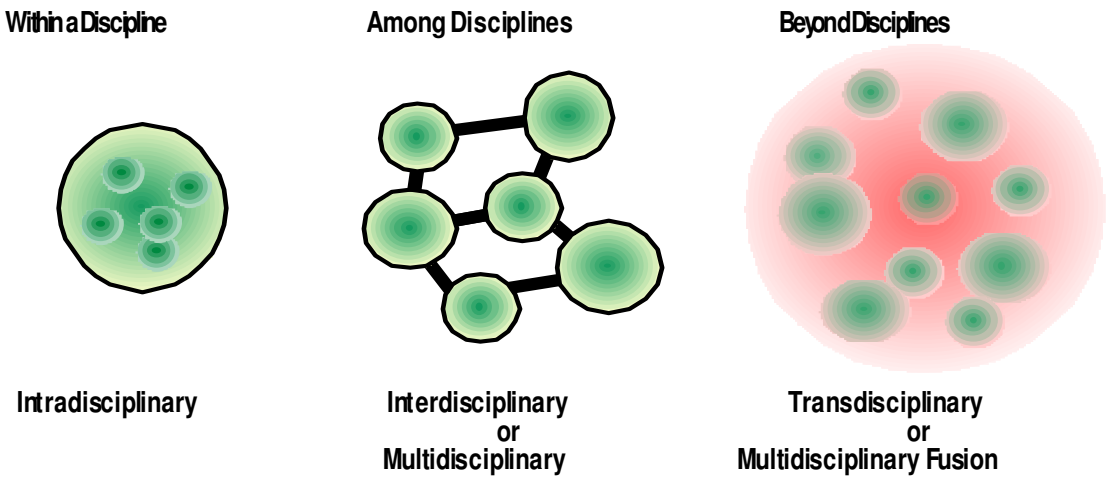

Figure 2: Transdisciplinarity Differs by the Elimination of Disciplinary Boundaries [34]

The introduction of the concept of transdisciplinarity across the spectrum of knowledge is a daunting task. Much confusion, and some aversion, to this concept are evident in many areas of research and education. A discipline is a comfortable armchair. This armchair represents safety, a sense of belonging, a feeling of control. It is not surprising that a conceptual model that seeks to, if not eliminate, reduce the use of this device is taken as a personal affront. The problem is that there is a limit to possibilities from this restrictive posture. One cannot mow the grass from this position. One cannot paint the house from this position. In other words, this condition is highly restrictive. The purpose of this metaphor is to illustrate the utility of a transdisciplinary approach to problem solving.

In a sense, the word *transdisciplinary* is, at best, confusing, and at worse, misleading. Many references have attempted to define this word in a universal and understandable manner; however, one common drawback persists throughout these efforts. In every case, there is a comparison between transdisciplinary, intra-disciplinary, inter-disciplinary, and multi-disciplinary. These three concepts all involve the relationship and functionality between diverse disciplines. Perhaps a better nomenclature for the concept of transdisciplinary would be anti-disciplinary or coalesant-discipilinarity. To present another analogy, when water and oil combine, the two constituents remain separated. Though they are together, they do not coalesce:

they are still in solution as separate entities. Their usefulness in this manner is questionable. Now consider water and cement. Apart, they are useful compounds, but when combined, they produce a new compound with far different characteristics. This combination creates a product that has changed the world in great ways. Figure 3 illustrates a possible symbol for transdisciplinarity.

Figure 3: Symbol for the Transdisciplinary Approach to Problem Solving

Application to this Study

The subject matter of this study is complex. Anytime a natural phenomenon interacts with mankind the results are often unpredictable. Nature appears to perform many of her demonstrations on a random basis. There is some sense of organization and repeatability on a grand scale, but on a local scale the variability is enormous. This is particularly evident in the case of severe weather, especially tornadoes. On a global scale, the surface and upper atmospheric conditions appear organized; however, small perpetrations in the scheme of orderly mechanisms have a profound effect on local conditions.

The jet stream typically moves northward during the winter months; thus, preventing the explosive collision of opposing air masses which can initiate severe

convection. In the spring and summer, the jet stream migrates southward, setting the stage for widespread severe weather across a broad area of the United States. Small changes in the track of the jet stream can produce tornadoes in the winter months, which often catch the population unprepared.

Even during the "peak" tornado season, some innocuous thunderstorms produce devastating tornadoes, while grandiose super cells produce no tornadoes. Tornadoes can form, as typically expected, in the southwestern region of a storm, or can form on the leading edge, spun up by the concentrated downdraft.

The interaction between these esoteric entities and humankind produces a myriad of complicated and dangerous scenarios. For this reason, it is difficult to predict what interactions are possible when tornadoes strike inhabited areas of our globe. However, there is no question that tornadoes pose a threat to life and property across most regions of the United States. Their effect on different structures is the best evidence in the attempt to prevent causalities. Unfortunately, there are many different levels of tornado destruction. Even within the structure of a tornado great differences in wind regimes exist. Additionally, there are many different kinds of structures that experience these powerful winds and debris impact environments. To further complicate the formula, the surrounding topographical environment also is a factor in damage evaluation and prevention: wind patterns change over hills and escarpments, surrounding vegetation affects the local windfield characteristics of tornadoes and debris concentration from surrounding structures directly contribute to the danger from impact destruction.

The three primary areas of expertise utilized in the generation of this research are meteorology, engineering, and home building; however, these represent only the major constituents. Obviously the contribution of meteorology is in the form of weather, thunderstorm, and tornado specifics. The engineer provides the knowledge and expertise with regards to the structural interaction between tornadoes and structures. The home builder understands the standard techniques of construction and utilizes the findings to provide improved principles for construction and strengthening of structures against tornado hazards. While this lists appears complete, many sub-

disciplines, and some totally unrelated disciplines, participated in this endeavor in an effort to complete the goals of this study.

The medical community offered good data in regards to the causality mechanisms. This is important for the understanding of how tornadoes inflict severe injuries and deaths. These data confirm that many survivors of serious tornadoes escaped death as a result of chance. It also supplemented the determination of what structural improvements would prove the most beneficial in providing an added margin of safety for the inhabitants.

Throughout this thesis, the term transdisciplinary will appear in conjunction with the processes and procedures used herein. The cooperation of multiple individuals contributed to the content of this essay; therefore, this presentation owes a debt of gratitude. It serves as a testament to the viability of using a transdisciplinary approach to the solution of a very complex problem.

CHAPTER 3

TORNADO PHYSICS

Introduction

Tornadoes are very complex entities. The constituents for tornado formation are numerous. Not only are the essential ingredients for a tornado necessary, but they must coalesce at the right time in the correct order and be of an acceptable magnitude. Even when all necessary components are in place and interact in the proper sequence, tornadoes do not always occur. This is the reason that tornadoes are so rare. This also amplifies the need for further research. If all of the conditions exist, yet tornadoes fail to form, then science does not recognize some factors. There are unknown constituents, or unknown processes, or unknown combinations of events that have thus far escaped science. This said, there are also circumstances where all ingredients are absent, yet a tornado occurs. It is worth repeating, tornadoes are complex.

Before proceeding, it is worth mentioning the state of tornado understanding. Many books and papers have been published in the past twenty years or so defining enormous progress in the knowledge of tornado formation, structure, and behavior. Many of these essays will be referenced throughout this study, but one is worthy of particular mention: *Severe Convective Storms.* [35] Published by the American Meteorological Society, it is a "collection of 13 review papers by a distinguished group of scientists, providing a summary of the current scientific understanding of convective storms and the weather they produce..." [35] The editor, Dr. Charles Doswell III is a renowned meteorology researcher, whose references appear throughout this dissertation for his many contributions to tornado research.

In order to provide a comprehensive description of tornado physics, it is necessary to regress to a discussion of basic meteorology.

Meteorology Basics

Three constituents of our planetary environment are responsible for the entire spectrum of weather: wind, temperature, and moisture. These ingredients exist in many forms. All of the diverse weather conditions experienced on the surface of the earth are due to the influence of various dynamics on these three items.

The earth's weather "engine" is the result of the transfer of energy. Heating and cooling processes, which contributes to the phase changes in water, create the dynamics that provide such a variation in our weather regimes. Considering the large scale on which these changes occur, the effect on weather is substantial. Depending on the process involved, water either releases energy or absorbs energy. These transitions in energy create what we know as weather.

Wind is the result of temperature variations. Solar warming of air at the surface results in the ascension of warm air. This absence of mass creates an atmospheric void where the warm air used to be located. The result is an area of atmospheric pressure that is lower than the surrounding area; therefore, more air moves in to replace the partial vacuum resulting in wind. The greater the pressure gradient between the low pressure area and the high pressure, the higher the wind. In the absence of any further acting forces, all winds would blow in straight lines (high pressure to low pressure); however, the earth rotates. This creates a force, known as the Coriolis force, which causes the winds to veer (to the right in the Northern hemisphere and to the left in the Southern hemisphere). This curvature of winds is but one of the complicating factors that greatly influence weather. As high pressure winds travel toward areas of lower pressure, the resultant curve follows the Coriolis Effect; therefore, the winds rotate in a clockwise direction. Conversely, as the air continues to create a void by the absence of air, winds rotate counter-clockwise into areas of low pressure. This is the reason that the wind field surrounding hurricanes (represented by very low pressure) in the Northern Hemisphere rotates counter-clockwise.

The previous paragraph explains the effect that temperature has on the creation of wind; thus, the formation of high and low pressure areas, but the effects of

temperature on weather phenomena do not stop here. As warm air ascends upward it experiences a cooling effect. This is due to the fact that as a parcel of air gets further away from the surface of the earth, the effects of gravity diminish. As altitude increases pressure decreases; therefore, the surrounding air is cooler. Mountain tops are a good example of this phenomenon. Since warm air can hold more water vapor that cool air, the initial parcel of air that ascended due to its higher temperature contains more moisture than the air surrounding it. If the temperature of this parcel of air cools to the dew point, the moisture condenses out in the form of water droplets. This phenomenon is a cloud.

Before proceeding to a more exhaustive description of the mechanisms that transform wind, temperature, and moisture from three benign constituents into factors that produce the most severe weather on earth, a clarification is necessary.

From a meteorological standpoint, the description of altitude differs from what is commonly used. Typically, the expression of altitude is feet, meters, miles, or kilometers (a height coordinate system). In meteorology, the units of altitude are millibars, abbreviated as mb (a pressure coordinate system). The reason is that meteorological analyses rely on pressure attributes rather than measurements above the ground. “To better explain this system, the 500 mb level, for example, represents the height to which a barometer would have to ascend to read 500 mb.” [36] The exception to this is in referring to concepts that are dependant on measurable distances, such as cloud top height or cloud base height.

Table 2 provides a generalized conversion from feet to millibars:

Table 2: Chart Describing the Correlation Between Millibars and Altitude
[36]

Pressure Level (mb)	Equivalent Height (ft)	Characteristics
1000	300	Surface conditions
850	5000	Storm forecasting
700	10,000	Short wave disturbances
500	18,000	Short wave disturbances
300	30,000	Long wave distrubances, wintertime jet stream
200	39,000	Long wave distrubances, summertime jet stream
100	54,000	Upper troposphere

Deep Moist Convection

There exist three modes of heat transfer: conduction, radiation, and convection. From the standpoint of meteorology, the role of conduction is not a driving force for thunderstorm study on a local scale. The energy available for any weather condition initially comes from the sun via solar radiation; however, for this study, radiation is not considered. Without question, the heat transfer mode of convection is the driving force in relation to weather, specifically severe weather. The relationship is so undeniable that the term *deep, moist convection* (DMC) is synonymous with the term thunderstorm. [37] These terms occur interchangeably throughout this paper.

As mentioned earlier, the changes of water phases are the primary contributor to variations in our weather. This statement progresses to proclaim that the changing phases of water, and the energy released in this process, is the source of the most hazardous weather that occurs.

According to Doswell, three constituents for the initiation of DMC are [38]:

- sufficient depth of moisture in the low or mid-troposphere,
- a steep lapse rate allowing for a substantial "positive area" on the graph, and
- a means of lifting an imaginary parcel of air sufficient for it to reach its level of free convection (LFC).

Since the phase change of water creates the energy used to "fuel" DMC, a substantial amount of moisture in the lower levels of the atmosphere is required. This

moisture influx occurs on a very large scale. Typically, this moisture supply results from winds on the western edge of an eastern high pressure area channeling toward a low pressure area to the west. Recall that winds gravitate from areas of high pressure to areas of low pressure.

The lapse rate refers to the decrease in temperature with height. A device called a radiosonde measures the vertical characteristics of the lower atmosphere. A radiosonde consists of a small barometer, a thermometer, and a hygrometer built into a cage attached to a balloon. The cage also contains a radio transmitter and batteries to relay the data back to a recording station. [39] As the balloon ascends, it travels horizontally with the wind at the various levels; thus, provides wind direction and speed at various altitudes. These data supplied by the radiosonde present the definition of the lower atmosphere. The recording of this information on a special graph represents the *sounding*. Soundings illustrate the relationship of a lifted parcel of air with its environment. This is particularly important in the determination of the stability of the atmosphere, or more precisely, the odds of the formation of DMC.

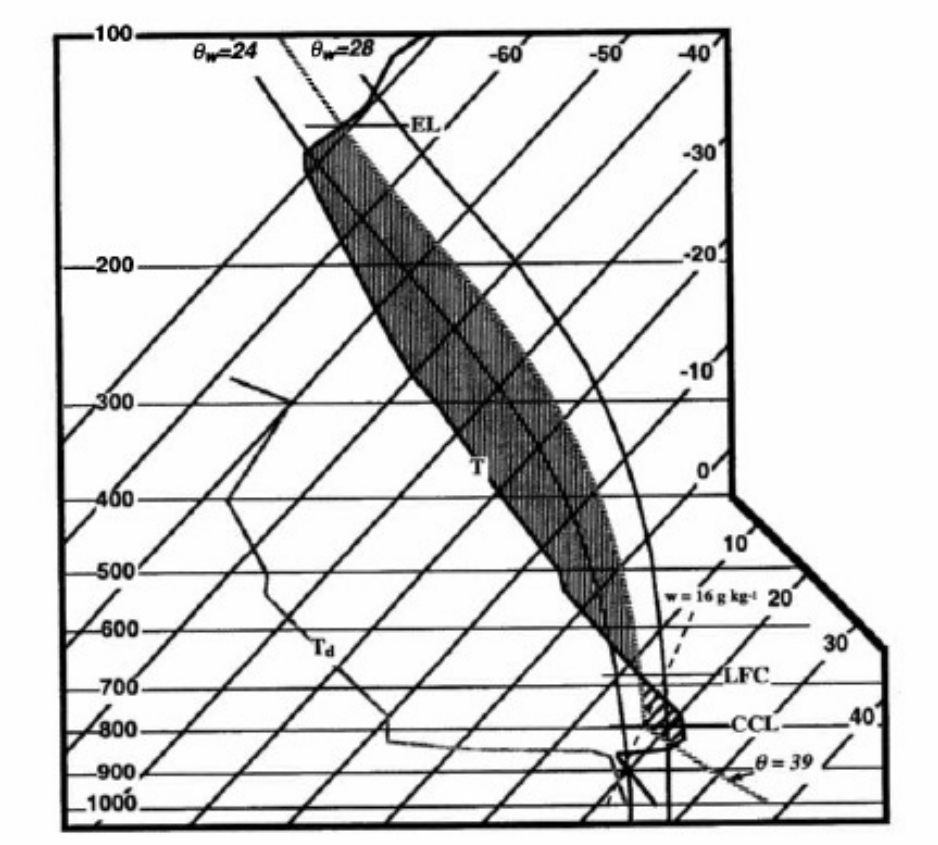

Figure 4: Typical Example of an Atmospheric Sounding
[35]

One of the necessary constituents of DMC listed above is the present of a "steep" lapse rate. A trace of the temperature of the parcel as it ascends has a steep lapse rate if the line leans strongly to the left, as the one shown in Figure 4. The area of the shaded portion of the figure represents the numerical value of the convective available potential energy (CAPE). This is the energy responsible for the convective updraft; thus, the higher the CAPE, the greater the potential for severe convection. [35]

Another useful characteristic revealed by the sounding is the presence of convective inhibition (CIN). This area, represented by the red area on the sounding, illustrates a capping inversion. This level of air inhibits convection by preventing its ascension. If this capping inversion is weak or absent, widespread DMC will likely occur. If the CIN is weak and the CAPE is steep, severe thunderstorms can form

rapidly and monopolize the moisture; thus, inhibiting further storm development. [40] If the CIN is strong, it can prevent DCM. Likewise a strong CAPE and a moderate CIN will suppress thunderstorm development until the parcel reaches a critical point and penetrates the CIN. In this case severe thunderstorms will develop explosively.

Once sufficient moisture exists, the vertical state of the atmosphere describes an adequate CAPE value, and a low to moderate CIN is in place, the addition of lift will most certainly initiate DMC. Surface heating of a local air parcel provides lift on a relatively small scale; however, other mechanical means often supplement this lifting on a more sizable scale. Frontal boundaries, dryline interaction, or outflow from neighboring convection can provide the necessary lifting to deepen the moisture layer, weaken the CIN, and allow the thermals to reach the LFC. [40] Figure 5 demonstrates how the interaction of a cold frontal boundary with warm moist air provides upward lift by "wedging" under the moist air regime.

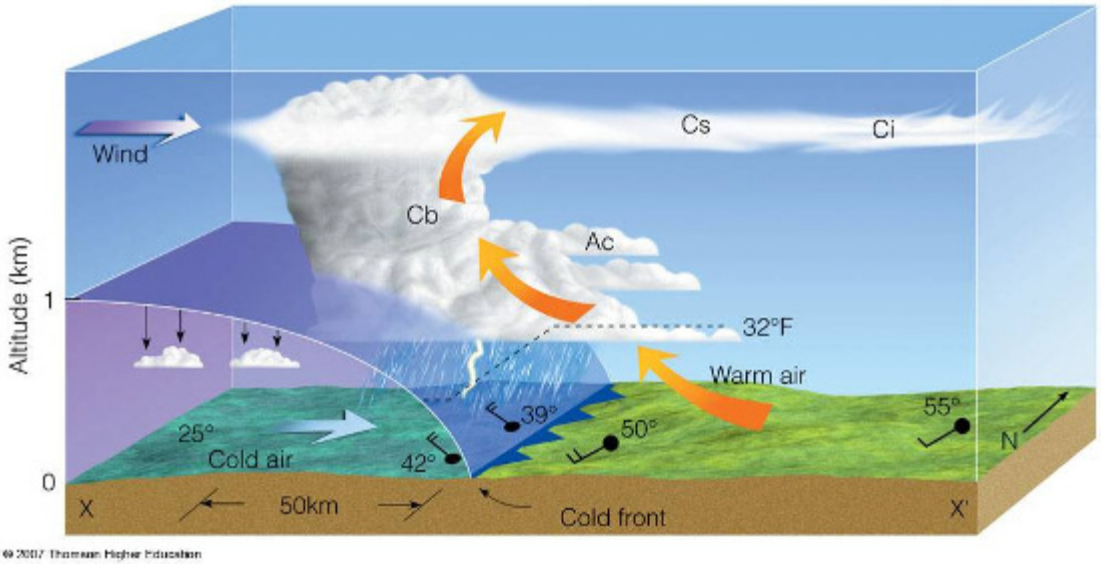

Figure 5: Cross-Section of Cold Frontal Wedge
[41]

As the above conditions coalesce, a thunderstorm is born. The next section describes the events that contribute to the formation of a tornado.

Supercells and Tornadogenesis

The preceding descriptions regarding the formation of DMC represent the current knowledge associated with thunderstorms. There is little doubt that the principles described above are valid and factually define the atmospheric conditions and interactions that result in the development of DMC. The study of the initiation of tornadoes lacks this level of confidence. Many unknowns still exist in terms of why some storms become tornado producers and some; seemly, identical storms are free of tornado activity.

Rotation is an inherent characteristic of our universe from the most macro scale imaginable to the microscopic, and possibly nanoscale dimension: solar systems rotate around in the universe, planets rotate around stars, satellites rotate around planets, planets rotate on their axes, and electrons rotate around nuclei. Furthermore, on our planet, atmospheric phenomena rotate within the atmosphere. High and low

pressure areas rotate in terms of wind flow regimes, and as the scales continue to get smaller, under certain conditions, individual storms rotate. Most important for the formation of severe weather is the *mesoscale*. While this scale of measurement is difficult to quantify, for this study mesoscale will encompass "phenomena occur(ing) on horizontal scales between ten and several hundred kilometers." [42]

The primary harbinger of severe weather on a more localized scale is the supercell. The distinguishable feature of a supercell is in its unique structure, which allows the storm to function as a rotating "engine". In a non-supercell thunderstorm, an update fuels the thunderstorm with latent energy in the form of a warm moist air injection. [43] This updraft is primarily vertical. As this inflow of air reaches a level that allows condensation to occur, physical changes cause the air to rapidly descend as a downdraft. Since this downdraft is competing with the updraft, the inflow is choked and the storm enters the stages of dissipation due to the lack of fuel. In a supercell, wind shear tilts the primary core of the thunderstorm; therefore, the updraft and the downdraft both exist without affecting one another. This permits the thunderstorm to intensify and results in a long-lived, rotating, and constantly evolving entity. Within this rotating thunderstorm there exists a unique area of rotation called a mesocyclone; also known as the "meso". [43]

The initiation of a supercell thunderstorm (or severe DMC) is broken down into to two sets of processes: preconditioning and triggering. [42] Newton distinguishes these factors that "precondition (destabilize)s the environment, for example, an approaching upper-level trough, differential horizontal advection, low-level jets, from those that release the instability, such as rapid lifting by fronts, cold domes from thunderstorms, drylines, and topography" [42].

The process that instigates the rotation of the meso in a supercell deals with the shearing of the winds. Wind shear is the result of winds at adjacent vertical levels blowing from different directions and at different speeds. For example, if the wind at the surface is blowing at 15 knots from the southeast and the wind at 1500 feet is blowing from the southwest at 20 knots, an environment of wind shear exists. The intersection of these two wind regimes would cause an imaginary parcel of air to

rotate. Imagine a length of flexible tubing suspended in the air with the southeasterly wind described above acting on the bottom of the tubing and the southwesterly wind described above acting on the top of the tubing. This would cause the tube to rotate. If a strong updraft occurs at the midpoint of the length of tubing, the flexible nature of the tubing allows the tube to bend upward in the center. As this bending continues, eventually the tubing on either side of the midpoint will be in a vertical orientation. This is a simplified representation describing the initiation of the rotation of the meso in a supercell thunderstorm.

Now that a thunderstorm has formed and it has developed into a supercell, what is necessary for this storm to produce a tornado? Alan Moller suggests, "The environments that produce supercells are becoming better understood, largely because of observations and cloud modeling experiments. It has been considerably more difficult to find atmospheric signs that reliably discriminate between tornadic and nontornadic supercells." [40] What is certain is that, "A buoyant updraft, rainy downdrafts, and a deep, mesocyclonic vortex (preexisting vertical vorticity) are tornadic supercell storm ingredients." [43]

Two classes of tornadoes exist based on the environments in which they initiate: type I and type II. Type I tornadoes typically form within the circulation of a mesocyclone. These represent the most long-lived violent tornadoes. Recent studies indicate that type I tornadoes often form when the parent mesocyclone circulation interacts with a preexisting thermal boundary such as an outflow from a previous storm or some type of frontal boundary. [43] This is thought to be due to the horizontal vorticity of the thermal boundary (flexible tubing example) being ingested into the updraft of the mesocyclone and vertically tilted and stretched into a tornado. "...type II tornadoes from along a stationary or slowly moving front or wind shift line apparently from the rolling-up of the associated quasi-vertical vortex sheet into individual vortices..."

Tornado Characteristics

More of interest to this dissertation than the formation mechanics of tornadoes is the characteristics of tornado behavior after formation has occurred. "Some essential elements of the tornado vortex are fairly well established. The flow spirals in a radial direction inward into a core flow that is basically a swirling, rising plume or jet, but often includes an inner downward jet along the axis. The radial flow toward the center of the vortex intensifies in the surface layer. The vortex flow is driven by the energy generated from latent heat release in a thunderstorm with appreciable rotation." [44] However, this is where the similarities end. No two trees are identical, no two clouds are identical, no two storms are identical, and no two tornadoes are identical. The diversity in tornado characteristics is widespread. "...some tornadoes display thin, relatively smooth, almost elegant single funnels on the ground, while others are composed of many highly turbulent secondary vortices revolving about the large central cores." [45] From the vast database of tornado photographs, there exists a plethora of tornado shapes, sizes, and colors. These differences in appearance, differences in size and intensity, differences in forward speed, and differences in longevity all contribute to the complexities of tornado/surface interactions.

Shape and size of a funnel in contact with the surface is not indicative of intensity. A relatively small, rope-like tornado can produce considerable damage, while a mile-wide "wedge" tornado can be less powerful than would be expected.

The forward speed of a tornado can vary from no translational motion to over 70 miles per hour. This is important because on the right side of a tornado vortex the translational speed is additive to the tornadoes wind speeds. For example, if the tornado vortex is producing winds of 130 mph and the forward speed of the tornado is 50 mph, then the windspeed along the right side of the vortex is actually 180 mph. Conversely, using this same concept, the relative winds on the left side of the vortex is 130 mph minus 50 mph, or 80 mph. (See Figure 6)

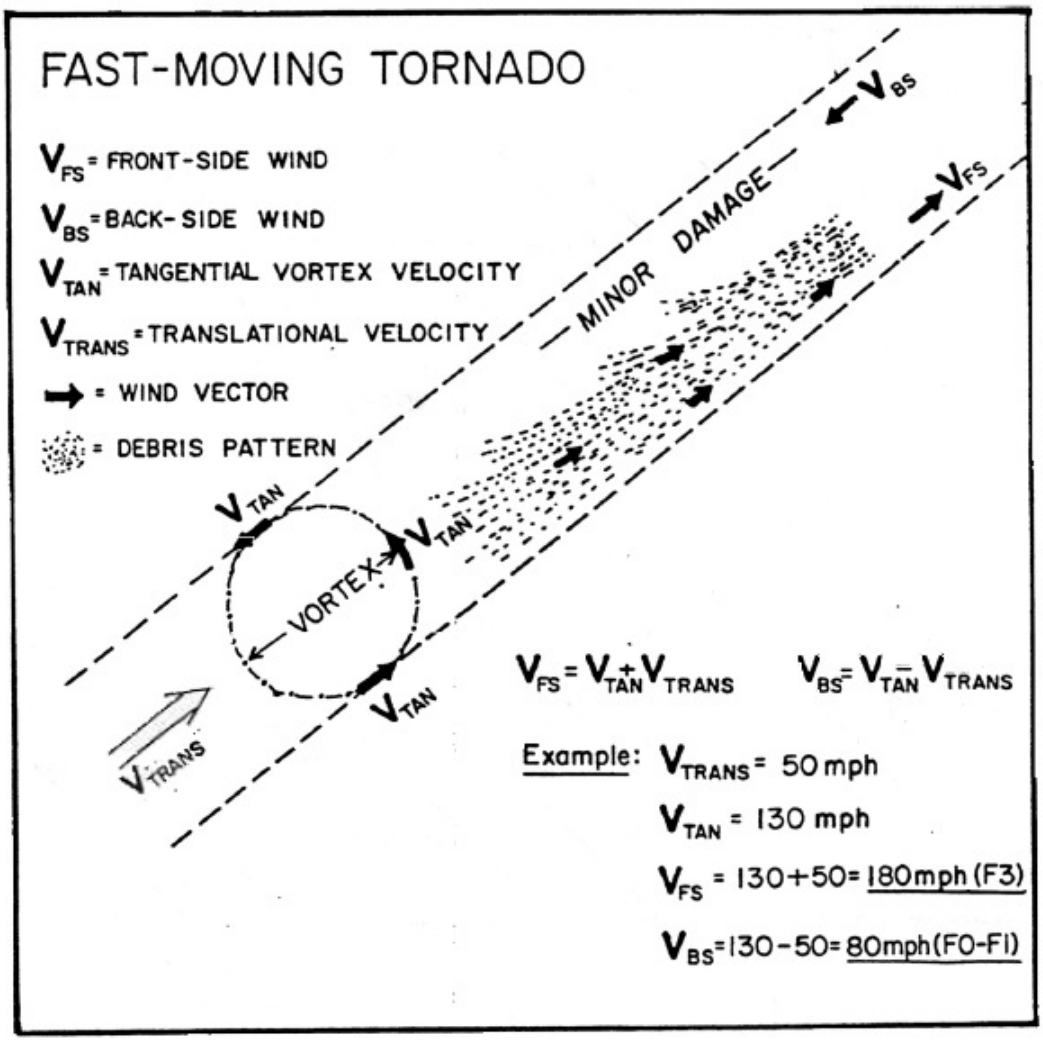

Figure 6: Wind Speed Distribution Within the Path of a Tornado
[46]

Due to numerous observations of tornado damage, tornadoes allegedly skipped. The fact that one house often experienced complete destruction while a house next door sustained only minor damage perpetuated this myth. The mistaken theory proliferated for many decades until Dr. T. Theodore Fujita noticed that in some aerial views of severe tornado damage, there existed the presence of cycloid-shaped ground markings within the tornado's damage path. [16] Further investigation revealed that the most severe damage and the majority of the fatalities occurred in the areas indicated by these strange markings. After studying video evidence, Dr. Fujita formulated that these marks were the result of smaller vortices within the primary

funnel. He called these aberrations, suction vortices. The discovery of these mini-tornadoes within the main vortex provided the explanation of why extreme damage often occurs on a smaller scale than the primary damage path. Figure 7 is Fujita's representation of the concept of suction vortices. The winds in the proximity to the "mini-funnels" are much greater than the surrounding winds.

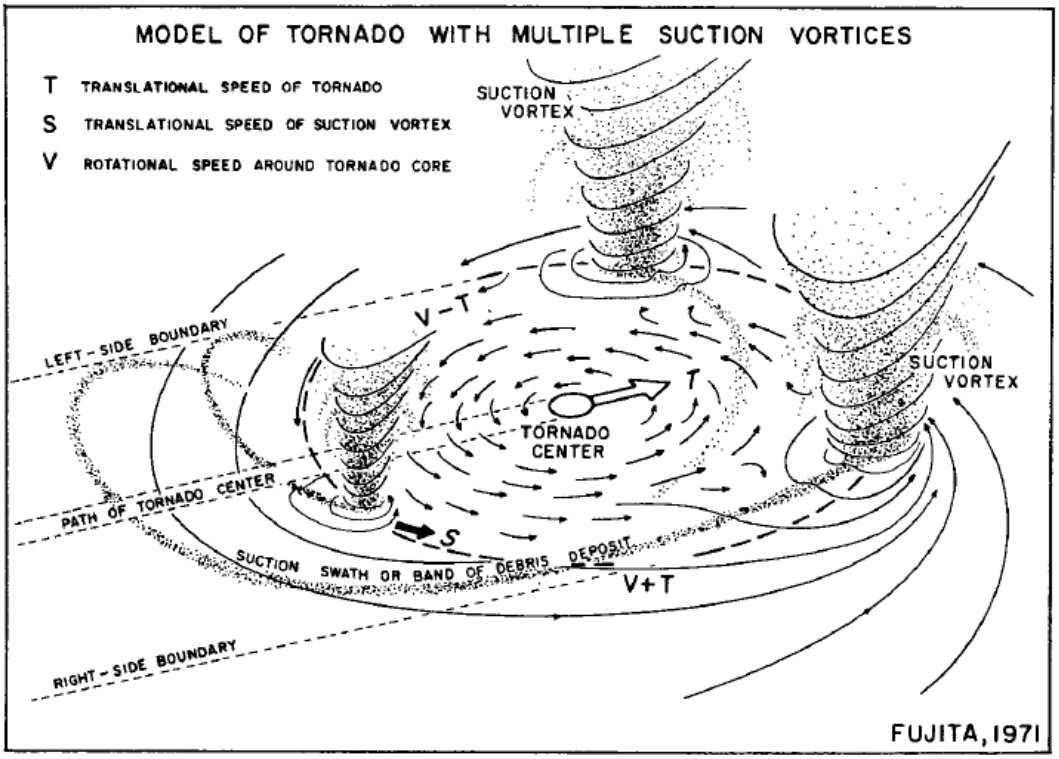

Figure 7: Fujita's Multi-Vortex Tornado Sketch
[47]

A study by Lewellen, et al. was able to recreate this phenomenon by the use of a simulator; thus, confirming the existence and formation characteristics of these suction vortices. [45] His paper states, "...the number of secondary (vortices) is not constant in time, and their evolution is often chaotic, but there are always a number of strong secondary vortices...with perturbation pressure deficits of twice that in the upper core of the main vortex."

The effect of these multiple vortices on the wind speed and associated damage is evident taking into consideration the explanation given above regarding the additive characteristics of the tornadoes forward speed. Suction vortices provide another constituent in the equation for determining the most intense winds speeds inside tornadoes. As previously shown, the translational speed of the main vortex is additive to the rotational speed of the main tornado vortex on the right side of the vortex. The existence of suction vortices complicates this topic. A tornado with a rotational speed of 130 mph and a translational speed of 50 miles per hour combined with 50 mph rotational-speed suction vortex located on the right side of the main tornado vortex results in an instantaneous wind speed of 230 mph. Add this to the various directional constituents of the comprehensive wind field and it is not difficult to explain catastrophic damage. Figure 8 illustrates one of the first photographs of this phenomenon.

Considering the descriptions given previously, it is easy to explain the variations of damage within a tornado's path. Visualize a tornado with a damage path width of 1000 feet. If the description described above is occurring on the right side of the funnel, there will be a wind speed 230 mph. At the center of the tornado vortex, the wind speed is almost zero. If the left side of the tornado in the example, simultaneously experiences no suction vortices, then the resultant instantaneous wind speed at this location would be the rotational speed of the main vortex (130 mph), minus the translational speed of the tornado (50 mph), resulting in an instantaneous wind speed of 80 mph as in the first example described. Therefore in the 1000 feet wide path of the same main tornado, there will be southerly winds approaching 230 mph on the right, 500 feet to the left, and the winds will be near zero, and 500 more feet to the left, the location will experience a northerly wind of 80 mph. Add to this the upward component of the winds throughout this funnel and it becomes obvious that the resulting forces felt by structures in the tornadoes path will experience a very convoluted application of pressure forces.

Figure 8: Photograph of Multi-Vortex Tornado in Dallas in 1957
[48]

As was previously illustrated, the overall wind field characteristics in and around a tornado are complicated. The study of tornado damage provides much evidence in the attempt to define tornado wind fields, but the most superior data in regards to the wind fields result from videos of actual tornadoes. Detailed analyses of tornado videos are possible by the use of a procedure known as photogrammetry. Knowing the frame speed of the video in addition to the identification of objects of known scale allows for comprehensive mapping of debris particles and cloud tags. From these analyses, the internal tornado wind perturbations and accurate wind speed estimates are calculated.

The first 16mm tornado film of sufficient quality to permit photogrammetry resulted from the Dallas tornado on April 2, 1957. There are several reasons for this tornado to be an excellent subject for photogrammetry research:

- The tornado occurred in the afternoon; therefore, adequate light was present
- The tornado occurred in the downtown area of a major metropolitan area; therefore, many opportunities for professional video existed
- The parent storm was not an extensive rain producer; therefore, obscurations were minimal
- The tornado was stable – it remained in the same stage of development for the majority of its lifecycle
- It was a single vortex tornado; therefore, its structure was not complicated by derivative elements of rotation
- The condensation funnel did not come in contact with the ground for much of its life; thus, the evidence of the interface between the wind regimes and the ground were phenomenal

Hoecker did an extensive study of this video resulting in the first three-dimensional comprehensive analysis of a major tornado's wind field distributions and wind speeds. [49] The maximum tangential windspeed resulting from this study was 170 mph. Correspondingly, the highest upward wind speed reached 150 mph. Figure 9 illustrates the distribution of the tangential and upward wind characteristics of the Dallas tornado.

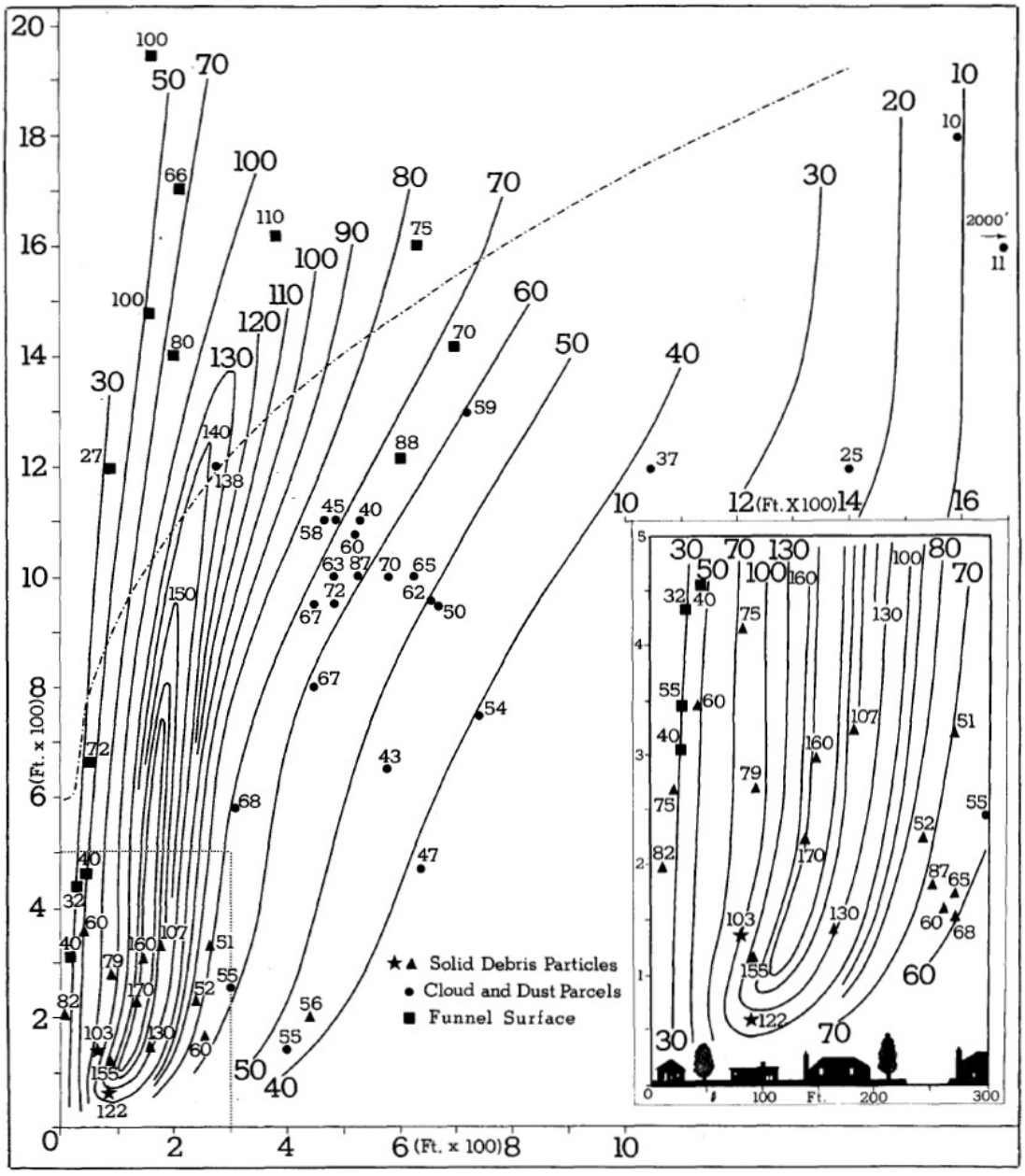

Figure 9: Cross Section of Dallas Tornado Windfield
[49]

Dr. Fujita was the master of photogrammetry. His obsession with detail and his talents for illustration combined to provide a very comprehensive study of every tornado that he analyzed. His painstaking procedure for analyzing tornado video evidence included six steps [16]:

- Exact tornado path detail and various tornado characteristics must be examined via an aerial and/or ground survey,
- Positioning at the site of the photographer allowed the surveyor to establish the azimuth angles of reference to the tornado,
- Prints of each frame of the video must be made,
- Prints must be registered to maintain a fixed frame of reference to minimize the effects of camera movement,
- Re-photograph the registered frames,
- Convert angular displacements from the stabilized movie to velocities via trigonometry

While photogrammetry provides a good approximation of the wind field associated with particular tornadic events, it does have drawbacks. One such limitation of photogrammetry is that only wind particles normal to the line of sight are candidates for measurement; therefore, radial velocity is not available for direct measurement. [16] Also, debris particles have mass (sometimes substantial mass); therefore, do not represent the wind speed, but the speed of the debris. Lastly, tornadoes do not always provide quality video recordings: they are often rain-wrapped, surrounded by debris or dust, occur at night, or transpire in areas where photographers are not available. Despite these limitations, photogrammetry has, and does, represent a viable method of estimating wind field characteristics and wind speed determination in tornadoes.

Why is there such a preoccupation with the wind speeds in a tornado? Does not other characteristics exist that represent important tornado information? One paper suggests that "...the most *intense* (italics are theirs) tornado may not necessarily be the most damaging one if the velocity maximum is suspended sufficiently far above the ground." [50] The answer is that the primary constituent of a tornado is the effect that the wind has on humanity. The wind speed defines the tornado's intensity. The damage that results from a tornado results from the wind. The injuries and fatalities

are the result of the interface of the wind with people. More importantly, the required precautions to increase survival in the event of a tornado are an attempt to counteract the effects of wind. The knowledge of the wind characteristics in and around a tornado allow for better definitions of safety measures.

The utilization of Doppler radar has also proven to be a valuable tool in the quest to determine the windspeed in a tornado. In a 1985 paper, the techniques for using Doppler radar to penetrate a tornado provided promising results. Despite the successes alluded to in this paper, the concluding remarks stated, "...high priority should be given to the development of a portable Doppler radar or lidar which could be transported by intercept teams to a position near the tornado..." [51]

CHAPTER 4

DAMAGE ANALYSIS AND SURVEYS

Introduction

After the May 1970 tornado that struck Lubbock, Texas, engineering entered the scientific study of tornadoes damage analysis. The foremost contribution to tornado research from engineering is the estimation of tornado windspeeds via load resistance calculations associated with wind-induced failure. Whether through an on-site physical survey or analysis of tornado damage artifacts, this method provides the best data for analysis. However, as this thesis demonstrates, information gathered from tornadoes that occurred long in the past provides valuable clues to tornado behavior and tornado/building interactions.

For tornado damage analyses, the principal artifacts are photographs. Photographs taken for the sole purpose of analysis of storm damage is indisputable evidence allowing engineers and meteorologists to perform forensic analyses without being present at the damage scene. Depending on the time-period of the tornado, the representative photographs can be of poor quality from the standpoint of structural study. Older photographs of this nature concentrate on subject matter important to the photographer rather than on damage particulars. The assumption that secular photographs will highlight data important to the study is sometimes optimistic. For this reason, the introduction of transdisciplinarity is required. Image manipulation processes can extenuate areas of concern and eliminate areas of no consequence. This becomes especially important when analyzing very old photographs. Optimally, the photographs should represent damage that was exclusively the result of structure/wind interaction or debris impact. In addition, debris transport photos can be very beneficial in determining casualty specifics and windfield characteristics. A preferred damage photograph would encompass damage from an obtainable direction, on a structure of known construction in which scale determination is possible. Photographs

of this nature can provide valuable evidence that permit wind-engineering analyses to estimate the wind speeds and modes of failure.

Over the past few decades, engineers have become increasingly interested in the damage caused by extreme winds, including those resulting from tornadoes. There are many successes in this field study including the introduction of the relatively new subset of engineering: Wind Engineering. Many of the primary references in this study come from individuals either currently or formerly associated with the Texas Tech Wind Engineering department. The goal of this work is not to diminish their contributions. On the contrary, the hope is that their efforts will provide a foundation for further study.

Given the aforementioned statements, the goals of a typical engineering study of damage in the wake of a tornado are twofold:

- "record engineering assessments of the response of structures to tornadic loadings – extreme winds, changes in atmospheric pressure, and missile impacts; and
- advance the scientific understand of tornadoes through the calculation of near-ground windspeeds, the characterization of near-ground windfields, and the contribution of pertinent facts observed during investigations" [8]

Wind Engineering

The field of wind engineering encompasses many diverse areas of concentration; however, for this application only two are included: severe wind structure interaction and debris impact phenomena.

When a structure is in a wind environment, the most basic form of the empirical equation describing this interaction is an application of the Bernoulli equation: [52]

$$p_s = p_a + \frac{1}{2}\rho V^2 \tag{1}$$

Where p_s represents the stagnation pressure exerted on a flat surface (i.e. the side of a building)

p_a is the ambient pressure in lbs/ft^2

ρ is the air density in slugs/ft^3

V is the wind velocity in ft/sec

On the surface of the earth, the air is at atmospheric pressure; therefore, the p_a term is zero. Under a standard atmospheric condition, which is adequate for wind pressure determinations, the air density is 0.00237 slug/ft^3 or 14.7 psi. This reduces to:

$$p_s = \frac{1}{2}(0.00237)V^2 \tag{2}$$

This illustrates an interesting phenomena in regards to wind /structure interaction. The wind exerted pressure on a surface is proportional to the wind velocity squared; therefore, the force on a building experiencing 147 ft/sec (100) mph) wind is not ten times the force of a 14.7 ft/sec (10 mph) wind, but 100 times the force. This exemplifies the phenomenal forces that act on a structure during a tornado.

With continued involvement from engineering, the equation showed above evolved to represent conditions that are more specialized. The American Society of Civil Engineers created a standard called "Minimum Design Loads for Buildings and Other Structures" which is the benchmark for studies related to structures under the influence of wind loads, as well as, snow loads, rain loads, ice loads, seismic anomalies, and other specifics to structure-influenced conditions. [17] Of particular importance to extreme wind studies to low rise-buildings, the equation of the influence of wind on structures has expanded as shown below:

$$p = q_h[(GCp_f) - (GCp_i)](lb/ft^2) \tag{3}$$

Where p represents the design wind pressure for Main Wind-Force Resisting System (MWFRS) of low-rise buildings

GCp_f is the external pressure coefficient found in [17] Figure 6-10

GCp_i is the internal pressure coefficient found in [17] Figure 6-5

q_h is the velocity pressure evaluated at height h and found by the following equation:

$$q_h = 0.00256 K_Z K_{ZT} K_d V^2 I (lbs/ft^2) \text{ [53]} \quad (4)$$

Where 0.00256 is the default air density (note that this is slightly different from the number used in the above equation - by determination of the ASCE)

K_Z is the exposure velocity pressure which estimates the change in wind speed with height as well as terrain roughness

K_{ZT} is the topographical factor for accounting for winds speeding up over hills and escarpments

K_d represents the directionality factor

V is the wind speed represented by a 3-s gust speed and is associated with an annual probability of 0.02

The aforementioned ASCE is a guide for the design of new structures; its formulation in part owes its derivation from studies of wind damage, and as such, can be utilized, or reverse-engineered, to aid in the determination of wind characteristics based on observed damage. Though these equations and illustrations are absent from the content of this study, they are important in regards to the advances for the field of wind engineering.

The second application of wind engineering in terms of extreme wind characterization is the aspect of debris impact. This phenomenon is the concentration

of this study. Chapters 5 and 6 go into much detail regarding this aspect of engineering.

A most important factor of wind engineering involves the accumulation of data needed to understand a high-wind event. These data are primarily the result of damage surveys.

General Survey Specifics

Over the past few years, damage surveys have provided substantial evidence dealing with the way tornadoes destroy homes. For instance, one survey found that during the 1980 Grand Island, Nebraska tornado, 49% of severe damage along the path of the tornado occurred in homes that had garage doors on the side of the house facing the approaching storm. [15] This was strong evidence that garage door failures allowed the winds to enter the roof-covered space; thus, internal pressures were greatly increased. This same phenomenon occurred during the 1999 Moore, Oklahoma tornado. [13] Figure 10 illustrates the fragility of a garage door. This home was lucky. Despite the damage incurred on the garage door, the remainder of the residence is mostly intact.

Figure 10: Garage Doors Represent One of the Weakest Elements of a Home
[54]

In 1993, the National Weather Service and the National Severe Storms Forecast Center developed a guideline for conducting wind damage surveys. [46] This guide illustrated specifically how surveys were to be performed, including equipment to be used, how to relate damage to the Fujita scale of tornado intensity (which has since been replaced by the Enhanced Fujita scale), how to determine if the episode was tornadic in nature or just downburst winds, and the basic goals of the survey. Even a worksheet was included to insure that no artifact escaped the survey team. The basic goals of a survey as enumerated in the "guide" were:

- construct a sketch of the path of damage, including path length and wide, an estimate of the times that the tornado was in contact with the ground, and a rough estimate of the F-rating
- interviews with any eyewitnesses and/or storm spotters
- attempt top get videos and photographs if available

- make note of any unusual characteristics and document missile trajectories
- Record the damage area using both video and still cameras for later analysis
- note any accounts from the tornado that could be useful in the NWS Preparedness Program [46]

Typically, the National Weather Service dispatches a survey team after each severe weather event. The information acquired from these surveys has proven to be invaluable in regards to tornado and damage mitigation research. Many reports resulting from specific tornado surveys exist, and this thesis uses many as examples. [11, 13, 14, 15, 55, and 56]

For the research in this dissertation, three surveys were undertaken. Each survey was different in terms of objectives; however, each illustrates the diversity and extreme power associated with a tornadic event. Please note that the information contained in regards to the surveys does not attain the level of serious scientific rigor. Their inclusion in this study is to provide a point of reference to illustrate the devastating effects associated with tornado episodes.

McKinney, Texas Tornado 1948

The first tornado survey investigates a tornado that occurred on May 3rd, 1948 in McKinney, Texas. The choice of this tornado for examination resulted from several factors:

- The author's familiarity with this community
- A long past tornado provides a good comparison of damage between home construction in a previous era to contemporary construction practices
- Allows an opportunity to highlight the advantages of transdisciplinary research and collaboration
- Exposes the plausibility of studying tornado damage when the damage is not recent, especially illustrates the quality of the artifacts that can be recovered

- This review will help answer some questions about this tornado in light of today's knowledge of severe convective weather

Since, this tornado occurred more than 60 years ago, accumulating viable data was challenging. Newspaper accounts, while not supportive of scientific study, did provide useful leads in terms of locating photographs, survivors, local meteorological data, and some useful statistics that were verifiable. In particular, a professional photographer in McKinney in 1948 supplied many of the photographs included in this study. Unless specified otherwise, all photographs of the McKinney tornado damage are courtesy of [57]. One photograph, of unknown origin, shows an aerial view of the damage area. [58] (See Figure 11) This photo indicates the possible locations for suction vortices within the parent tornado due to the irregular severe damage pattern. Also noted are the locations of the author's family and one of the fatalities during this storm.

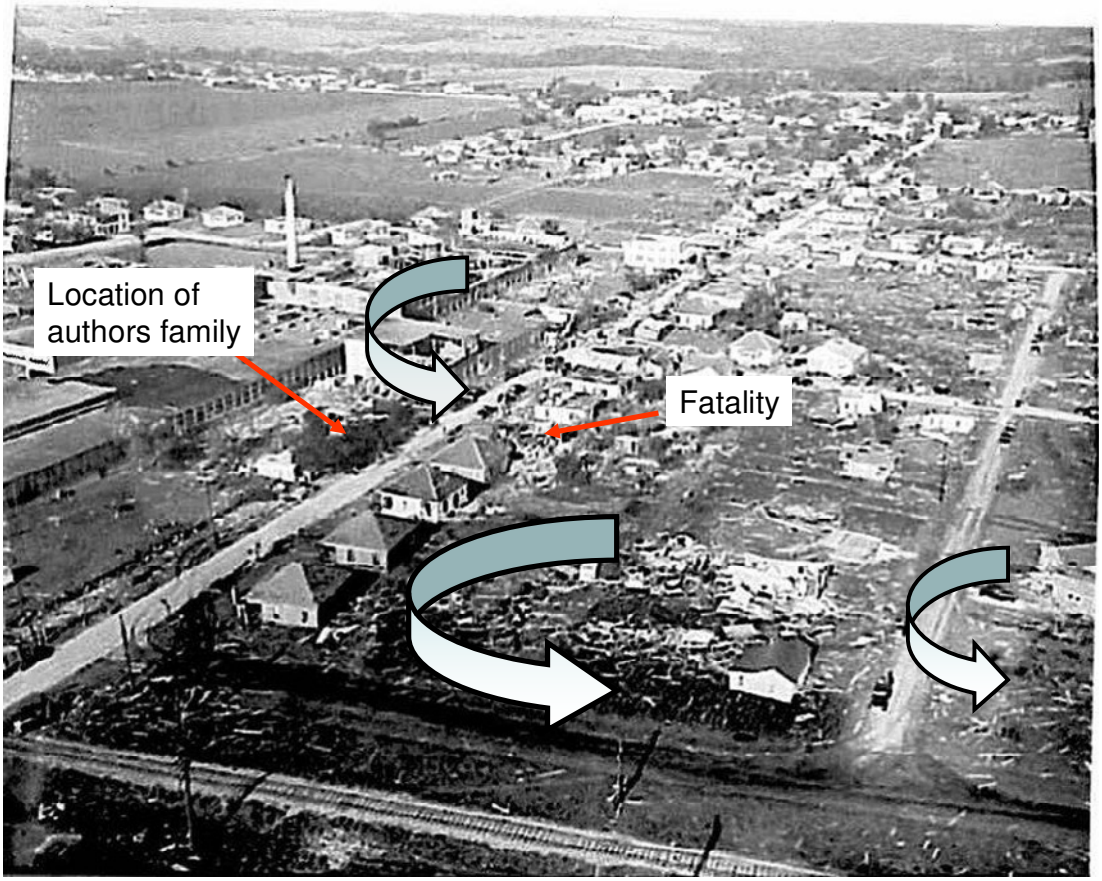

Figure 11: Rare Aerial View of 1948 McKinney Tornado Damage
[58]

An effort to regenerate specifics related to a 60-year-old tornado event resulted only through the transdisciplinary collaboration of various entities. A generic concept map shown in Figure 12 illustrates a generic representation of this contingency of cooperation. Similar to the concept map shown in Chapter 1, the process for this forensic examination concentrated on three primary areas of research: Meteorological evidence, analyzing the statistical evidence from various sources, and compiling and analyzing damage artifacts.

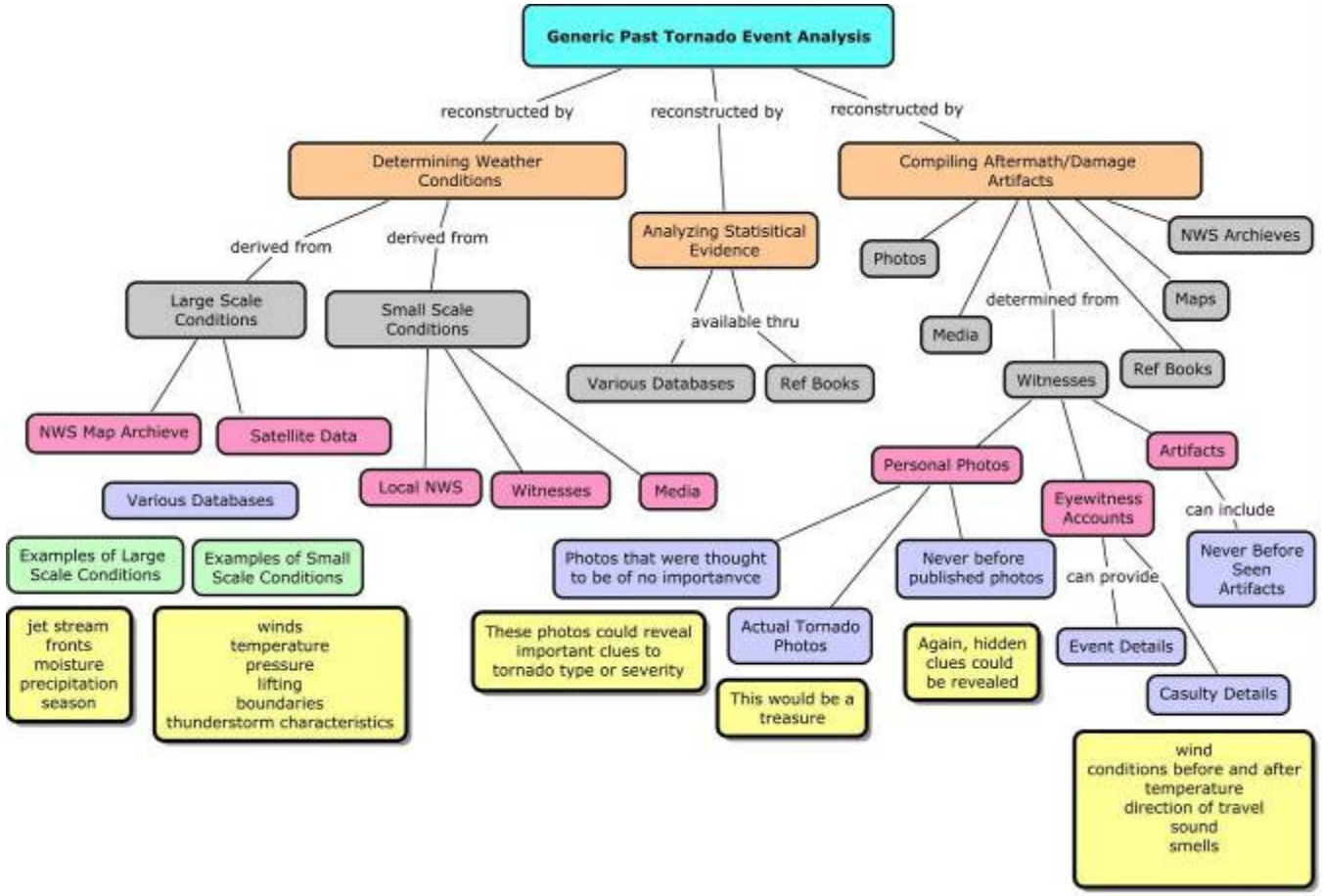

Figure 12: Concept Map Defining 1948 McKinney Tornado Research

The unfettered cooperation of many individuals, professionals, city historians, and news outlets exemplified the success of the nature of transdisciplinarity of this project. The concept map illustrated in Figure 13 represents the fan-out of this research and the individual contributing entities. Despite a sixty year elapsed time since the event, the artifacts in terms of photographs, survivors, historical records, and meteorological data was overwhelming. Since the official National Weather Service database, known as "storm Data" only goes back to 1950, this event predated this documentary service by two years. Still the availability of useful information existed in great quantity.

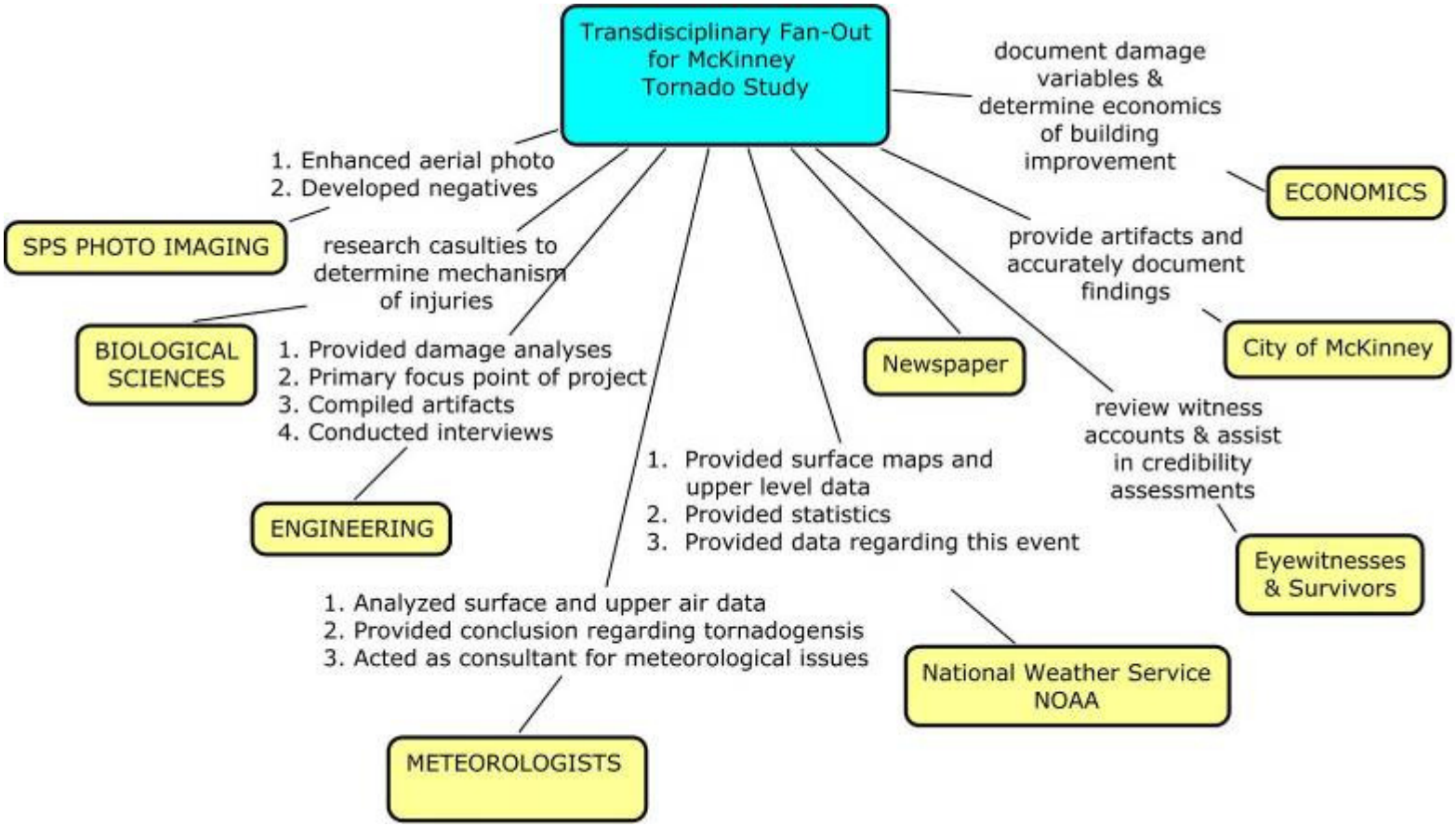

Figure 13: Concept Map Defining the Details of the Research Project

Severely damaged during this tornado was the primary employer in McKinney: the Texas Textile Mills (referred to hence forth as the mill). The tornado not only struck this business, but it hit at 3PM, which was shift change. This means that the maximum number of people witnessed this storm at its peak intensity. Yet only two deaths resulted.

The next several photographs highlight some of the damage to the mill. In Figure 14, the second floor experienced considerable damage. Even though very large wooden beams supported the second floor, much of the floor is absent. It is interesting that very few of the windows are broken, owing to the direction of the strongest winds. It is interesting that the fence is intact, despite the abundance of periphery debris.

Figure 14: The Mill Sustained Great Damage to 2nd Floor, but Most Windows Survived

Figure 15: The Damage Adjacent to the Mill was Severe

Figure 15 is one of the most damaged areas of the mill. Steel beams failed, the fence sustained severe damage, and there is considerable debris present. There is also a destroyed water tower shown in the center-left of the photo.

Figure 16: The Mill's Water Tower Sustained Total Destruction

Figure 16 highlights the damage to the water tower and surrounding structures. Notice the abundance of cotton debris. Sheets of metal also exist which indicates that

flying debris during this storm was severe. Metal beams experienced contortion as the wind forces removed whatever materials adhered to them.

Figure 17: Debris Scattered Around the Mill Illustrates Flying Debris

Figure 17 represents the eastern section of the mill damage. Second floor damage shows, as well as, debris from homes across the street. In terms of damage associated with residences, this tornado left sporadic severe damage along a path of little to moderate damage. This is further evidence of a multi-vortex tornado.

Homes built in this area in the 1940's were considerably different from homes built today. The foundations were usually wooden blocks with the floor joist held to

these blocks by gravity. This design would allow wind to get underneath the home and either lift it up or roll it off the foundation. Figure 18 illustrates the result of an inferior home to foundation interface.

Figure 18: House Rolled Due to Inferior Attachment to Foundation

Figure 19 further shows the foundation deficiency typical of homes during this time (notice that house on the right is built on a very fragile foundation). Also seen is the automobile that has sustained major damage and was obviously moved from somewhere to its final resting place on the grass. The automobile windows are all broken, and small debris is widespread, yet the house on the right is virtually undamaged despite the weak building constituents. Across the street, a frail garage is intact, while the second floor of the factory behind sustained major damage. (The author's family took refuge in this frail garage during this storm).

Figure 19: A Good Illustration of Minor Damage alongside Severe Destruction

Much of the home damage witnessed is attributable to weaknesses in connections, especially weak connections between walls and roofs. Many examples of roof to wall failure illustrate this fact. During this time, the roofs attachment mechanism to the walls consisted of concept known as toe nailing. This is where a nail driven in at an angle sufficient to penetrate the roof member connects to the plate across the top of the wall. This methodology provides a very poor connection between these components; however, during this period, the alternatives were limited.

.

Figure 20: After the Roof Failed, the Walls Collapsed

The home shown in Figure 20 experienced complete roof failure. The displaced roof is evident in the front yard and appears to be intact. The major structural elements of the roof are 2 x 6 timbers. The failure mechanism most certainly responsible for this failure was pressure forces on the underside of the roof due to wind intrusion into the residence. Perhaps the failure of a window or door allowed wind entrance, which created a strong uplift environment. In the absence of the structure's cohesion aided by the roof connections, the front wall collapsed outward.

Figure 21: Another Example of Roof Failure

Figure 21 illustrates a failure mechanism similar to that in the previous photograph. Since the windows are missing, it appears that the wind gained entrance into the structure through the openings, lifted the roof, and the wall collapsed due to the absent cohesion of the roof structure. Much of the furniture remains in the house. This photograph also illustrates the construction of the interior walls. They consist of 2 x 4 timbers covered on both sides with solid wood. This provides a much stronger wall than sheetrock.

Figure 22: Failure of Roof due to Overhanging Porch

This home failed under the force of the tornado winds due to the overhanging porch giving the wind an entrance under the roof. When the roof failed the rest of the home failed like a house of cards. This phenomenon is less evident today due to the limitation of expansive porches, but the materials utilized today provide inferior structural support.

Figure 23: Catastrophic Damage due to Roof Failure and Racking

The damage in the photograph labeled as Figure 23 is particularly interesting. Though the roof is completely gone and considerable debris is present all around the home, much of the envelope of the home is intact. The house on the left seems to have experienced only minor damage.

Figure 24 is a graphical representation of the effect of wind pressures on walls and roofs after wind penetration occurs. Tremendous forces act on the exterior walls and roofs causing failures at these weak connections.

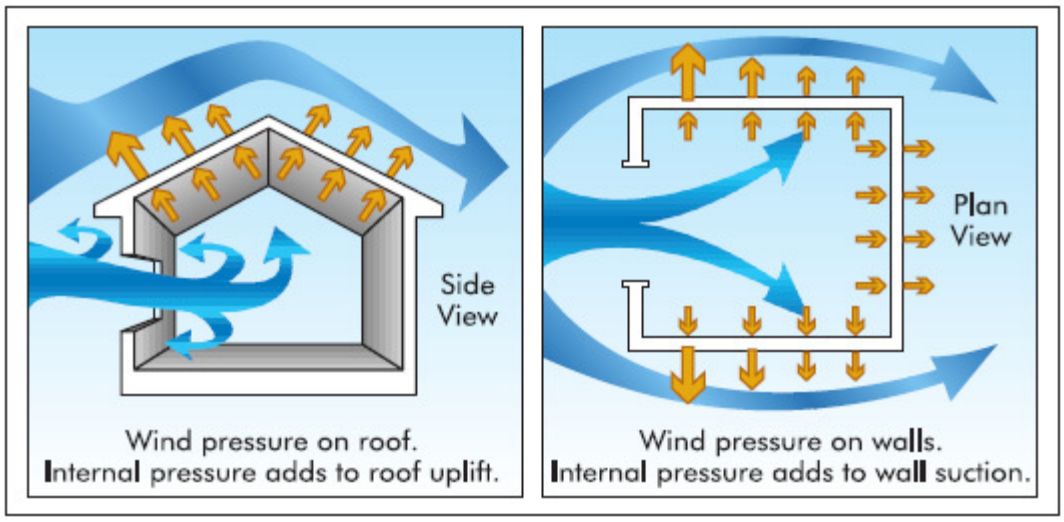

Figure 24: How Internal Pressure Affects Home
[59]

Figure 25: Roof Loss due to Porch Overhang

Figure 25 illustrates the loss of a roof via a different mechanism. In this case, the roof connection failure did not result in wind intrusion into the house, but via the wind getting under the roof from the front porch, similar to the structure in Figure 22. The roof failed at the connection, as before, but due to the porch creating an area under which the wind could gain a "hold", the forces were adequate to lift the roof away from the structure. As in some previous illustrations, the walls remained standing. This illustrates another testament to the structure that existed within the exterior and interior walls common in 1948.

Homes not only fail from wind intrusion, but also by wind effects on the outside surface to the home. Figure 26 highlights other means of failures typical when structures experience tornado force winds.

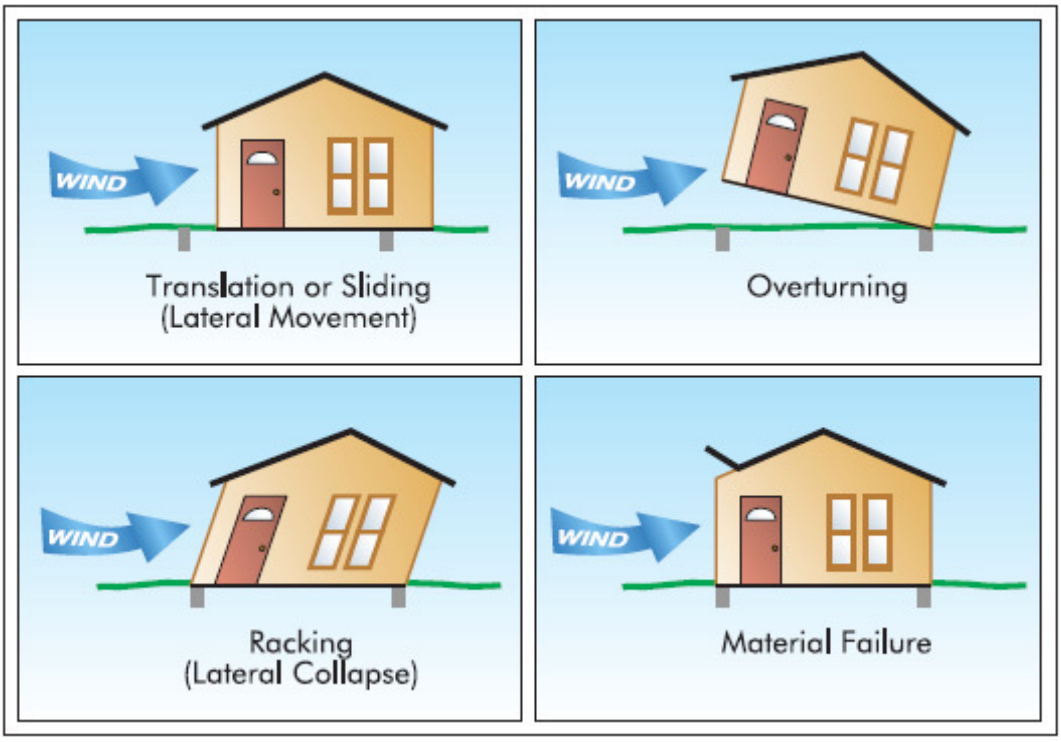

Figure 26: Various Mechanisms can Cause Structural Failure
[59]

The home illustrated in Figure 27 experienced severe racking.

Figure 27: Failure via Racking

Another form of artifacts from the McKinney tornado came in the form of survivor testimony. Even though the tornado occurred 60 years in the past, vivid memories still existed for many of the respondents. Of all of the contacts, each one had the same overall description: The day started out very humid and cloudy. As the day progressed, it became partly cloudy and very warm and oppressive. No one saw the funnel itself, and no rain occurred prior to the tornado. This would suggest that the tornado was already (or rapidly becoming) rain-wrapped. It likely formed on the southwestern part of the thunderstorm and moved eastward (since it struck Princeton, 7 miles to the east) as the main thunderstorm moved northeastward. All eyewitnesses report that they saw a rolling black cloud approaching from the west. This wall was probably the tornado approaching, hidden behind a curtain of rain. Without exception, each respondent reported that it was dark as midnight. They each stressed that this

was not an exaggeration. The tornado struck suddenly as the wind went from calm to ferocious in an instant. [60, 61, 62, and 63]

From a meteorological standpoint, the tornado should not represent a great surprise with today's knowledge. Unfortunately, in 1948 this was not the case. There were no radars, no satellites, no storm spotters, and no computers. In 1948, there were no tornado watches or warnings, and no televisions to see the approach of a storm. However, in retrospect, the conditions were favorable for the development of isolated tornadoes. Figure 28 indicates that a severe weather event may be in the near future.

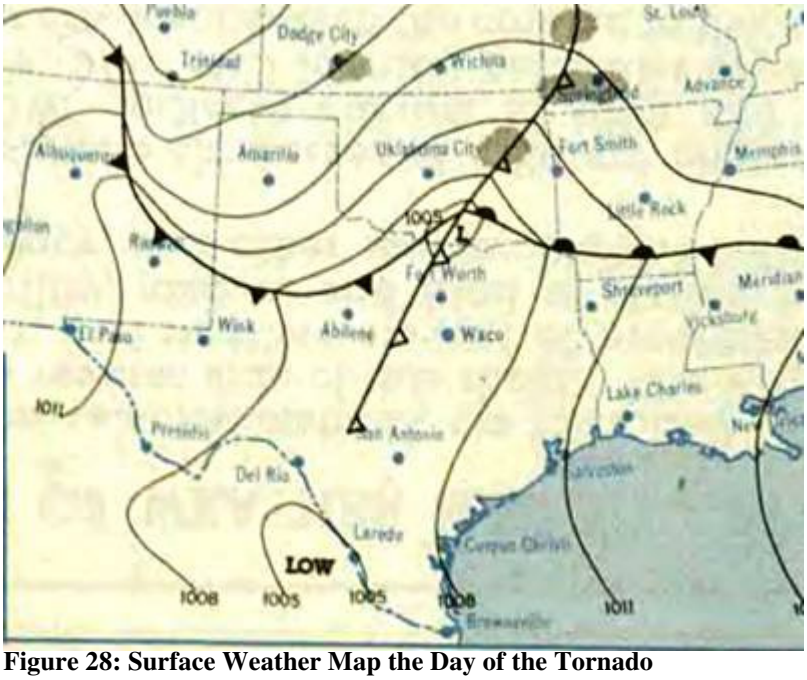

Figure 28: Surface Weather Map the Day of the Tornado
[64]

A dryline has formed along a retreating warm front. In addition, a surface low is located on the Texas/Oklahoma border just north of the McKinney area, and the warm front sector west of the low is moving southeastward as a cold front. As thunderstorms form along this intersection of air masses, outflow boundaries will result. These boundaries will become a focus for the development of further thunderstorms, especially as daytime heating provides the "fuel" needed for development. Personal communication with the Fort Worth National Weather Service

forecast office confirmed this scenario. Having access to upper level archival data, their assessment of the situation noticed a 500-mb trough over the New Mexico/Colorado area containing west-southwest winds of 45 knots. This confirms the existence of deep layer shear. An 850-mb low over the Texas Panhandle with winds approximately 20 knots provided borderline low-level shear. Lifting indices greater than minus-six existed in the most unstable regions; therefore, sufficient instability existed. Along with the surface characteristics mentioned earlier, the region in question was definitely under the threat of scattered severe thunderstorms, with likely rotation. [65] This proved correct about 2 ½ hours after the surface map in Figure 28 documented the conditions.

Judging from the damage region, it first touched down about ½ mile west of the mill (along Barnes Street). At this point, it struck the Hall residence. One of the respondents to interview for this research was the late Helen Hall, husband of the late Roy Hall. She stated that her husband saw the storm coming and was trying to get the baby to safety when the tornado struck their home. He and the baby hit the floor just as the roof flew away. At this point, he looked up into what must have been the interior of the tornado. Roy Hall is purported to be one of two credible tornado survivors to have looked into the eye of a tornado. The following is an excerpt from his interview with *Weatherwise* magazine in 1951.

> "[T]he bottom of the rim was about 20 feet off the ground. The interior of the funnel was hollow; the rim itself appearing to be not over 10 feet in thickness and, owing possibly to the light within the funnel, appeared perfectly opaque. Its inside was so slick and even that it resembled the interior of a glazed standpipe. The rim had another motion which was, for a moment, to dazzling to grasp. Presently I did. The whole thing was rotating, shooting past from right to left with incredible velocity." (66)

The official death count from this tornado is three; however, there is some doubt regarding this number. Figures 29, 30, and 31 are the death certificates from the

individuals reported to have died because of this tornado. The first two victim's causes of death are compound skull fracture and skull fracture. This is consistent with tornado related causalities. The third certificate lists the cause of death as electrocution from a lightning strike; therefore, not a tornado related death. The names of the victims are not included out of respect.

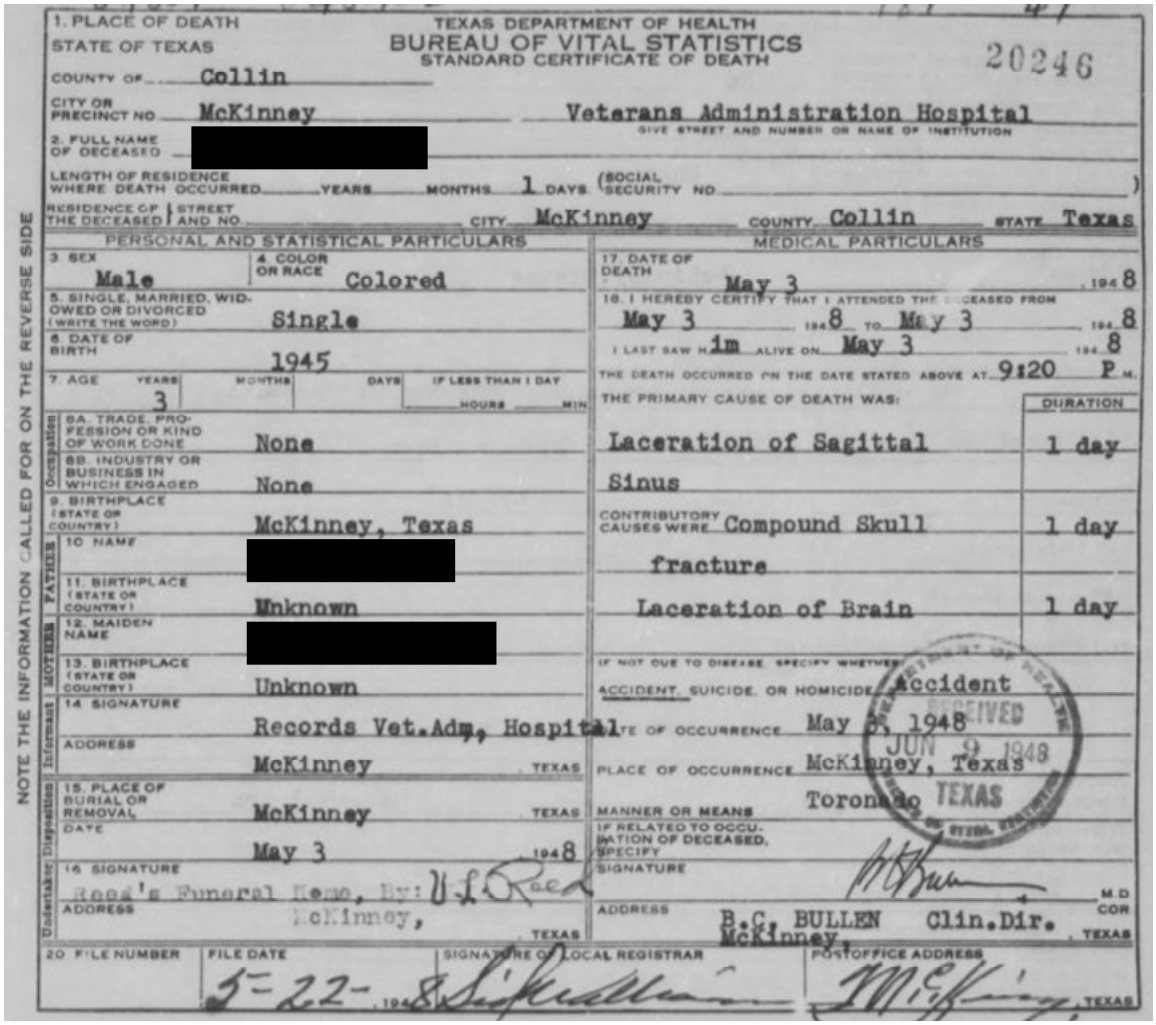

1. PLACE OF DEATH
STATE OF TEXAS
TEXAS DEPARTMENT OF HEALTH
BUREAU OF VITAL STATISTICS
STANDARD CERTIFICATE OF DEATH
20246

COUNTY OF Collin
CITY OR PRECINCT NO McKinney
Veterans Administration Hospital
GIVE STREET AND NUMBER OR NAME OF INSTITUTION
2. FULL NAME OF DECEASED [redacted]
LENGTH OF RESIDENCE WHERE DEATH OCCURRED ... YEARS ... MONTHS 1 DAYS (SOCIAL SECURITY NO ...)
RESIDENCE OF THE DECEASED | STREET AND NO. ... CITY McKinney COUNTY Collin STATE Texas

PERSONAL AND STATISTICAL PARTICULARS

3. SEX: Male
4. COLOR OR RACE: Colored
5. SINGLE, MARRIED, WIDOWED OR DIVORCED (WRITE THE WORD): Single
6. DATE OF BIRTH: 1945
7. AGE: YEARS 3 MONTHS DAYS IF LESS THAN 1 DAY HOURS MIN
Occupation
8A. TRADE, PROFESSION OR KIND OF WORK DONE: None
8B. INDUSTRY OR BUSINESS IN WHICH ENGAGED: None
9. BIRTHPLACE (STATE OR COUNTRY): McKinney, Texas
FATHER
10. NAME [redacted]
11. BIRTHPLACE (STATE OR COUNTRY): Unknown
MOTHER
12. MAIDEN NAME [redacted]
13. BIRTHPLACE (STATE OR COUNTRY): Unknown
Informant
14. SIGNATURE: Records Vet.Adm, Hospital
ADDRESS: McKinney TEXAS
Disposition
15. PLACE OF BURIAL OR REMOVAL: McKinney TEXAS
DATE: May 3 1948
Undertaker
16. SIGNATURE: Reed's Funeral Home, By: U.L.Reed
ADDRESS: McKinney, TEXAS

MEDICAL PARTICULARS

17. DATE OF DEATH: May 3 1948
18. I HEREBY CERTIFY THAT I ATTENDED THE DECEASED FROM May 3 1948 TO May 3 1948
I LAST SAW HIM ALIVE ON May 3 1948
THE DEATH OCCURRED ON THE DATE STATED ABOVE AT 9:20 P.M.

THE PRIMARY CAUSE OF DEATH WAS:	DURATION
Laceration of Sagittal Sinus	1 day
CONTRIBUTORY CAUSES WERE Compound Skull fracture	1 day
Laceration of Brain	1 day

IF NOT DUE TO DISEASE, SPECIFY WHETHER ACCIDENT, SUICIDE, OR HOMICIDE: Accident
DATE OF OCCURRENCE May 3, 1948
PLACE OF OCCURRENCE McKinney, Texas
Toronado
MANNER OR MEANS
IF RELATED TO OCCUPATION OF DECEASED, SPECIFY
SIGNATURE
ADDRESS B.C. BULLEN Clin.Dir. McKinney, TEXAS
M.D. COR

RECEIVED JUN 9 1948 TEXAS VITAL STATISTICS

20 FILE NUMBER | FILE DATE 5-22-1948 | SIGNATURE OF LOCAL REGISTRAR | POST OFFICE ADDRESS McKinney, TEXAS

NOTE THE INFORMATION CALLED FOR ON THE REVERSE SIDE

Figure 29: Death Certificate of Young Boy
[67]

This small boy died from severe head injuries, likely caused from flying debris.

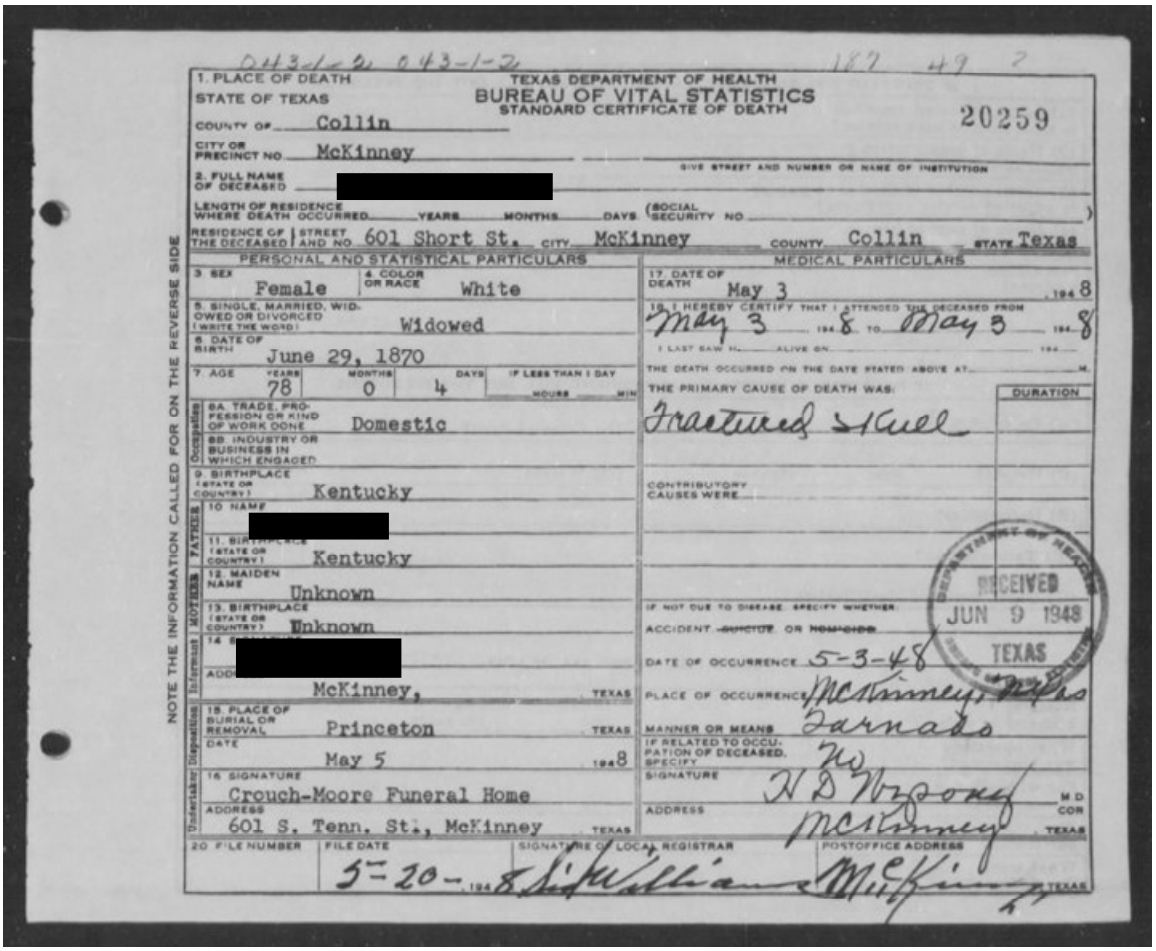

043-1-2 043-1-2 187 49 7

1. PLACE OF DEATH
STATE OF TEXAS
COUNTY OF Collin
CITY OR PRECINCT NO McKinney

TEXAS DEPARTMENT OF HEALTH
BUREAU OF VITAL STATISTICS
STANDARD CERTIFICATE OF DEATH

20259

GIVE STREET AND NUMBER OR NAME OF INSTITUTION

2. FULL NAME OF DECEASED [redacted]

LENGTH OF RESIDENCE WHERE DEATH OCCURRED ____ YEARS ____ MONTHS ____ DAYS (SOCIAL SECURITY NO ____)

RESIDENCE OF THE DECEASED | STREET AND NO. 601 Short St. CITY McKinney COUNTY Collin STATE Texas

NOTE THE INFORMATION CALLED FOR ON THE REVERSE SIDE

PERSONAL AND STATISTICAL PARTICULARS

3. SEX Female
4. COLOR OR RACE White
5. SINGLE, MARRIED, WIDOWED OR DIVORCED (WRITE THE WORD) Widowed
6. DATE OF BIRTH June 29, 1870
7. AGE YEARS 78 MONTHS 0 DAYS 4 IF LESS THAN 1 DAY HOURS MIN

Occupation
8A. TRADE, PROFESSION OR KIND OF WORK DONE Domestic
8B. INDUSTRY OR BUSINESS IN WHICH ENGAGED

9. BIRTHPLACE (STATE OR COUNTRY) Kentucky

FATHER
10. NAME [redacted]
11. BIRTHPLACE (STATE OR COUNTRY) Kentucky

MOTHER
12. MAIDEN NAME Unknown
13. BIRTHPLACE (STATE OR COUNTRY) Unknown

Informant
14. [redacted]
ADDRESS McKinney, TEXAS

Undertaker Disposition
15. PLACE OF BURIAL OR REMOVAL Princeton TEXAS
DATE May 5 1948
16. SIGNATURE Crouch-Moore Funeral Home
ADDRESS 601 S. Tenn. St., McKinney TEXAS

MEDICAL PARTICULARS

17. DATE OF DEATH May 3 1948
18. I HEREBY CERTIFY THAT I ATTENDED THE DECEASED FROM May 3 1948 TO May 3 1948
I LAST SAW H____ ALIVE ON ____
THE DEATH OCCURRED ON THE DATE STATED ABOVE AT ____ M.
THE PRIMARY CAUSE OF DEATH WAS: DURATION
Fractured Skull
CONTRIBUTORY CAUSES WERE

IF NOT DUE TO DISEASE, SPECIFY WHETHER ACCIDENT, SUICIDE OR HOMICIDE
DATE OF OCCURRENCE 5-3-48
PLACE OF OCCURRENCE McKinney, Texas
MANNER OF MEANS Tornado
IF RELATED TO OCCUPATION OF DECEASED, SPECIFY No
SIGNATURE W D Woods M.D.
ADDRESS McKinney TEXAS

RECEIVED JUN 9 1948 TEXAS

20. FILE NUMBER
FILE DATE 5-20-1948
SIGNATURE OF LOCAL REGISTRAR
POSTOFFICE ADDRESS

Figure 30: Death Certificate of Elderly Woman
[67]

This woman also died from severe head injury; almost certainly from flying debris.

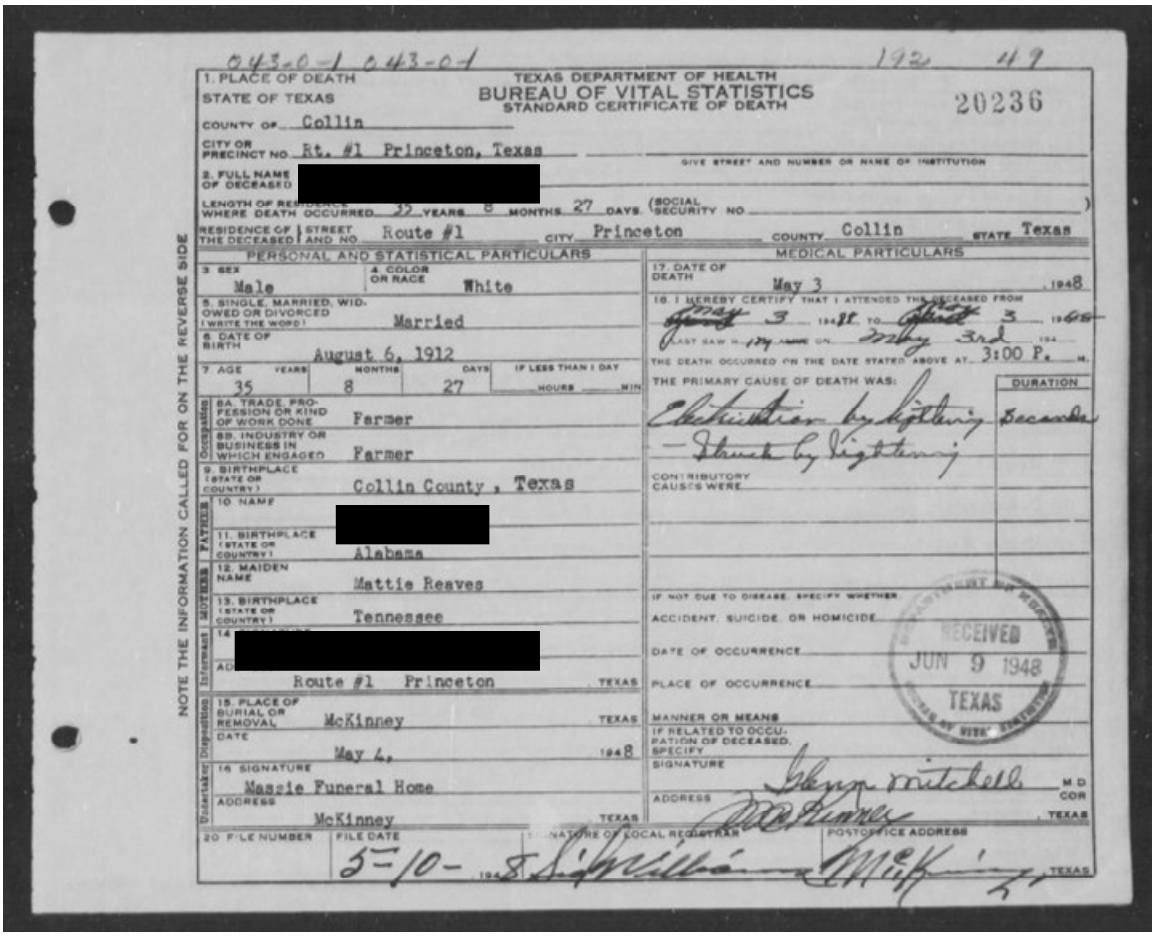

043-0-1 043-0-1 192 49

1. PLACE OF DEATH
STATE OF TEXAS
TEXAS DEPARTMENT OF HEALTH
BUREAU OF VITAL STATISTICS
STANDARD CERTIFICATE OF DEATH
20236

COUNTY OF Collin
CITY OR PRECINCT NO Rt. #1 Princeton, Texas
GIVE STREET AND NUMBER OR NAME OF INSTITUTION

2. FULL NAME OF DECEASED [redacted]
LENGTH OF RESIDENCE WHERE DEATH OCCURRED 32 YEARS 8 MONTHS 27 DAYS (SOCIAL SECURITY NO)
RESIDENCE OF THE DECEASED STREET AND NO Route #1 CITY Princeton COUNTY Collin STATE Texas

PERSONAL AND STATISTICAL PARTICULARS

3. SEX Male
4. COLOR OR RACE White
5. SINGLE, MARRIED, WIDOWED OR DIVORCED (WRITE THE WORD) Married
6. DATE OF BIRTH August 6, 1912
7. AGE YEARS 35 MONTHS 8 DAYS 27 IF LESS THAN 1 DAY HOURS MIN

Occupation
8A. TRADE, PROFESSION OR KIND OF WORK DONE Farmer
8B. INDUSTRY OR BUSINESS IN WHICH ENGAGED Farmer

9. BIRTHPLACE (STATE OR COUNTRY) Collin County, Texas

FATHER
10. NAME [redacted]
11. BIRTHPLACE (STATE OR COUNTRY) Alabama

MOTHER
12. MAIDEN NAME Mattie Reaves
13. BIRTHPLACE (STATE OR COUNTRY) Tennessee

Informant
14. [redacted]
ADDRESS Route #1 Princeton TEXAS

Disposition
15. PLACE OF BURIAL OR REMOVAL McKinney TEXAS
DATE May 4, 1948

Undertaker
16. SIGNATURE Massie Funeral Home
ADDRESS McKinney TEXAS

20 FILE NUMBER FILE DATE 5-10-48 SIGNATURE OF LOCAL REGISTRAR POST OFFICE ADDRESS TEXAS

NOTE THE INFORMATION CALLED FOR ON THE REVERSE SIDE

MEDICAL PARTICULARS

17. DATE OF DEATH May 3 1948
18. I HEREBY CERTIFY THAT I ATTENDED THE DECEASED FROM May 3 1948 TO May 3 1948
LAST SAW HIM ALIVE ON May 3rd 1948
THE DEATH OCCURRED ON THE DATE STATED ABOVE AT 3:00 P. M.
THE PRIMARY CAUSE OF DEATH WAS: DURATION
(a) Electrocution by lightning Seconds
(b) Struck by lightning
CONTRIBUTORY CAUSES WERE
IF NOT DUE TO DISEASE, SPECIFY WHETHER ACCIDENT, SUICIDE, OR HOMICIDE
DATE OF OCCURRENCE
PLACE OF OCCURRENCE
MANNER OR MEANS
IF RELATED TO OCCUPATION OF DECEASED, SPECIFY
SIGNATURE Glenn Mitchell M D
ADDRESS Princeton TEXAS

RECEIVED JUN 9 1948 TEXAS

Figure 31: Death Certificate of Lightning Victim
[67]

This man listed as a tornado victim, actually died due to a lightning strike.

None of the McKinney photographs extenuated debris impacts. It would be incomprehensible to assume that debris penetration did not initiate much of the damage and casualties of this tornado. Unfortunately, this knowledge is lost to time. However, by utilizing all available sources of information in combination with the knowledge of today's meteorologists and engineers, the event from May 3rd, 1948 becomes much more understandable.

Jackson, Mississippi Tornado 2008

Unlike the McKinney tornado, the tornado that struck Jackson Mississippi on the evening of February 5, 2008 was only one of dozens of tornadoes that tore through the mid-south. Unless otherwise specified, all photographs from the Jackson, Tennessee tornado are courtesy of the National Weather Service office in Memphis, Tennessee. [54] Figure 32 maps the specific tornado activity that occurred on that evening with the EF ratings shown along with the path lengths and widths.

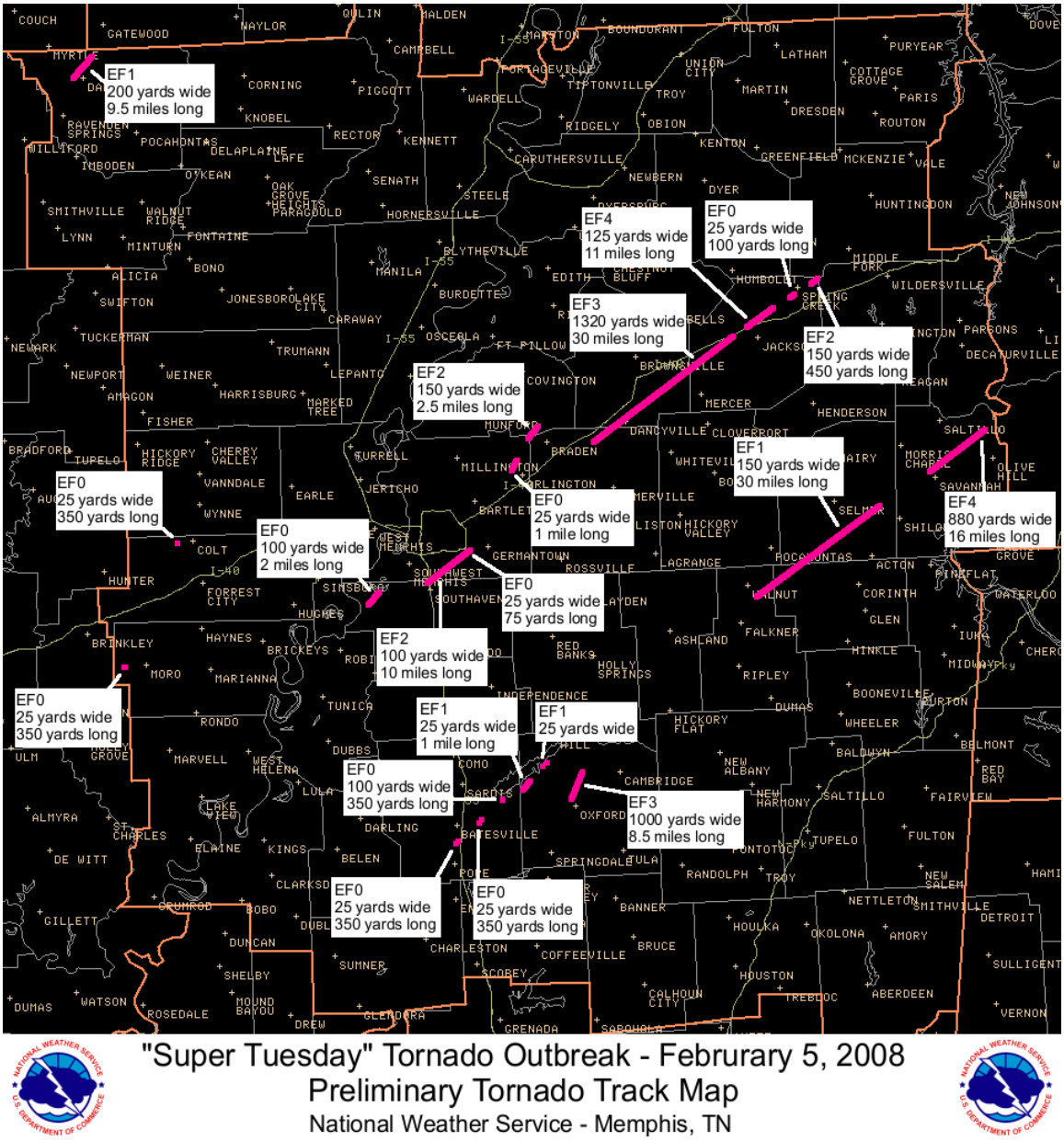

Figure 32: Tornadoes from 5 February, 2008

One of the strongest tornadoes, rated an EF-4 ripped though the Union University campus in Jackson Tennessee. This survey included a visit to Union University, the National Weather Service office in Memphis, and other related damage sites.

The damage at Union University was severe. Automobiles became debris and some of the dormitories suffered catastrophic damage. Figures 33 and 34 are indicative of the damage that results when automobiles are involved with tornadic winds. This exemplifies that automobiles offer no shelter during tornadoes.

Figure 33: Automobiles are no Match for 200+ mph Winds

This photograph of automobiles was located on the campus of Union University. An EF-4 tornado such as this is quite capable of tossing around very large objects such as cars.

Figure 34: The original Location of these Automobiles are Unknown

It was miraculous that no deaths occurred on the Union campus considering the massive devastation. However, there were many serious injuries. Since the campus buildings consisted of "engineered" structures, the injuries were more consistent with "trapped and crushed" injuries than injuries from debris impacts.

During this survey, it was possible to locate the emergency room record from the Jackson, Tennessee hospital. Table who knows details the injuries, mostly from the Union University campus. [68]

This event was traumatic to the extent that a book now exists relating the specific details of the students from the Union University campus. [69]

Table 3: Jackson, Tennessee Causality List
[68]

Age of victim	Sex	Details of Injury	Disposition
20	F	Cuts and abrasions	Discharged
20	M	Contusions/lacerations, lower extremity sprain	Discharged
21	F	Concussion	Discharged
51	M	Fractured hand	Admitted
70	M	Carbon monoxide poisoning	Admitted
69	F	Carbon monoxide poisoning	Admitted
20	F	Multiple contusions	Discharged
20	M	Scalp contusion	Discharged
52	M	Puncture wound, foot	Admitted
20	M	Crush injuries, compartment syndrome, rhabdomyolsis, acute renal failure	Admitted
18	F	Cuts and abrasions	Discharged
20	M	Multiple abrasions and contusions	Discharged
21	F	Sprained ankle	Discharged
20	M	Lacerations	Discharged
64	F	Crush injury, fractured elbow, pulmonary contusion and hemothorax	Admitted
38	M	Fractured finger	Admitted
46	M	Fractured clavicle	Admitted
20	F	Crush injuries, multiple rib fractures, spleen laceration, pulmonary contusion	Admitted
71	M	Penetrating wound by large stick to leg	Admitted
25	F	Foreign body in right arm	Admitted

Figure 35: Cinder Block Construction Caused Many Crushing Injuries

Figure 35 demonstrates the level of destruction that occurred on the campus of Union University. The primary construction of the dormitories consisted of cinder block walls and roofs. When exposed to winds of an EF-4 tornado, these walls toppled over causing many crushing types of injures as shown in Table 3. Though this construction was no match for the tornado, many of the walls collapsed against each other leaving "caverns" of relative safety. This may be in part one of the reasons for the lack of fatalities.

Figure 36: Miracle is that No Fatalities Occurred

Figure 36 is another example of the failure of the cinder block construction. This type of construction has some advantages in terms of debris protection, but structurally, most structures are unable to withstand the forces present during tornadoes. This is especially true of tornadoes rated as high as this EF-4.

Individual homes did not escape the destruction of this tornado outbreak. Scenes reminiscent of the McKinney tornado also existed after this powerful early-season tornado. Though the neighborhoods missed the most intense portion of the tornado, considerable damage occurred in scattered places. Figure 37 shows how modern building techniques do not exempt one from tornado damage.

Figure 37: Typical Home Construction Failed During Tornado

The brick veneer to this home offered no resistance from the tremendous wind forces. When the roof failed, the walls collapsed, as was often seen in the McKinney tornado.

Figure 38: Complete Failure of Home Structure

In some cases, the destruction caused complete devastation, as shown in Figure 38. Considerable debris surrounding this home suggests that the destroyed homes upwind contributed to the debris cloud that accompanied this storm. In more densely populated areas, flying debris from neighboring homes result in more severe localized damage.

Figure 39: Roof Failure due to an Inferior Roof Structure Connection

In other areas, the damage was less complete. The home shown ion Figure 39 lost a roof much like the homes in McKinney 60 years earlier. The same deficiencies in home construction from the 40s still exist in the 2000s.

Figure 40: Roof Failure due to Wind Intrusion

The residence in Figure 40 suffered major damage as the wind gained entrance through broken windows and a failed garage door. Note that the section of serious roof damage is above the area where the window and garage door allowed the winds to penetrate the envelope.

Figure 41: Another Example of Wind Intrusion Failure

Figure 41 is an excellent example of how a garage door failure results in severe roof damage directly over the garage. The roof surrounding the garage only sustained minor damage.

Figure 42: Heavy Metal Objects Become Dangerous Debris

Figure 42 illustrates that dangerous debris is often carried great distances in strong tornadoes. Significant damage would have resulted had these metal artifacts struck a person or a home,.

The Jackson, Tennessee occurred at a time when warnings routinely provide several minutes before the actual event for protective actions. The best suggestions for increasing safety are widely distributed; therefore, most people are aware of precautions and procedures to avoid the hazards of tornado events. The episode at Union University confirms that even during a devastating tornado, the options for increasing ones odd of survival are appropriate and successful.

Lone Grove, Oklahoma Tornado 2009

Scarcely a year passed since the Tennessee tornado outbreak when a catastrophic tornado hit a small community in southern Oklahoma. Unfortunately, this powerful EF-4 tornado hit the most vulnerable portion of the population: a large mobile home community. Eight people died in this storm: one when the tornado struck a moving truck and seven in the mobile home community. This survey proved most sobering in that the survey took place soon after the event, and the fact that several residents were present and going through the rubble.

Due to the unimaginable damage that occurred in this area, there will be a minimal amount of narrative in this section. Photographs with explanative captions exist; however, the necessity for extensive narration is unwarranted. There is not much to explain regarding what happened on a February evening in late February, 2009.

Figure 43: This Automobile was Transported over 100 Yards

Figure 43 shows an automobile that was adjacent to a mobile home park. An entire row of mobile homes experienced destruction and this automobile was carried a considerable distance. The mobile homes were unrecognizable about the storm.

Figure 44: Permanent Residences also Suffered Severe Damage

The inhabitants of the home shown in Figure 44 survived the storm in the small closet shown in the interior of the house. Even though they survived, the closet's door failed and never found. The room closest to the camera was the living room. Despite the tremendous damage to the residence, the window on the side of the storm's approach is not broken. The destructive winds completely removed the roof, and as shown earlier, the brick veneer offered little in the way of resistance.

Figure 45: A Fence is all that remains of this Mobile Home

Figure 45 is a panoramic view of a large portion of the mobile home park. No mobile homes in the path of this tornado survived. Often, severe damage is scattered around a neighborhood, but in this case is was universal. This scene of total devastation reinforces the fact that a mobile home is one of the worse places to seek shelter during a tornado.

Figure 46: Even the trees experienced severe damage

Figure 46 shows another view of the mobile home park. Mobile home parts, furniture, clothing, insulation, toys, and automobiles covered many acres adjacent to the mobile home park. The possibility of survival in one of these structures is almost impossible. Eight people died in this mobile home park. Many more sustained serious injuries. Only the ones who were not home escaped uninjured.

Figure 47: Heavy Framing Thrown a Great Distance

It is hard to imagine the forces associated with such a tremendous storm, but this steel mobile home frame showed no resistance as it struck this tree. Even objects such as this heavy frame became a source of flying debris. Figure 47 illustrates that the windfield associated with a very strong tornado completely devastates mobile homes.

Figure 48: Original Location of this Mobile Home is Unknown

Figure 48 shows another artifact of deadly flying debris. This mobile home frame hit the ground with sufficient force to impale the ground. The original location of this artifact could not be determined; likewise, the location of the rest of the mobile home remained unknown.

Figure 49: Broken Tie-Down Strap

Figure 49 illustrates the ineffectiveness of mobile home tie-downs. These may be useful during a high wind, but when exposed to tornado force winds, the tie-downs fail allowing the mobile home to become airborne. Even the residents could not identify the debris from their own homes.

The photographs taken at Lone Grove, Oklahoma clearly illustrates that there is no safe refuge in a mobile home. Wind can get underneath and cause failure of any tie-down mechanism devised. Projectiles will penetrate the home at almost any wind speeds associated with any tornado. The pressure exerted on the walls and ceiling by the winds cause immediate explosive destruction. No mobile home is ever safe during a tornado.

CHAPTER 5

PENETRATION MECHANICS BACKGROUND AND MATHEMATICAL MODELLING

Introduction

Extensive research exists on penetration problems by many distinguished researchers to develop fundamental relationships applied to areas such as hypervelocity impact, shaped-charge penetration, long-rod penetration, small arms, ballistic protection, and armor design.

The fundamental understanding of penetration mechanics is as follows. Given a projectile, a target, and details of the initial geometry, kinematics, and materials properties; investigate whether or not target perforation occurs. If perforated, investigate what the residual characteristics of projectile and target will be, and if not, investigate the depth of penetration.

In this chapter, there is a discussion of analytical, numerical, and experimental approaches to penetration and perforation problems by scientists and researchers. Particular emphasis is on experimental and analytical modeling of projectile impact into plywood.

Background

Penetration mechanics is one of the most difficult problems in the research field of mechanics and researchers have been working on the solutions many years. Solution approaches exist on three different levels as follows [70]:

1. Data correlation
2. Engineering models
3. Numerical simulation

Data correlation

Data correlations rely on extensive testing with large sample sizes. When good correlations exist, they are extremely useful for interpolation to predict other dissimilar cases. Using this approach many researchers conducted very interesting studies related to penetration problems. In a review article by Wright [23] the following formula calculates the unknown limit velocity; V_L - Limit velocity is the minimum striking velocity for penetration.

$$\frac{\rho_p V_L L}{E_t T \sec\theta} = f(T\sec\theta / D, E_p / E_t, L/D....) \tag{5}$$

In Eqn. (5), L is the length and D is the diameter of the penetrator. T is the thickness of the target when the angle between the line of flight and target normal is θ. Subscripts *p* and *t* stand for penetrator and target, ρ is density and E is a characteristic stress or energy per unit volume. The left hand side of Eqn. (5) represents the ratio of available kinetic energy per unit cross sectional area of penetrator to the energy that can be absorbed per unit area of target. The non-dimensional terms in Eqn. (5) such as density and energy characteristics are an attempt to account for the material properties of penetrator and target. In some cases other material properties, such as fracture toughness, material hardness, etc. are included in the dimensional analysis to make the model more complete [23].

Engineering Models,

The development of engineering models relies on approaches similar to those used successfully in strength of materials and hydraulics. The goal of an engineering model is to drive a simple mathematical equation at the same time adequately representing the physics of the problem in question.

Numerical Simulation

Numerical simulations may, in general, include all the relevant physics. However, other difficulties arise, such as the development of efficient algorithms for highly distorted materials, and the accurate representation of material behavior.

The following section addresses some of the important studies that exist from scientists and researchers in penetration mechanics.

Previous research on Penetration Mechanics

In 1988, many research studies occurred resulting in reasonably accurate simulations of penetration problems [71, 72, 73, 74, and 75]. Zukas and Anderson reviewed the state of the art of numerical simulations which describes the impact and penetration mechanics plus provided a comprehensive review [76]. They discussed the general capabilities and limitations of numerical simulations. They clearly stated that as the size and speed of computers have increased during that time; therefore, so has the complexity of codes used for these purposes, but certain characteristic difficulties persist [70].

Vadim et al. investigated three-dimensional solutions of perforation and damage of multilayered and multi-sheet bumpers under high- and hypervelocity impact of single particles, and performed numerical investigations of rod particle's orientation influence on penetration effect. [77]

Rozenberg and Dekel studied the process of long-rod penetration into thick metallic targets through a series of two-dimensional simulations. The goal of the research was to uncover the inherent material similarities in this process. In particular, the search was for non-dimensional parameters accounting for the depth of penetration, such as the density ratio, and the relative strengths of penetrator and target. They reported that the research results match existing empirical data, shedding

more light on the penetration process and emphasizing the difficulties in achieving an overall normalization procedure for the process [78].

Forsell et al. investigated the identification of failure properties of ventricular tissue from experimental data of deep penetration with cylindrical punches, which is of particular clinical and industrial interest to understand the mechanisms of perforation of pacemaker electrodes [79]. Other researchers conducted similar studies. [80, 81, and 82]

Chen [21] investigated numerical simulations of the penetration processes in aluminum blocks by spherical-nose steel rods. The investigation included 152-mm diameter 6061-T651 aluminum bars impacted by spherical-nose projectiles machined from T-200 mar aging steel rods at nominal impact velocities between 300 and 1000 m/s. The transient dynamic finite element code LS-DYNA 2D provided the numerical analysis. A comparison of the calculated results to the experimental data indicated good correlation.

Kovtunenko presented a numerical simulation of some plane Lamé problems with a rectilinear crack under non-penetration conditions. He formulated that the non-linear crack problem is a variation of inequality. He calculated the approximate solution using penalty iteration and the finite-element method. [83]

Huang et al., have investigated the RHT concrete strength model and failure using numerical simulations of composite projectile penetrating concrete targets. Their results showed that RHT parameters, specifically the failure parameters, greatly influence the penetration depth and exit velocity. Comparisons between numerical analysis and experimental results were also discussed [84].

Godwin and Chapyak investigated the apparent enhancement of target strength in the steady-state. They used the Tate model together with the Birkhoff jet model in their study. By explicitly including strength terms in both Bernoulli's Law and Newton's Second Law, they derived a more general strength multiplier. This multiplier was a function of the penetrator velocity as well as the density and strength of both the penetrator and target [22].

Walters et al. derived the velocities, lengths and penetrations as an explicit function of time by employing a perturbation solution of the nondimensional Alekseevski–Tate equations. They obtained a third-order perturbation solution which includes both penetrator and target strength terms. They compared the exact solution to the perturbation solutions, illustrated a typical comparison between the exact and approximate solutions for a tungsten rod impacting a semi-infinite steel armor target. They further showed that the perturbation solution is accurate for the perforation of finite thickness (short penetration time) targets. [85]

Forrestal and Hanckhak conducted depth-of-penetration experiments with ogive-nose steel projectiles and limestone targets to determine the penetration limit velocity. [86]

Although, the penetration equations that describe the behavior of an eroding long rod while penetrating at a high velocity were developed by Alekseevski [87] and Tate [88] in the mid 1960s, solution methods to improve the resulting accuracy is still a challenging research interest.

Luttwak et al. investigated oblique impact and penetration of long rods both experimentally and numerically. In the experiments, a long copper rod obliquely impacted an aluminum plate at a velocity of 850 m/sec. They carried out the numerical simulations in the multi-material Euler-with-strength processor of the three dimensional code MSC/DYTRAN. This revealed a good agreement between the computations and the experimental results, as to the shape of the projectile and target during the penetration process [89].

Bassette and Littlefield [90] analyzed the loading history for the hypervelocity impact of a long-rod striking a moving flat plate at an oblique angle using the EPIC code. They assessed the effect of an EPIC input parameter (the erosion strain) for the numerical treatment of eroding interfaces with specific attention focused on the predictions of peak loads, mass loss, and final configuration of the rod.

Nesterenko et al. investigated the results of penetration test with tungsten (93%) heavy alloy penetrators of solid and porous composite samples of Ti-6Al-4V alloy with different microstructures (Widmanstatten pattern and equiaxed). Composite materials with alumina rods and tubes filled with B4C powders demonstrated a new feature of penetration: projectile deflection with a self sealing of the hole and forced shear localization caused by tubes fracture. They reported that the results demonstrated the applicability of HIPing for Ti-based armor materials [91].

Malaise et al. investigated new ballistic experiments (encapsulated rod experiments) enabling a pressurization of the front face of the ceramic block (dynamic confinement) and compared these to results obtained from standard unconfined configurations (DOP tests). They proposed a modeling approach based on a description of the fragmentation process of the ceramic. They have reported that comparisons between Eulerian computation and the experiments show that conditions for rod dwell link to immobilizing fragments of ceramic in front of the projectile [92].

Daneshjou et al. investigated the penetration depth of long-rod electromagnetic projectiles on semi-infinite targets with a numerical approach. They reported that the results obtained from this study are comparable with recent studies. The theoretical models used in the analysis of long-rod penetration on semi-infinite targets were Tate, Grace, and Vahedi models [93].

Huang et al. studied a series of depth-of-penetration (DOF) tests to investigate the ballistic performance of armor ceramics. Based on the experimental results, this study presented an improved differential efficiency factor (DEF). They showed that the density, internal friction, and compression strength of ceramics are crucial factors that affect the ballistic performance of ceramics significantly through the interaction between the long-rod projectiles and thick-tile armor [94].

Rolc et al., [95], studied the interaction of the flying plate with the long-rod penetrator both experimentally and numerically using the LS DYNA 3D finite element code. Detailed investigations exist on the influence of the plate velocity and plate material on this interaction. They reported that numerical results showed relatively

large damage to the projectiles. The numerical simulation of the damaged projectiles with some targets also exists.

Wlodarczyk and M. Magier investigated a problem of the dynamics of long-rod penetrators loaded with gunpowder combustion products. They solved the problem, in closed form, by using the wave method (d'Alambert). The derivation of the analytic recurrence formulae defines the fields of longitudinal stress and particle velocity in the rod penetrator [96].

For more than a century, scientists and researchers have investigated the subject of long rod penetrators into targets. [97, 98, 99, 100, 101, 102, 103, 104, 105].

The main focus of this chapter is to develop equations which predict the dynamic response of walls (brick, plywood, concrete, etc) when impacted by tornado missiles such as 2x4 wood timbers. The development of the included equations is on the previous researchers' work sited above. To derive the equations in this study, there is the assumption that the impacts result in rigid body penetration and plastic failure.

Derivation of Penetration Equations

Of particular interest is a study from the Army Ballistics Laboratory undertaken to predict the effects of explosive derivative shrapnel on the human body. This is of interest because the material used to simulate the human body is plywood. Though there are some significant differences between this scenario and the impact of tornado debris on residential walls, it proved to be a good starting point. W. Bruchey and Amy Tank authored this report [106 and 107], but for the sake of brevity, hereafter, I will refer to these as the Bruchey equations.

Like many preceding researchers, Bruchey began with the penetration equations shown below as equations (6-9) as derived by Alekseevski [87] and Tate [88].

$$\frac{1}{2}\rho_p (v-u)^2 + Y_p = \frac{1}{2}\rho_t u^2 + R_t \Rightarrow \quad \text{Interface stress balance} \tag{6}$$

$$\frac{dV}{dt} = -\frac{Y_p}{l\rho_p} \Rightarrow \text{Rod deceleration} \tag{7}$$

$$\frac{dl}{dt} = U - V \Rightarrow \text{Erosion kinematics} \tag{8}$$

$$U = \frac{dP}{dt} \Rightarrow \text{Penetration definition} \tag{9}$$

where

V : Penetrator velocity

U : Penetration velocity

P : Penetration depth

l : Penetrator length

t : Time after impact

R_t : Target strength

Y_p : Penetrator strength

ρ_p : Penetrator density

ρ_t : Target density

Since Bruchey's projectiles were steel, aluminum, and granite cubes, the resulting penetration was of a rigid body characterization (the length of the projectile remains constant); therefore.

$\frac{dl}{dt} = 0$, then

$$U = V \tag{10}$$

Though his actual derivation is absent from the report, his presented differential form of the penetration equation is

$$-mv(\frac{dv}{dx}) = \frac{1}{2} rbAV^2 + sA \tag{11}$$

where

$r = \rho = 0.35 \frac{g}{cm^3}$ the density of the target.

$s =$ strength of plywood in $\frac{dynes}{cm^2}$

$A =$ average presented area of fragment (cube) in cm^2

$v = V_0 =$ striking velocity in $\frac{cm}{\sec}$

$m =$ mass of the projectile in g

$X = x =$ plywood depth of penetration in cm

$a = \alpha = \frac{A}{m}$

$g = \gamma = \frac{r}{2}$

$b = \beta =$ a shape factor

Upon integrating equation (11), Bruchey's equation for penetration depth is

$$X = \frac{-1}{2} \times \frac{\ln(\sigma) - \ln(V_0^2 \bullet \gamma \bullet \beta + \sigma)}{\alpha \bullet \gamma \bullet \beta} \tag{12}$$

The differences between the equations used in this study and Dr. Bruchey's concerns that of universal application. Bruchey's equations are valid exclusively for predicting the characteristics of the impacts of small cubes of dense materials (steel, aluminum, and granite) into various thickness of plywood. His equations require the development of two terms, explained momentarily. The equations described herein

are more applicable to a variety of applications, including composite walls systems) which will be illustrated later.

The characteristic that forces Bruchey's equations to have limited utility is the determination of his strength term. First, the derivation of this term is absent, except to say that it is based on testing results. The strength term, though not specifically related to plywood, has a basis on some reaction between the projectile material and the target material. At any rate, no explanation exists; therefore, is not applicable for other circumstances.

In contrast, this thesis utilizes the "published" tensile strength value for the strength term in all of the equations. This seems appropriate after studying the Alekseevski-Tate paper, and its use proved most valuable. This allows for the consideration of a variety of target materials without the requirement for extensive testing.

Additionally, Bruchey has included a term that he refers to as a shape factor, beta. Again, this term derives from testing and neither its derivation nor explicit definition is included in the presentation.

The above paragraphs do not suggest that Bruchey's equations are incorrect. On the contrary, they prove most efficient for predicting the results of the testing that he explains. There are differences between the Bruchey circumstance and the objective of this dissertation. In the Bruchey situation, the projectiles have a density from 7 ½ to 21 times the densities of the target. In the case of 2 x 4 timber impacting plywood (or even brick), the densities are more equal. It was previously mentioned that the "cube" projectiles "tumbled, while the 2 x 4 projectiles always strike perpendicular to the target (this would represent the worse case in the real world), resulting in the same "presented" area each time. Furthermore, the velocities of the projectiles in the Bruchey tests ranged from 335 mph to 2237 mph. The maximum projectile velocity expected in a tornado impact is 100 mph. The use of his equations is simply limited, especially in terms of composite wall systems. There is no

methodology to combine different materials and predict the results from Bruchey's equations.

Bruchey's next step was to solve equation (12) for V_0 to determine the limit velocity. The resulting limit velocity equation becomes

$$V_0 = \frac{1}{e^{(-2)x\alpha\gamma\beta} \bullet \gamma\beta}\left[(-e^{(-2)x\alpha\gamma\beta})\gamma\beta\sigma(e^{(-2)x\alpha\gamma\beta} - 1)\right]^{\frac{1}{2}} \tag{13}$$

The development of the equations for this thesis also begins with equations (6-9) as the foundational equations. As in the Bruchey example, the impact assumption is rigid; therefore, the length of the penetrator is constant and equation (10) is valid. From this point on, the derivations and associated applications are exclusive to this thesis.

For the remainder of this study the following applies. As in equation (6), the symbol used for the strength of the plywood is R_T. This parameter is no longer an unknown that must be determined through testing, but will represent the actual "published" tensile strengths of the target materials. Furthermore, since the velocities are relatively low and the trajectories do not vary, the shape factor β is not required.

For the application considering the impact of 2 x 4 projectiles against various wall surfaces, the following derivations are developed.

Using Eqn (7) and (10), Eqn (6) becomes

$$-\frac{dV}{dt} l\rho = \frac{1}{2}\rho_t V^2 + R_T \tag{14}$$

Using eqn (10), Eqn (9) becomes

$$V = \frac{dP}{dt} \Rightarrow dt = \frac{1}{V} dP \tag{15}$$

Substituting Eqn (15) into Eqn (14) yields

$$-V\frac{dV}{dP}l\rho_p = \frac{1}{2}\rho_T V^2 + R_T \tag{16}$$

Multiplying both sides of Eqn (16) by the penetrator average cross-sectional area, A, yields

$$-V\frac{dV}{dP}l\rho_p A = \frac{1}{2}\rho_T A V^2 + R_T A \tag{17}$$

Since $l\rho_p A = m$ is the mass of the penetrator, Eqn (17) becomes

$$-mV\frac{dV}{dP} = \frac{1}{2}\rho_T A V^2 + R_T A \tag{18}$$

Dividing Eqn (18) by m, we obtain

$$-V\frac{dV}{dP} = V^2\gamma\alpha + \alpha R_T \tag{19}$$

where

$$\alpha = \frac{A}{m} \tag{20}$$

$$\gamma = \frac{1}{2}\rho_T \tag{21}$$

By rearranging Eqn (19), the basic integration equation results

$$-\int \frac{V}{\gamma V^2 + R_T} dV = \int \alpha \, dP \tag{22}$$

Derivation of Penetration Depth, P

Using Eqn (22) achieves the penetration depth when the striking velocity V_0 becomes zero. Thus, with proper integral limits, Eqn (22) becomes

$$-\int_{V_0}^{0} \frac{V}{\gamma V^2 + R_T} dV = \int_{0}^{P} \alpha \, dP \tag{23}$$

Integrating Eqn (23) yields

$$\frac{-\ln R_T}{2\beta\gamma} + \frac{\ln(V_0^2\gamma + R_T)}{2} = P\alpha \tag{24}$$

From Eqn (24), the penetration depth is derived which is almost identical to the Bruchey depth of penetration equation (12) offering further validation of this derivation process. The only difference is the absence of the β term and the utilization of actual tensile strength properties.

$$P = -\frac{1}{2} \times \frac{\ln R_T - \ln(V_0^2\gamma + R_T)}{\alpha\gamma} \tag{25}$$

Derivation of Residual Velocity, V_r

Knowing the striking velocity, the remaining velocity (residual velocity) exists after the penetrator passes through the thickness of the target. Changing the integral limits of Eqn (23) accordingly gives

$$-\int_{V_0}^{V_r} \frac{V}{\gamma V^2 + R_T} dV = \int_0^w \alpha dP \tag{26}$$

Where w indicates the target thickness. Integrating Eqn (26) yields

$$-\frac{\ln(V_r^2\gamma + R_T)}{2\gamma} + \frac{\ln(V_0^2\gamma + R_T)}{2\gamma} = w\alpha \tag{27}$$

Rearranging Eqn (27) gives

$$\ln(V_r^2\gamma + R_T) - \ln(V_0^2\gamma + R_T) = -2\alpha\gamma w \tag{28}$$

or

$$\ln\left(\frac{V_r^2\gamma + R_T}{V_0^2\gamma + R_T}\right) = -2\alpha\gamma w \tag{29}$$

Considering "ln" terms on both sides of Eqn (29) yields

$$\frac{V_r^2\gamma + R_T}{V_0^2\gamma + R_T} = e^{-2\alpha\gamma w} \Rightarrow V_r^2\gamma + R_T = (V_0^2\gamma + R_T)e^{-2\alpha\gamma w} \tag{30}$$

then

$$V_r^2 = \frac{1}{\gamma}[(V_0^2\gamma + R_T)e^{-2\alpha\gamma w} - R_T] \tag{31}$$

Taking the square root of Eqn (31) yields

$$V_r = \sqrt{\frac{1}{\gamma}[(V_0^2\gamma + R_T)e^{-2\alpha\gamma w} R_T]} \tag{32}$$

Using Eqn's (20), (21) and (32), we have

$$V_r = \sqrt{\frac{1}{\frac{1}{2}\rho_T}[(V_0^2\,\frac{1}{2}\rho_T + R_T)e^{-2\frac{A}{m}\frac{1}{2}\rho_T w} - R_T]} \tag{33}$$

or

$$V_r = \sqrt{\frac{2}{\rho_T}[(\frac{1}{2}\rho_T V_0^2 + R_T)e^{\frac{-A\rho_T w}{m}} - R_T]} \tag{34}$$

Rearranging Eqn (34) gives

$$V_r = \sqrt{[(V_0^2 + \frac{2R_T}{\rho_T})e^{\frac{-A\rho_T w}{m}} - \frac{2R_T}{\rho_T}]} \tag{35}$$

Finally, residual velocity is

$$V_r = \sqrt{[(V_0^2 e^{\frac{-A\rho_T w}{m}} - \frac{2R_T}{\rho_T}(1 - e^{\frac{-A\rho_T w}{m}})]} \tag{36}$$

Derivation of Limit Velocity, V_L

Limit velocity, as before, is the minimum velocity level for penetration to embed the projectile in the target. In other words, when the penetrator passes through the thickness of the target, remaining velocity becomes zero. For striking velocities smaller than the penetration limit velocity, the projectile rebounds from the target. The limit velocity derivation comes from Eqn (23) by changing the integral limits to

$$-\int_{V_L}^{0} \frac{V}{\gamma V^2 + R_T} dV = \int_0^w \alpha \, dP \tag{37}$$

Where w is the thickness of the target.

Integrating Eqn (37) gives

$$\frac{-\ln R_T}{2\gamma} + \frac{\ln(V_L^2 \gamma + R_T)}{2\gamma} = w\alpha \tag{38}$$

or

$$\ln(\frac{V_L^2 \gamma + R_T}{2\gamma}) = 2\alpha\gamma w \tag{39}$$

Considering “ln” transformation gives

$$V_L^2 \gamma + R_T = R_T e^{2\alpha\gamma w} \tag{40}$$

Finally, the limit velocity equation becomes

$$V_L = \sqrt{\frac{R_T}{\gamma}(e^{2\alpha\gamma w} - 1)} \tag{41}$$

To add a composite wall capability, modify Eqn (41) to

$$V_L = \sqrt{\frac{R_T}{\gamma}(e^{2\alpha\gamma_{eq} w_{eq}} - 1)} \tag{42}$$

Where

$$w_{eq} = w_{primary} + \int_{i=2}^{n} w_i \frac{\rho_i}{\rho_{primary}} \tag{43}$$

and

$$\gamma_{eq} = \frac{1}{2}(\rho_{primary} + \int_{i=2}^{n} w_i \frac{\rho_i}{\rho_{primary}}) \tag{44}$$

or

$$V_L = \sqrt{\frac{R_T}{\gamma}(e^{2\alpha[\frac{1}{2}(\rho_{primary} + \int_{i=2}^{n} w_i \frac{\rho_i}{\rho_{primary}})]\times[w_{primary} + \int_{i=2}^{n} w_i \frac{\rho_i}{\rho_{primary}}]} - 1)} \tag{45}$$

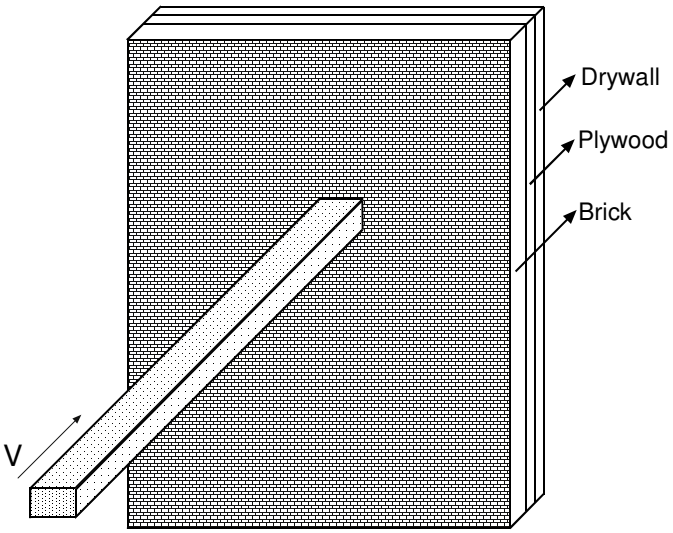

Figure 57: Composite wall consist of brick, plywood and drywall.

Eqn's (43) and (44) provide equivalent thickness and the equivalent density of the composite wall. In other words, the thickness and the density of the composite wall develop in terms of the assumed primary material of the wall. As shown in Figure 57, if the brick is the primary material of the composite wall, equivalent thickness and the density is:

$$w_{eq} = w_{brick} + w_{plywood}\frac{\rho_{plywood}}{\rho_{brick}} + w_{drywall}\frac{\rho_{drywall}}{\rho_{brick}} \tag{45}$$

$$\gamma_{eq} = \frac{1}{2}(\rho_{brick} + w_{plywood}\frac{\rho_{plywood}}{\rho_{brick}} + w_{drywall}\frac{\rho_{drywall}}{\rho_{brick}}) \tag{46}$$

By adapting the foundational penetration equations, it is possible to construct empirical equations to predict the behavior of wall systems when impacted by tornado debris. Alekseevski and Tate modified the Bernoulli equation to produce more usable penetration equations, Bruchey modified the Alekseevski-Tate equations to provide

for a specific condition, and this study took the next step in developing equations useful for tornado debris impact.

The following figures illustrate comparisons between the Bruchey equations, debris testing at Texas Tech, and the use of the equations developed for this dissertation. Chapter 6 goes into greater detail regarding the specifics of the testing and the explanations of the comparisons; however, in order to demonstrate the ineffectiveness of the Bruchey equations to circumstances described herein, they are included here.

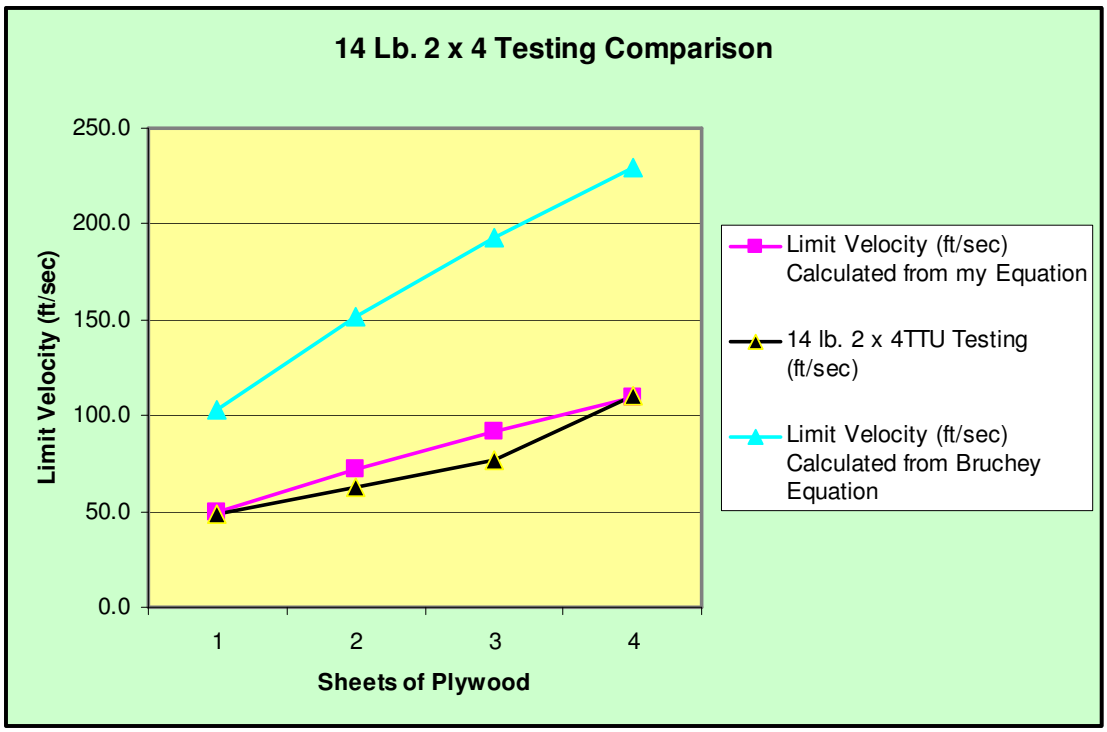

Figure 50: Comparison of Bruchey equations, TTU testing, and equations from this study for a 14 lb. projectile

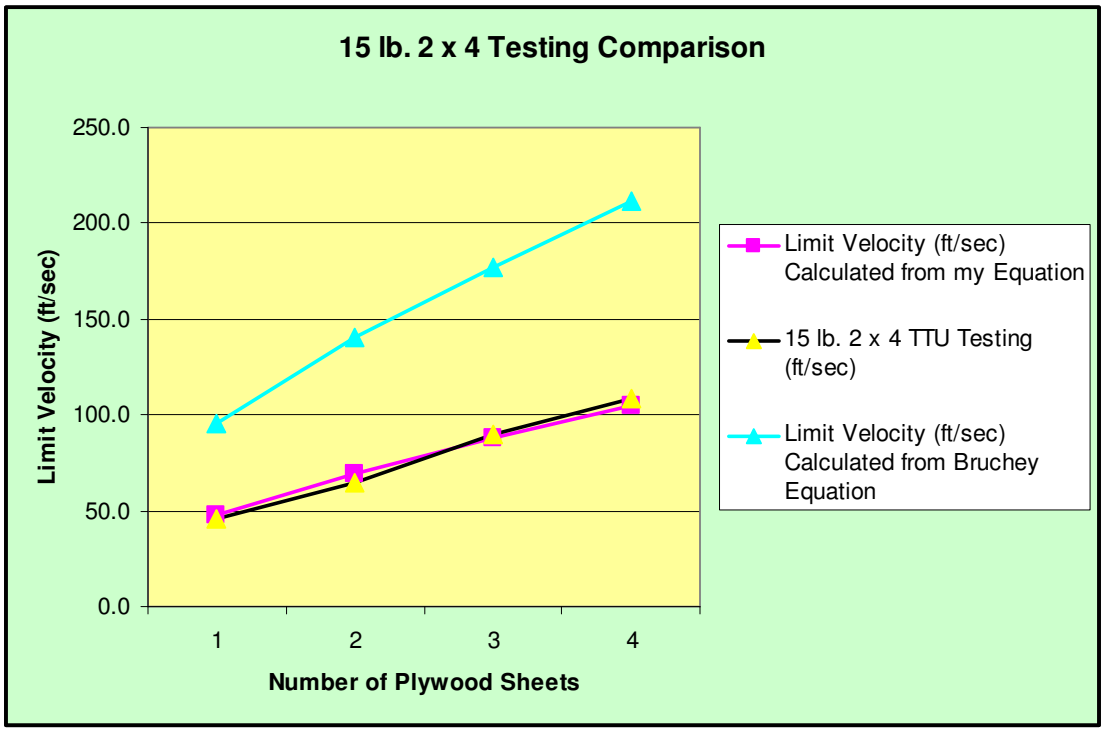

Figure 51: Comparison of Bruchey equations, TTU testing, and equations from this study for a 15 lb. projectile

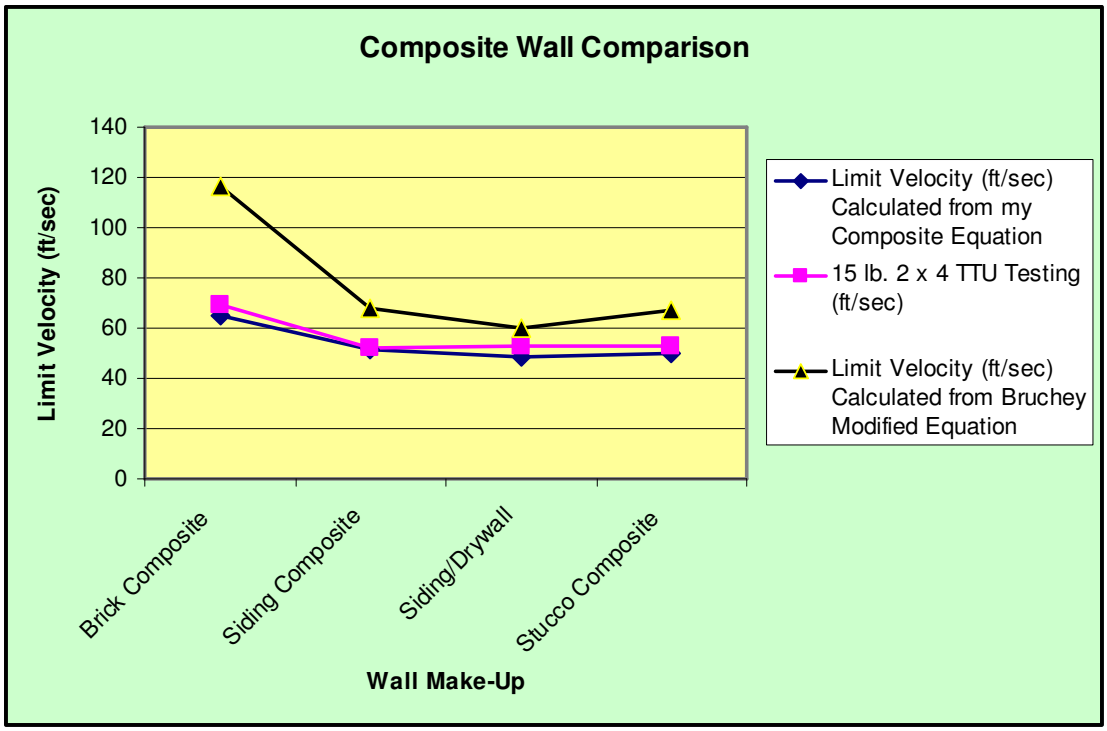

Figure 52: Comparison of Bruchey equations, TTU testing, and equations for this study of various composite wall systems

As these comparisons clearly demonstrate, the Bruchey equations do not correlate with the actual test results. Furthermore, the figures illustrate the excellent matching of the Texas Tech testing and the equations developed for this thesis. Again, Chapter 6 contains the details of the testing and the utilization of the included equations.

CHAPTER 6

TORNADO IMPACT MITIGATION TECHNIQUES

Introduction

As this study has illustrated, the two primary failure mechanisms involved when tornado force winds interact with residences are structural failure and debris impact. Structural failure occurs when the wind pressures exceed the load carrying capability of the home itself in which case the roof, walls, or both collapses. During initial construction, increasing resistance to wind forces is relatively inexpensive. Various products are available to help secure the baseplates to the foundation, the studs to the baseplates, the top plates to the studs, and the rafters and joists to the top plates. Simpson-Strongtie has a very good product line offering superior protection from high winds, mostly marketed for new construction. [109] Unfortunately, retrofitting these into an existing home would require considerable demolition; therefore, the costs would be very high.

Another dilemma associated with expending effort and money to prevent structural damage is the fact that within the tornado's strong windfield there will likely be a substantial debris cloud. Especially in urban areas, the tornado will have accumulated debris from structures damaged downrange. Unless, the entire community has exercised diligence in building their homes resistant to high winds, the associated debris can cause extensive damage and casualties. [55] Furthermore, debris impact is often the primary cause of structural failure. If a substantial debris artifact strikes a home and the structural envelope fails, wind pressures can drastically increase inside the home and result in catastrophic failure.

In order to protect life, this study is concentrated on in-home protection from debris and associated failure mechanisms. A safe room inside a home will not specifically minimize damage to the home, but it will provide a level of protection to

the occupants. A safe room is not dependant on the quality of construction of the neighboring buildings, and this option is adaptable into an existing home without the expensive of hardening the home envelope.

Determination of Baseline Projectile Impact Velocities

In order to determine the projectile speeds in defining the construction of the safe room, it is necessary to review a document from the Federal Emergency Management Agency. FEMA 361 has defined the design wind speeds and associated projectile speeds for vertical (walls) and horizontal (ceiling) surfaces of a safe room. Table 4 includes these values. In the same reference there is a graphic depicting the expected maximum wind speeds for locations within the United States. Figure 51 illustrates these areas of risk. [110]

Table 4: Derived Impact Velocities

Safe Room Design Wind Speed	Missile Speed (15 lb. 2 x 4) and Safe Room Impact Surfaces
250 mph	Vertical Surfaces (Walls): 100 mph Horizontal Surfaces (Ceilings): 67 mph
200 mph	Vertical Surfaces (Walls): 90 mph Horizontal Surfaces (Ceilings): 60 mph
160 mph	Vertical Surfaces (Walls): 84 mph Horizontal Surfaces (Ceilings): 56 mph
130 mph	Vertical Surfaces (Walls): 80 mph Horizontal Surfaces (Ceilings): 53 mph

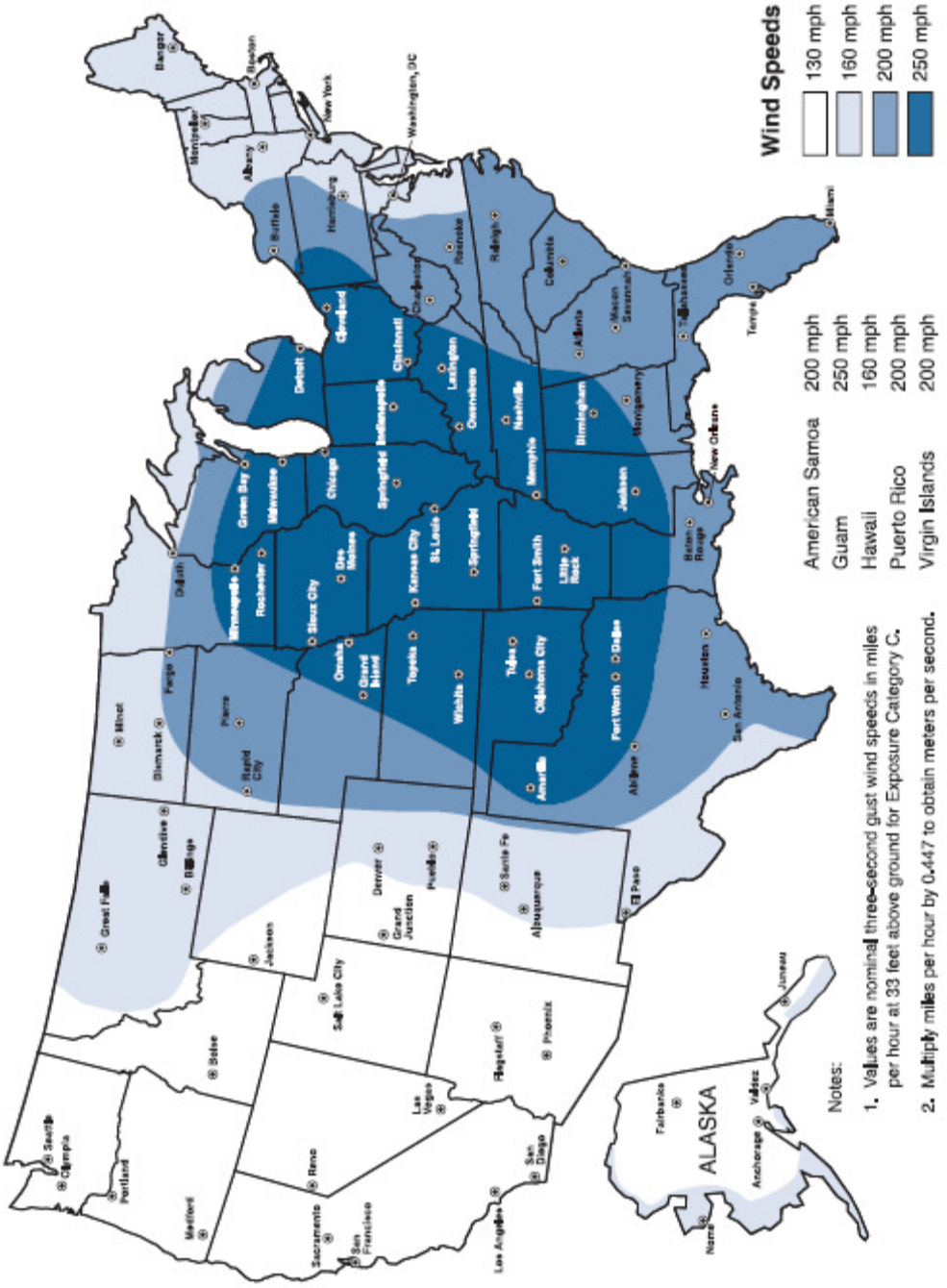

Figure 53: Wind Velocity Distribution Across the United States
[110]

Since the safe room, design will reflect the categories listed in the Enhanced Fujita damage intensity scale, Table 5 defines these categories.

Table 5: Enhanced Fujita Wind Categories
[110]

Enhanced Fujita Scale Categories	3-Second Gust Wind Speed (mph)
EF0	65-85
EF1	86-110
EF2	111-135
EF3	136-165
EF4	166-200
EF5	>200

In Table 4, the projectile impact speeds are different from the preceding designed wind speeds. The expectation is that the speed of the debris will not reach the full velocity of the highest design wind speeds, partially due to the projectile estimated short fight time before impact occurs. Furthermore, the FEMA chart does not include winds below 130 mph.

In comparing the wind speed categories in Table 4 with the maximum 3-second gust wind speed in the Fujita scale, the wind speeds do not exactly correlate. For example, the FEMA Table notes a safe room design wind speed of 160 mph, while the EF Scale category closest to this value corresponds closely to an EF3 upper limit of 165 mph. For the purpose of this study, EF wind predictions per Table 5 constitute the limits of consideration. This requires some modifications to the expected debris travel velocities. The first two rows in Table 4 correlate with the EF4 and EF5 wind scales in Table 5; therefore, these missile speeds remain unchanged. Table 4 rows 3 and 4 differ slightly from the Fujita predictions; therefore, the missile speed adjustment is necessary. In Table 4, row 3, the safe room design windspeed is 160 mph with a corresponding missile speed listed as 84 mph. This ratio represents a reduction of 52.5%. Since this study uses the Fujita speeds as the baseline, the 165 mph windspeed shown in Table 5 reduced equally by 52.5% gives a missile speed of 87 mph. In Table 4, row 4, the safe room design windspeed is 130 mph and the missile speed is 80 mph. This ratio represents a reduction of 61.5%. As before, the 135 mph windspeed shown in Table 5 translated to a 61.5% reduction to give a missile

speed of 83 mph. In addition, projectile speeds associated with safe room design speeds of less than 130 mph required estimation. This allowed a direct comparison between each category of EF damage intensity scale versus safe room design criteria.

The EF0 and EF1 categories are absent from the FEMA chart because at these lower wind speeds the damage from debris is expected to be minimal. To offer a comprehensive evaluation of all EF categories, these projectile velocities are included in this exercise. Since the percentage of safe room design windspeed to projectile windspeeds show an increasing trend as the windspeeds under consideration decreases, it was estimated that for the maximum EF1 and EF0 expected windspeeds of 110 mph and 85 mph respectively, a percentage of 70% and 80% produced a conservative estimate. This resulted in projectile speeds for the EF1 and the EF0 to be 77 mph and 68 mph respectively.

One final calculation was necessary to define the projectile characteristics of an internal safe room. FEMA estimated (as shown in Table 4), a value for expected projectile speeds for debris, which affects the top of the safe room. Since most debris striking the ceilings of safe rooms result from falling debris rather than blowing debris, the estimated impact velocities are lower than those expected to strike the vertical surfaces. Across the range of categories, these vertical debris speeds are 66% of the horizontal expected projectile speeds.

Table 6 illustrates the final values used in this research for safe room projectile velocities.

Table 6: Design Velocities for this Study
[110]

Enhanced Fujita Category	Max Expected Windspeeds (mph)	Designed Projectile Windspeeds for Walls (mph)	Designed Projectile Windspeeds for Ceilings (mph)
EF0	85	68	45
EF1	110	77	51
EF2	135	83	55
EF3	165	87	58
EF4	200	90	60
EF5	>200	100	67

For all of the following calculations, the material properties of the various materials are from the following sources [111, 112, 113, 114, and 115]

As mentioned in the previous chapter, many studies exist regarding impact dynamics, some with various projectiles of various configurations. [116, 117] The 2 x 4 projectiles in this research are blunt-nosed, without any point on the end of the wood; however, is beyond the scope of this discussion.

Depth of Penetration Calculations

The first use of the equations from Chapter 5 determines the depth of penetration into plywood of a 15 lb. 2 x 4 traveling at the speeds developed in the last section. This data defines the thickness of plywood required to prevent projectiles from penetrating the wall sections (45, 51, 55, 58, 60, 67 for ceilings; 68, 77, 83, 87, 90, 100 for walls). Using (eqn 25):

The following values represent the numbers in this series of calculations.

P = penetration depth in feet

R_T = tensile strength of plywood target = 1500 lb/in^2 [2.16 (10)^5 lb/ft^2]

Note: since plywood by its nature has varying characteristics depending on the specific sample used, this parameter exists in the literature as a range

from 1500 – 4000 lb/in^2 – to guarantee the most conservative approach to storm safety, the lower end of this parameter is used

V = velocity of the projectile in ft/sec

ρ = 26 lb/ft^3

γ = ρ/2 = 13

A = "presented area" = 1.5 in x 3.5 in [.125 ft x .292 ft] = .0365 ft^2

M = w/g = 15/32.2 = .465

α = A/M = .0365/.465 = .078

For 66 ft/sec [45 mph]:

P_{66} = .12 feet [1.4 inches]

For 74.8 ft/sec [51 mph]:

$P_{74.8}$ = .15 feet [1.8 inches]

For 80.6 ft/sec [55 mph]:

$P_{80.6}$ = .17 feet [2.0 inches]

For 85 ft/sec [58 mph]:

P_{85} = .18 feet [2.2 inches]

For 88 ft/sec [60 mph]:

P_{88} = .20 feet [2.3 inches]

For 98.2 ft/sec [67 mph]:

$P_{98.2}$ = .23 feet [2.8 inches]

For 99.7 ft/sec [68 mph]:

$P_{99.7}$ = .24 feet [2.9 inches]

For 112.9 ft/sec [77 mph]:

$P_{112.9}$ = .29 feet [3.5 inches]

For 121.7 ft/sec [83 mph]:

$P_{121.7}$ = .33 feet [3.9 inches]

For 127.5 ft/sec [87 mph]:

$P_{127.5}$ = .35 feet [4.2 inches]

For 131.9 ft/sec [90 mph]:

$P_{131.9}$ = .37 feet [4.4 inches]

For 146.6 ft/sec [100 mph]:

$P_{146.6}$ = .42 feet [5.1 inches]

Figure 54 illustrates these results graphically. As can be seen, the results are almost linear in nature, which is expected.

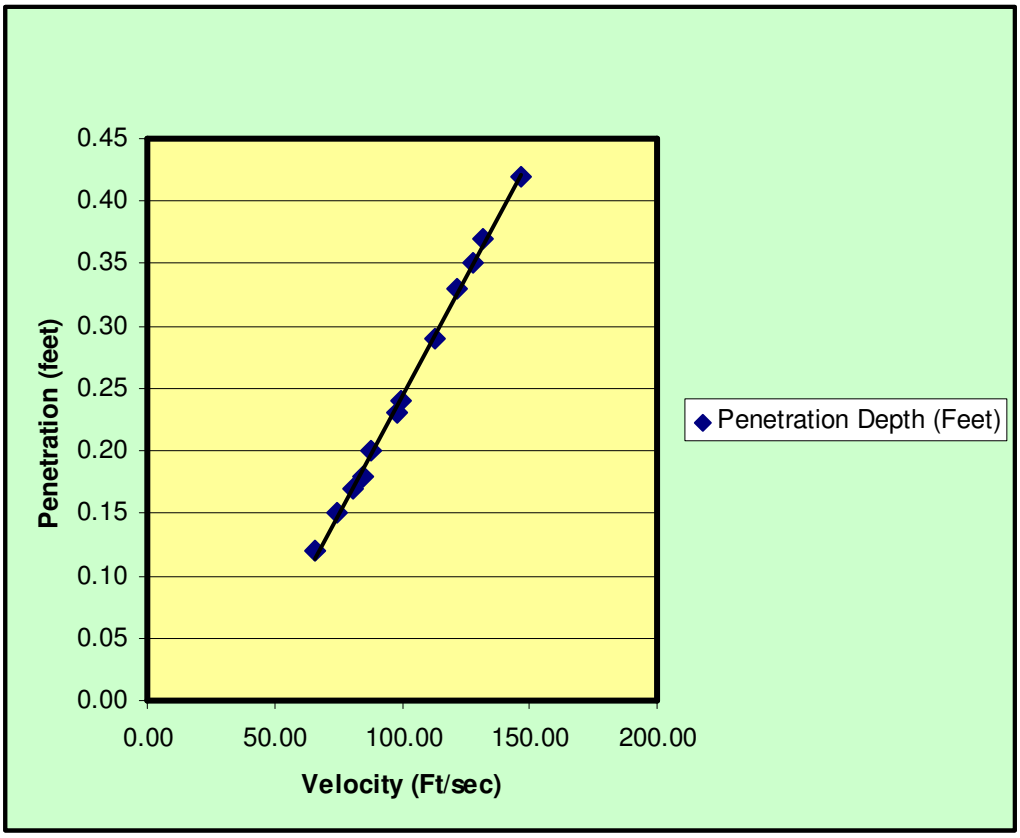

Figure 54: Projectile Penetration Depth

The penetration depth is of particular importance because it allows a determination regarding the thickness of plywood (or number of plywood sheets) required to repel debris impacting at the velocities defined in the previous section. Table 7 describes the number of plywood sheets required with each corresponding EF Scale category.

Table 7: 3/4" Plywood Requirements

Enhanced Fujita Category	Thickness of Plywood Required for Ceiling (inches)	Equivalent Sheets of 3/4" Plywood for Ceiling	Thickness of Plywood Required for Walls (inches)	Equivalent Sheets of 3/4" Plywood for Walls
EF0	1.5	2	2.9	4
EF1	1.8	3	3.6	5
EF2	2.1	3	4.0	5
EF3	2.3	3	4.3	6
EF4	2.4	4	4.5	6
EF5	2.9	4	5.2	7

Figure 55 represents a graphic illustration of the results shown in Table 7.

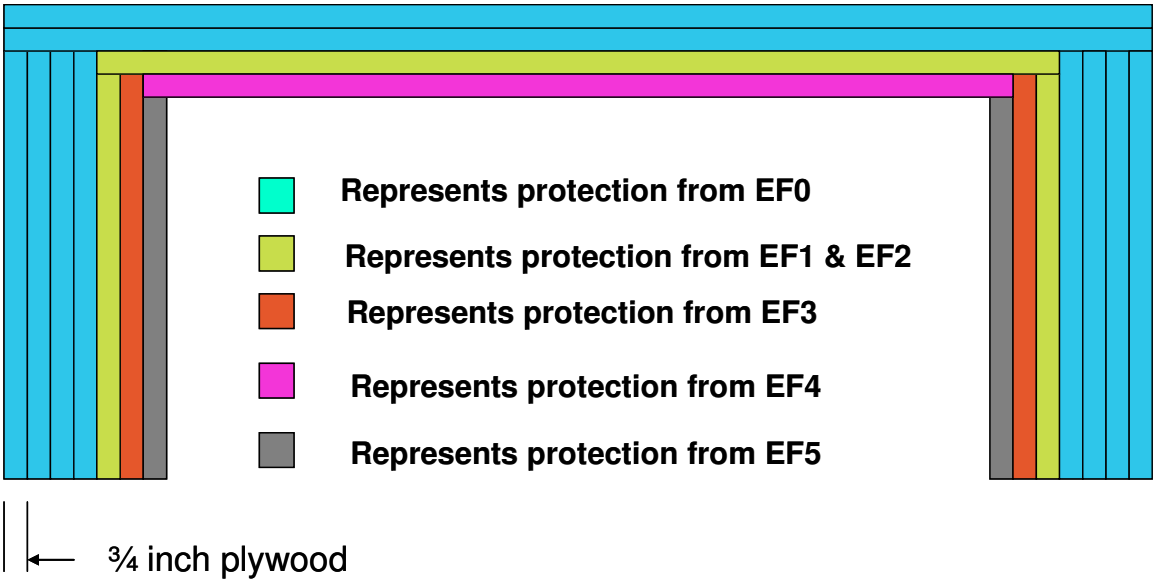

Figure 55: Graphical Presentation of Storm Room Options

Though not particularly included in this thesis, the penetration of concrete by a steel pipe represents an adequate test of validation since data exists regarding this scenario. Due to the dangers associated with a tornado striking a nuclear power facility, the construction techniques of such a structure is critical. In 1978, such a

study occurred. [118] Part of this research included the firing of a 743 lb., 12 inch diameter schedule 40 steel pipe at concrete barriers. Table 8 includes the illustration of this testing, along with the depth of penetration results from the testing and from the penetration depth equation. Figure 56 shows that no correlation exists between the test results and the equation. This suggests that the failure mechanism of steel onto concrete has major differences to 2 x 4 timbers into plywood.

Table 8: Particulars of Concrete Penetration Testing

Test Number	Velocity of Pipe (ft/sec)	Penetration Depth from Testing (inches)	Penetration Depth from Equation (inches)
1	202	7.0	62.0
2	198	6.8	60.3
3	202	6.8	59.9
4	143	5.0	46.0
5	98	4.5	36.9
6	92	3.9	35.1
7	152	5.3	48.5
8	92	3.5	36.0
9	157	4.1	50.1

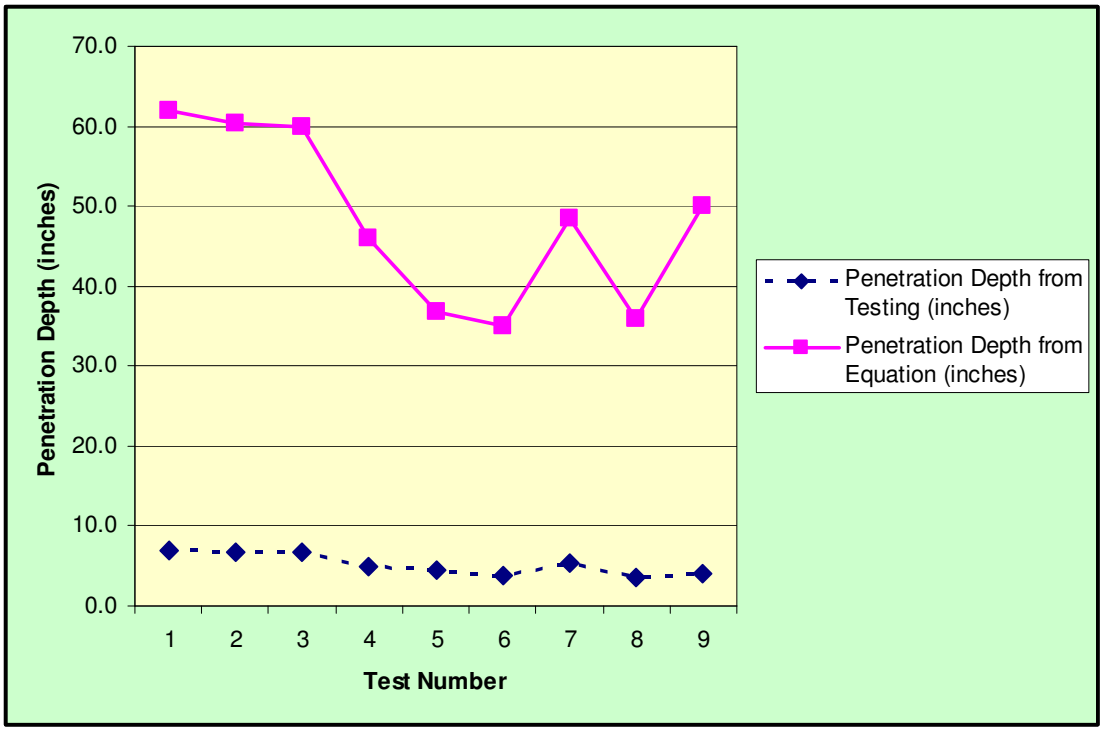

Figure 56: No Correlation Exists Between Testing and Calculations

The conclusions from this comparison illustrate that by deviating from the primary assumptions of this study, results are invalid. For one, the penetration of the steel pipe into concrete does not represent a rigid body penetration. The length of projectile is not constant throughout the penetrating phase; therefore, this violates the premise of a rigid body penetrator. Second, the failure mechanism is not completely plastic, as was the case with 2 x 4 projectiles against plywood. There is a large difference in the densities between steel pipe and concrete; therefore, the failure mechanism is more of a "scabbing" nature, quite different from the penetration of wooden 2 x 4's and plywood targets. By violating the fundamental characteristics of this study and experiencing inferior results, our original guidelines regarding the usefulness of the derived equations prove to be valid.

Limit Velocity Calculations

One of the most important parameters involved in safe room design is the determination of the projectile limit velocity in terms of the proposed wall and ceiling construction. The limit velocity is the velocity that a projectile must attain to penetrate the surface under study. Equation (41) provided the means for calculation of this metric.

Unlike the penetration depth explained in the previous section, the limit velocity is useful for wall systems other than plywood. The importance of penetration depth in plywood provides valuable data in regards to the number of layers required to prevent penetration; however, in composite wall systems, the depth of penetration is less vital than the velocity needed to allow full penetration. The equations repeat until the number of sheets corresponds to a success with a projectile at 100 mph (in this case seven sheets). Debris penetration in a brick or steel substrate is not as important because additional layers of brick or steel are not likely to be an option. In order to achieve penetration protection from projectile speeds up to 146.6 ft/sec, the calculations listed below include up to seven sheets of plywood. The projectile as before is a 15 lb 2x4.

The parameters used for these calculations are:

R_T = 1500 lb/in^2 [2.16 (10)^5 lb/ft^2]

ρ = 26 lb/ft^3

γ = ρ/2 = 13

A = "presented area" = 1.5 in x 3.5 in [.125 ft x .292 ft] = .0365 ft^2

M = w/g = 15/32.2 = .465

α = A/M = .0365/.465 = .078

w = thickness in feet

Note: w is the only parameter that changes between the calculations for limit velocity based on thickness of plywood

For one sheet of ¾" plywood (w = .0625):

V_L = 47.5 ft/sec [32.4 mph]

For two sheets of ¾" plywood (w = .125):

V_L = 69.5 ft/sec [47.4 mph]

For three sheets of ¾" plywood (w = .1875):

V_L = 88.0 ft/sec [60.0 mph]

For four sheets of ¾" plywood (w = .250):

V_L = 105.2 ft/sec [71.7 mph]

For five sheets of ¾" plywood (w = .3125):

V_L = 121.8 ft/sec [83.0 mph]

For six sheets of ¾" plywood (w = .375):

V_L = 138.2 ft/sec [94.2 mph]

For seven sheets of ¾" plywood (w = .4375):

V_L = 154.8 ft/sec [105.5 mph]

Figure 57 illustrates the results of these calculations.

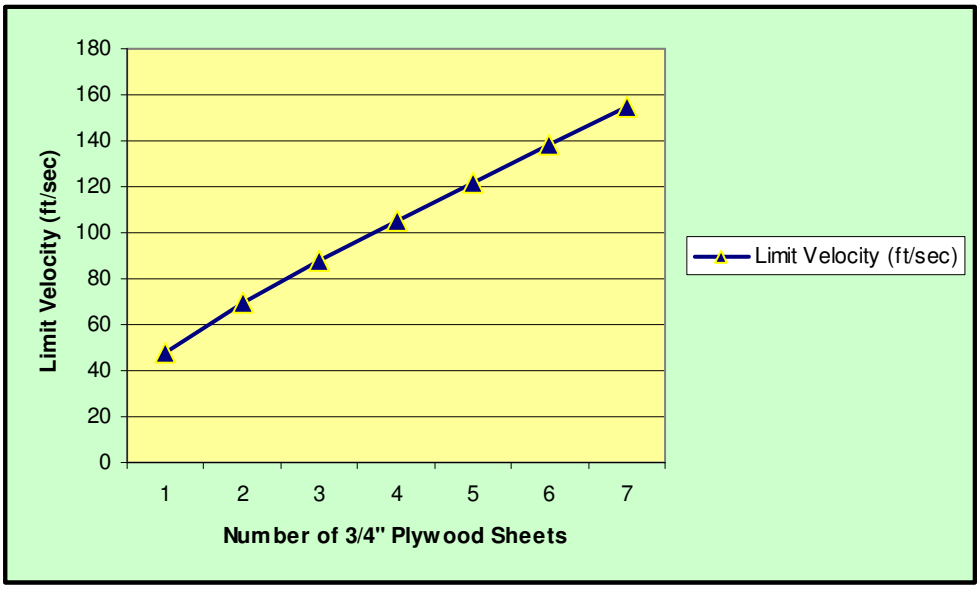

Figure 57 : Limit Velocity (ft/sec) Calculated from Equation

The limit velocity is the only calculated parameter in this study that allows some level of validation by comparing the findings with Texas Tech testing results and by the use of kinetic energy estimation. Since the equation for the limit velocity is a derivative of the equation on penetration depth, the validation of the limit velocity equation correspondingly validates the penetration depth evaluation.

The Texas Tech testing of a 15 lb. 2 x 4 missile against plywood structures comprise some of the testing documented in the university's Debris Impact Testing Report [18]. In this case, the projectile is a 15 lb. 2 x 4, 12 feet long. There could be some discrepancies here because a pine 2 x 4 has a density of 0.450 g/cm^3 (or .016 lb/in^3). This would indicate a weight of 12.069 pounds for a 12-foot long specimen; however, the 15 lb. recorded number comprises this comparison. Furthermore, there was a plastic "sabot" placed on the end of the projectile to facilitate firing pressures, since the shape of the projectile was rectangular and the barrel of the "cannon" was round. The weight of this sabot is not included in the literature. It is likely that this additional mass resulted in the 15 lb. weight. Table 9 lists the results of this testing.

Table 9: Equations Compared to TTU Testing

Number of 3/4" Plywood Sheets	TTU Testing (ft/sec)
1.00	45.5
2.00	64.5
3.00	89.5
4.00	108.5

The results of the comparison are in Figure 58. Due to the limited number of TTU tests, only four data points were available. Still the correlation of the two curves indicates that the calculated values track the TTU testing data very closely. The fluctuation in the testing results comes from the fact that plywood is variable across its surface in terms of strength. This is expected and has no negative consequence to the validity of the equation.

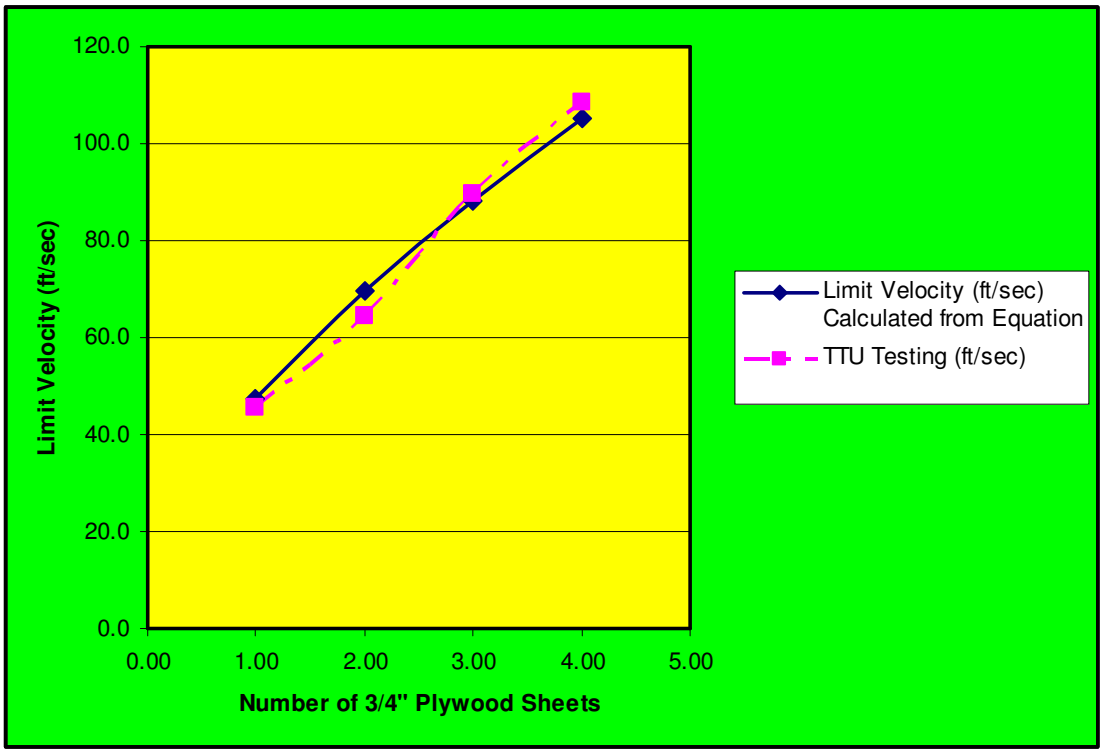

Figure 58: Limit Velocity Comparison between Equation and TTU Testing

An additional estimate of limited velocity, using the kinetic energy of the missile, also lends credence to the equations. The equation for the kinetic energy of a moving projectile is a function of the mass and the velocity squared.

$$T_{energy} = \frac{1}{2} m V^2 or \frac{1}{2} \frac{wgt}{g} V^2 \tag{47}$$

In this application, the mass is constant; therefore, the equation is dependant on the velocity only. This permits a methodology that consists of summing the squares of the individual constituent velocities and taking the square root. For example, the limit velocity is determined for the first sheet of plywood using the equation. Squaring this velocity and then multiplying this by the number of sheets of plywood under consideration gives a resultant. The square root of this total represents the estimate of limit velocity.

$$V_L = \sqrt{\sum_{1}^{n} (n) V_1^2} \tag{48}$$

V_1 is the limit velocity of the first sheet of plywood.

Table 10 lists the limit velocities determined using this methodology.

Table 10: Comparison of Velocities using Kinetic Method

Number of Sheets of 3/4" Plywood	Limit Velocity (ft/sec) Calculated from Equation	Limit Velocity (ft/sec) Kinetic Energy Method
1	32.43	32.43
2	47.36	45.86
3	60.00	56.17
4	71.70	64.86
5	83.01	72.52
6	94.23	79.44
7	105.54	85.80

Table 11: Deviation between Equation and Kinetics

Number of Sheets of 3/4" Plywood	Limit Velocity (ft/sec) Calculated from Equation	Limit Velocity (ft/sec) Kinetic Energy Method	Percent Difference from the Expected Value
1	32.43	32.43	0.0
2	47.36	45.86	3.3
3	60.00	56.17	6.6
4	71.70	64.86	9.8
5	83.01	72.52	12.9
6	94.23	79.44	16.0
7	105.54	85.80	19.0

Though the differences are significant, the variability indicates an interesting pattern. By visualizing the physical characteristics of the situation, the differences become more reasonable. The equations consider the plywood to be a finite thickness, the number of actual sheets do not play into equation. However, the kinetic exercise assumes individual and does not account for the added strength resulting from the plywood sheets attachment to each other. Each subsequent sheet reinforces the strength of the previous sheet; therefore, the sheets act as a singular entity. Closer examination of the data indicates that with each added sheet of plywood, the difference between the kinetic results and the calculated results is linear and in the same magnitude. Table 11 exemplifies this difference, as it accumulates. Note that with each added sheet, this additional "stiffness" difference between the calculated velocities and the test results are approximately 3.3%. This theory will become more obvious later in this chapter when other examinations reinforce this theory.

Though not necessary to indicate validity, the following modification to equation (41) provides a result closer to the calculated values by considering this "stiffness" theory.

$$V_L = (1 + .033n)\sqrt{\sum_{1}^{n}(n)V_1^2} \tag{49}$$

Figure 59 illustrates these accumulating discrepancies, with each additional sheet of plywood. In addition, superimposed on the chart is also the TTU testing.

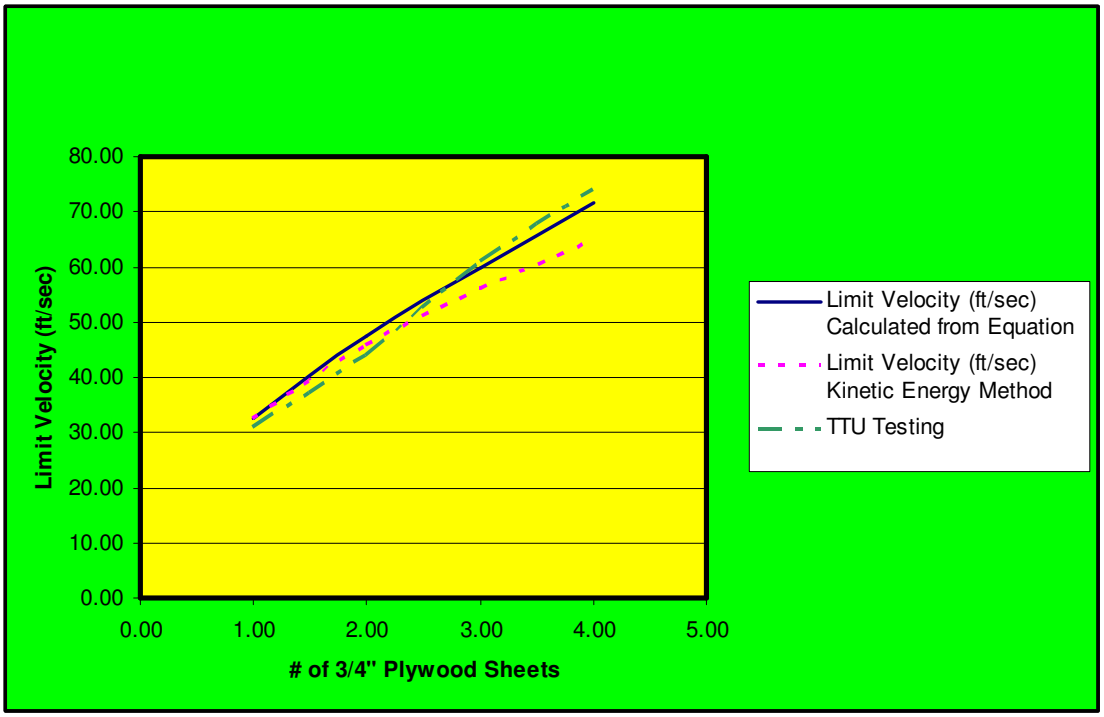

Figure 59: Overall Comparison of Results

The examination of a second set of TTU testing provides another level of credence to this procedure. This set of tests has a projectile with slightly different characteristics. It is still a 2 x 4 timber, but with a weight of 14 lbs. rather than 15 lbs. [119]. The equations remain the same for the limit velocity, but the values of the mass and subsequent alpha are different.

For these experiments, the mass becomes 14.0lbs./32.2 = .435; therefore, α becomes .0365/.435 or .084.

<u>For one sheet of ¾" plywood (w = .0625)</u>:

V_L = 49.3 ft/sec [33.6 mph]

For two sheets of ¾" plywood (w = .125):

V_L = 72.2 ft/sec [49.2 mph]

For three sheets of ¾" plywood (w = .1875):

V_L = 91.6 ft/sec [62.5 mph]

For four sheets of ¾" plywood (w = .250):

V_L = 109.8 ft/sec [74.8 mph]

For five sheets of ¾" plywood (w = .3125):

V_L = 127.4 ft/sec [86.9 mph]

For six sheets of ¾" plywood (w = .375):

V_L = 145.0 ft/sec [98.9 mph]

For seven sheets of ¾" plywood (w = .4375):

V_L = 162.9 ft/sec [111.1 mph]

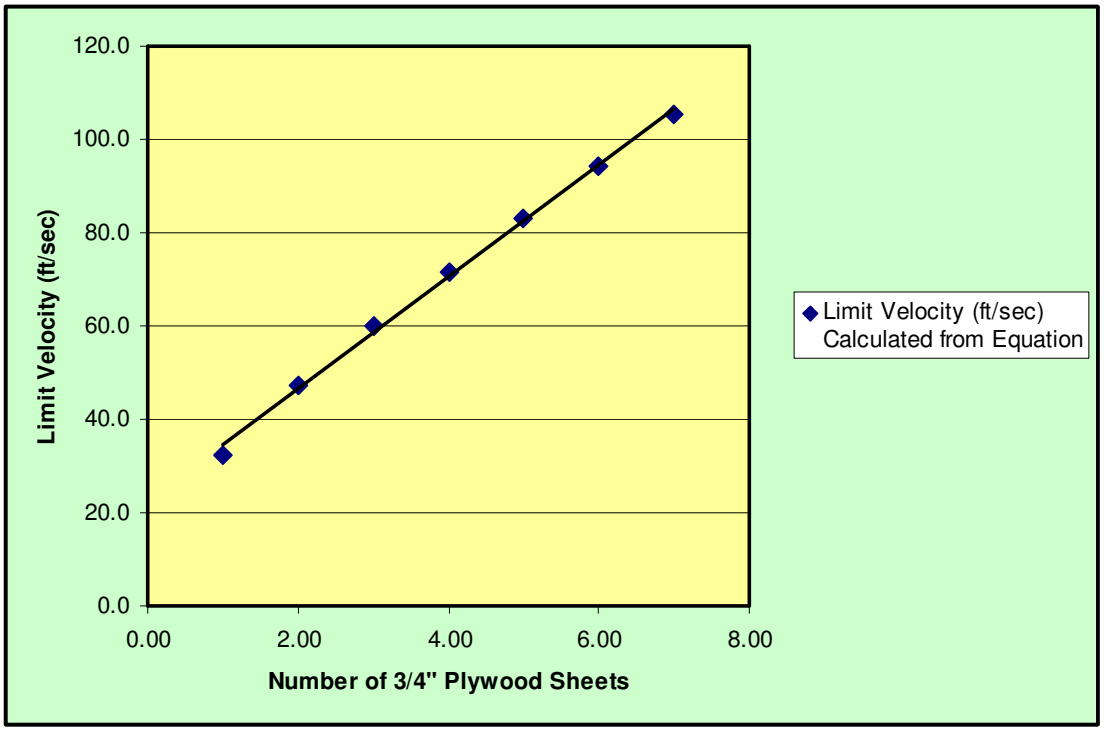

Figure 60: Limit Velocity from Equations

The trend line in Figure 60 illustrates, as in the previous set of data, the corresponding limit velocities are mostly linear in nature.

Table 12 lists the results of the Texas Tech testing.

Table 12: Plywood Sheets from TTU Testing

Number of 3/4" Plywood Sheets	TTU Testing (ft/sec)
1.00	48.4
2.00	63
3.00	76.6
4.00	110.2

A comparison between the calculated limit velocities and the TTU measured limit velocities for the 14 lb projectile indicates that the correlation is again very reasonable. As shown in Figure 61, some discrepancies exist (as would be expected) due to the variability of plywood strength across its surface.

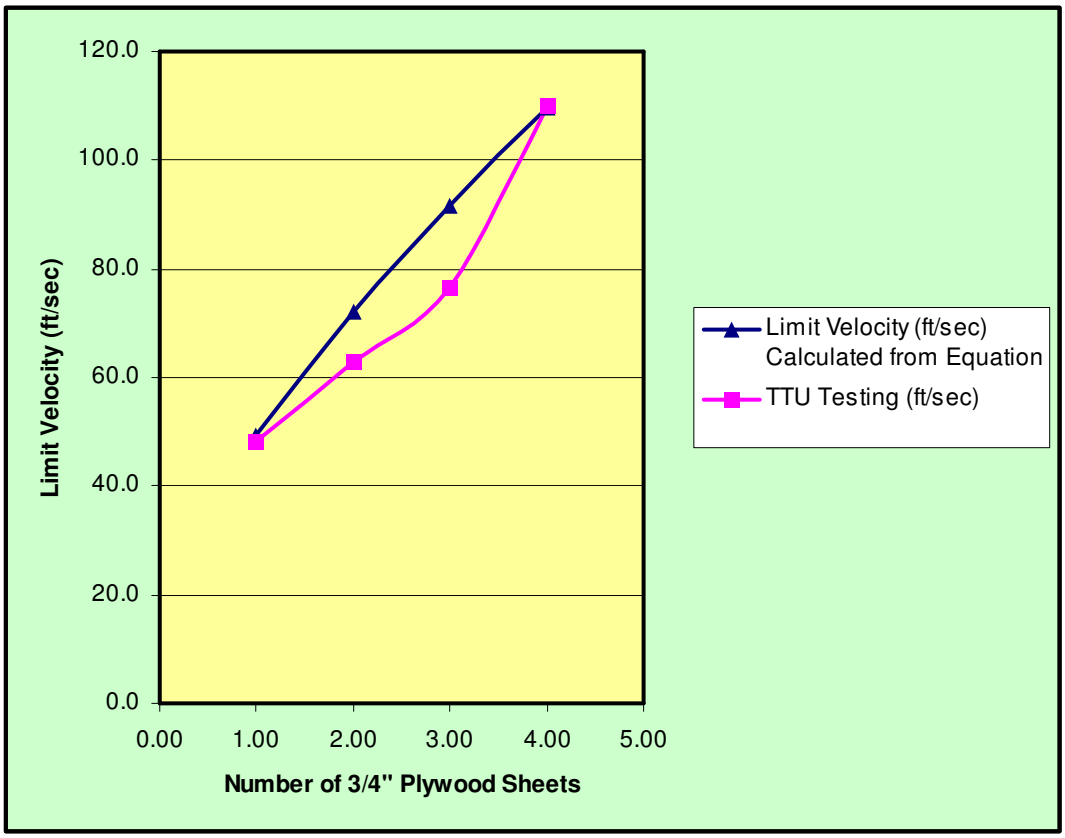

Figure 61: Comparison between Equations and TTU Tests

Another series of tests conducted at Texas Tech involved a 15 lb. 2 x 4 and four sheets of plywood. While this test did not concentrate on determining the velocities of failure, but it still adds credibility to the equations under considerations here. As Table 13 indicates, the predictions from the equations prove successful when compared with the results of the testing.

Table 13: Further Validation of Equations

Texas Tech Testing Projectile Velocity in mph	Limit Velocity Predicted from the Equations	Comments
103.1	71.7	Perforated target 7'
100.8	71.7	Perforated target 4'
97.7	71.7	Perforated target 2'
91.0	71.7	Perforated target 1'
90.6	71.7	Perforated target 3'
89.7	71.7	Perforated target 2'
86.1	71.7	Perforated target 3'
82.8	71.7	Perforated target 3'

One of the benefits of using the equations described herein is the fact that they are useful for composite targets, as well as, one-material targets. This becomes beneficial when investigating the limit velocities of surfaces that contain a variety of materials, such as exterior walls or storm room walls consisting of plywood and steel.

In the past, research and recommendations for safe rooms inside of a residence have not taken one aspect of this situation into consideration: There is a significant possibility that the projectile must past through an exterior wall prior to striking the safe room. Though this intermediate surface provides some level of protection, in this thesis, this represents another element of conservatism and therefore ignored during the recommendation phase of this report. However, it is this phenomenon, which illustrates the utility of the residual velocity. Figure 62 illustrates this conception of initial debris impact. If the laundry room became the safe room, the debris would have to pass through at least one exterior wall prior to reaching the laundry room.

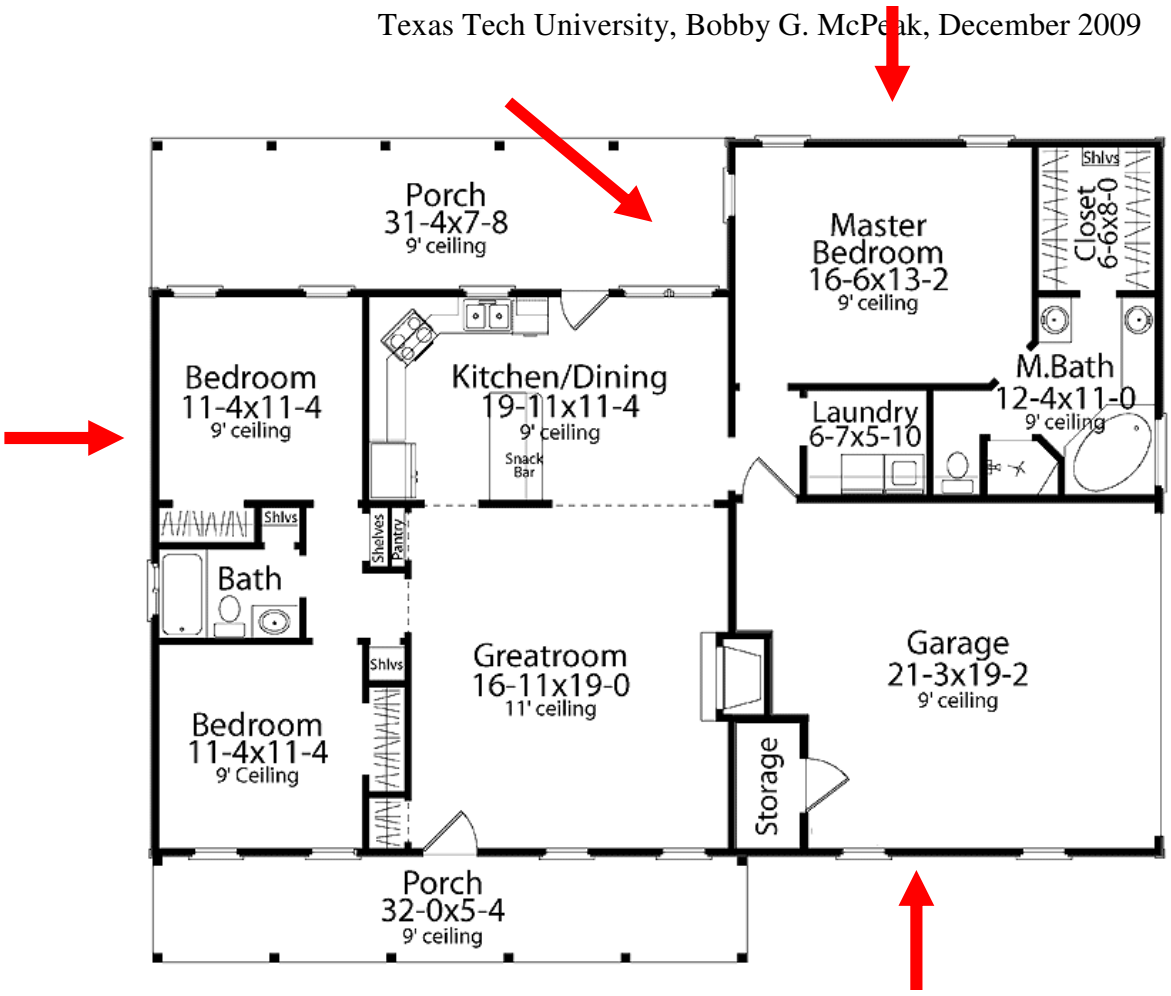

Figure 62: Typical Floor Plan Indicating Debris Incursion
[120]

Even a very modest home can achieve some level of protection by the strengthening of an interior room as shown in Figure 63. Again, the debris has to penetrate at least one wall prior to striking the master walk-in closet.

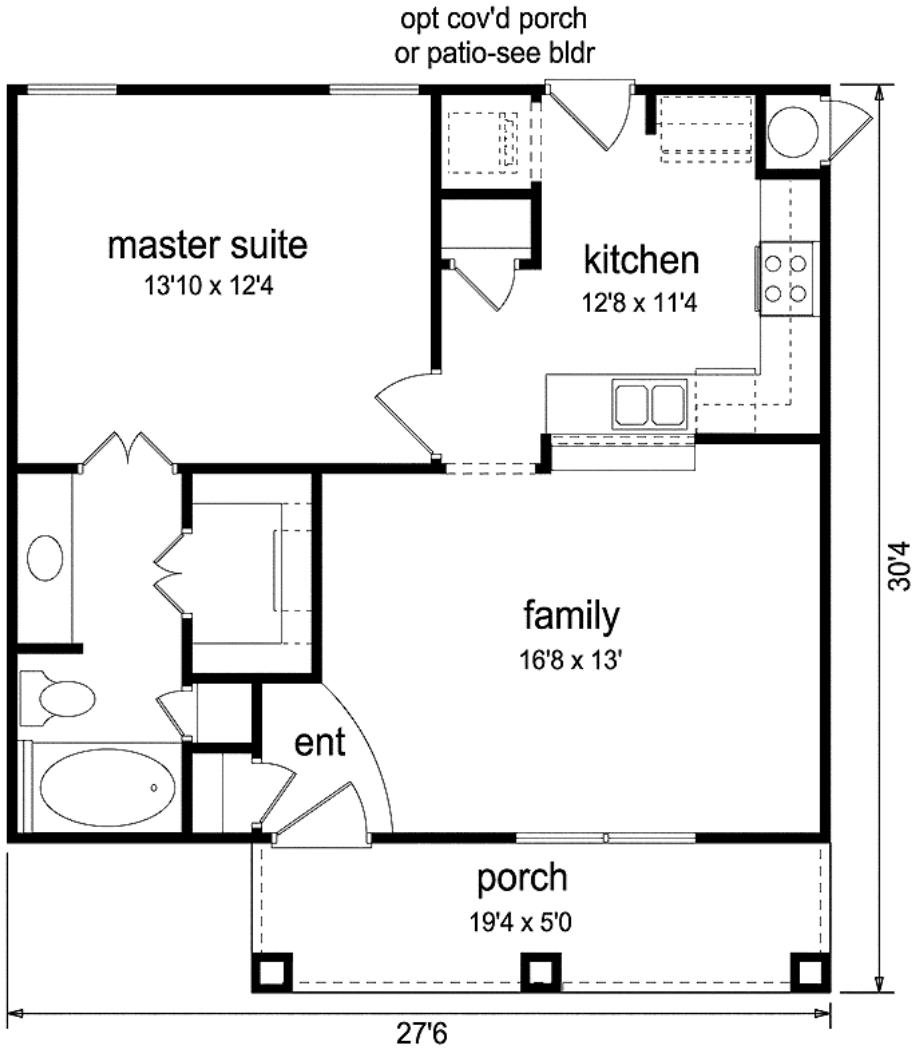

Figure 63: Small Floor Plan
[120]

One of the most typical exterior wall systems consist of brick, plywood, then sheetrock (gypsum). A composite wall with different materials greatly complicates the physics of penetration. Even the order of the wall materials can have an effect on the limit velocity. [119, 121, and 122] Since the wall contains different materials, the typical equation requires modification to include equivalent parameters. These calculations utilized (egn's 42, 43, and 44 to result in eq. 45)

R_T = 300 lb/in^2 [43200 lb/ft^2]

This strength terms refers to the strength of the primary constituent of the wall, in this case the brick

ρ_{brick} = 120 lb/ft^3

ρ_{ply} = 26 lb/ft^3

ρ_{sr} = 48 lb/ft^3

w_{brick}= .25 feet

w_{ply}= .0625 feet

w_{sr}=.052 feet

$$\rho_{eq} = \rho_{brick} + w_{ply}\frac{\rho_{ply}}{\rho_{brick} + \rho_{sr}} + w_{sr}\frac{\rho_{sr}}{\rho_{brick} + \rho_{ply}} =$$

$$120 + .0625(\frac{26}{120+48}) + .052(\frac{48}{120+26}) = 120.036$$

$$w_{eq} = w_{brick} + w_{ply}\frac{\rho_{ply}}{\rho_{brick} + \rho_{sr}} + w_{sr}\frac{\rho_{sr}}{\rho_{brick} + \rho_{ply}} =$$

$$.25 + .0625\frac{26}{120+48} + .052\frac{48}{120+26} = .276$$

γ_{eq} = ρ/2 = 60.018

A = "presented area" = 1.5 in x 3.5 in [.125 ft x .292 ft] = .0365 ft^2

M = w/g = 15/32.2 = .465

α = A/M = .0365/.465 = .078

$$V_L = \sqrt{\frac{43200}{(60.018)}(e^{2(.078)(60.018)(.276)} - 1)}$$

V_L= 95.1 ft/sec (64.9 mph)

Only one of the testing scenarios at Texas Tech uses the same wall components as this example. The resulting limit velocity in their test was 69.4 mph. Again, this value closely matches the calculated value.

In the plywood-only examples, a kinetic energy relationship demonstrated the viability of the limit equations. As remarked, since the plywood sheets attached to each other, a "stiffness" factor explained the discrepancies between the calculated values and the kinetic energy related values. In this example, the components of the wall do not connect; therefore, the conclusion is much closer. The calculated limit velocities of the constituent components squared, summed, and the square root taken results in the estimated limit velocity of the whole.

First, the limit velocities of the constituents are developed.

For the brick portion, the following parameters define the variables in the equation::

R_T = 300 lb/in^2 [43200 lb/ft^2]

ρ = 120 lb/ft^3

γ = ρ/2 = 60

A = "presented area" = 1.5 in x 3.5 in [.125 ft x .292 ft] = .0365 ft^2

M = w/g = 15/32.2 = .465

α = A/M = .0365/.465 = .078

w = thickness in feet = .25

$$V_L = \sqrt{\frac{43200}{(60)}(e^{2(.078)(60)(.250)} - 1)}$$

$V_{L(brick)}$ = 82.8 ft/sec (56.5 mph)

For the sheetrock portion, the following parameters define the variables in equation:

R_T = 220 lb/in^2 [31700 lb/ft^2]

ρ = 48 lb/ft^3

γ = ρ/2 = 24

A = "presented area" = 1.5 in x 3.5 in [.125 ft x .292 ft] = .0365 ft^2

M = w/g = 15/32.2 = .465

α = A/M = .0365/.465 = .078

w = thickness in feet = .052

$$V_L = \sqrt{\frac{31700}{(24)}(e^{2(.078)(24)(.052)} - 1)}$$

$V_{L(sr)}$ = 15.0 ft/sec (10.2 mph) *This is not unexpected as sheetrock offer little resistance to impact.*

The limit velocity of a single plywood sheet equaled 32.4 mph in an earlier example.

With this data:

$V_L = \sqrt{\sum_1^n V^2} = \sqrt{56.5^2 + 10.2^2 + 32.4^2}$ for a composite limit velocity of 65.9 mph

Table 14 includes the results of these comparisons.

Table 14: Limit Velocity Comparison

Methodology of Determination	Limit Velocity Value (mph)
Equations from this study	64.9
Texas Tech Test	69.4
Kinetic Energy	65.9

A second testing at Texas Tech uses a 12.5 lb. 2 x 4 striking a wall constructed of brick, ½" insulation board, and ½" of sheetrock.

The values used for this scenario follows:

R_T = 300 lb/in^2 [43200 lb/ft^2]

ρ_{brick} = 120 lb/ft^3

$\rho_{ins.bd.}$ = 2.64 lb/ft^3

ρ_{sr} = 48 lb/ft^3

w_{brick}= .25 feet

$w_{ins.bd.}$= .0417 feet

w_{sr}=.0417 feet

$$\rho_{eq} = \rho_{brick} + w_{ins.bd.}\frac{\rho_{ins.bd.}}{\rho_{brick} + \rho_{sr}} + w_{sr}\frac{\rho_{sr}}{\rho_{brick} + \rho_{ins.bd.}} =$$

$$120 + .0417(\frac{2.64}{120 + 48}) + .0417(\frac{48}{120 + 2.64}) = 120.017$$

$$w_{eq} = w_{brick} + w_{ins.bd.}\frac{\rho_{ins.bd}}{\rho_{brick} + \rho_{sr}} + w_{sr}\frac{\rho_{sr}}{\rho_{brick} + \rho_{ins.bd.}} =$$

$$.25 + .0417\frac{2.64}{120 + 48} + .0417\frac{48}{120 + 2.64} = .2670$$

γ_{eq} = ρ/2 = 60.0085

A = "presented area" = 1.5 in x 3.5 in [.125 ft x .292 ft] = .0365 ft^2

M = w/g = 12.5/32.2 = .3882

α = A/M = .0365/.3882 = .0940

$$V_L = \sqrt{\frac{43200}{(60.0085)}(e^{2(.094)(60.0085)(.2670)} - 1)}$$

V_L= 124.5 ft/sec (84.9 mph)

Again, only one of the testing scenarios at Texas Tech uses the same wall components as this example. The resulting limit velocity in their test was 81.8 mph. Again, this value closely matches the calculated value.

The kinetic energy method is repeated as before with new characteristics due to the difference in projectile weight, ½" insulation board and the ½" sheetrock.

For the brick portion, the following parameters define the variables in the equation:

R_T = 300 lb/in^2 [43200 lb/ft^2]

ρ = 120 lb/ft^3

γ = ρ/2 = 60

A = "presented area" = 1.5 in x 3.5 in [.125 ft x .292 ft] = .0365 ft^2

M = w/g = 12.5/32.2 = .3882

α = A/M = .0365/.3882 = .094

w = thickness in feet = .25

$$V_L = \sqrt{\frac{43200}{(60)}(e^{2(.094)(60)(.250)} - 1)}$$

$V_{L(brick)}$ = 106.6 ft/sec (72.7 mph)

For the sheetrock portion, the following parameters define the variables in the equation:

R_T = 220 lb/in^2 [31700 lb/ft^2]

ρ = 48 lb/ft^3

γ = ρ/2 = 24

A = "presented area" = 1.5 in x 3.5 in [.125 ft x .292 ft] = .0365 ft^2

M = w/g = 12.5/32.2 = .3882

α = A/M = .0365/.3882 = .0940

w = thickness in feet = .0417

$$V_L = \sqrt{\frac{31700}{(24)}(e^{2(.094)(24)(.0417)} - 1)}$$

$V_{L(sr)}$ = 16.5 ft/sec (11.3 mph)

For the insulation board portion, the following parameters define the variables in the equation:

R_T = 65 lb/in^2 [9360 lb/ft^2]

ρ = 2.64 lb/ft^3

γ = ρ/2 = 1.32

A = "presented area" = 1.5 in x 3.5 in [.125 ft x .292 ft] = .0365 ft^2

M = w/g = 12.5/32.2 = .3882

α = A/M = .0365/.3882 = .0940

w = thickness in feet = .0417

$$V_L = \sqrt{\frac{9360}{(1.32)}(e^{2(.094)(1.32)(.0417)} - 1)}$$

$V_{L(ins.\ bd.)}$ = 8.59 ft/sec (5.85 mph)

$V_L = \sqrt{\sum_1^n V^2} = \sqrt{72.7^2 + 11.3^2 + 5.85^2}$ for a composite limit velocity of 73.8 mph

Table 15 includes the results of these comparisons.

Table 15: Limit Velocity Comparison

Methodology of Determination	Limit Velocity Value (mph)
Equations from this study	81.7
Texas Tech Test	81.8
Kinetics Methodology	73.8

Another wall structure that is common in the construction of homes is termed a "frame" house. In contrast to a brick house, the exterior of a "frame" house consists of either clapboard siding, Masonite (engineered wood) siding, or some similar non-masonry material. Texas Tech has performed some limiting testing on these wall systems, which provide good data for estimating characteristics of these wall systems. In a paper by McDonald [123] walls constructed in the fashion indicated above cannot resist a 2 x 4 projectile at speeds greater than 50 mph. Using the equivalent equation (45), Figure 64 illustrates the results of performing these calculations against TTU testing.

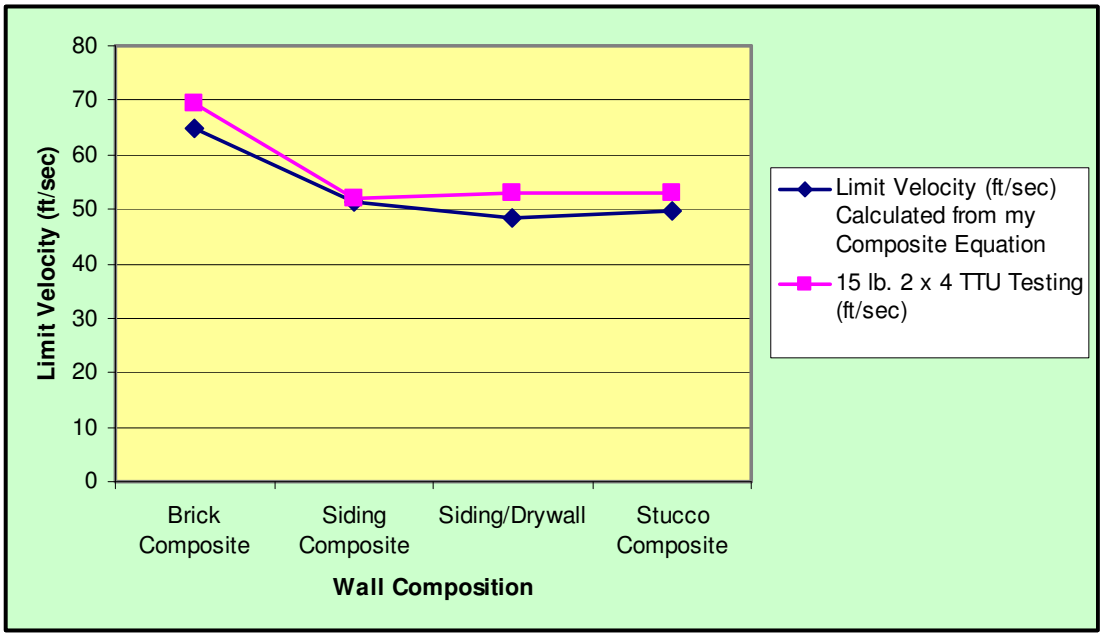

Figure 64: Comparison of Composite Wall System Limit Velocities Between TTU Testing and equations

Again, almost perfect correlation exists between the testing and utilization of the equations. This represents a major step forward in the determination of tornado debris against a variety of wall systems.

Of particular importance is the viability of a concrete shelter system in the presence of tornado debris. Earlier in the depth of penetration discussion, the validity of the equations for concrete walls experiencing impact from steel pipes indicated a very positive application of this equation for such a combination of projectile and target. Since these equations apply, the following is the result of using the equations to determine the limit velocity of a 15 lb. 2 x 4 striking various thickness of concrete.

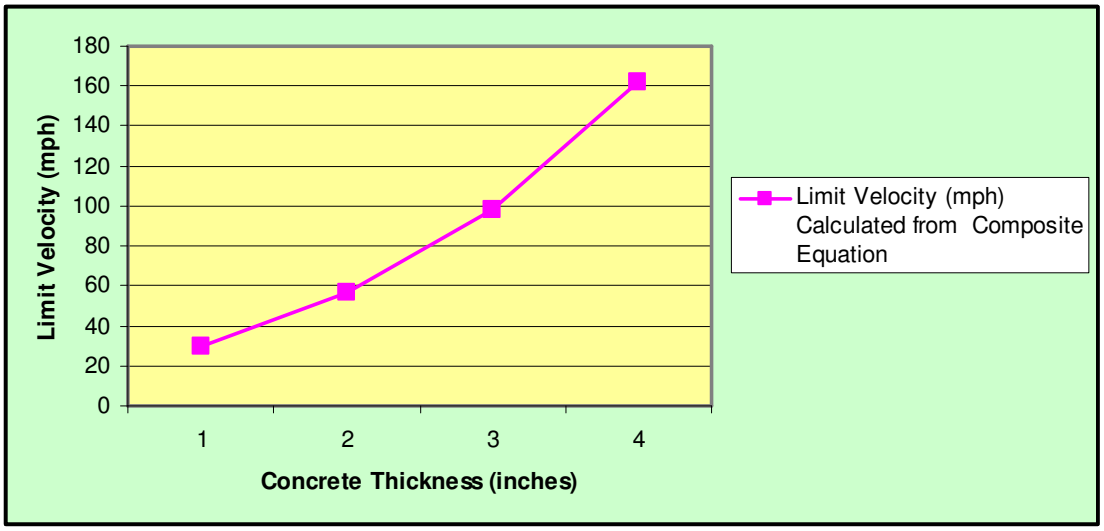

Figure 65: Limit Velocities for Concrete of Various Thicknesses

As illustrated in Figure 65, a projectile with a velocity of 100 mph would just penetrate a concrete wall three inches thick. For this reason, the recommendation is to construct all concrete shelters with a minimum concrete wall thickness of four inches. For an example of such a shelter, see Appendix A.

The last investigation of the phenomena associated with the limit velocity is composite walls systems that have a plate of steel as a constituent. The steel component of the composite system complicates the situation enormously. First, the layers of material that make up the wall are often in contact with each other. Since this puts dissimilar materials in contact with one another, the equations are possibly affected. In addition, the mechanisms of failure for steel sheets are different that the characteristics of brick or wood based failures. Steel lacks the brittle element of the previous materials. Instead of a plugging or pedaling failure common with plywood and like materials or the brittle failure usually seen with brick and concrete walls, steel fails from crack propagation and ultimately fracture. Additionally, steel has a characteristic that is lacking with other considered materials. Instead of shattering like masonry or pedaling like wood, it has the ability to deform. Steel structurally deforms prior to rupture; therefore, predicting the limit velocity is further complicated. [124 and 125] Adding steel to a wall system allows more energy transfer from the projectile to the wall and this energy spreads over a larger area, resulting in a superior

penetration resistive wall. Unfortunately, there are some disadvantages from the standpoint of this study. Adding steel to a composite wall system greatly complicates the ability to predict the event via the use of equations; however, the equations demonstrated in this study provides a conservative estimate of the expected limit velocities associated with wall surfaces containing a steel component.

This study does not suggest that steel does not provide superior protection for penetration of a safe room. However, since this exercise concentrates on an inexpensive alternative to a safe room that provides "near absolute protection", steel will not be included in the section on recommendations for the following reasons:

- The cost of steel is much higher than other suggested strengthening materials
- Procurement, transport, and handling of steel make it very difficult to maneuver
- Cutting and attaching steel to the wall surfaces requires skills that many homeowners lack
- Safe rooms surrounded by steel might diminish communications from cell phones and weather radios
- In the case of a rescue situation, steel could complicate emergency personnel entrance
-

Though steel is not included in the recommendations of this paper, calculations and associated comparisons with test results are included for the sake of completeness.

As before, since different materials compose the walls under consideration, the equation used includes the equivalent parameter modifications.

In case 1, the walls consist of two layers of plywood and one layer of 16-gauge steel.

$R_T = 58{,}000$ lb/in^2

This strength terms refers to the strength of the primary constituent of the wall, in this case the steel

$\rho_{steel} = 491$ lb/ft^3

ρ_{ply} = 26 lb/ft^3

w_{steel}= 16-gauge = .060 inches (.00498 feet)

w_{ply}= .125 feet

$$\rho_{eq} = \rho steel + w_{ply}\frac{\rho_{ply}}{\rho_{steel\,sr}} =$$

$$491 + .125(\frac{26}{491}) = 491.007$$

$$w_{eq} = wsteel + w_{ply}\frac{\rho_{ply}}{\rho_{steel}} =$$

$$.00498 + .125\frac{26}{491} = .0116$$

γ_{eq} = ρ/2 = 245.503

A = "presented area" = 1.5 in x 3.5 in [.125 ft x .292 ft] = .0365 ft^2

M = w/g = 15/32.2 = .465

α = A/M = .0365/.465 = .078

$$V_L = \sqrt{\frac{8352000}{(245.503)}(e^{2(.078)(245.503)(.0116)} - 1)}$$

V_L= 138.5 ft/sec (94.4 mph)

In case 2, the walls consist of four layers of plywood and one layer of 16-gauge steel.

R_T = 58,000 lb/in^2 [8,352,000 lb/ft^2]

This strength terms refers to the strength of the primary constituent of the wall, in this case the steel

ρ_{steel} = 491 lb/ft^3

ρ_{ply} = 26 lb/ft^3

w_{steel}= 16-gauge = .060 inches (.00498 feet)

w_{ply}= .250 feet

$$\rho_{eq} = \rho steel + w_{ply}\frac{\rho_{ply}}{\rho_{steel\,sr}} =$$

$$491 + .250(\frac{26}{491}) = 491.013$$

$$w_{eq} = wsteel + w_{ply}\frac{\rho_{ply}}{\rho_{steel}} =$$

$$.00498 + .250(\frac{26}{491}) = .0182$$

γ_{eq} = ρ/2 = 245.507

A = "presented area" = 1.5 in x 3.5 in [.125 ft x .292 ft] = .0365 ft^2

M = w/g = 15/32.2 = .465

α = A/M = .0365/.465 = .078

$$V_L = \sqrt{\frac{8352000}{(245.507)}(e^{2(.078)(245.507)(.0182)} - 1)}$$

V_L= 186.0 ft/sec (126.8 mph)

The results of this comparison (See Table 16) indicates that the results the testing could be suspect. Notice that for the case with two layers of plywood and one layer of 16-gauge steel, the velocity is only 9.2 ft/sec less than the case with twice the thickness of plywood and thicker steel. Nonetheless, the equations seem to have supplied a reasonable estimate of the limit speed.

Table 16: Steel Composite Limit Velocity

Sheets of Plywood	Limit Velocity (ft/sec) Calculated from Equation	Limit Velocity (ft/sec) Calculated from Texas Tech Testing
2	138.5	147.7
4	186.0	156.9

These results clearly illustrate that the calculations are not valid for composite walls constructed with steel.

Residual Projectile Velocities

The velocities of the projectiles after penetration are a characteristic that is very useful in determining safety aspects of a storm room. The equation for determining the residual velocity occurs in Chapter 5, equation (36).

The first series of calculations represent the residual velocities of a 15 lb 2 x 4 with an impact velocity of 100 mph (146.7 ft/sec) into one to seven layers of ¾" plywood. Using equation (36), the following results were obtained.

R_T = 1500 lb/in^2 [2.16 (10)^5 lb/ft^2]

ρ = 26 lb/ft^3

$\gamma = \rho/2 = 13$

A = "presented area" = 1.5 in x 3.5 in [.125 ft x .292 ft] = .0365 ft^2

M = w/g = 15/32.2 = .465

α = A/M = .0365/.465 = .078

w = thickness in feet

V_0 = Velocity of the projectile

For one sheet of ¾" plywood:

V_{r1} = 130.1 ft/sec (88.7 mph)

For two sheets of ¾" plywood:

V_{r2} = 113.7 ft/sec (77.5 mph)

For three sheets of ¾" plywood:

V_{r3} = 96.9 ft/sec (66.1 mph)

For four sheets of ¾" plywood:

V_{r4} = 79.2 ft/sec (54.0 mph)

For five sheets of ¾" plywood:

V_{r5} = 59.5 ft/sec (40.6 mph)

For six sheets of ¾" plywood:

V_{r6} = 33.5 ft/sec (22.9 mph)

For seven sheets of ¾" plywood:

Since V_{r7} results in a negative number under the radical – the projectile does not does not penetrate (confirms penetration depth calculations and limit velocity calculations in previous sections)

The illustration of this data is in Figure 66:

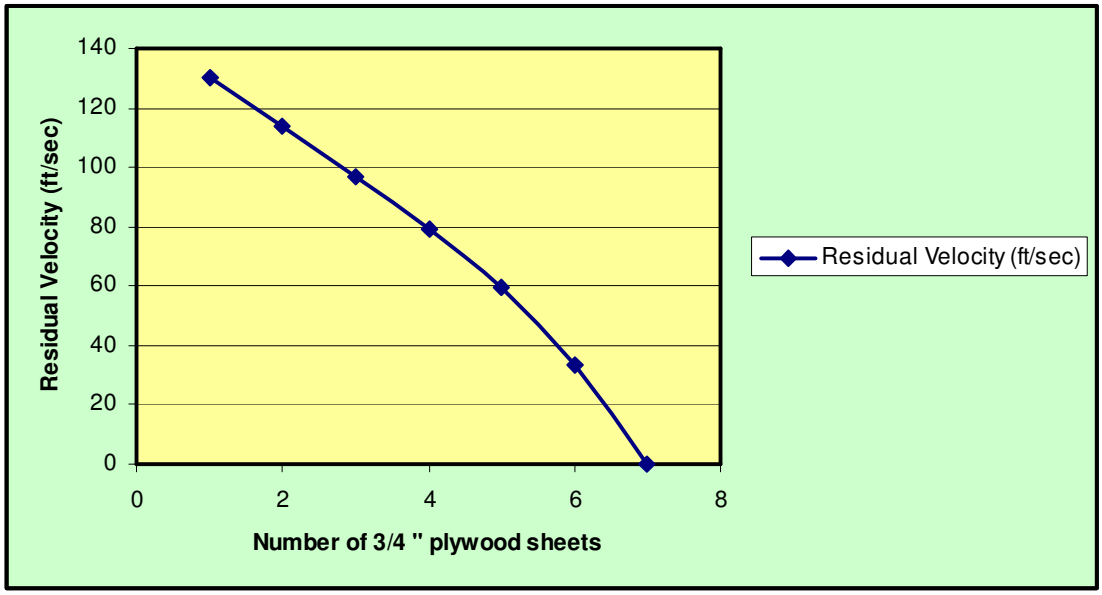

Figure 66: Residual Velocity

In terms of debris striking the external envelope of a home an important composite wall section is brick, ¾" plywood, and 5/8" sheetrock. As in previous examples, the first step is developing the values for the various parameters in a composite structure: the *equivalent* parameter values.

R_T = 300 lb/in^2 [43200 lb/ft^2]

ρ_{brick} = 120 lb/ft^3

ρ_{ply} = 26 lb/ft^3

ρ_{sr} = 48 lb/ft^3

w_{brick}= .25 feet

w_{ply}= .0625 feet

w_{sr}=.052 feet

$$\rho_{eq} = \rho_{brick} + w_{ply}\frac{\rho_{ply}}{\rho_{brick} + \rho_{sr}} + w_{sr}\frac{\rho_{sr}}{\rho_{brick} + \rho_{ply}} =$$

$$120 + .0625(\frac{26}{120+48}) + .052(\frac{48}{120+26}) = 120.03$$

$$w_{eq} = w_{brick} + w_{ply}\frac{\rho_{ply}}{\rho_{brick} + \rho_{sr}} + w_{sr}\frac{\rho_{sr}}{\rho_{brick} + \rho_{ply}} =$$

$$.25 + .0625\frac{26}{120+48} + .052\frac{48}{120+26} = .277$$

γ_{eq} = ρ/2 = 60.015

A = "presented area" = 1.5 in x 3.5 in [.125 ft x .292 ft] = .0365 ft^2

M = w/g = 15/32.2 = .465

V= Velocity in feet/sec

The use of Equation (45) permits these calculations.

Since the premise of this study is to define levels of protection correlated to the EF Scale of tornado damage intensity, the velocities used for this exercise match the velocities developed earlier.

EF0: Upper debris velocity for walls – 99.7 ft/sec (68 mph)

V_{rEF0} = 8.0 ft/sec (5.5 mph)

EF1: Upper debris velocity for walls – 112.9 ft/sec (77 mph)

V_{rEF1} = 16.4 ft/sec (11.2 mph)

EF2: Upper debris velocity for walls – 121.7 ft/sec (83 mph)

V_{rEF2} = 20.5 ft/sec (14.0 mph)

EF3: Upper debris velocity for walls – 127.6 ft/sec (87 mph)

V_{rEF3} = 23.0 ft/sec (16.4 mph)

EF4: Upper debris velocity for walls – 132 ft/sec (90 mph)

V_{rEF4} = 24.8 ft/sec (16.9 mph)

EF5: Upper debris velocity for walls – 146.7 ft/sec (100 mph)

V_{rEF5} = 30.3 ft/sec (20.6 mph)

The illustration of this data appears in Figure 67.

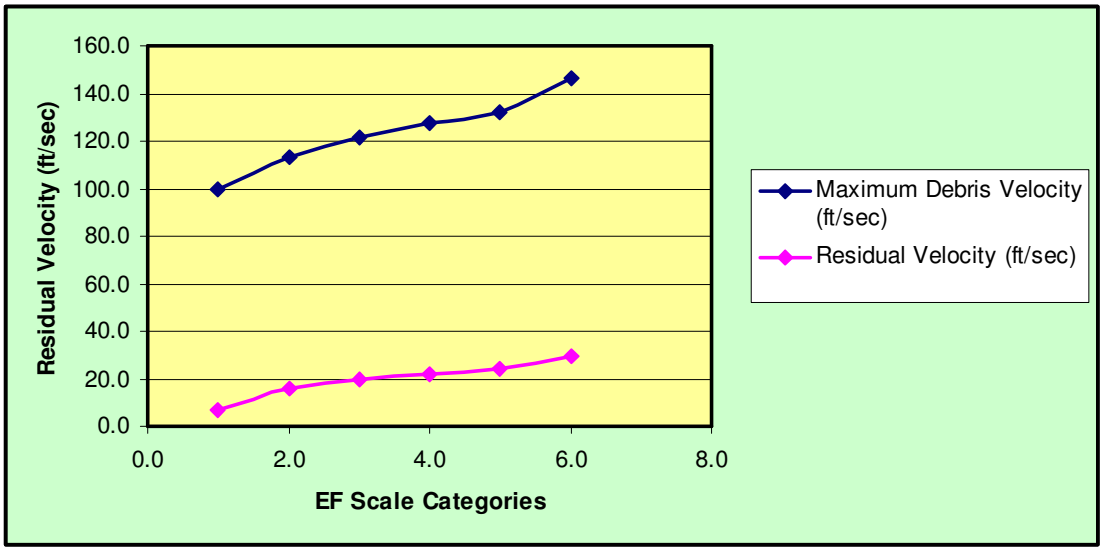

Figure 67: Residual Velocity after Brick Penetration

This concept has valuable corollaries in terms of predicting residual velocity for wall construction with unknown parameters such as density or strength. For example, if a door assembly is tested and the threshold velocity determined, the residual velocity can be determined from these equations. Assume the door testing reveals that the threshold for failure is 47 mph with a 15 lb 2 x 4. This is approximately the same limit velocity found earlier for two sheets of plywood. Input the parameters in the plywood velocity equation into the residual velocity equation to provide an estimate of the residual velocity for a projectile striking the door at any velocity.

Door example for a velocity of 146.7 ft/sec (100 mph)

$$V_r = \sqrt{(146.7^2 e^{\frac{-(.0365)(26)(.187)}{.465}} - \frac{216000}{(26)})(1 - e^{\frac{-(.0365)(26)(..187)}{.465}})}$$

V_{rEF5} = 96.9 ft/sec (66.1 mph)

Since McDonald stated that exterior non-masonry walls could not expect to resist penetration at debris speed in excess of 50 mph, the above example can predict

the residual velocities of debris striking non-masonry wall surfaces. As described in the door example, the characteristics of a non-masonry external wall is very close to the same as for a wall constructed of two sheets of plywood; therefore, the plywood characteristics used in the equations for residual velocity will predict the residual velocities of debris impacting exterior non-masonry walls.

EF0: Upper debris velocity for walls – 99.7 ft/sec (68 mph)

V_{rEF0} = 62.9 ft/sec (42.9 mph)

EF1: Upper debris velocity for walls – 112.9 ft/sec (77 mph)

V_{rEF0} = 78.3 ft/sec (53.4 mph)

EF2: Upper debris velocity for walls – 121.7 ft/sec (83 mph)

V_{rEF0} = 87.9 ft/sec (60.0 mph)

EF3: Upper debris velocity for walls – 127.6 ft/sec (87 mph)

V_{rEF0} = 94.2 ft/sec (64.2 mph)

EF4: Upper debris velocity for walls – 132 ft/sec (90 mph)

V_{rEF0} = 98.8 ft/sec (67.4 mph)

EF5: Upper debris velocity for walls – 146.7 ft/sec (100 mph)

V_{rEF0} = 113.7 ft/sec (77.5 mph)

The illustration of this data appears in Figure 68.

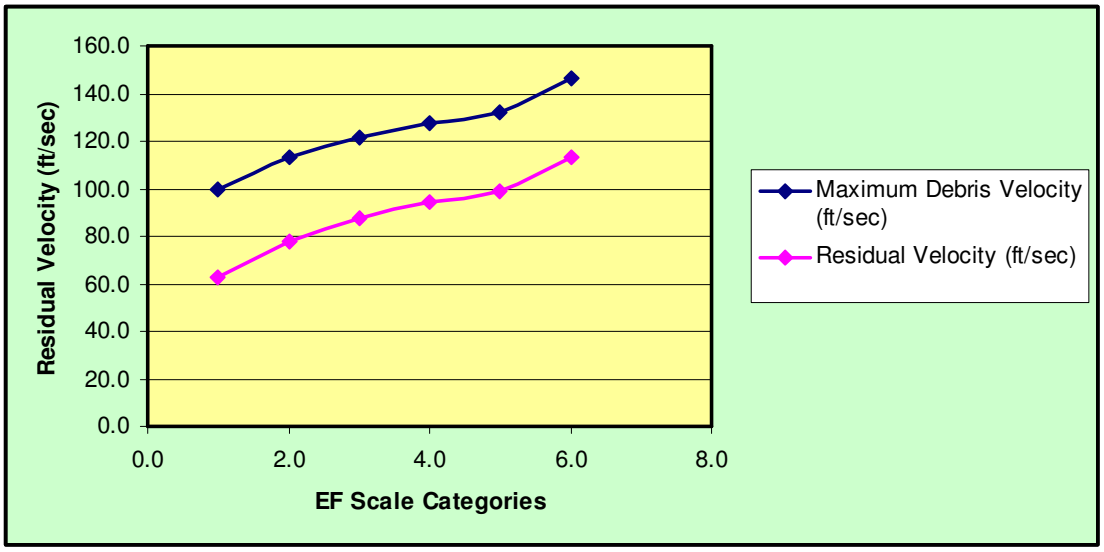

Figure 68: Velocity after Frame Wall Penetration

As illustrated, the equations described in Chapter 5 are useful and valid for predicting penetration depth, limit velocity, and residual velocity for a large number of projectile and target geometries.

Probability Considerations

Since this chapter concentrates on examples resulting in useful data for making decisions in regards to storm room construction, the element of probability is included here.

Since statistical data is a fluid target and changes often, the probabilities of tornadoes and associated maximum damage requires frequent attention. The U.S. Nuclear Regulatory Commission is quite interested in tornado data and damage effects. Their latest publication dated February 2007, includes the new boundaries defined by the Enhanced Fujita Damage Scale [126]. This document goes into finite detail in terms of tornado strikes, wind characteristics, path length and width, and other specifics about tornadoes.

The decision to construct a safe room or supplemental tornado shelter involves several variables: what are the chances of a tornado strike, how bad is it likely to get, what specifics in terms of damage is avoidable. [127]

The probability of a single structure experiencing a tornado depends on the location of the structure. Throughout the United States, there is great variability in the odds of a tornado. The aforementioned document details the probability of tornado strikes within the U.S. by dividing the country into one-degree areas of latitude and longitude. According to the NRC report, the highest probability of a tornado of any intensity striking a "point structure" occurs in the central United States and the estimated frequency is 3.58×10^{-4}.

Determining the probability of a tornado strike within a given EF range involves two separate probabilities: the probability of a tornado strike of any intensity (called event 1 and noted as E1), and the probability that the winds will exceed the threshold of one of the EF categories (called event 2 and noted as E2). This represents a situation called conditional probability meaning that E1 must occur before E2 can occur. This uses equation (50):

$$P_P\langle u \geq u_0 \rangle = P_P \times \langle u \geq u_0 \,|\, s \rangle \tag{50}$$

P_P is the probability that a point structure will experience a tornado

$u \geq u_0$ is the probability of a wind speed u exceeding some wind speed u_0

therefore:

$P_P\langle u \geq u_0 \rangle$ is the probability that given a tornado occurs the wind speed will exceed some specified wind speed

Event 2 is an exhaustive event because if event 1 occurs one of the categories of the EF scale exists.

Table 17 illustrates the probability of tornadoes by EF category [126].

Table 17: Probability of EF Category Wind Speeds (E2)

Enhanced Fujita Category	Percentage of Occurrence
EF0	53.80%
EF1	22.30%
EF2	11.90%
EF3	7.00%
EF4	3.30%
EF5	1.70%

E1 = 3.58 x 10^{-4}

E2= the percentage shown in Table 17

The probability of experiencing a tornado within each EF category is:

$$P_{EF0} = (3.58\times10^{-4})(0.538) = 1.926\times10^{-4}$$

$$P_{EF1} = (3.58\times10^{-4})(0.223) = 7.983\times10^{-4}$$

$$P_{EF2} = (3.58\times10^{-4})(0.119) = 4.260\times10^{-5}$$

$$P_{EF3} = (3.58\times10^{-4})(0.070) = 2.506\times10^{-5}$$

$$P_{EF4} = (3.58\times10^{-4})(0.033) = 1.181\times10^{-5}$$

$$P_{EF5} = (3.58\times10^{-4})(0.017) = 6.086\times10^{-6}$$

As an adjunct to the analyses illustrated above and to further validate the theories presented in this study, a finite element analysis is included. This will generate another level of verification and provide the framework for further study apart from this research.

The software package utilized in this effort is LS-DYNA. In general, LS-DYNA allows for the solutions of complex problems which involve material nonlinearities and large deformations. Simulations provided by LS-DYNA provide predictions which ultimately guide product development and safety assessments.

As mentioned throughout this dissertation, there exists limitations in terms of TTU experimental data availability; therefore, the finite element analysis provides an additional supplement to validate the results of this study. Of primary interest is the examination of the residual velocity conclusions, which are valid throughout this study, based on the derivation of the equation. TTU test results guide the finite element model development. The following chapter illustrates the degree of confidence in the analysis results.

CHAPTER 7

FINITE ELEMENT SIMULATION

Introduction

The main focus of this chapter is to develop a finite element simulation using the LS-DYNA analysis code to predict the dynamic response of plywood when impacted by tornado missiles such as 2 x 4 wood timbers. The purpose is to provide an additional layer of confidence to the results shown by the equations developed in this research study. This additional verification supplements the limited TTU experimental data.

To guide the finite element model development, existing TTU experimental results are used. LS-DYNA simulation results allow crosschecking and correlation against the existing TTU experimental test data described throughout this research. Correlation of simulated data to TTU experimental data helps in providing confidence in the construction and solutions of the simulation model.

One Layer Pine Wood Finite Element Model Simulation of Plywood

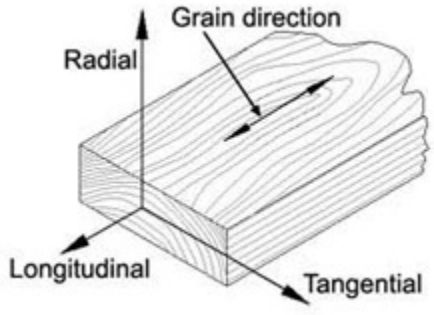

Figure 69: Illustration of Wood Grain Coordinates
[128]

Due to the paucity of adequate plywood property definitions, the consideration is that plywood has similar properties as a single layer pine target. Stiffness and strength properties of the wood (as with plywood) vary as a function of orientation between the longitudinal, tangential, and radial directions. As shown in Figure 69, the longitudinal direction is the fiber or grain direction. Stiffness and strength are at their maximum values in this direction.

Based on the symmetry of the problem, the models consist of only one quarter of the geometry. The projectiles and the targets consist of 8-node hexahedron solid elements, using one integration point. Figure 70 illustrates the finite element mesh. The target has 5 elements through the thickness to emulate the 5 layers of a plywood substrate. The contact region has a fine mesh with an element size of 3.175 mm x 3.175 mm x 3.81 mm. The transition region has an element size of 3.175 mm x 3.175 mm x 3.81 mm with a course mesh size of 6.35 mm x 6.35 mm x 3.81 mm. The element size for the projectile is the same as that of the impact zone of the target, which is 3.175 mm x 3.175 mm x 3.175 mm. Targets and projectiles have 19,320 and 1,008 brick elements respectively.

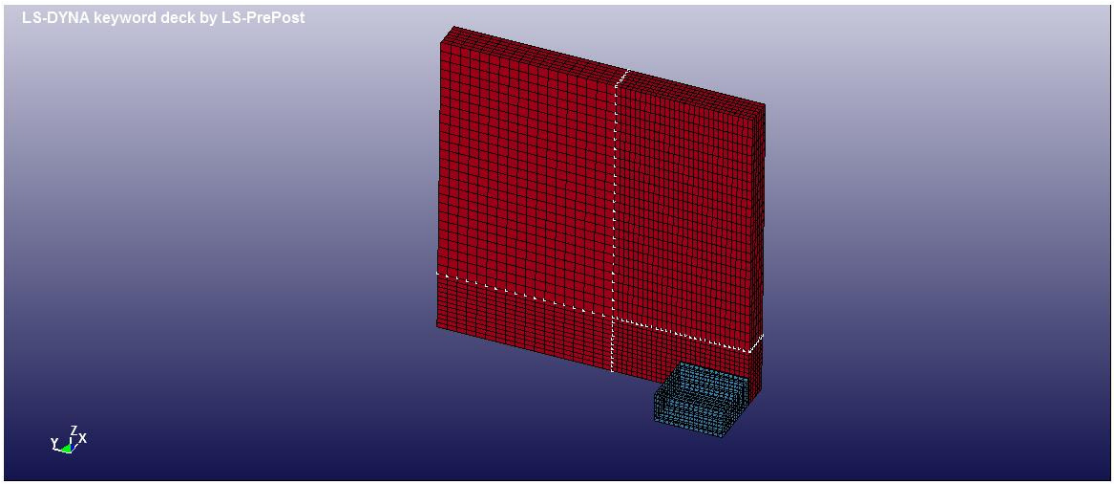

Figure 70: Finite Element Mesh

As shown in Figure 71, the symmetry boundary conditions exist on the bottom and right-hand faces of the targets and projectiles. The upper and right-hand faces of the targets have fixed boundary conditions.

Modeling approximates the impact forces between the projectiles and the targets with "eroding contact surfaces". The contact surfaces redefine themselves after an element fails, and are removed from the model; therefore, accurately tracking the force between the projectile and the target.

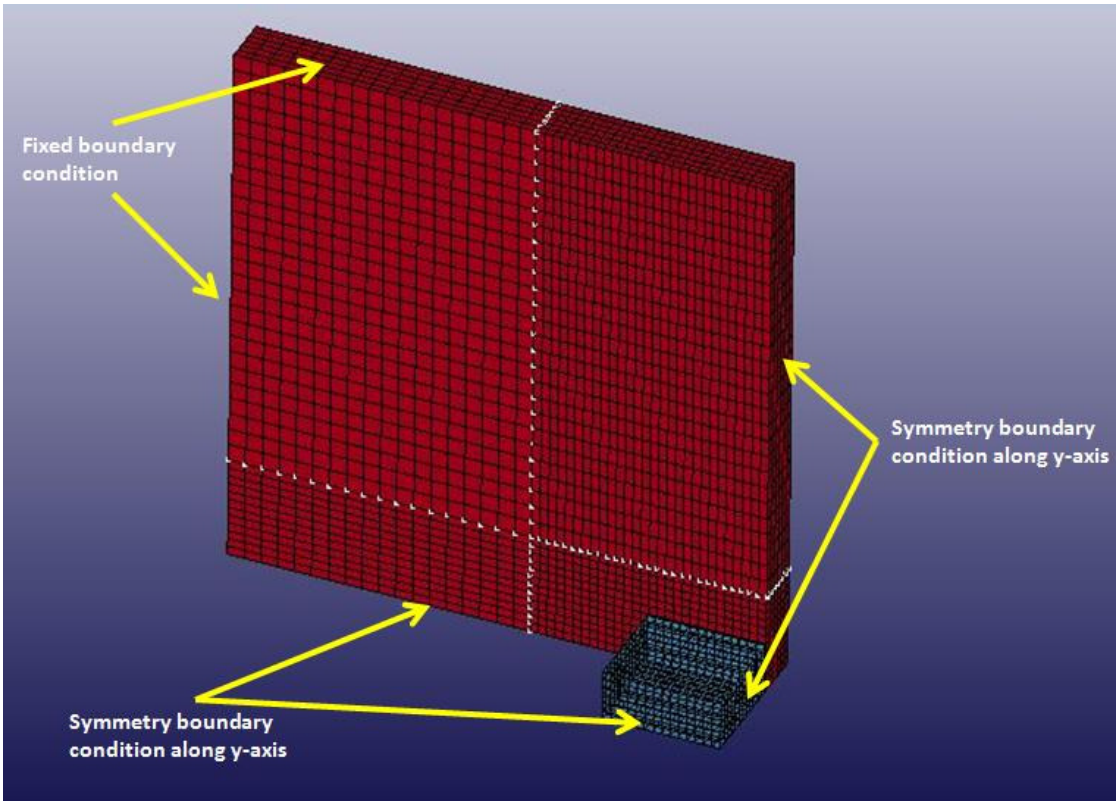

Figure 71: Due to Symmetry - 1/4 of Target is Modeled

Material Model

The Material Model 143 (MAT_WOOD_PINE) models the targets and Material Model 20 (MAT_RIGID) models the projectiles. The AOPY option represents the ply direction for the targets. The longitudinal direction is set along the y-axis and the transverse direction is set in the z-direction.

The primary features of the Material Model 143 (MAT_WOOD_PINE) are:

- Transverse isotropy is used for the elastic constitutive equations (different properties are modeled parallel and perpendicular to the grain)
- Yielding, with associated plastic flow characteristics, is modeled with separate yield (failure) surfaces for the parallel- and perpendicular-to-the-grain modes
- Hardening in compression is formulated with translating yield surfaces
- Post-peak softening is formulated with separate damage models for the parallel- and perpendicular-to-the-grain modes
- Strength enhancement at high strain rates is included

Table 18 describes the default material properties used for the Southern Pine Wood.

Table 18: Southern Pine Material Properties

All units are kg, mm, ms, kN, Gpa)	
Property	**Value**
Density	6.731E-07
Stiffness:	
Parallel Normal Modulus, EL	11.35000
Perpendicular Normal Modulus, ET	0.24680
Parallel Shear Modulus, GLT	0.71520
Perpendicular Shear Modulus, GLR	0.08751
Parallel Major Poisson's Ratio, PR	0.15680
Strength:	
Parallel Tensile Strength, Xt	0.04003
Parallel Compressive Strength, Xc	0.01332
Perpendicular Tensile Strength, Yt	0.00096
Perpendicular Compressive Strength, Yc	0.00257
Parallel Shear Strength, Sxy	0.00428
Perpendicular Shear Strength, Syz	0.00599
Damage:	
Parallel Fracture Energy in Tension, Gf1	0.02005
Parallel Fracture Energy in Shear, Gf2	0.04148
Parallel Softening Parameter, Bfit	30
Parallel Maximum Damage, Dmax	0.999
Perpendicular Fracture Energy in Tension, Gf1	0.00040
Perpendicular Fracture Energy in Shear, Gf2	0.00830
Perpendicular Softening Parameter, Dfit	30
Perpendicular Maximum Damage, Dmax	0.99
Hardening:	
Parallel Hardening Initiation, Npar	0.5
Parallel Hardening Rate, Cpar	1008
Perpendicular Hardening Initiation, Nper	0.4
Perpendicular Hardening Rate, Cper	252

The projectile considered throughout this thesis is a 15 lb, 12 foot long 2 x 4 timber. Modeling a projectile with this geometry would require tremendous computational time (primarily due to the length); therefore, the model consists of a simulated projectile. The simulated projectile possesses the identical dynamic properties of the original projectile in a more compact package without affecting the results of the simulation. The model projectile dimensions are 3.175 mm x 3.175 mm x 3.175 mm. The use of 3-D solid elements allow for additional ease of use and superior stability for contact problems. The basis of the simulation requires solutions of deformable body mechanic equation systems with a finite element methodology. 3-D steps solve the problems. Throughout the analyses, projectiles are rigid and the targets (plywood) possess geometric nonlinearity caused by large strain due to impact.

As a result of the simulation, projectile penetration or lack of penetration through the target provides results. In the case of penetration through the target, the remaining kinetic energy allows for the prediction of the residual velocities. Impact velocity is the primary parameter used in the simulation analysis.

Results and Discussions

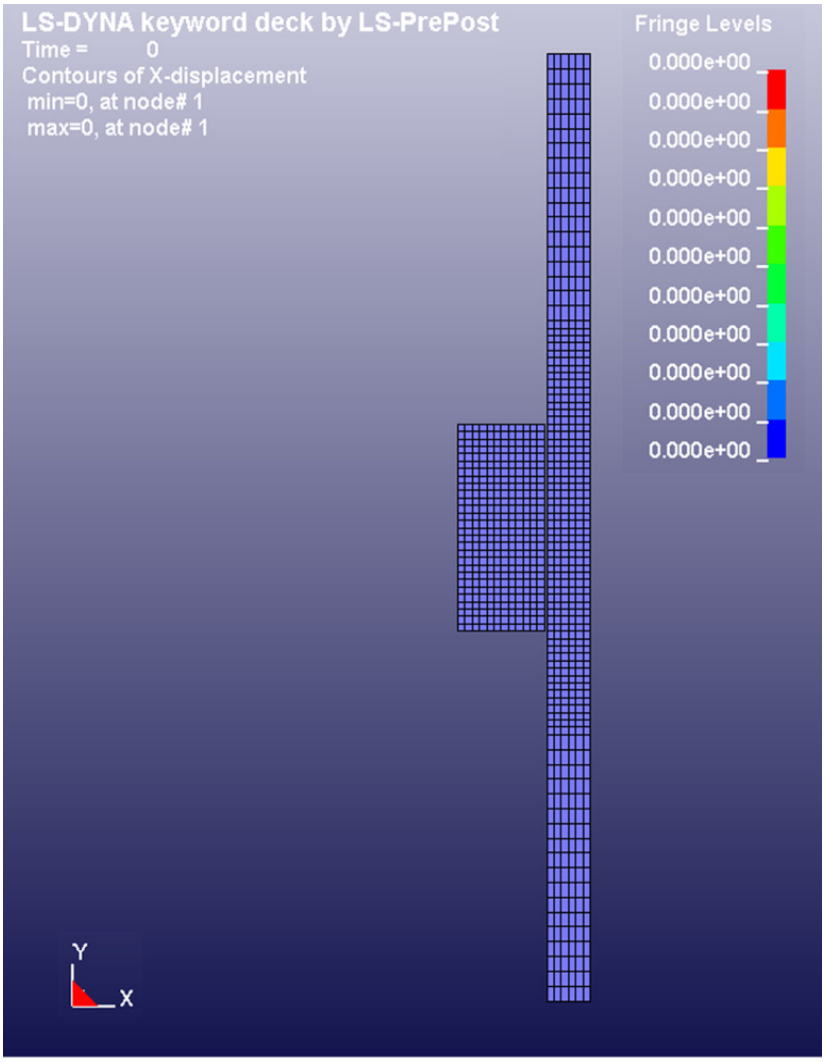

Figure 72: Side View of Finite Element Mesh

Figure 72 shows the lateral view of the computational finite element model with no impact at time zero. To find the limiting value of impact velocities for penetration, simulations are performed for velocities of 4 m/s, 6 m/s, 8 m/s, 10 m/s, 12 m/s, 13 m/s, 14 m/s, 15 m/s, 17 m/s, 18 m/s, 20 m/s, 22.5 m/s. Figures 73-84 show the impact velocity profiles. Figure 73 illustrates the first example. At a projectile velocity of 4 m/s, the total energy absorption by the plywood deformation causes the projectile to bounce back at approximately 3.5 m/s in the negative direction of X. Note that in Figures 73-78, the rigid body velocities go into the negative (below zero) region of the charts. Similar behavior exists until the impact velocity reaches approximately 14 m/s (31.3 mph), as shown in Figure 79. At this impact velocity, the projectile penetrates the plywood and travels with a residual velocity of 1.87 m/s (4.2 mph). Note that the rigid body velocity does not go into the negative region of the chart. Simulation at this impact velocity is important as it predicts the limiting velocity for penetration. TTU test results indicate that the range of limiting impact velocity for penetration is between 13.2 and 14 m/s (29 and 31 mph). [18] Note that since the simulation result at this impact velocity indicates that the remaining (residual) velocity is 1.87 m /s, the limiting velocity for penetration is somewhere below 14 m/s (31.3 mph). This is in reasonable agreement with the TTU experimental results.

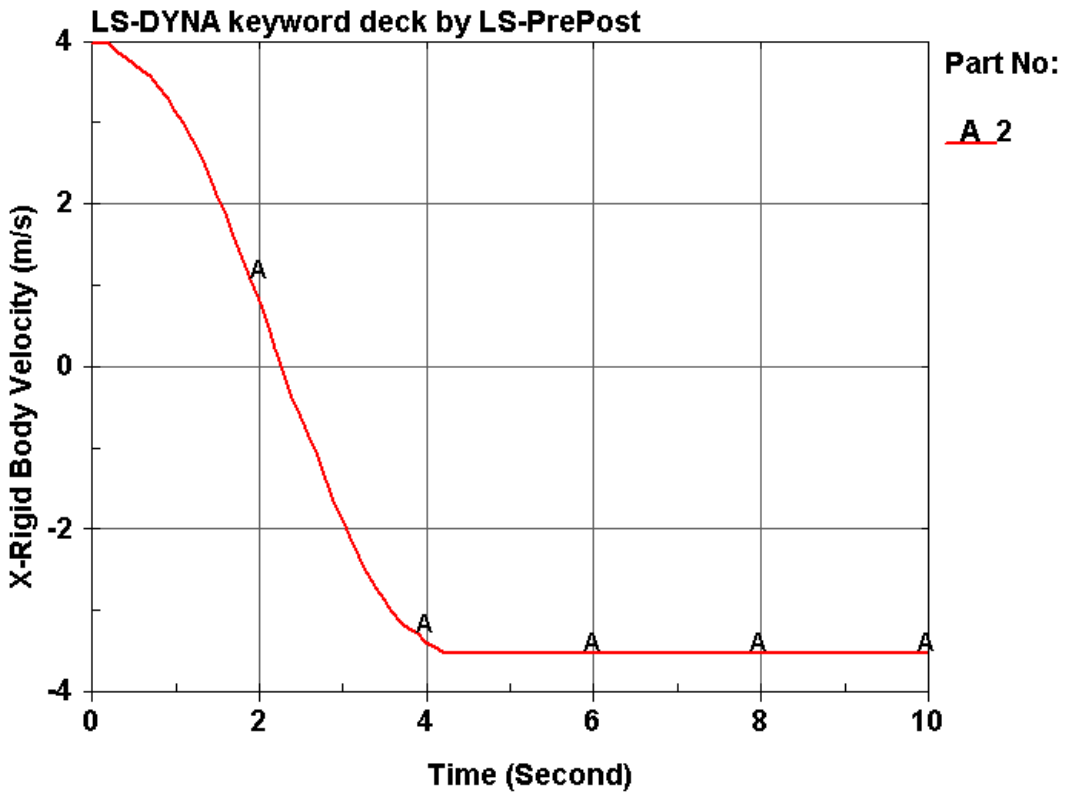

Figure 73: 4 m/s Impact Velocity Time History

At 4 m/s, the projectile strikes the target and is repelled in the direction from which it came. Note the transition of the velocity from a positive value to a negative value in Figure 73. At this impact velocity, the rebound velocity is 3.5 m/s. This represents a rebound velocity that is 88% of the initial impact velocity. This suggests that the target absorbed very little of the kinetic energy.

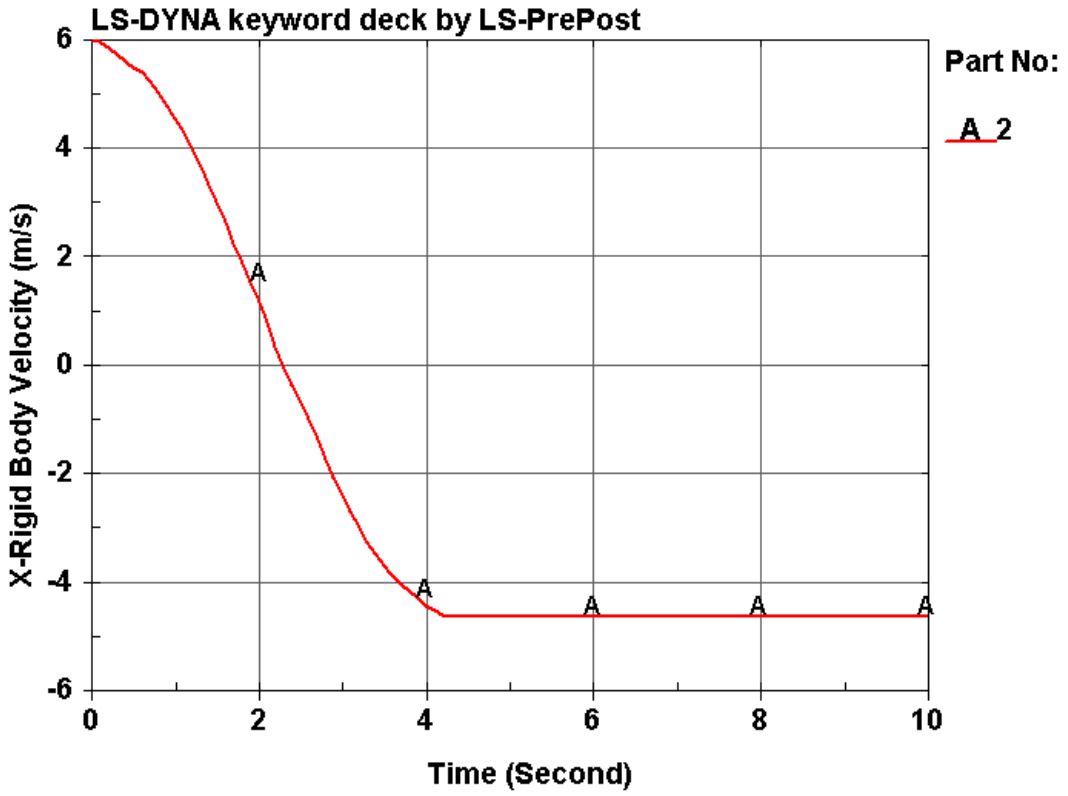

Figure 74: 6 m/s Impact Velocity Time History

At 6 m/s, as in the previous example, the projectile strikes the target and is repelled in the direction from which it came. Again there is a transition of the velocity from a positive value to a negative value as shown in Figure 74. At this impact velocity, the rebound velocity is 4.6 m/s. This represents a rebound velocity that is 77% of the initial impact velocity. This suggests that the target absorbed a larger amount of the kinetic energy than at the 4 m/s impact.

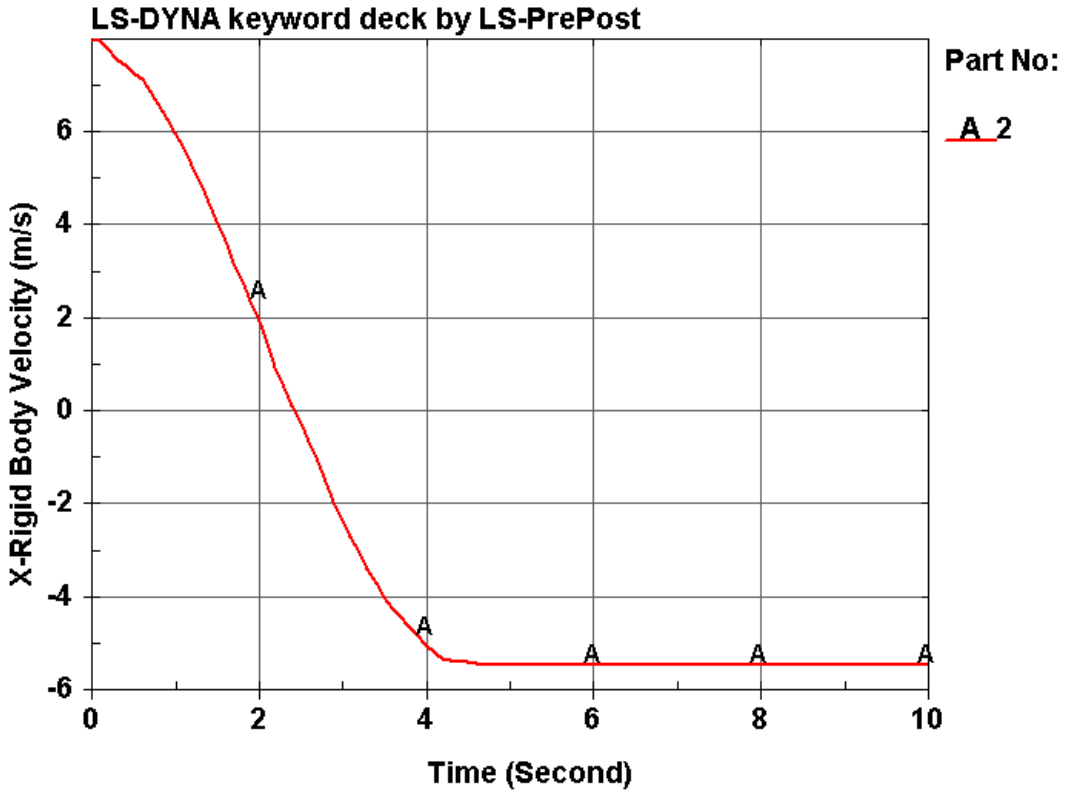

Figure 75: 8 m/s Impact Velocity Time History

At 8 m/s, as in the previous examples, the projectile strikes the target and is repelled in the direction from which it came. Again there is a transition of the velocity from a positive value to a negative value as shown in Figure 75. At this impact velocity, the rebound velocity is 5.43 m/s. This represents a rebound velocity that is 68% of the initial impact velocity. This suggests that the target is absorbing more of the energy as the impact velocity increases. As this trend continues, the target starts to show more deformation and higher levels of stress, which is illustrated later.

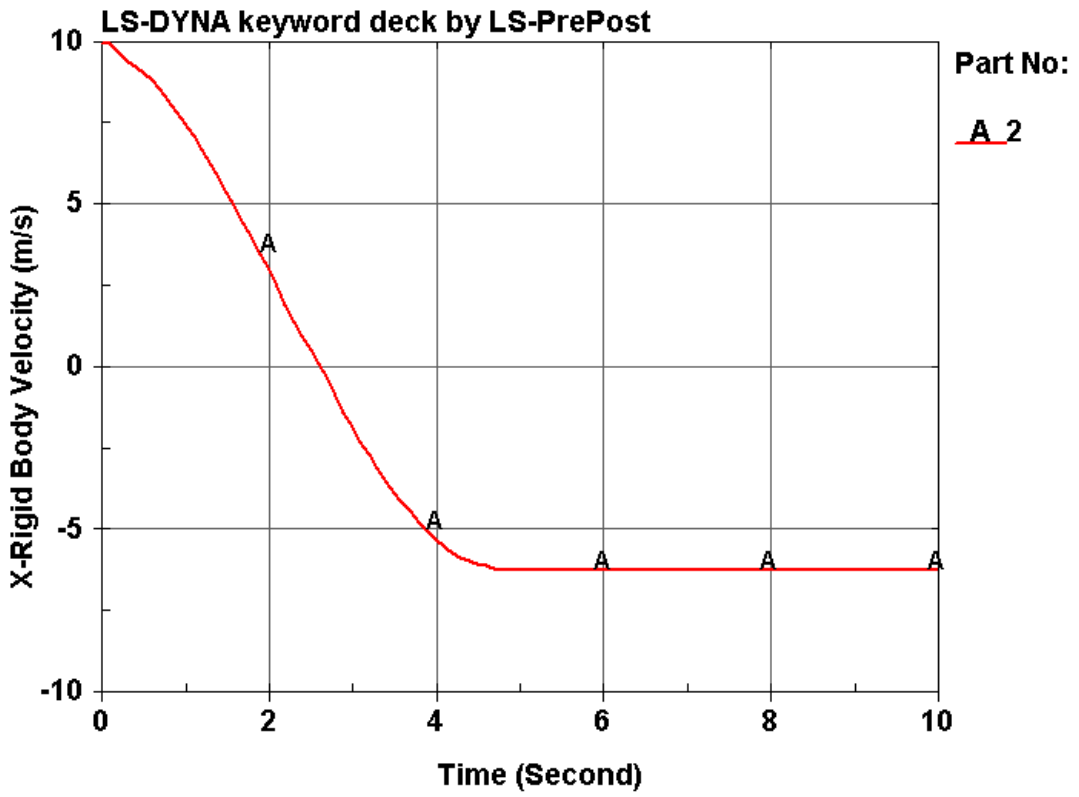

Figure 76: 10 m/s Impact Velocity Time History

At 10 m/s, as in the previous examples, the projectile strikes the target and is repelled in the direction from which it came. Again there is a transition of the velocity from a positive value to a negative value as shown in Figure 76. At this impact velocity, the rebound velocity is 6.22 m/s. This represents a rebound velocity that is 62% of the initial impact velocity. Again, this confirms that the target is absorbing more of the energy as the impact velocity increases. As this trend continues, the target shows more deformation and higher levels of stress, which is illustrated later.

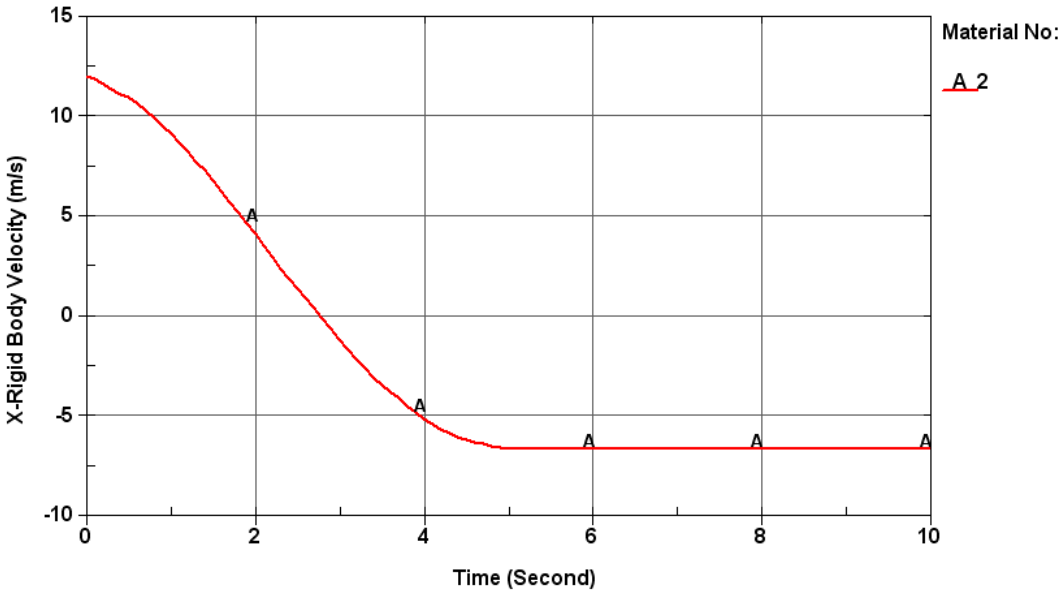

Figure 77: 12 m/s Impact Velocity Time History

At 12 m/s, as in the previous examples, the projectile strikes the target and is repelled in the direction from which it came. Again there is a transition of the velocity from a positive value to a negative value as shown in Figure 77. At this impact velocity, the rebound velocity is 6.65 m/s. This represents a rebound velocity that is 55% of the initial impact velocity. Again, this confirms that the target is absorbing more of the energy as the impact velocity increases. As this trend continues, the target shows more deformation and higher levels of stress, which is illustrated later.

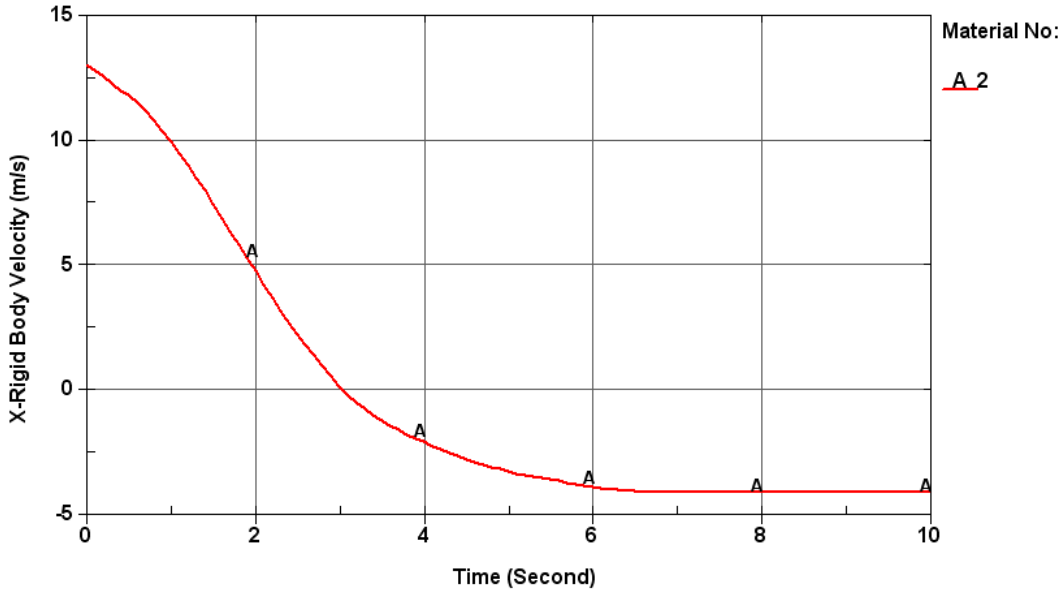

Figure 78: 13 m/s Impact Velocity Time History

At 13 m/s, as in the previous examples, the projectile strikes the target and is repelled in the direction from which it came; however, there is a definite change in the trend at this impact velocity because penetration is eminent at this point. There is still a transition of the velocity from a positive value to a negative value as shown in Figure 78, but the rebound velocity decreases. At this impact velocity, the rebound velocity is 4.13 m/s. This represents a rebound velocity that is only 31% of the initial impact velocity. The fact that the target is absorbing a greater portion of the energy than in the previous examples, thus the rebound velocity decreases as penetration nears.

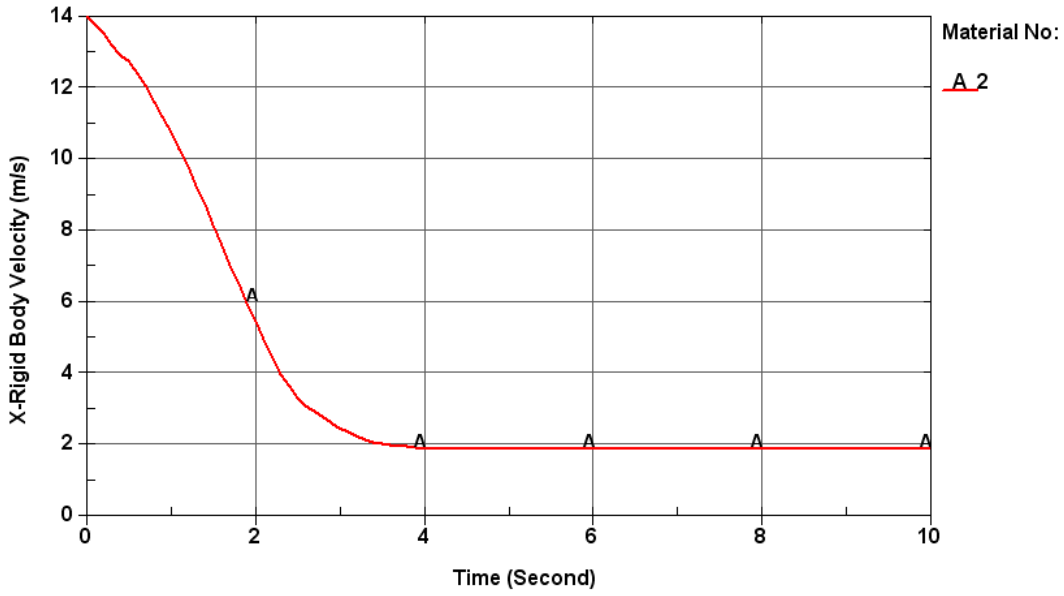

Figure 79: 14 m/s Impact Velocity Time History

At 14 m/s, the projectile penetrates the target. In this case the velocity does not enter the negative region of the graph as shown in Figure 79. Note that the velocity of the projectile decreases considerably, but remains in the positive X direction. At this impact velocity, there is no rebound phenomenon, but a projectile residual velocity exists. The residual velocity is quite low at 1.87 m/s (only 13% of the impact velocity) because the target absorbs most of the energy.

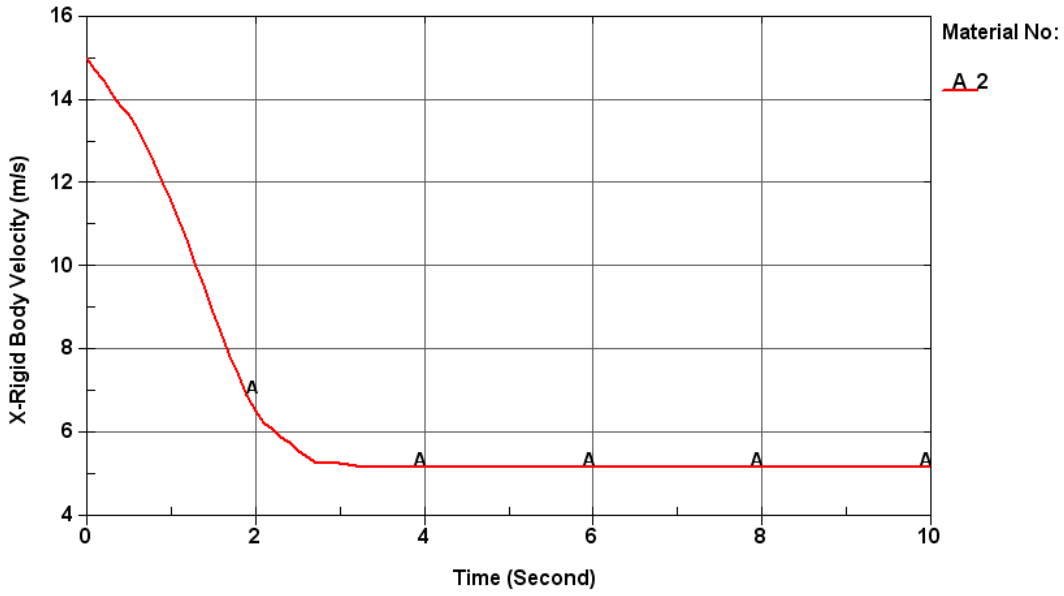

Figure 80: 15 m/s Impact Velocity Time History

At 15 m/s, the projectile again penetrates the target. As previously, the velocity does not enter the negative region of the graph as shown in Figure 80, but the velocity of the post-penetrating projectile has increased since the previous example to 5.169 m/s. This represents 34% of the velocity of the impact projectile. This suggests that the target has absorbed a great percentage of the energy; however, there exist enough left over to increase the residual velocity from the previous example.

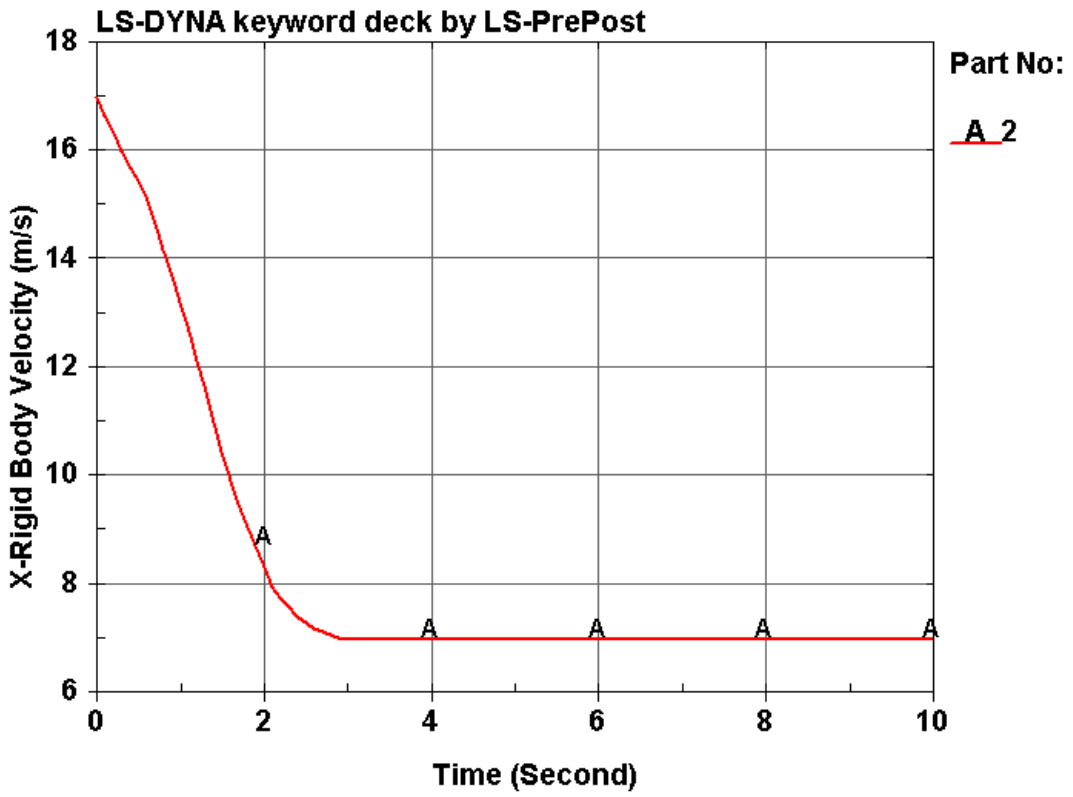

Figure 81: 17 m/s Impact Velocity Time History

At 17 m/s, the projectile again penetrates the target. Note that the post-penetrating projectile velocity continues to increase, as indicated in Figure 81, but the velocity of the post-penetrating projectile continues to increase since the previous example to 6.996 m/s. This represents 41% of the velocity of the impact projectile. This suggests that the target is absorbing a lesser percentage of the energy, allowing the projectile to continue to increase in velocity after impact.

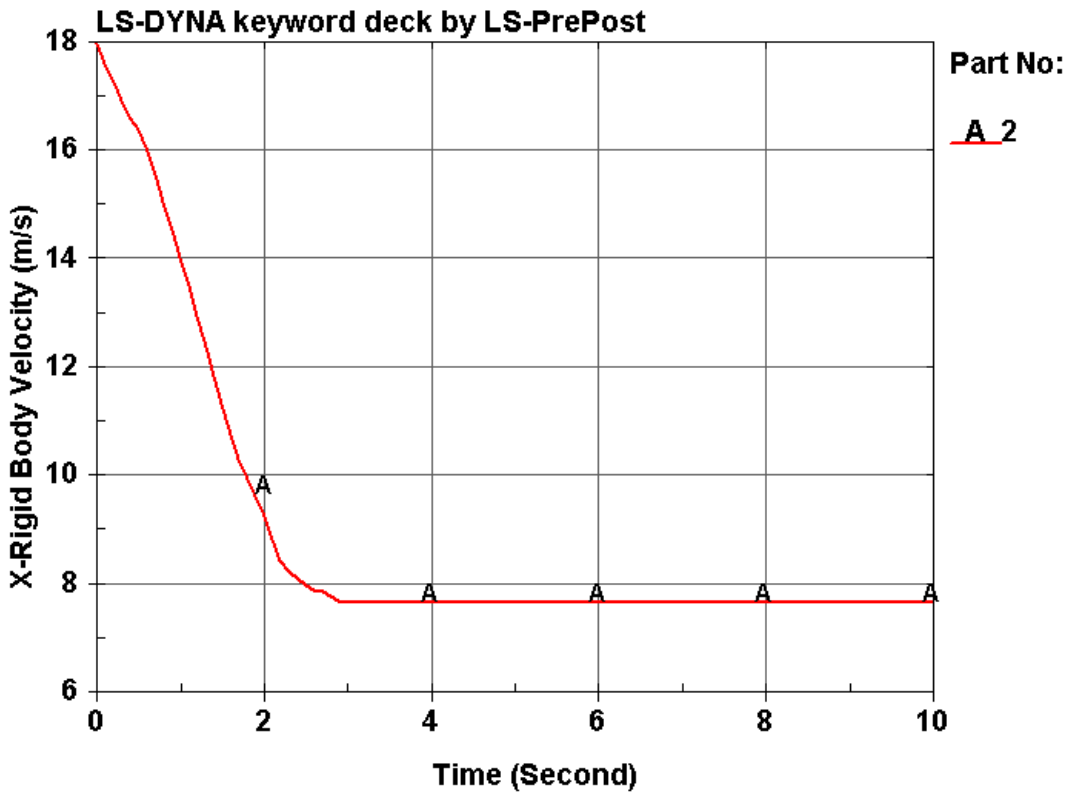

Figure 82: 18 m/s Impact Velocity Time History

At 18 m/s, the projectile continues to penetrate the target. Note that the post-penetrating projectile velocity continues to increase, as indicated in Figure 82, but the velocity of the post-penetrating projectile continues to increase since the previous example to 7.66 m/s. This represents 43% of the velocity of the impact projectile. This suggests that the target is absorbing a lesser percentage of the energy, allowing the projectile to continue to increase in velocity after impact.

.

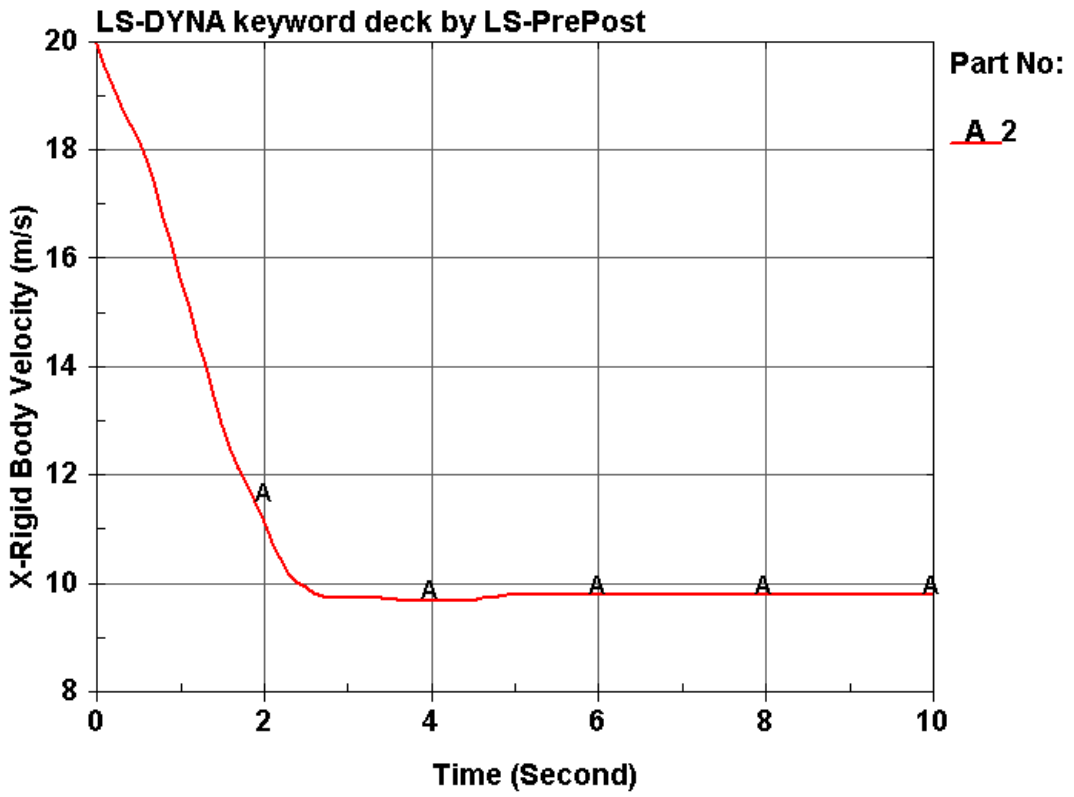

Figure 83: 20 m/s Impact Velocity Time History

At 20 m/s, the projectile, as expected, penetrates the target. Note that the post-penetrating projectile velocity continues to increase, as indicated in Figure 83, but the velocity of the post-penetrating projectile continues to increase since the previous example to 9.71 m/s. This represents 49% of the velocity of the impact projectile. This suggests that the target is absorbing a lesser percentage of the energy, allowing the projectile to continue to increase in velocity after impact. As is illustrated later, at this impact velocity, the target is starting to experience extensive damage.

.

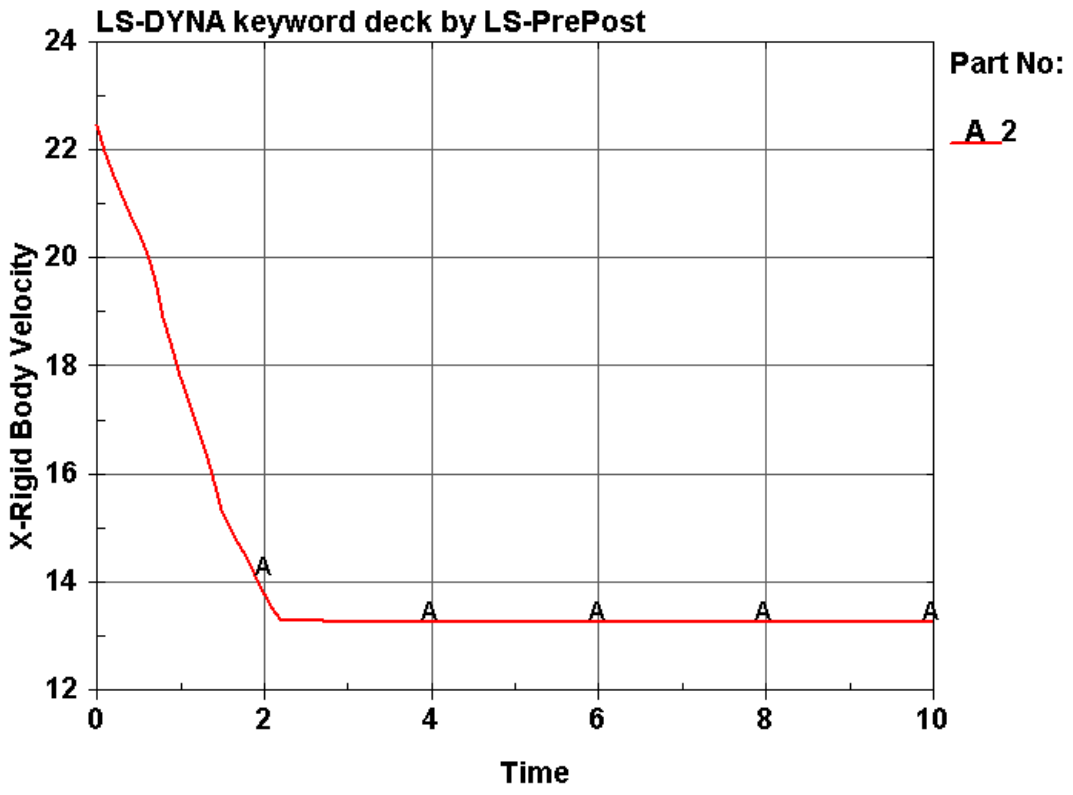

Figure 84: 22.5 m/s Impact Velocity Time History

At 22.5 m/s, the projectile, as expected, penetrates the target. Note that the post-penetrating projectile velocity continues to increase, as indicated in Figure 84, but the velocity of the post-penetrating projectile continues to increase since the previous example to 12.22 m/s. This represents 54% of the velocity of the impact projectile. This suggests that the target is absorbing a lesser percentage of the energy, allowing the projectile to continue to increase in velocity after impact. As is illustrated later, at this impact velocity, the target has experienced catastrophic failure and occurs to further protection as an impact barrier.

Figure 85 illustrates how the residual velocity changes with respect to impact velocity. It is interesting to note that this change remains linear until the impact velocity reaches approximately 15 m/s. After this velocity, the residual velocity changes to show a more non-linear behavior until the impact velocity of 18 m/sec and then remains linear again.

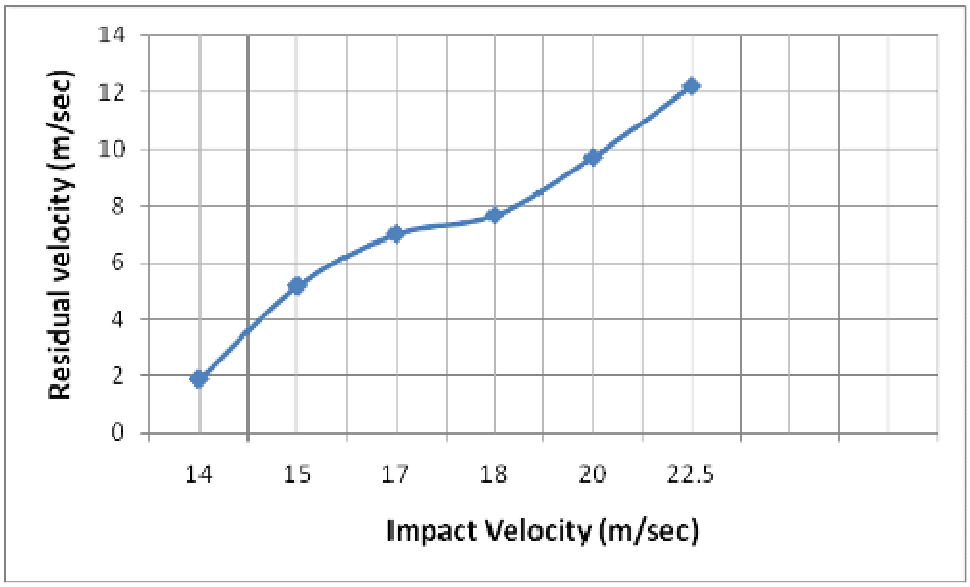

Figure 85: Relationship between Impact Velocity and Residual Velocity

The following figures illustrate the simulated effect that the projectile has on the target at various impact velocities.

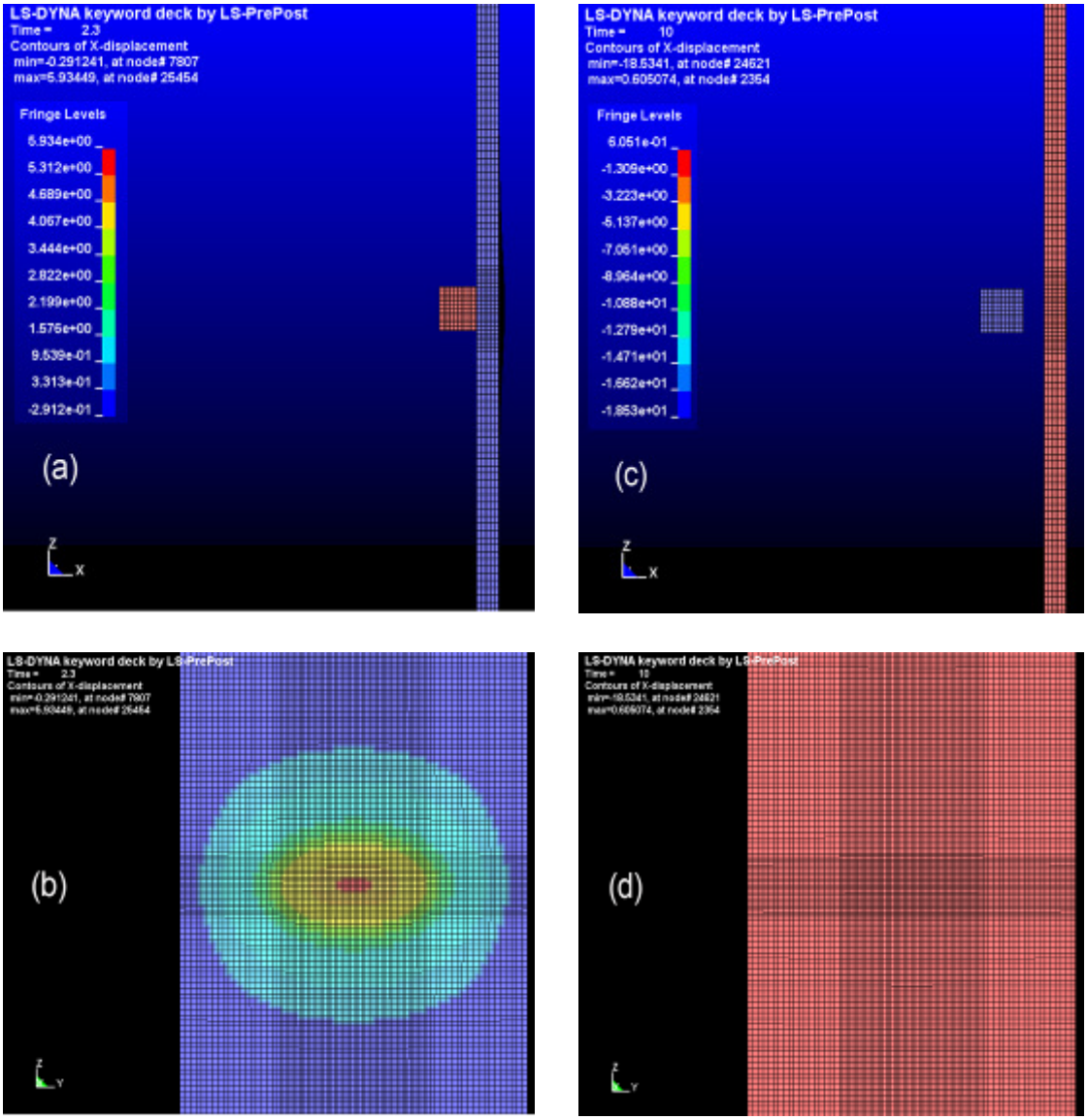

Figure 86: Plywood Subjected to 4 m/s Impact

In Figure 86, panes (a) and (b) are the lateral and top views respectively at 2.3 seconds after initial impact. Panes (c) and (d) are the lateral and top views respectively of the final deformed configuration (at 10 seconds after initial impact). Note that there is no damage observed after impact; therefore, the deformation is all elastic.

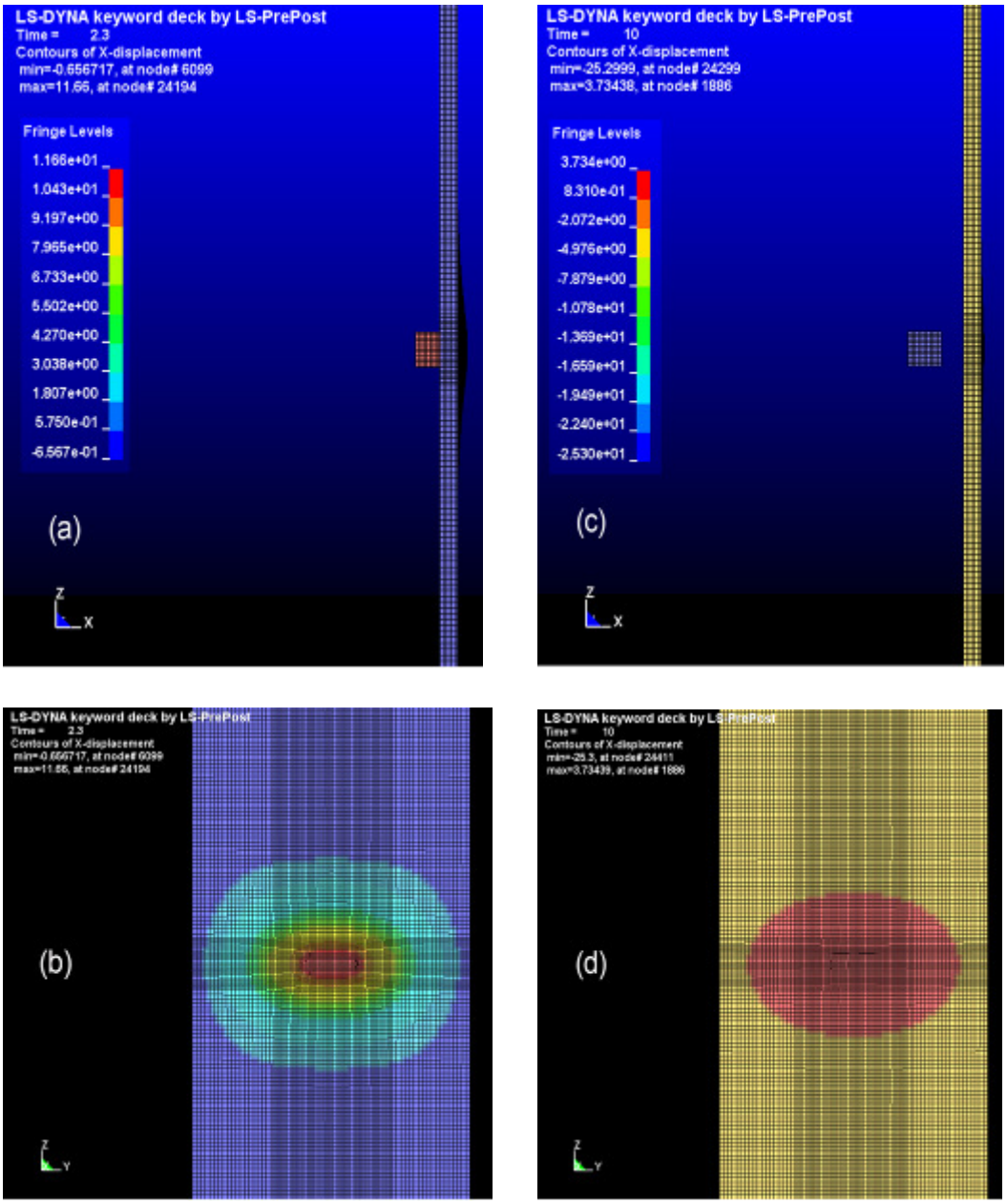

Figure 87: Plywood Subjected to 8 m/s Impact

In Figure 87, panes (a) and (b) are the lateral and top views respectively at 2.3 seconds after initial impact. Panes (c) and (d) are the lateral and top views respectively of the final deformed configuration (at 10 seconds after initial impact). Note that some residual target changes have occurred.

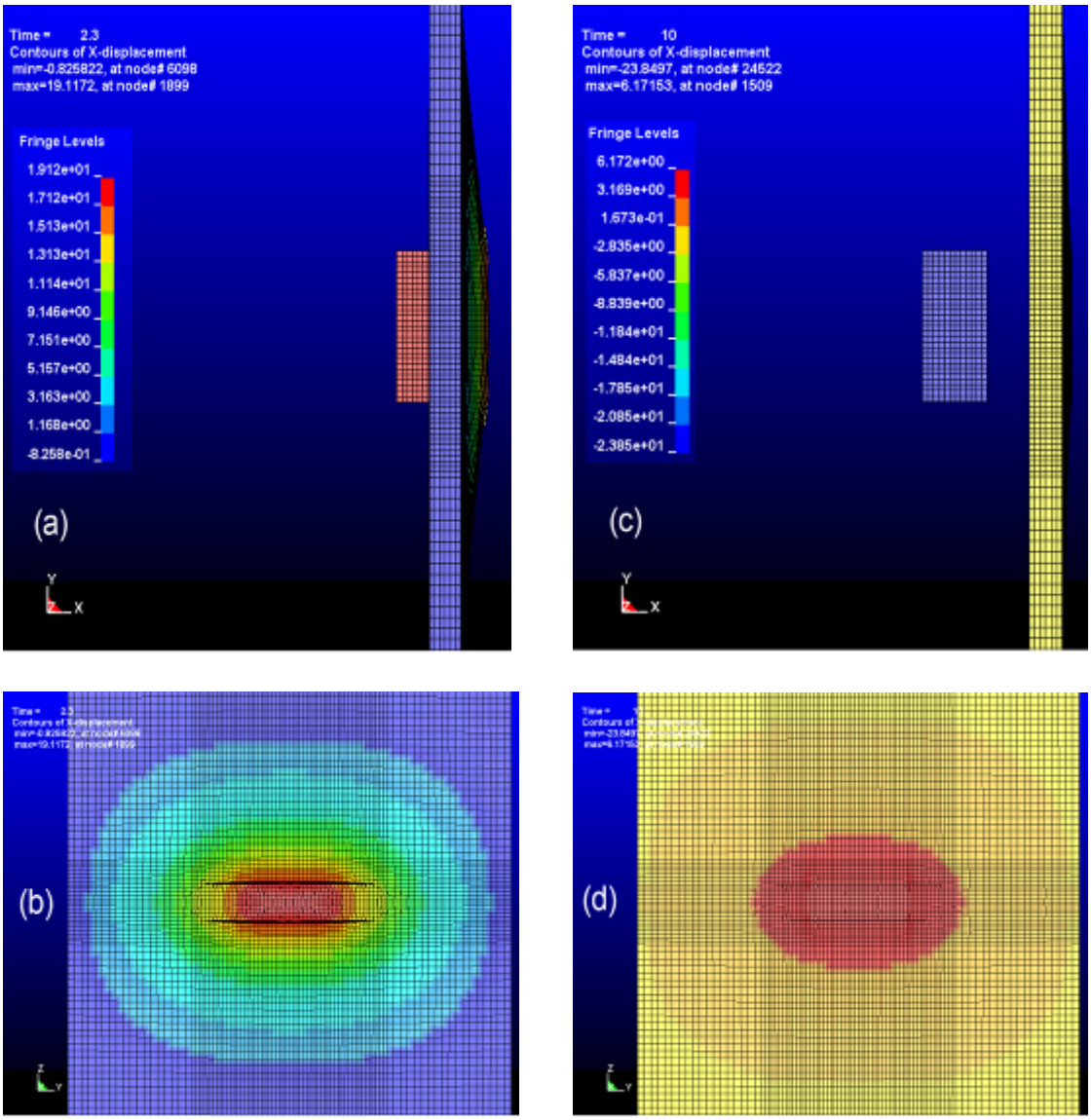

Figure 88: Plywood Subjected to 12 m/s Impact

In Figure 88, panes (a) and (b) are the lateral and top views respectively at 2.3 seconds after initial impact. Panes (c) and (d) are the lateral and top views respectively of the final deformed configuration (at 10 seconds after initial impact). Note that the level of permanent deformation is increasing in area and intensity.

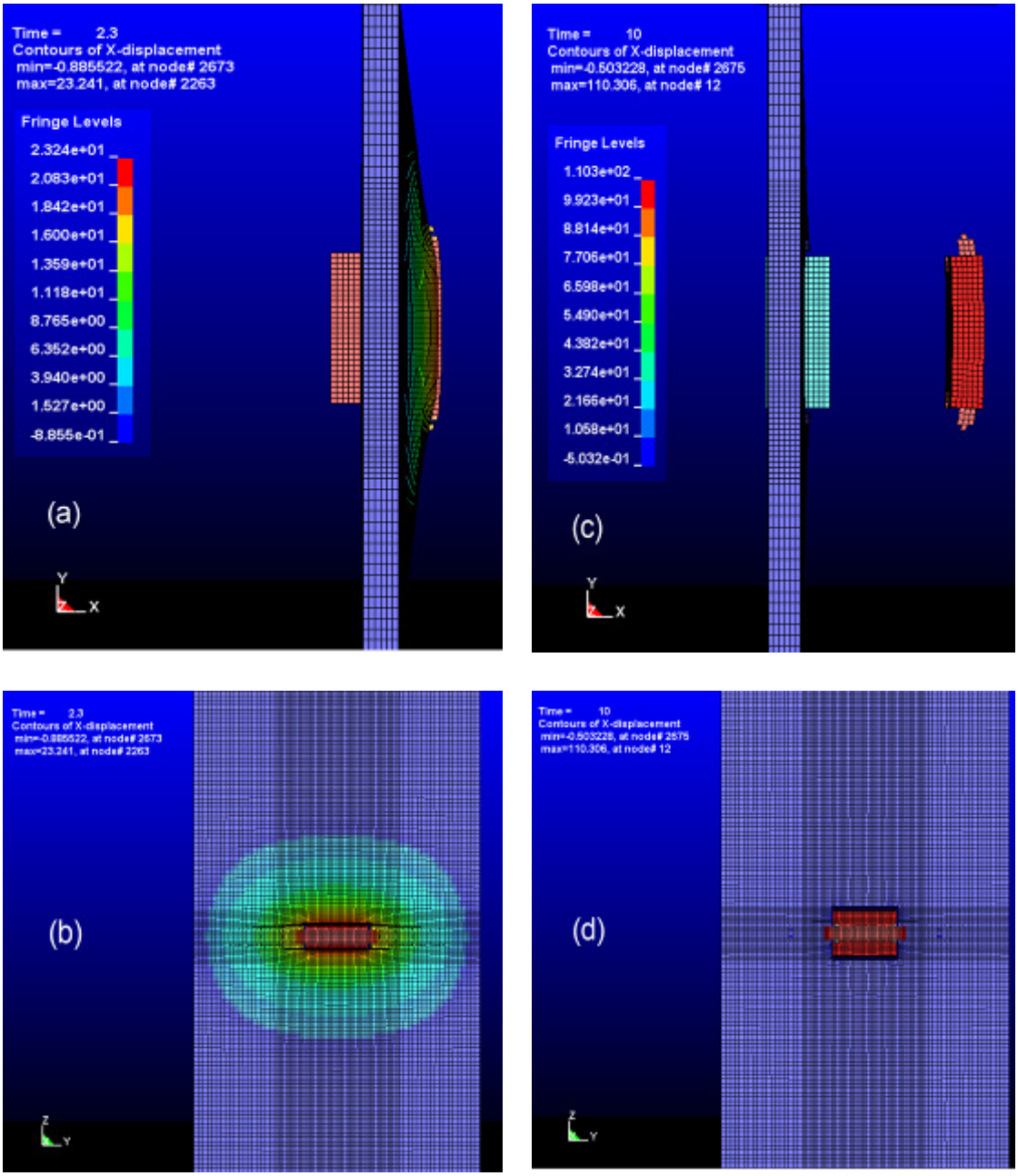

Figure 89: Plywood Subjected to 14 m/s Impact

In Figure 89, panes (a) and (b) are the lateral and top views respectively at 2.3 seconds after initial impact. Panes (c) and (d) are the lateral and top views respectively of the final deformed configuration. Penetration has now occurred and a solid plug ejects from the impact face of the target (see (c)).

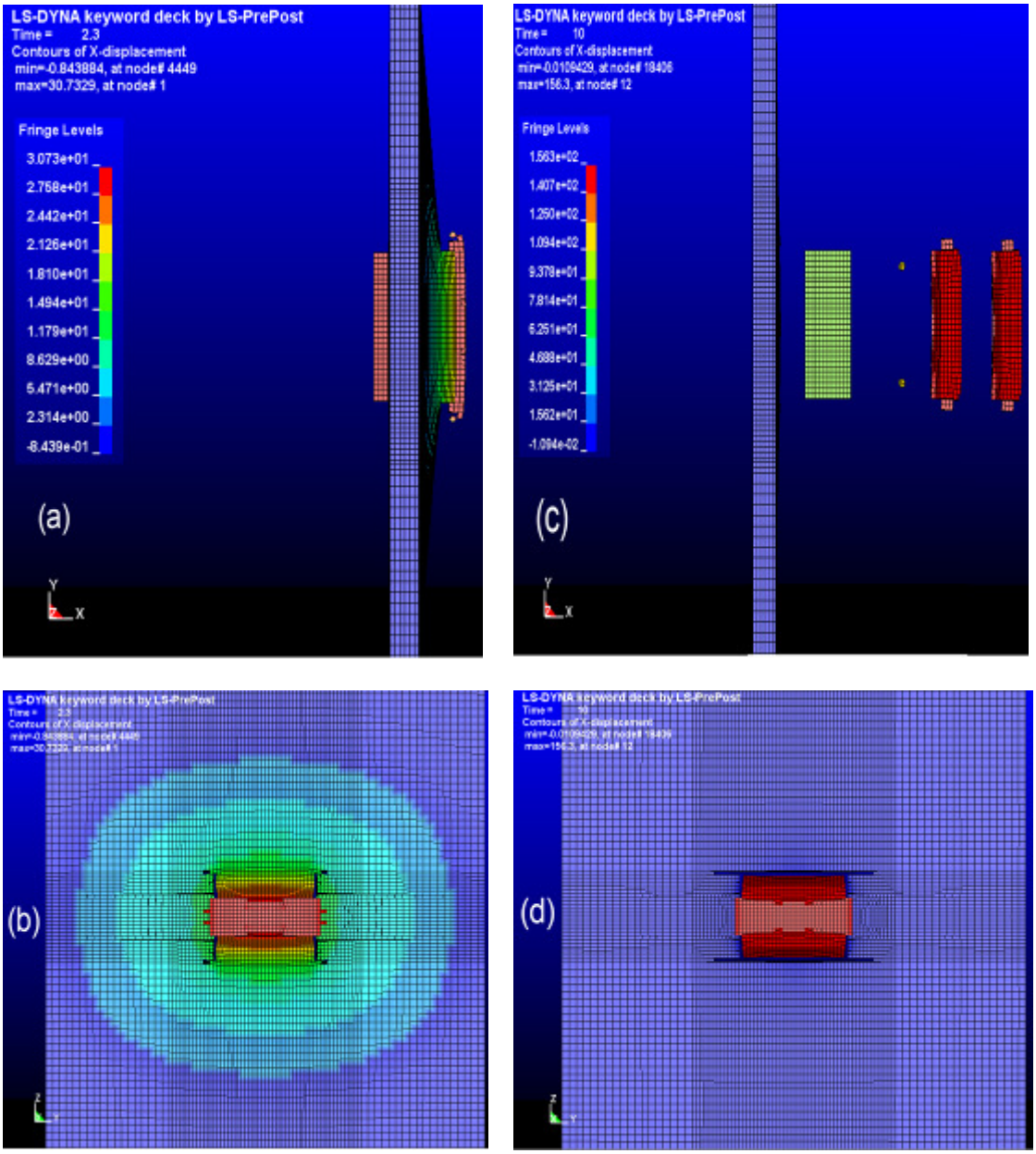

Figure 90: Plywood Subjected to 17 m/s Impact

In Figure 90, panes (a) and (b) are the lateral and top views respectively at 2.3 seconds after initial impact. Panes (c) and (d) are the lateral and top views respectively of the final deformed configuration. As before, the penetrating projectile has dislodged two pieces of plugs plus some debris.

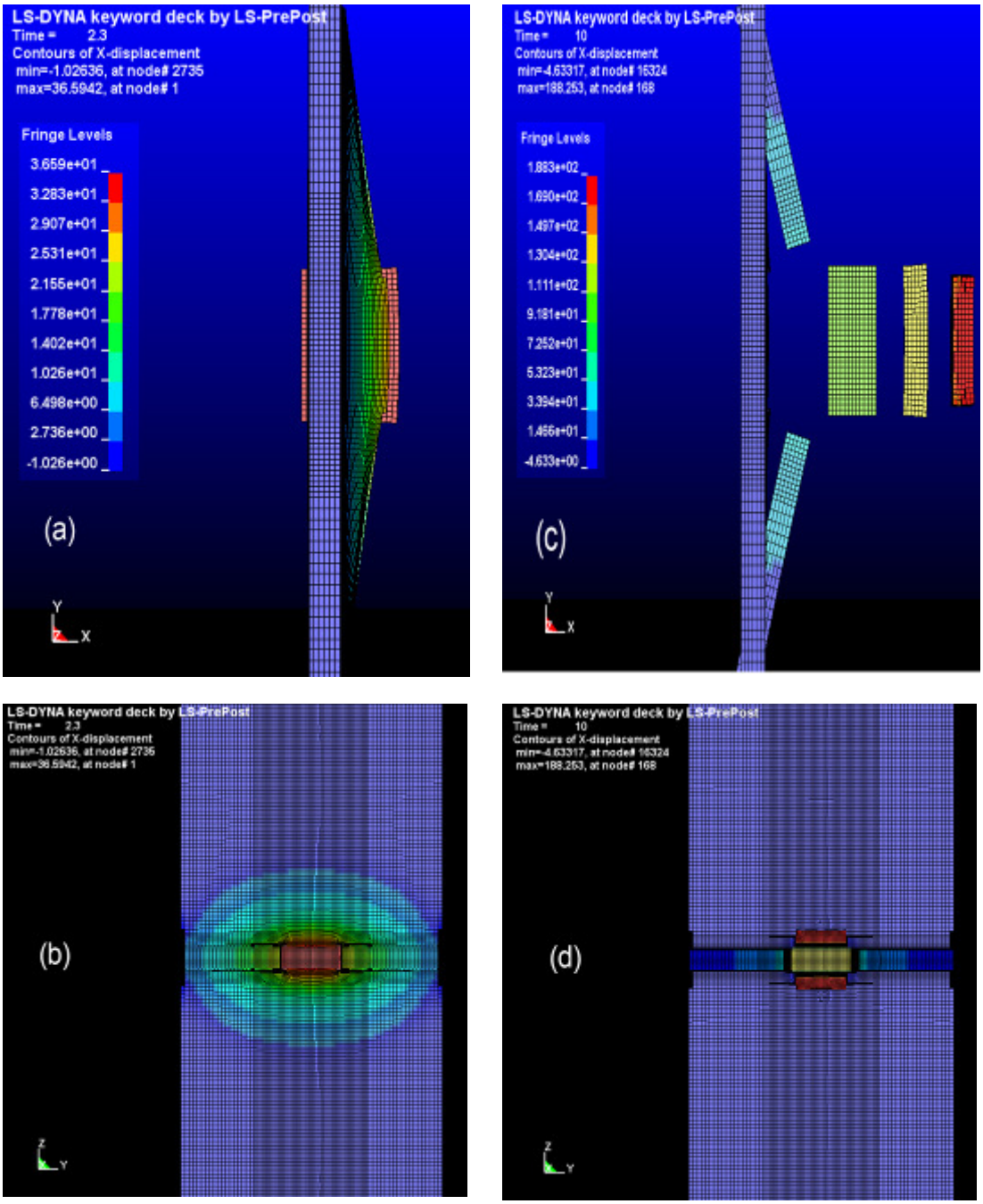

Figure 91: Plywood Subjected to 20 m/s Impact

In Figure 91, panes (a) and (b) are the lateral and top views respectively at 2.3 seconds after initial impact. Panes (c) and (d) are the lateral and top views

respectively of the final deformed configuration. In this case the stresses are sufficient to cause the beginning of catastrophic failure. Additionally, two broken pieces of target are observed.

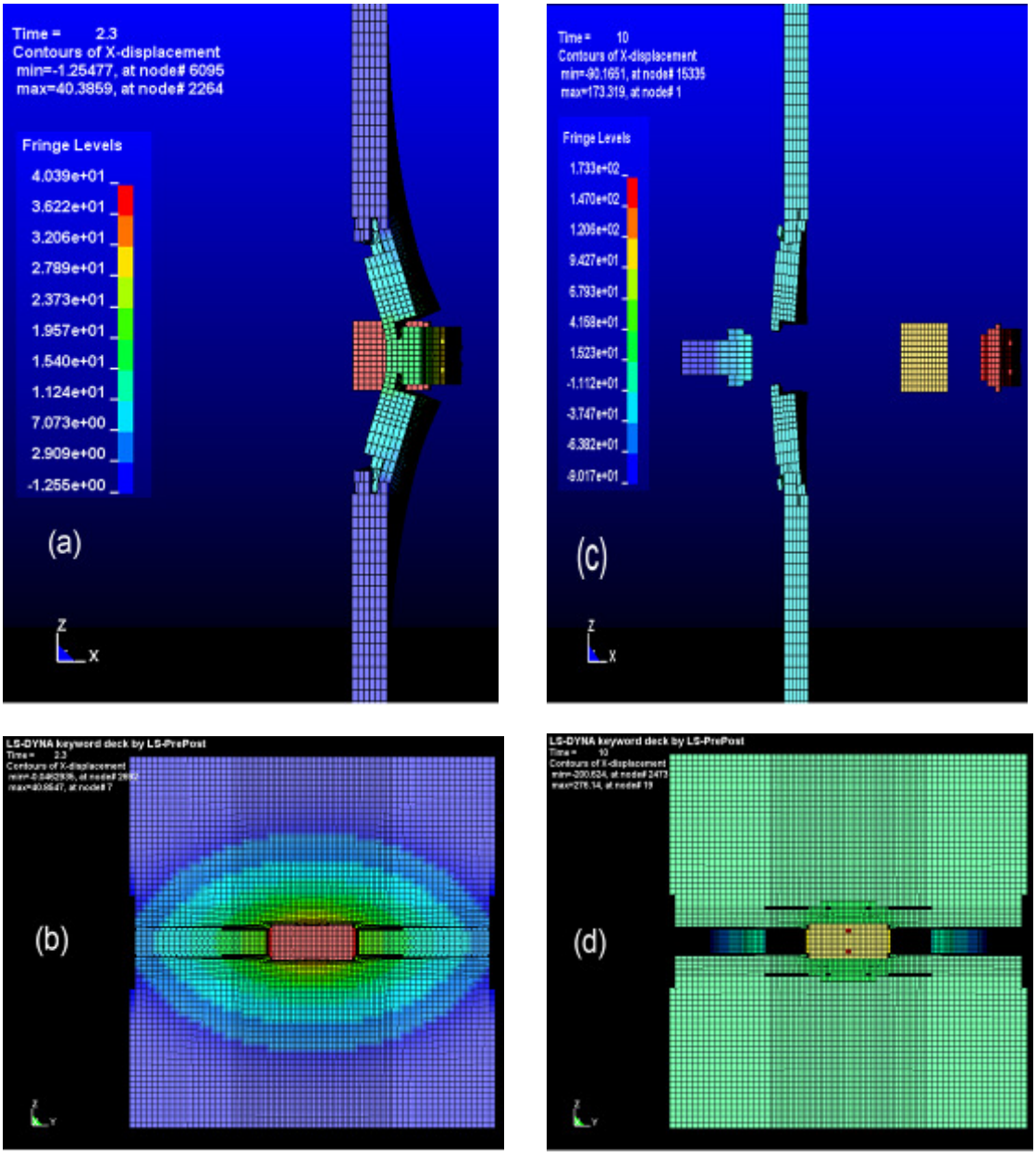

Figure 92: Plywood Subjected to 22.5 m/s Impact

In Figure 92, panes (a) and (b) are the lateral and top views respectively at 2.3 seconds after initial impact. Panes (c) and (d) are the lateral and top views respectively of the final deformed configuration. In this case the forces are very high causing complete failure of the target material. Note that the failure characteristic is entirely different from the previous cases.

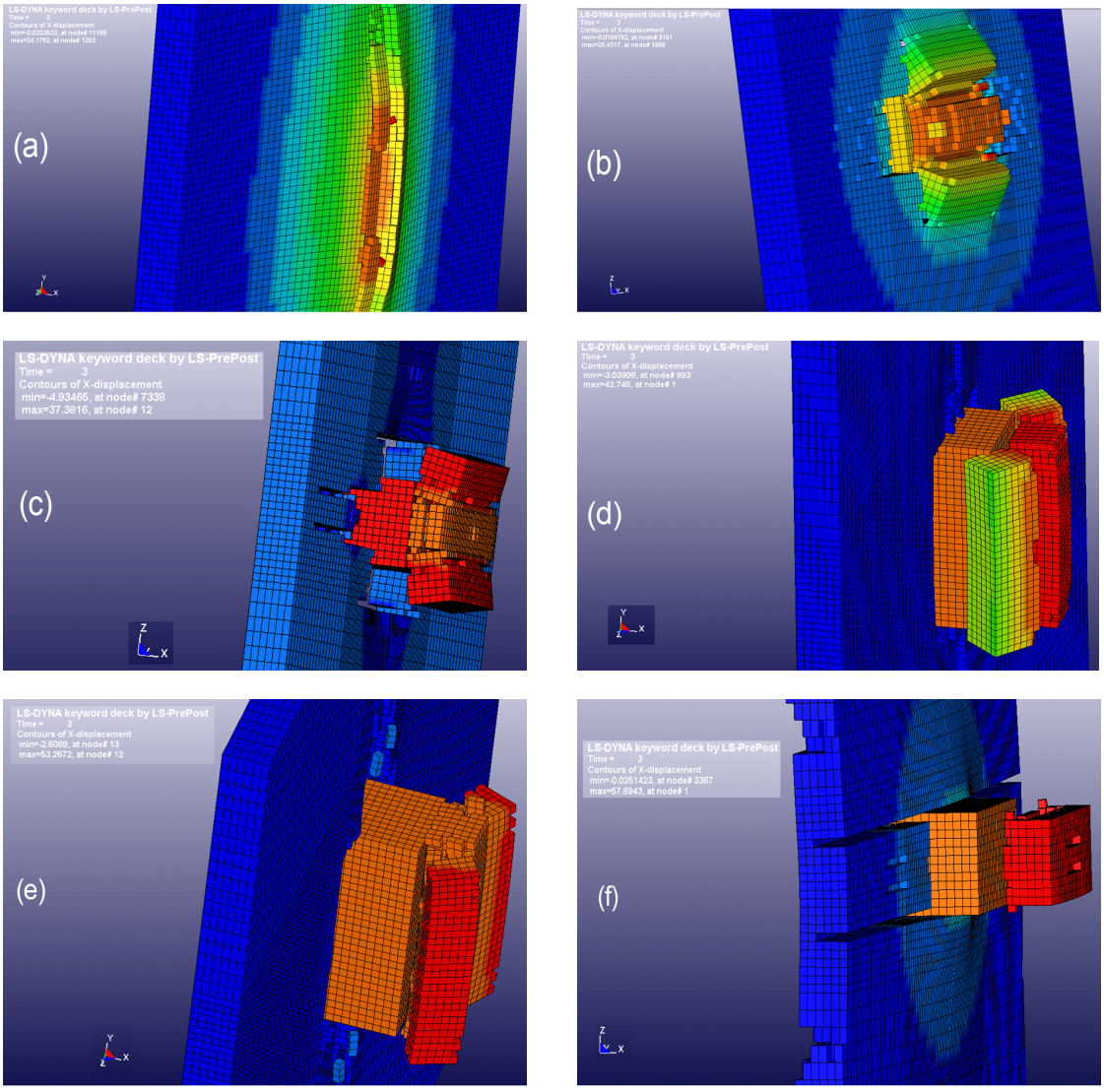

Figure 93: Damage Characteristics at Different Impact Velocities (3 sec after impact)

More insight into the characteristic of the damage on plywood results by examining Figure 93. This figure shows the plywood damage at different impact velocities. These images, at approximately 3 seconds after impact, illustrate the damage pattern in the pine target. The impact velocities are 12 m/s, 13 m/s, 14 m/s, 15 m/s, 18 m/s, and 22.5 m/s as shown in panes (a), (b), (c), (d), (e), and (f) respectively.

At an impact velocity of 12 m/s, there is no penetration and only slight damage on the rear face of the plywood. At impact velocities greater than 13 m/s, the projectile penetrates and the residual velocities exist, as recorded in the projectile velocity time histories in the preceding Figures 79-84.

In pane (a), it is observed that the 12 m/s projectile causes considerable deformation to the target. As the limit velocity is approached the rebound velocity decreases as the target absorbs more of the energy.

In pane (b), the situation described above is intensified. At an impact velocity of 13 m/s, extensive deformation is observed and some target debris is released on the non-impact surface of the target.

Pane (c) illustrates the actual penetration. At 14 m/s, not only is there a plug expelled, but the projectile has now entered the enclosure under protection from the plywood barrier.

Pane (d) illustrates the post limit-velocity penetration. At 15 m/s, the damage to the target has increased as the energy is becoming sufficient to cause not only penetration, but also target deterioration.

Pane (e) illustrates the impending structural failure of the target. With an impact velocity of 18 m/s, target areas surrounding the projectile are delaminating and being expelled into the “safe-area of the enclosure.

In Pane (f), catastrophic failure of the target is beginning. Projectile penetration and target debris are combining to produce a very dangerous environment on the safe side of the barrier.

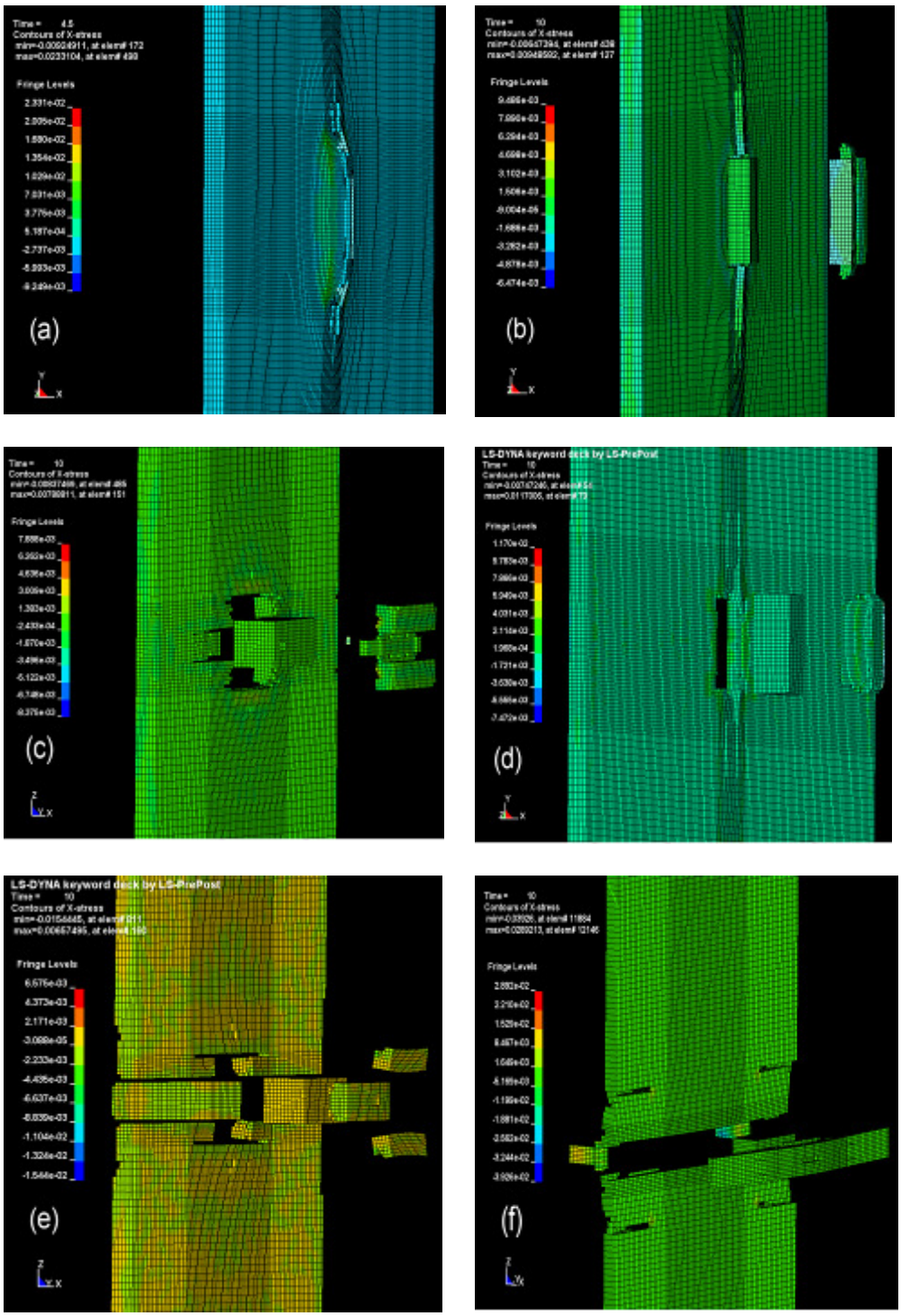

Figure 94: Damage Characteristics at Different Impact Velocities

Stress illustrations in Figure 94 occur after the final deformation has occurred at approximately 10 seconds after initial impact except in pane (a). This case is at the impact velocity of 13 m/sec and occurred at 4.5 seconds which represents the highest stress level at this impact velocity. Deformation after impact velocities of 14 m/s, 15 m/s, 18 m/s, 20 m/s, and 22.5 m/s are illustrated in panes (b), (c), (d), (e), and (f), respectively.

Though pane (a) represents pre-penetration, considerable deformation occurs to the target. As the velocity increases above this level, penetration occurs. Pane (b) illustrates that after an impact of 14 m/s, a substantial target plug itself becomes a projectile. As the velocities increase, this becomes more severe. In panes (c) and (d), impacts of 15 m/s and 18 m/s has caused considerable damage in the target. In pane (e), considerable debris is present in addition to the projectile. Finally in pane (f), the target experiences catastrophic failure and looses any semblance to a protective barrier.

In Figures 95 through 105, there is an examination of the kinetic energy of the plywood target when impacted at various projectile velocities. Since kinetic energy is highly dependant on velocity-squared, the velocities of the substrates (either actual relocation of particles or just vibration) are the primary drivers of the energy value.

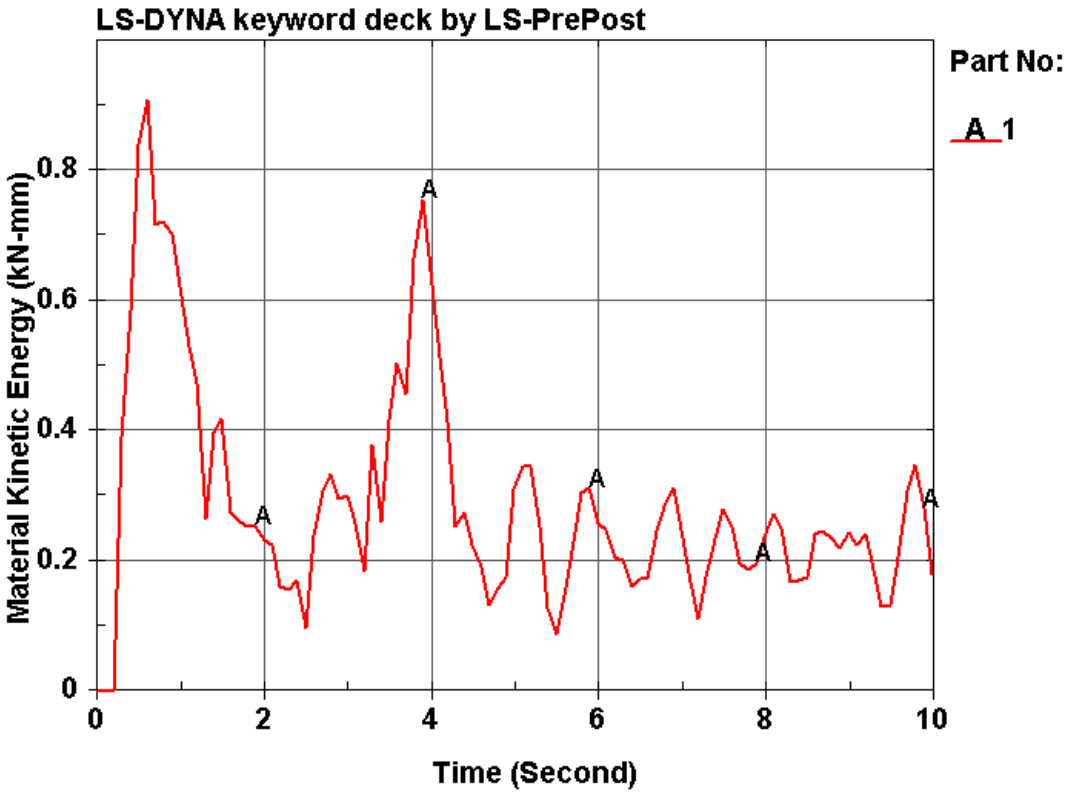

Figure 95: Kinetic Energy Absorbed by Target from 4 m/s Impact

As illustrated in Figure 95, the initial impact creates a spike in kinetic energy in the target. Damped vibration causes a reduction in the initial energy spike followed by a supplemental spike as the material goes through a vibratory regime before damping out at the conclusion.

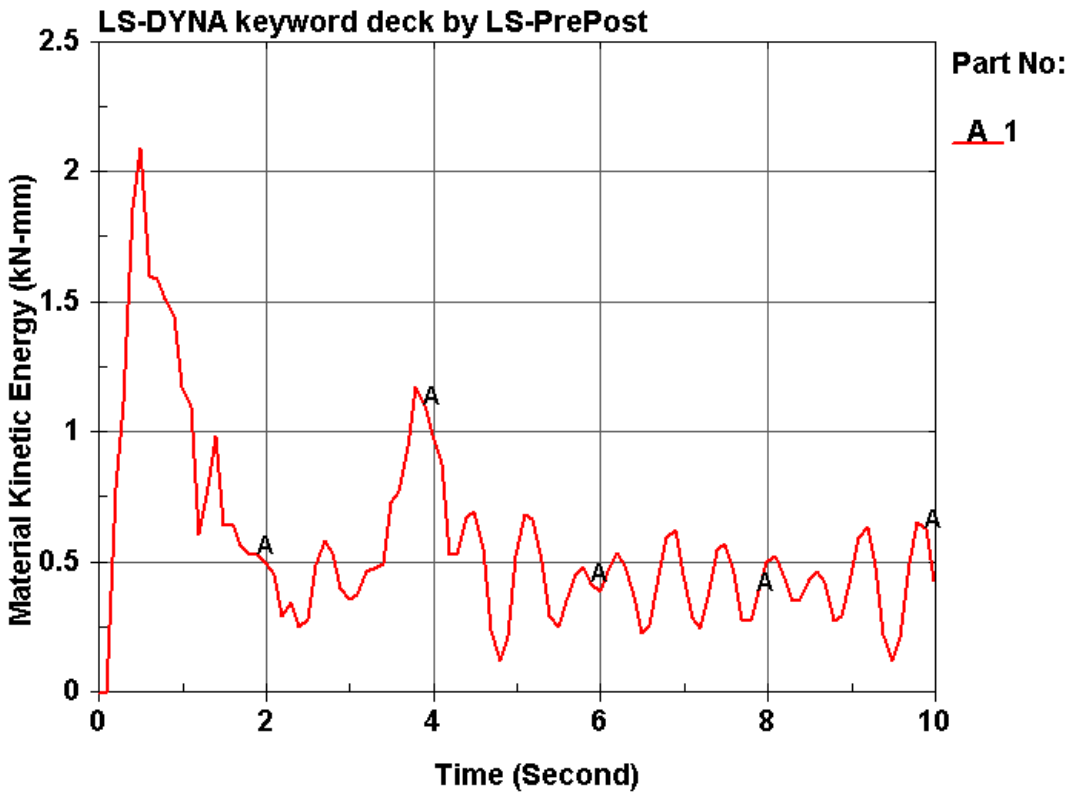

Figure 96: Kinetic Energy Absorbed by Target from 6 m/s Impact

As illustrated in Figure 96, as with the 4 m/s velocity, the initial impact creates a spike in kinetic energy in the target. Damped vibration causes a reduction in the initial energy spike followed by series of lower energy spikes as the material goes through a vibratory regime before damping out at the conclusion.

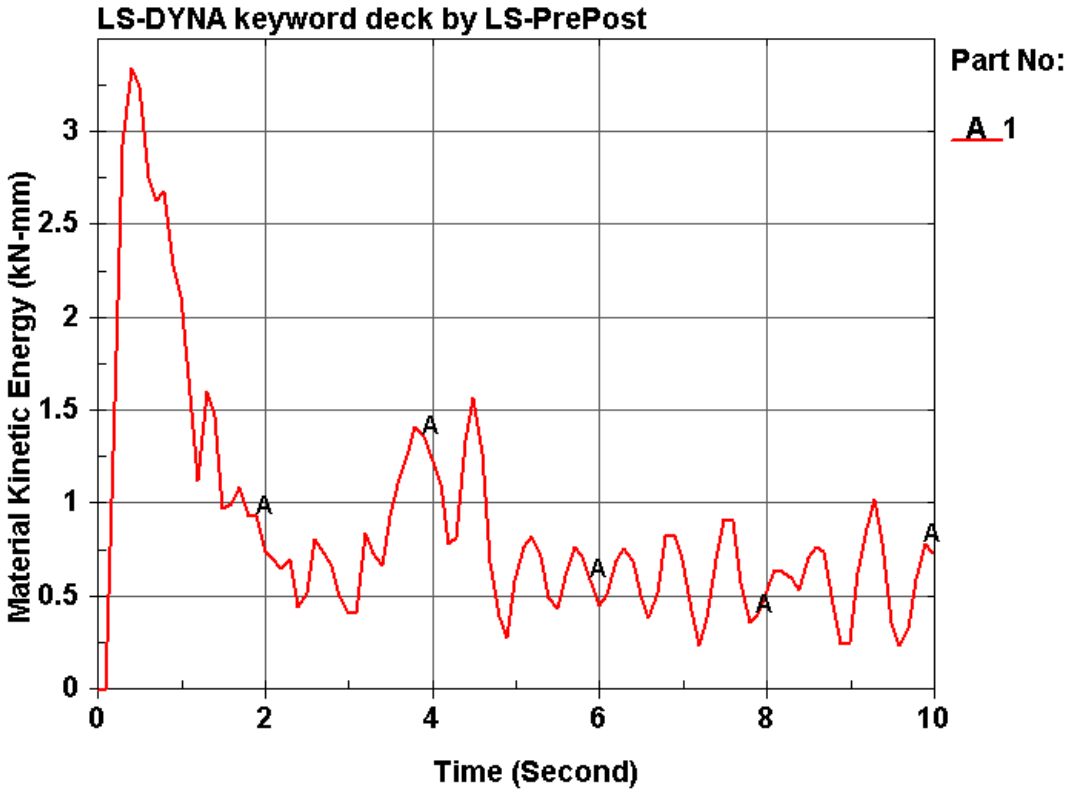

Figure 97: Kinetic Energy Absorbed by Target from 8 m/s Impact

As illustrated in Figure 97, as previously seen, the initial impact creates a spike in kinetic energy in the target. Damped vibration causes a reduction in the initial energy spike followed by series of lower energy spikes as the material goes through a vibratory regime before damping out at the conclusion. Note that the magnitude of second spike is decreasing as the impact velocity increases.

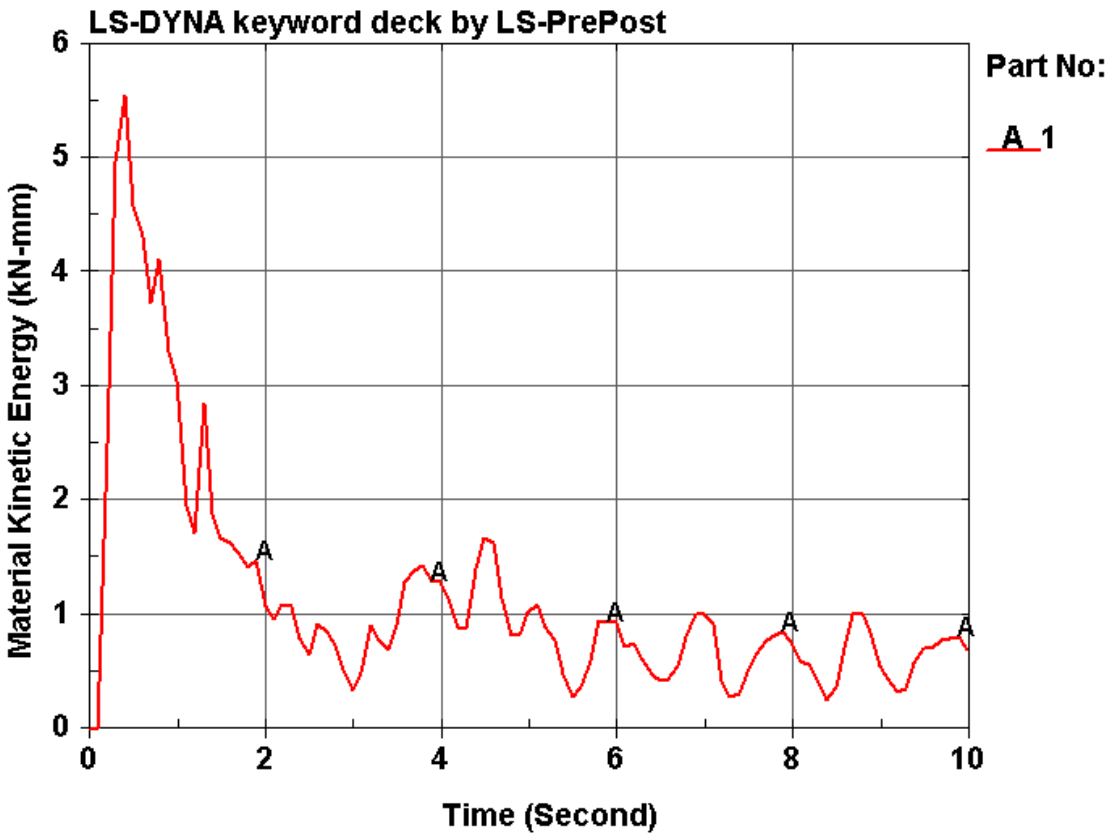

Figure 98: Kinetic Energy Absorbed by Target from 10 m/s Impact

As illustrated in Figure 98, the initial impact again creates a spike in kinetic energy in the target. Damped vibration causes a reduction in the initial energy spike followed by series of lower energy spikes as the material goes through a vibratory regime before damping out at the conclusion.

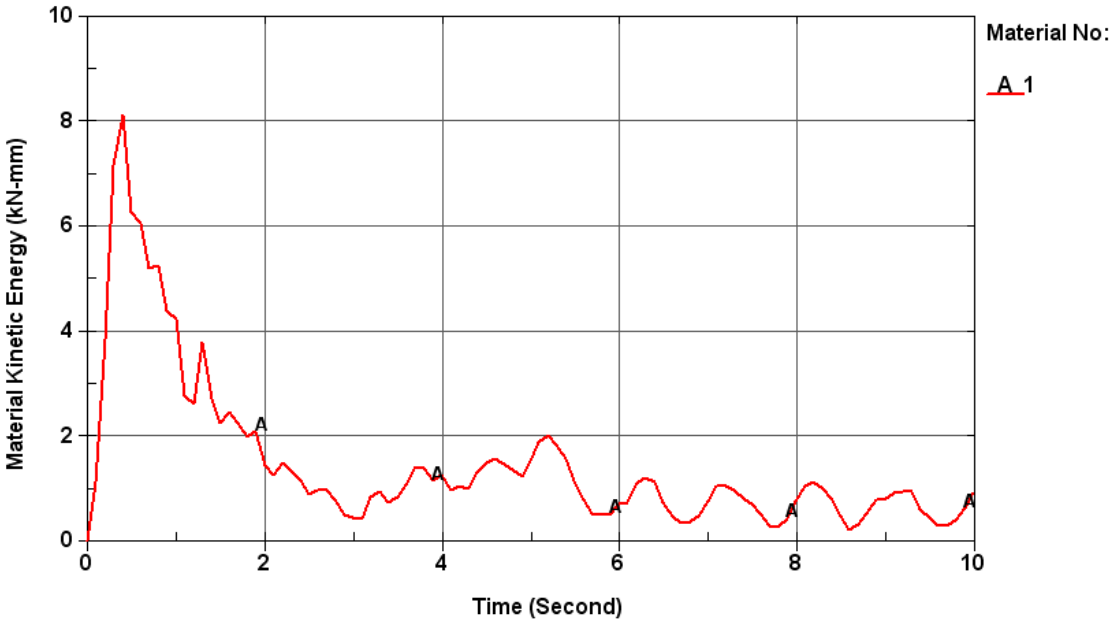

Figure 99: Kinetic Energy Absorbed by Target from 12 m/s Impact

Figure 99 provides a different energy profile than that seen on the previous illustrations. At this impact velocity, penetration is very close. The initial impact spike is still evident, but closely followed by a secondary spike in kinetic energy in the target. This results because the target is absorbing the penetration energy. A damping vibration follows this as the energy decreases after the impact concludes.

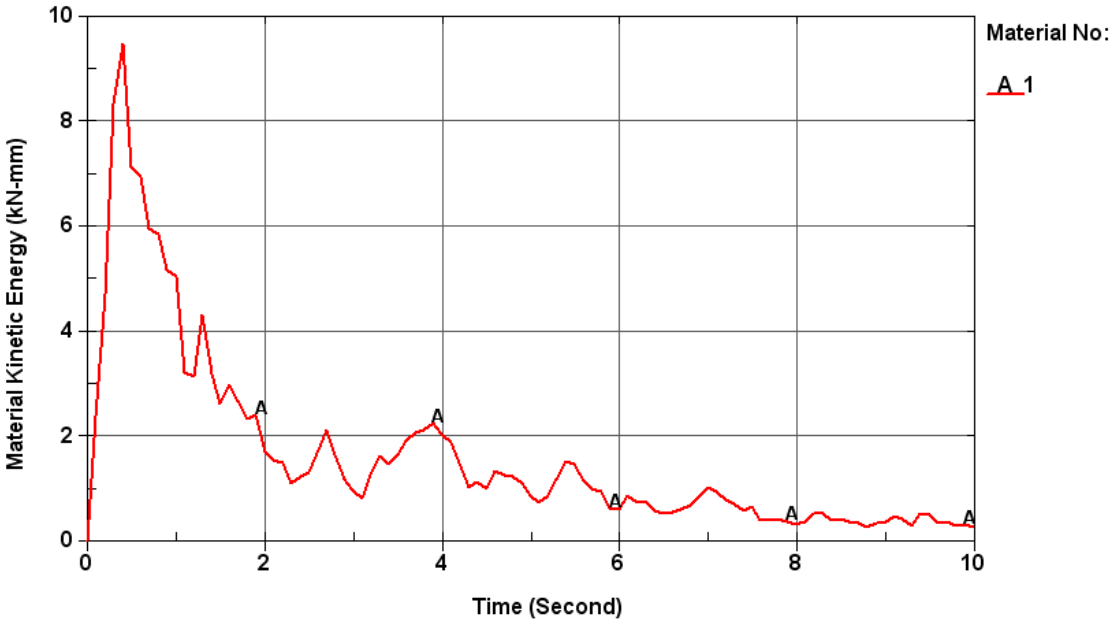

Figure 100: Kinetic Energy Absorbed by Target from 13 m/s Impact

Figure 100 provides an energy profile similar to the previous chart where the penetration is eminent. Again, the initial impact spike is still evident, but closely followed by an increased secondary spike due to the energy absorbed and the target absorbs the maximum energy. Again, a damping vibration follows this phenomenon as the energy decreases after the impact subsides. It is interesting to note that just before the limit velocity of penetration second spike almost diminished.

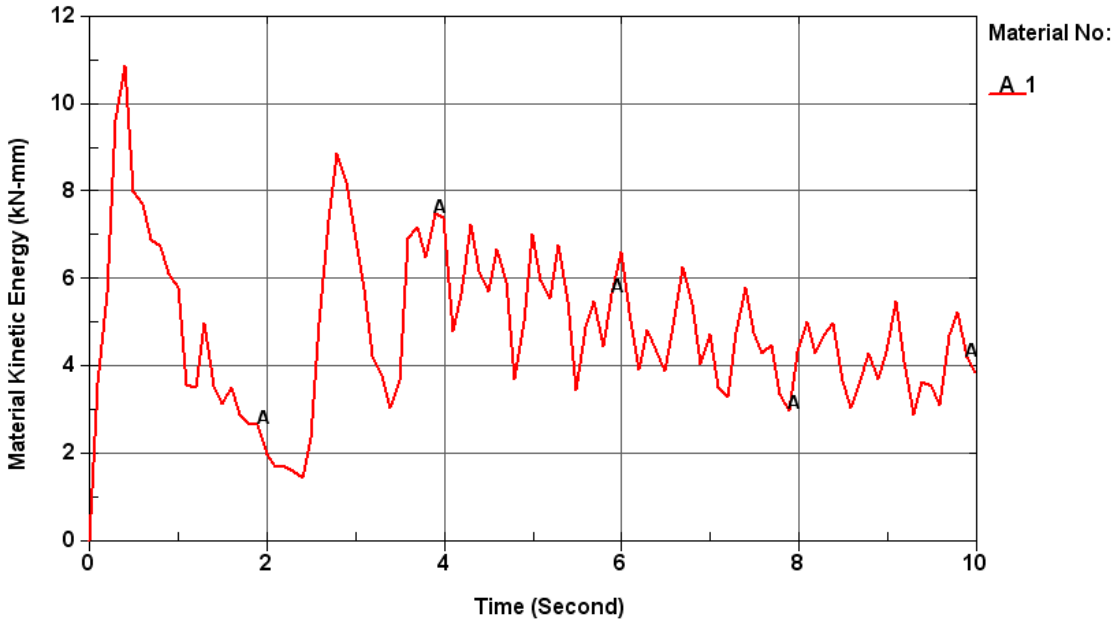

Figure 101: Kinetic Energy Absorbed by Target from 14 m/s Impact (penetration starts)

Figure 101 provides an energy profile different from the previous charts where the penetration had not occurred. Again, the initial impact spike is still evident, and again followed by an increased secondary spike. Again, a damping vibration follows this as the energy decreases after the impact concludes. It is worth noting that the second spike reaches to its maximum value approximately at 3.0 sec as shown in Figure 101. At this time, projectile is almost penetrated the whole thickness of the plywood and the broken piece of plywood (plug) is almost ready to dislocate from the impact face of the target.

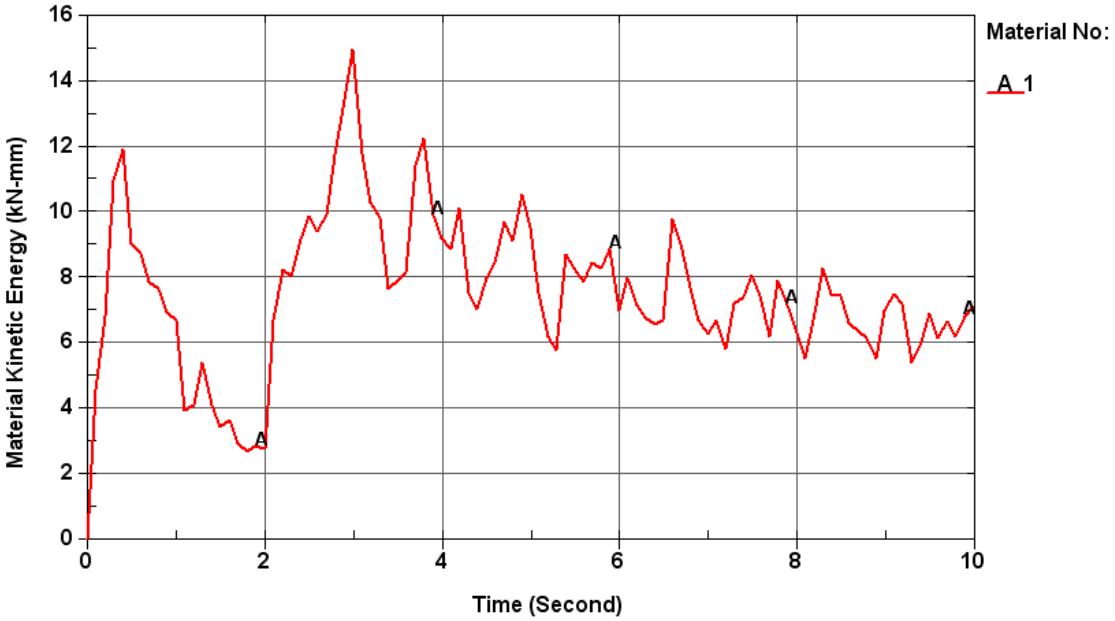

Figure 102: Kinetic Energy Absorbed by Target from 15 m/s Impact

Figure 102 provides an energy profile similar to the previous charts where the penetration occurred. Again, the initial impact spike is still evident, and again followed by an increased secondary spike. Again, a damping vibration follows as the energy decreases after the impact concludes. Observing simulation at 15 m/sec shows that the second spike is noticeably higher than the first spike. Approximately at 3.0 sec of simulation where the second spike occurs, majority of the projectile was out of plywood and the solid plug was ejected from the impact face of the target. Similar situations were observed when the impact velocity is increased as shown in Figures 103-105. The results of the higher impact velocities revealed that second spike increases as the impact velocities increase.

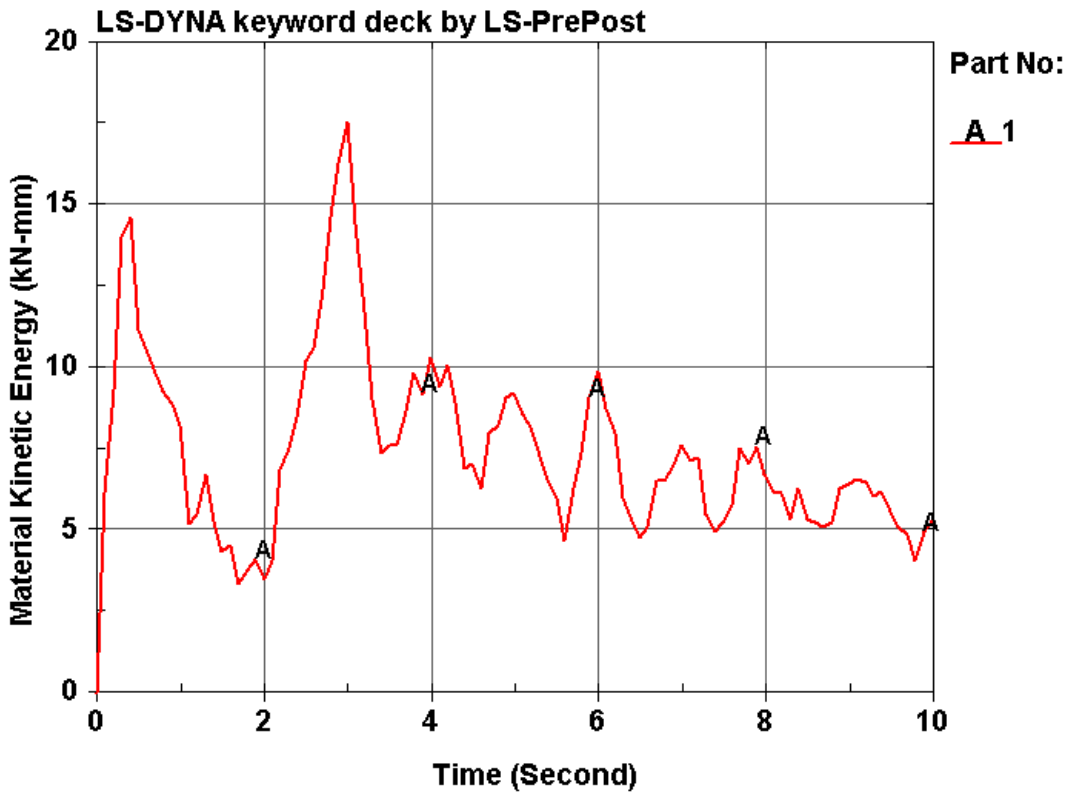

Figure 103: Kinetic Energy Absorbed by Target from 17 m/s Impact

Figure 103 provides an energy profile similar to the previous charts where the penetration occurred. Again, the initial impact spike is still evident, and again followed by an increased secondary spike. Again, a damping vibration follows as the energy decreases after the impact concludes. Observing simulation at 15 m/sec shows that the second spike is noticeably higher than the first spike. Approximately at 3.0 sec of simulation where the second spike occurs, majority of the projectile was out of plywood and the solid plug was ejected from the impact face of the target.

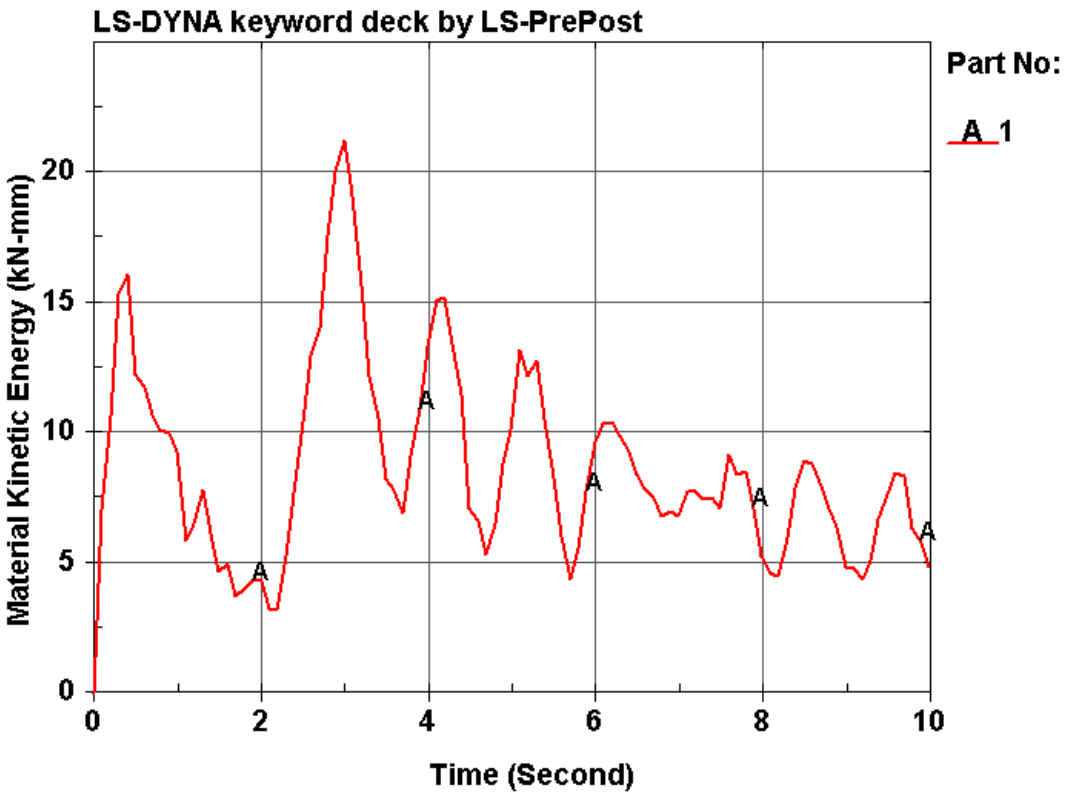

Figure 104: Kinetic Energy Absorbed by Target from 18 m/s Impact

Figure 104 provides an energy profile similar to the previous charts where the penetration occurred. Again, the initial impact spike is still evident, and again followed by an increased secondary spike. Again, a damping vibration follows as the energy decreases after the impact concludes. Observing simulation at 15 m/sec shows that the second spike is noticeably higher than the first spike. Approximately at 3.0 sec of simulation where the second spike occurs, majority of the projectile was out of plywood and the solid plug was ejected from the impact face of the target.

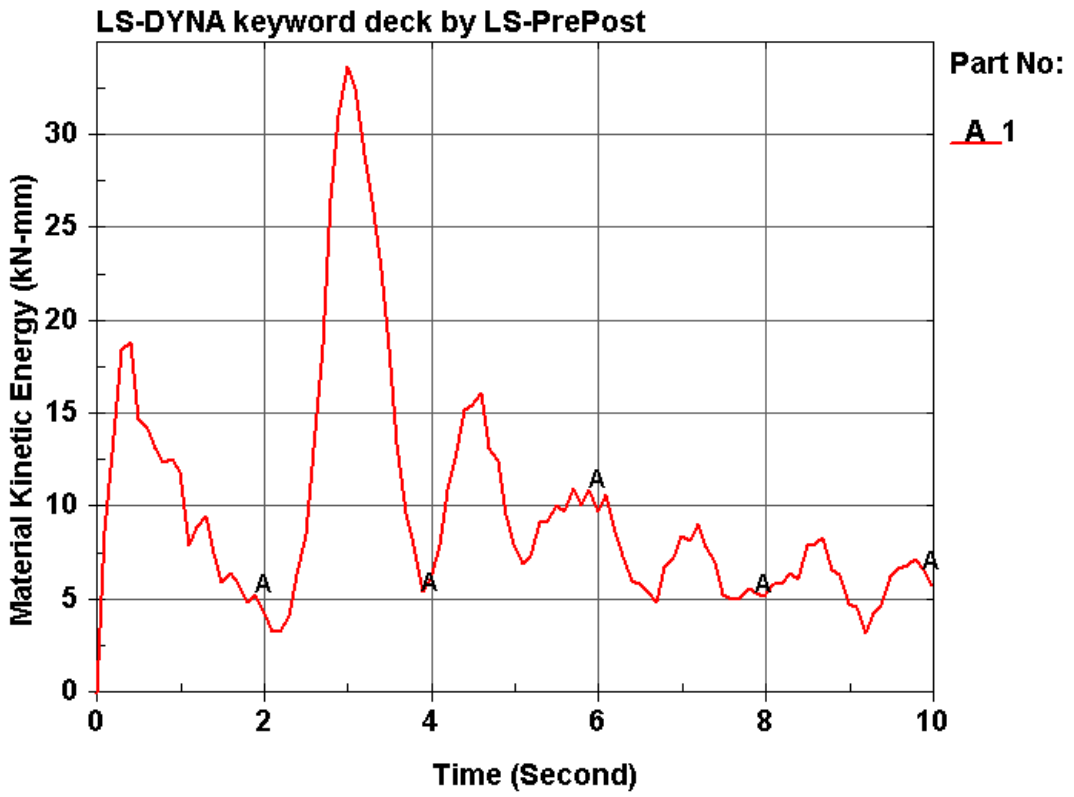

Figure 105: Kinetic Energy Absorbed by Target from 20 m/s Impact

Figure 105 provides an energy profile similar to the previous charts where the penetration occurred. Again, the initial impact spike is still evident, and again followed by an increased secondary spike. Again, a damping vibration follows as the energy decreases after the impact concludes. Observing simulation at 15 m/sec shows that the second spike is noticeably higher than the first spike. Approximately at 3.0 sec of simulation where the second spike occurs, majority of the projectile was out of plywood and the solid plug was ejected from the impact face of the target

As explained earlier, when penetration does not occur there is a rebound condition. Figure 106 illustrates these conditions. In situations where the impact velocity is between 4 m/s and 13 m/s, the rebound velocity increases almost linearly. These result shows sudden drop when the impact velocity gets close to 13 m/s (which is the velocity just before the penetration): specifically when the impact velocity approaches the penetration limit velocity, the rebound velocity decreases.

Further understanding of this phenomenon results from examining Figure 107. As the figure illustrates, the kinetic energy absorbed by the plywood increases as the impact velocity increases (for the non-penetrating situations). There is a sharp increase in absorbed kinetic energy by the plywood at the impact velocity that is near to the penetration limit velocity which reduces the rebound velocity of the projectile as shown in Figure 106.

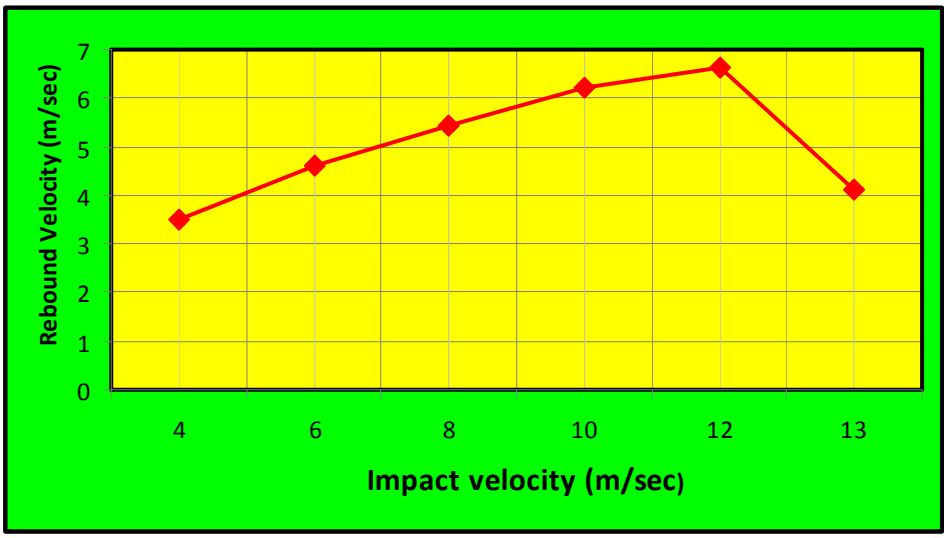

Figure 106: Rebound Velocities in Non-Penetrated Plywood

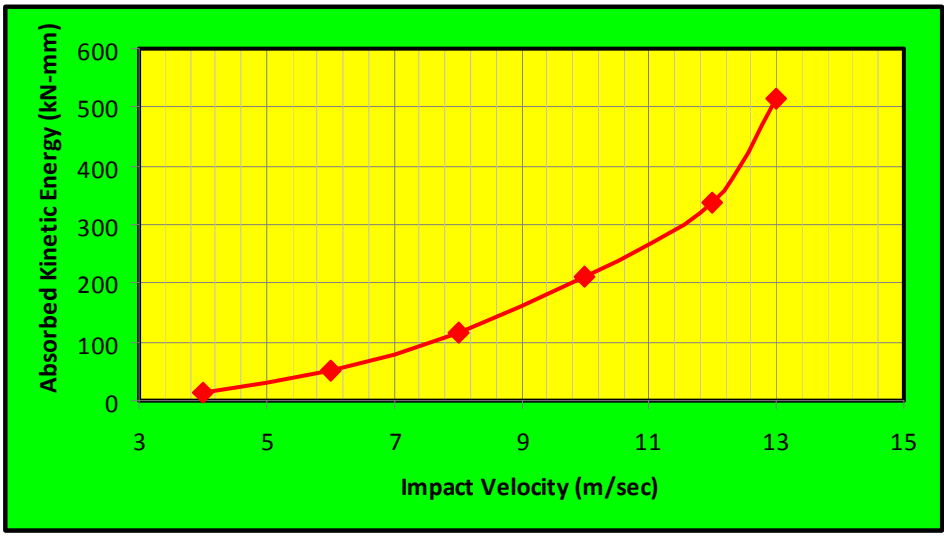

Figure 107: Absorbed Energies for Non-Penetrated Plywood

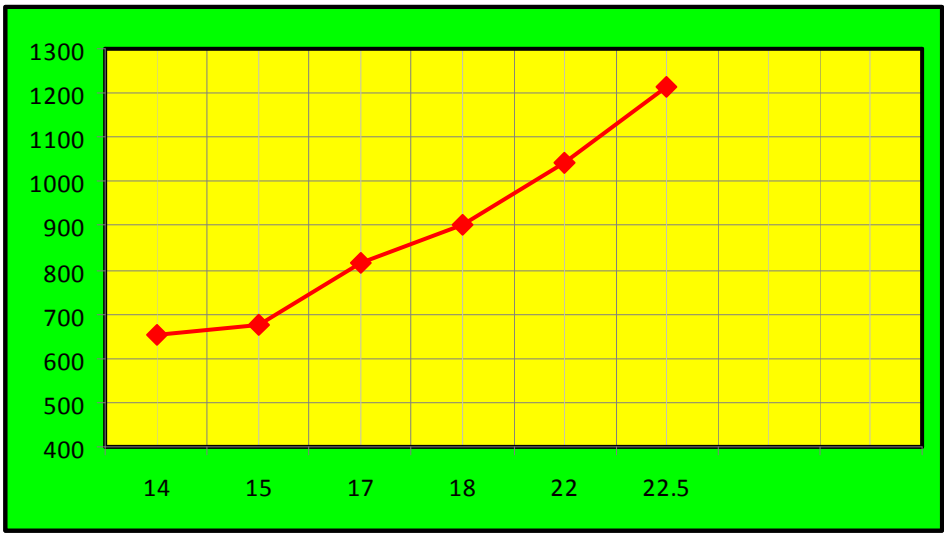

Figure 108: Absorbed Energies for Penetrated Plywood

Figure 108 shows the final absorbed kinetic energy by the plywood at various impact velocities when penetration occurs. In this instance, the final absorbed energy by the plywood allows calculation by reducing the residual kinetic energy from the initial kinetic energy. As shown in the figure, at first the trend of the curve is

fluctuating at the low impact velocities whereas at the high velocities kinetic energy absorption becomes linear.

While the previous figures illustrated the kinetic energy in the target at various impact velocities, Figures 109 through 120 illustrate the kinetic energy absorption in the projectile. Note that as was the case in the target energy charts, after penetration occurs (velocities >13 m/s), the curve tends to have a change its trend. Instead of a "recovery" of the energy, the energy depletes and mostly transfers to the target.

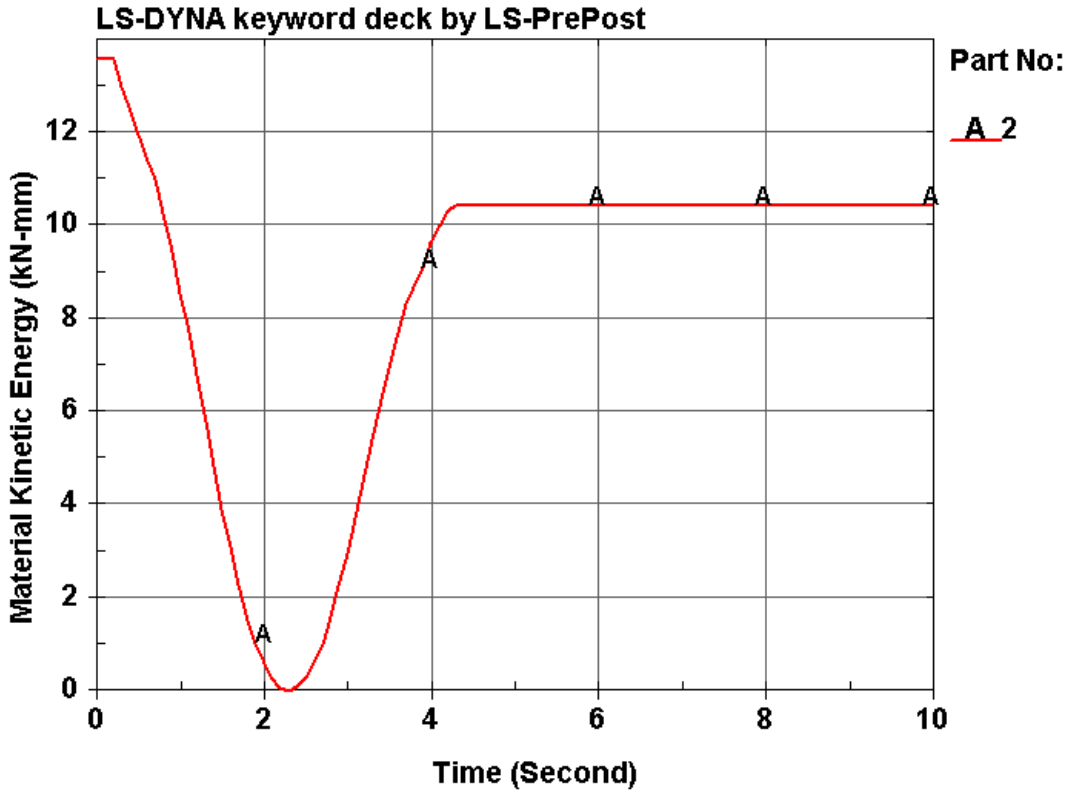

Figure 109: Projectile Energy at 4 m/s Impact

As Figure 109 illustrates, the projectile experiences a rapid decrease in energy (due to the rapid deceleration) immediately after impact. Since it is repelled in this situation, the velocity goes to zero as it changes directions then the velocity (in a

negative direction) again becomes a major contributor to the sudden rise in the kinetic energy.

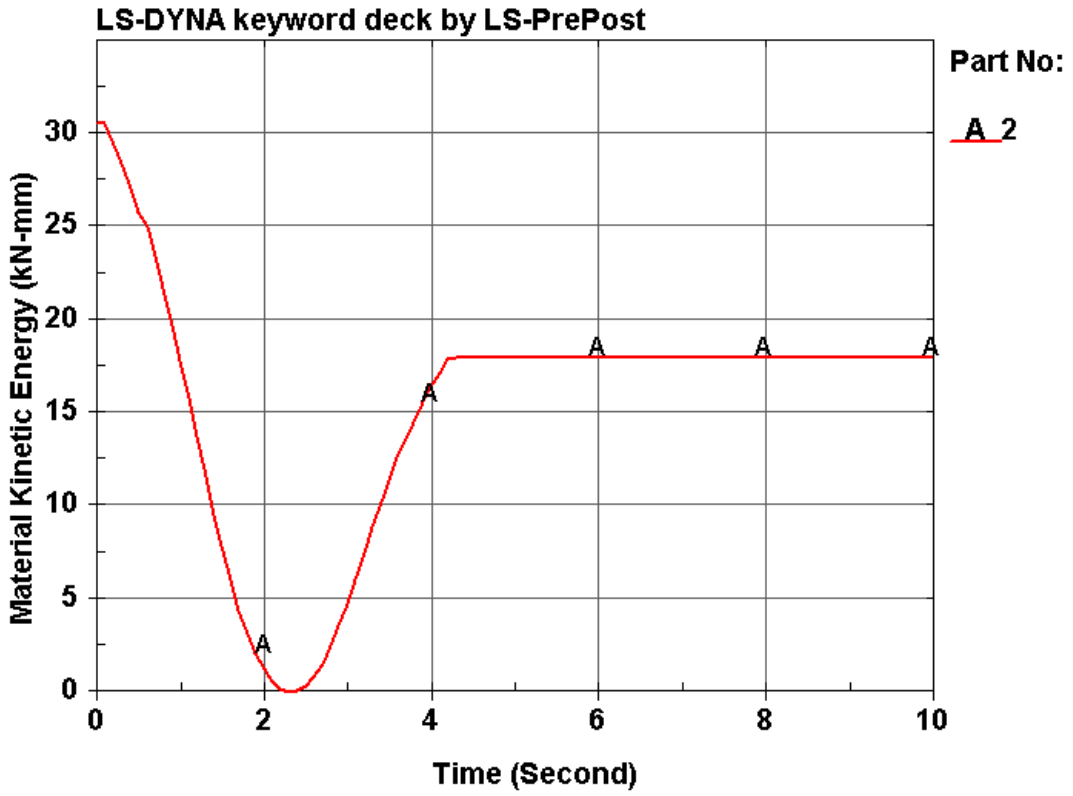

Figure 110: Projectile Energy at 6 m/s Impact

As Figure 110 illustrates, the projectile again experiences a rapid decrease in energy (due to the rapid deceleration) immediately after impact. Since it is again repelled in this situation, the velocity goes to zero as it changes directions then the velocity (in a negative direction) again becomes a major contributor to the sudden rise in the kinetic energy.

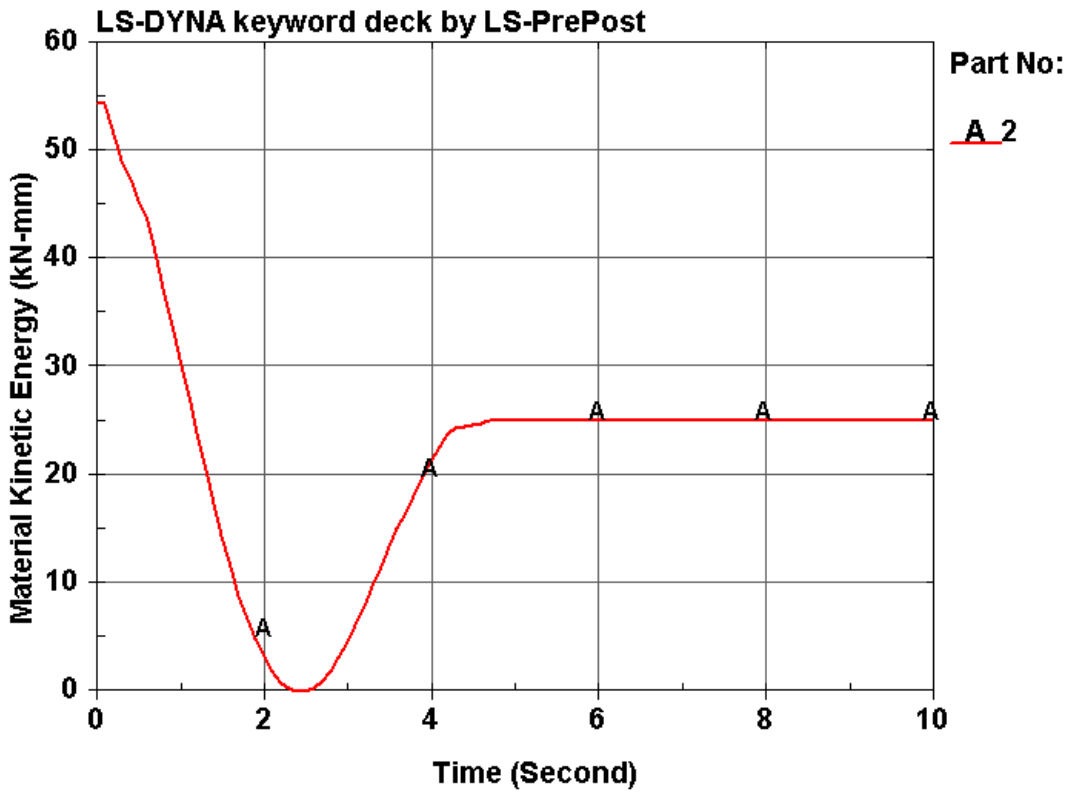

Figure 111: Projectile Energy at 8 m/s Impact

As Figure 111 illustrates, the projectile again experiences a rapid decrease in energy (due to the rapid deceleration) immediately after impact. Since it is again repelled in this situation, the velocity goes to zero as it changes directions then the velocity (in a negative direction) again becomes a major contributor to the sudden rise in the kinetic energy. As the impact velocity increases, the repelled velocity, thus the kinetic energy in the projectile also increases accordingly.

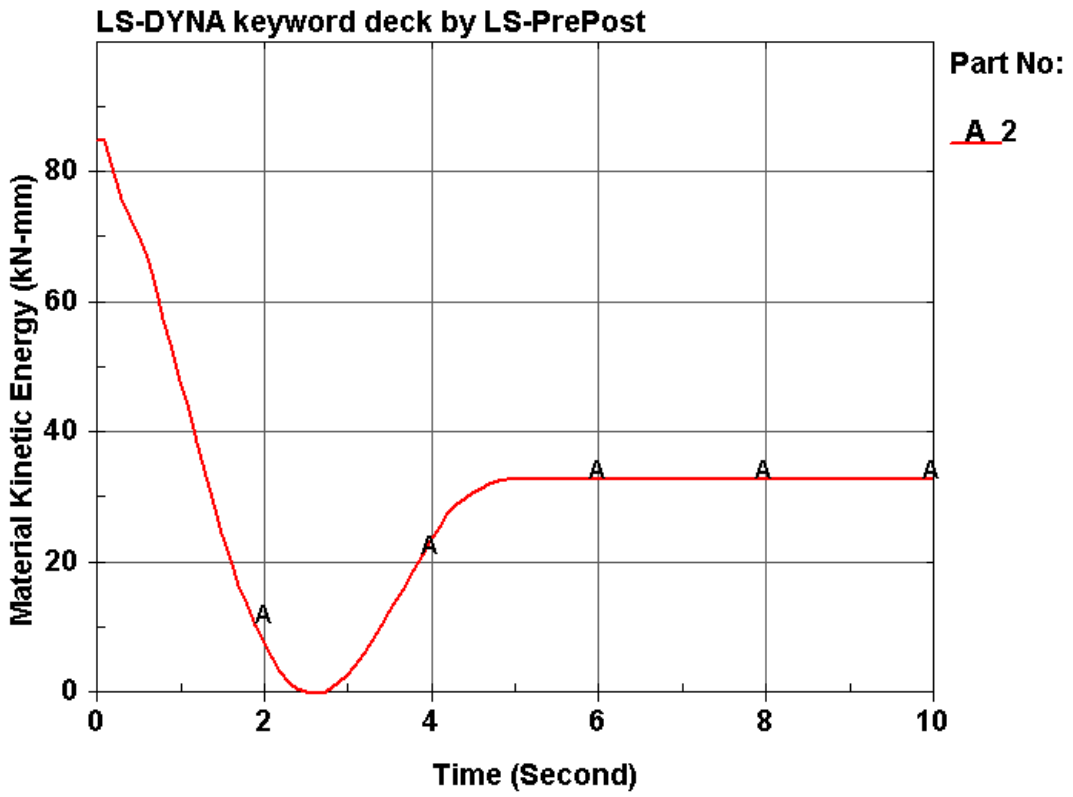

Figure 112: Projectile Energy at 10 m/s Impact

As Figure 112 illustrates, the projectile again experiences a rapid decrease in energy (due to the rapid deceleration) immediately after impact. Since it is again repelled in this situation, the velocity goes to zero as it changes directions then the velocity (in a negative direction) again becomes a major contributor to the sudden rise in the kinetic energy. As the impact velocity increases, the repelled velocity, thus the kinetic energy in the projectile also increases accordingly.

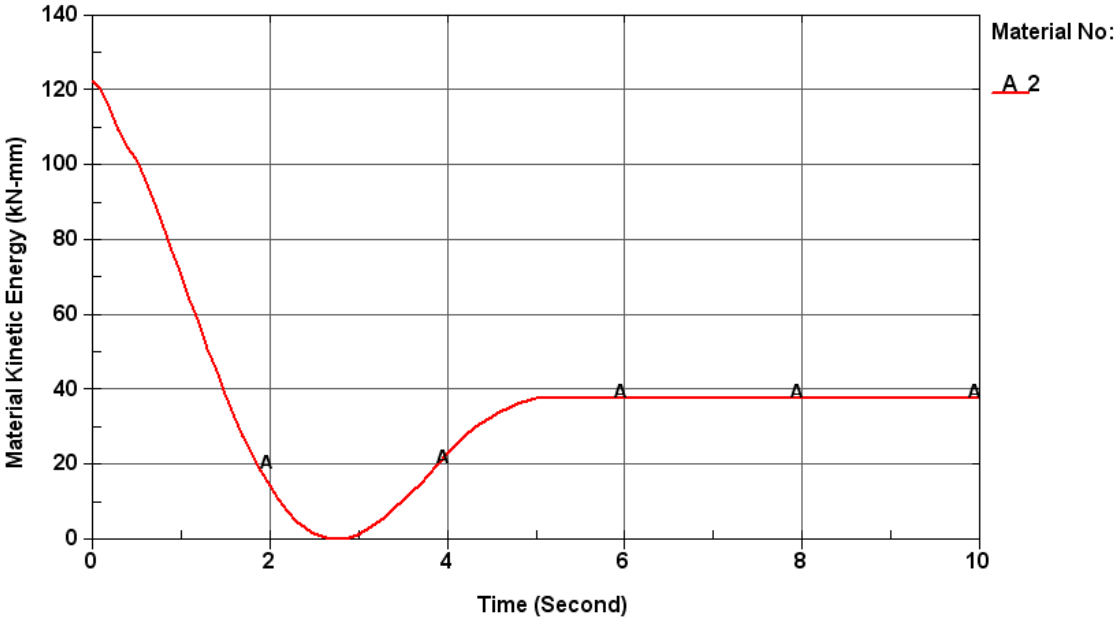

Figure 113: Projectile Energy at 12 m/s Impact

As Figure 113 illustrates, the projectile again experiences a rapid decrease in energy (due to the rapid deceleration) immediately after impact. Since it is again repelled in this situation, the velocity goes to zero as it changes directions then the velocity (in a negative direction) again becomes a major contributor to the sudden rise in the kinetic energy. As the impact velocity increases, the repelled velocity, thus the kinetic energy in the projectile also increases accordingly.

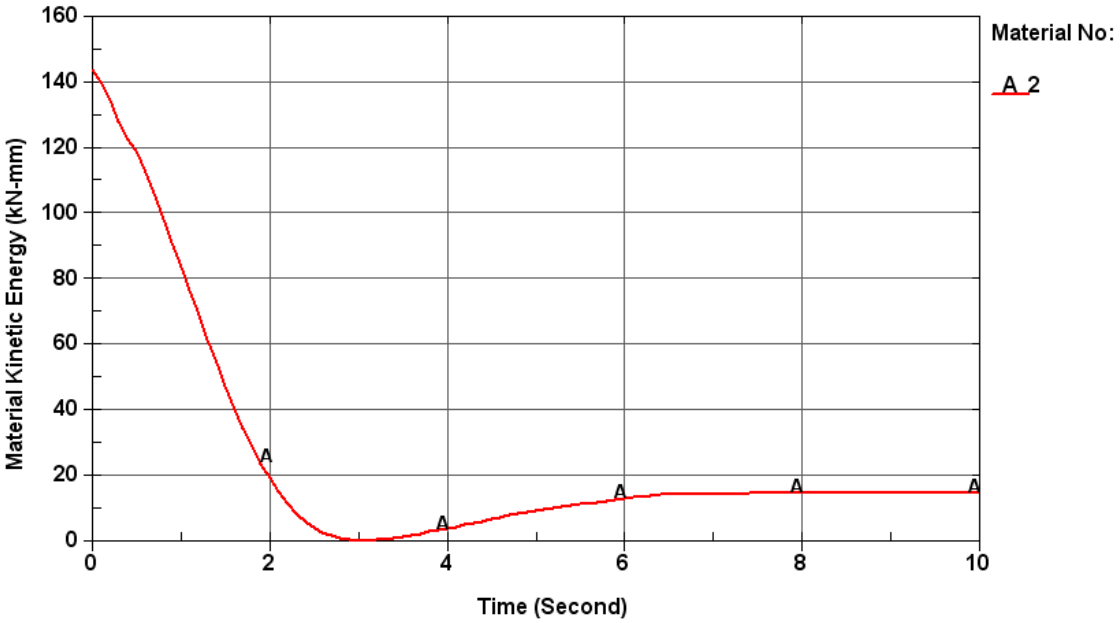

Figure 114: Projectile Energy at 13 m/s Impact

As Figure 114 illustrates, the projectile again experiences a rapid decrease in energy (due to the rapid deceleration) immediately after impact. Since it is again repelled in this situation, the velocity goes to zero as it changes directions then the velocity (in a negative direction) again becomes a major contributor to the sudden rise in the kinetic energy. As the impact velocity nears the penetration point, the "after-zero energy is less than in the previous example. Some of the energy expires due to the damage done to the target as shown previously at 12 m/s.

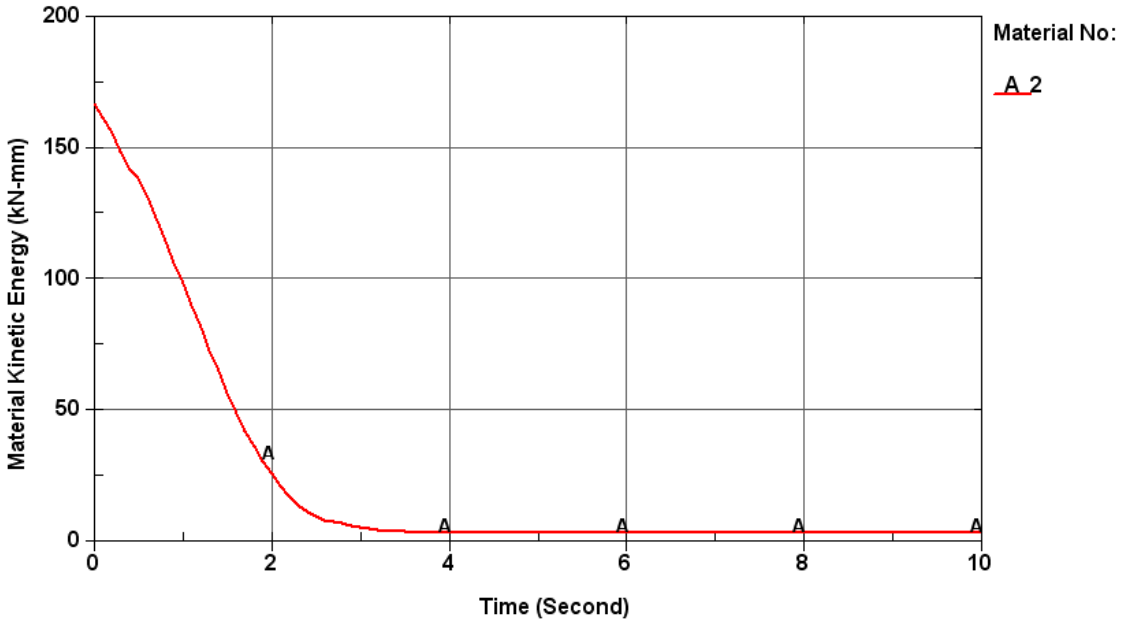

Figure 115: Projectile Energy at 14 m/s Impact

As Figure 115 illustrates, the projectile as before experiences a rapid decrease in energy immediately after impact; however, it does not recover. This is because penetration has occurred and the target material absorbs the majority of the energy.

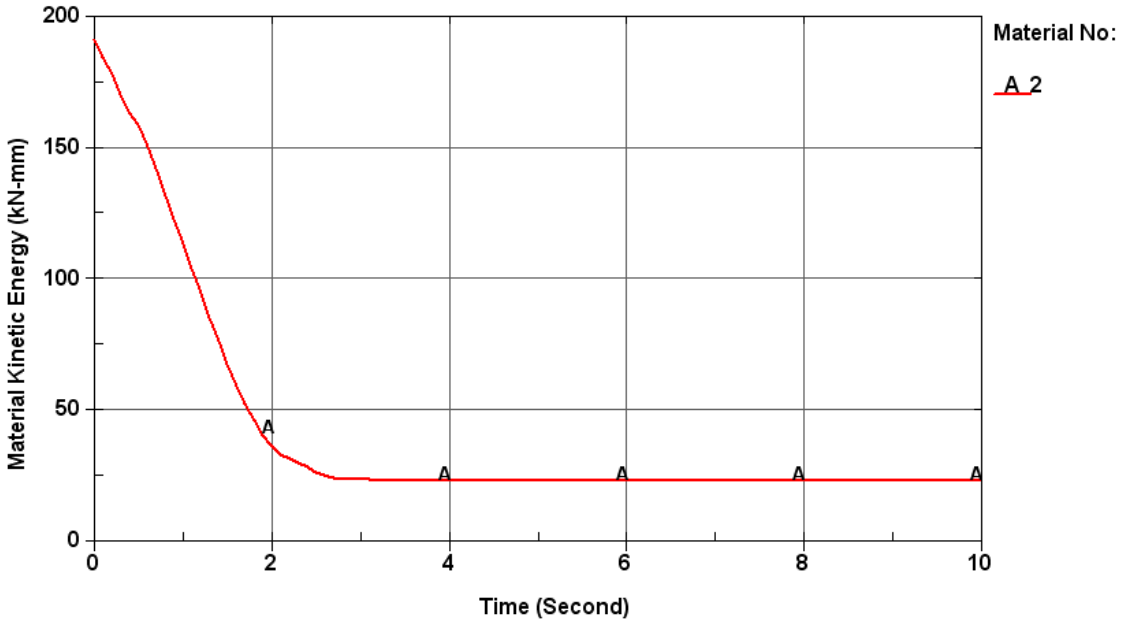

Figure 116: Projectile Energy at 15 m/s Impact

As Figure 116 illustrates, the projectile as before experiences a rapid decrease in energy immediately after impact; however, it does not recover. Again, this is because penetration has occurred and the target material absorbs the majority of the energy.

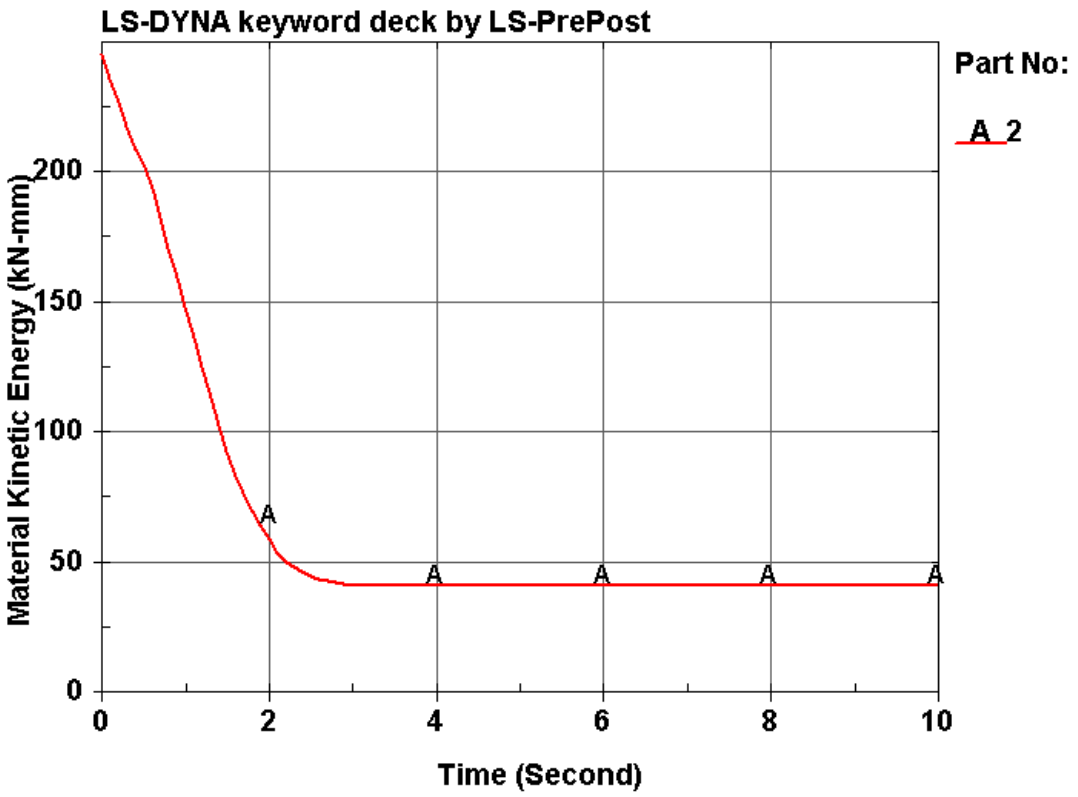

Figure 117: Projectile Energy at 17 m/s Impact

As Figure 117 illustrates, the projectile as before experiences a rapid decrease in energy immediately after impact; however, the impact force is sufficient to allow some recovery in the kinetic energy in the projectile.

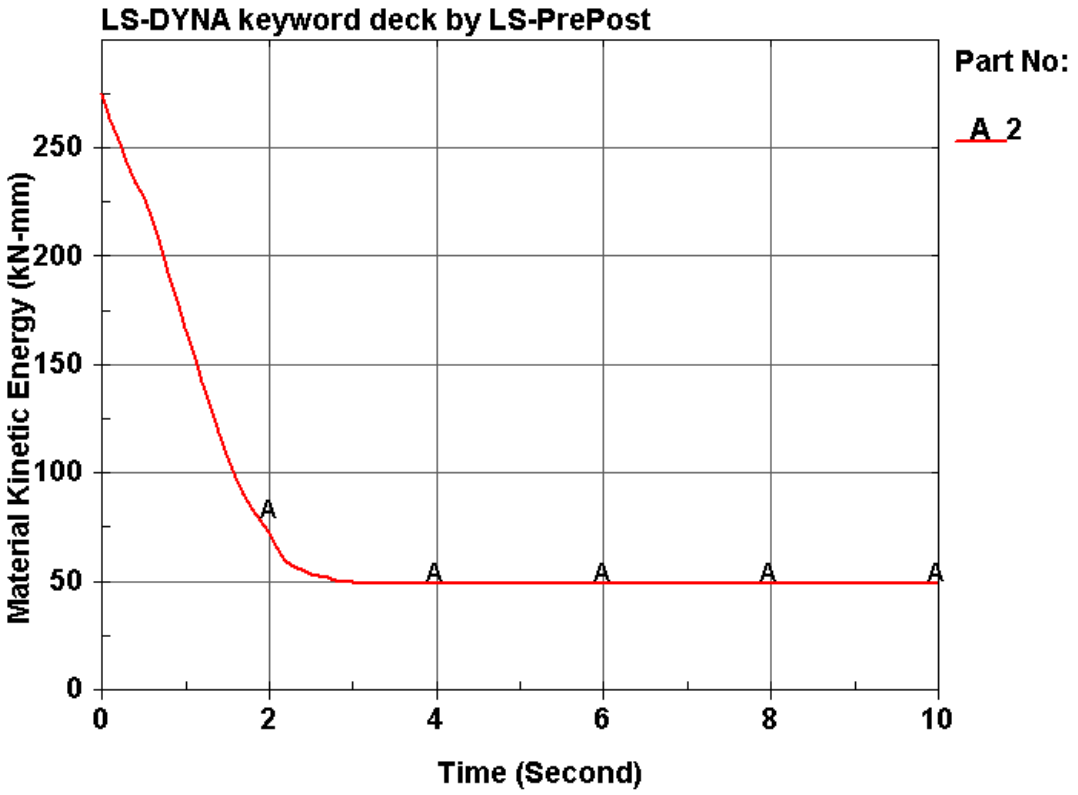

Figure 118: Projectile Energy at 18 m/s Impact

As Figure 118 illustrates, the projectile as before experiences a rapid decrease in energy immediately after impact; however, the impact force is sufficient to allow some recovery in the kinetic energy in the projectile.

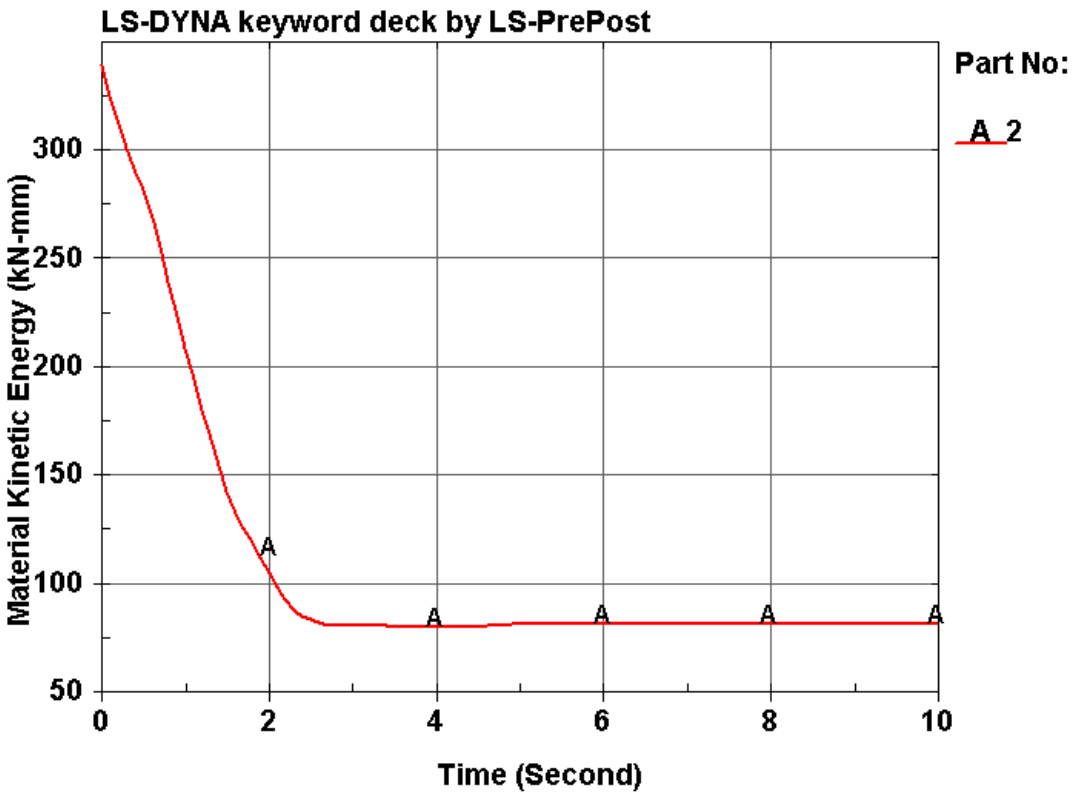

Figure 119: Projectile Energy at 20 m/s Impact

As Figure 119 illustrates, the projectile as before experiences a rapid decrease in energy immediately after impact; however, the impact force is again sufficient to allow some recovery in the kinetic energy in the projectile.

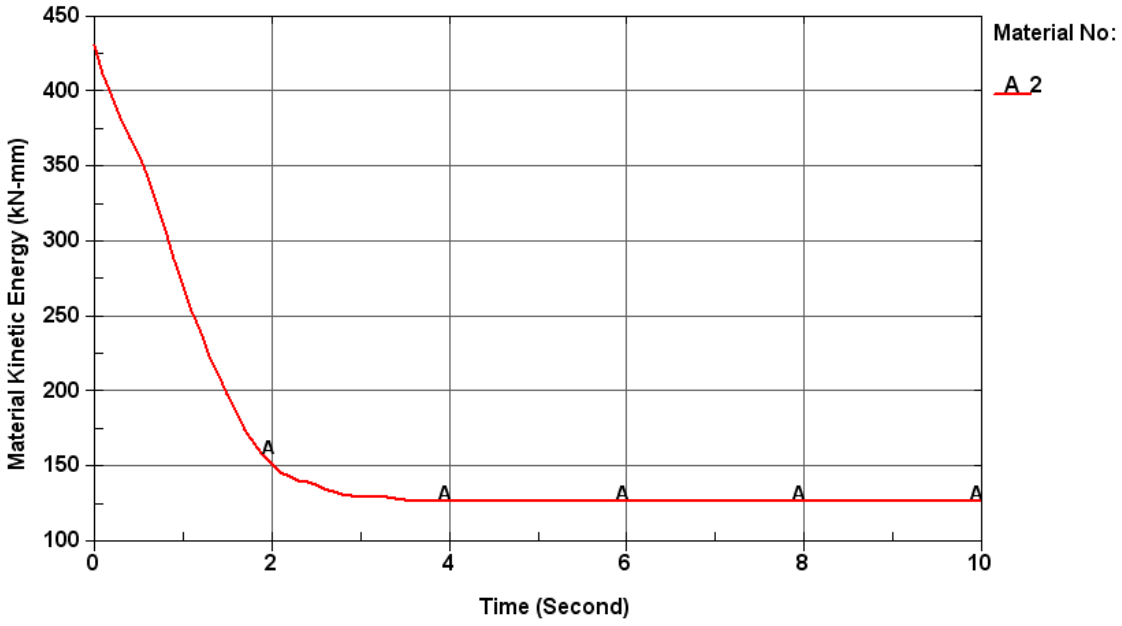

Figure 120: Projectile Energy at 22.5 m/s Impact

As Figure 120 illustrates, the projectile as before experiences a rapid decrease in energy immediately after impact; however, the kinetic energy again does not recover. Since this impact velocity produce catastrophic failure of the plywood, no residual energy returns back to the projectile.

As shown in figures 109-120, the general trend of the energy curves changes after the penetration velocity reaches 14 m/s. Note that the kinetic energies of the projectiles shown in the preceding figures are for the ¼ model mentioned earlier; therefore, the total kinetic energy is this value multiplied by four.

Throughout the preceding descriptions, the details of the finite element analysis are presented as four basic data elements: the impact velocity time histories, a series of impact simulation charts, charts illustrating the energy absorption of the target, and charts showing the energies inherent in the projectiles. These attributes have been described separately; however, there is a definite connection between these elements of the impact dynamics. Table 19 is a mapping of the figures categorized by the impact velocities.

Table 19: Finite Element Data Figures vs Impact Velocities

Impact Velocity	Impact Velocity Time History	Impact Simulations	Target Absorbed Energy	Projectile Energy
4 m/s	Figure 73	Figure 86	Figure 95	Figure 109
6 m/s	Figure 74		Figure 96	Figure 110
8 m/s	Figure 75	Figure 87	Figure 97	Figure 111
10 m/s	Figure 76		Figure 98	Figure 112
12 m/s	Figure 77	Figure 88	Figure 99	Figure 113
13 m/s	Figure 78		Figure 100	Figure 114
14 m/s	Figure 79	Figure 89	Figure 101	Figure 115
15 m/s	Figure 80		Figure 102	Figure 116
17 m/s	Figure 81	Figure 90	Figure 103	Figure 117
18 m/s	Figure 82		Figure 104	Figure 118
20 m/s	Figure 83	Figure 91	Figure 105	Figure 119
22.2 m/s	Figure 84	Figure 92		Figure 120

This table provides a correlation between the various figures included in the previous descriptions based on the impact velocities. By comparing these illustrations at each impact velocity, the comprehensive process taking place during these impacts is clearer.

Summary

In terms of the limit velocities required for a 2 x 4 timber to penetrate a plywood target, the comparison of the results is reasonably good. Since Texas Tech testing included the determination of the limit velocity needed for penetration, there can be a direct comparison between this testing, the equations described in this paper, and the simulation results. Figure 121 illustrates the limit velocity spread for the different methodology of determination.

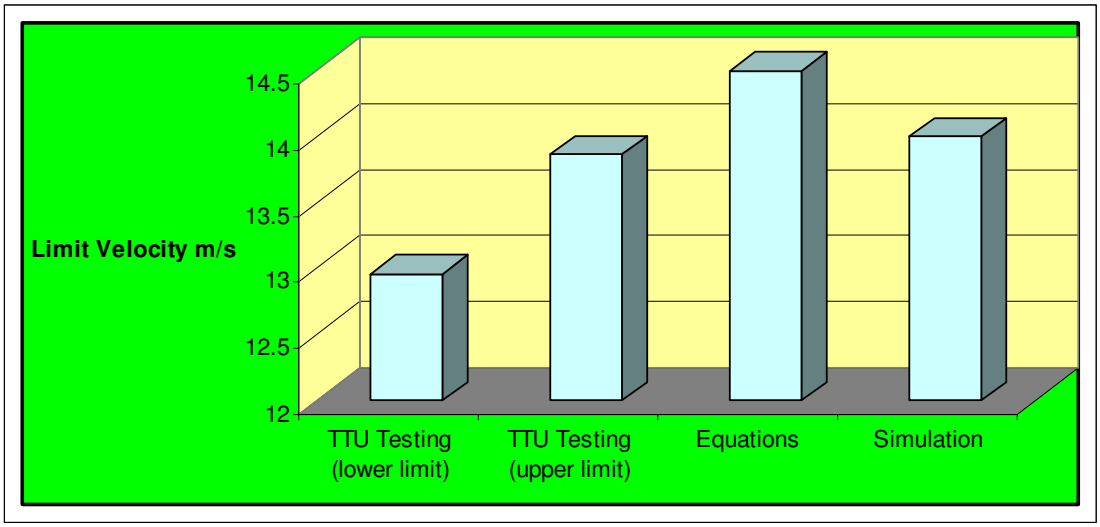

Figure 121: Comparison between Limit Velocity Determinations

Though the spread appears somewhat large at first glance, notice that the lowest to the highest value only differ by 1.5 m/s. This expresses good correlation for a parameter of impact dynamics that is dependant on a myriad of factors. These data definitely provide a level of confidence in the findings of this study.

From the standpoint of residual velocity, only two methodologies are involved: Texas Tech testing did not record the residual velocities of the projectiles after penetration. Table 20 and Figure 122 illustrate the comparison between the simulation and the calculations from the equations presented in this dissertation.

Table 20: Residual Velocity Comparison

Impact Velocity (m/s)	Simulation Residual Velocity (m/s)	Calculated Residual Velocity (m/s)
14	1.871	
14.5	3.579	2.264
15	5.169	3.6742
17	6.9956	8.336
18	7.6644	10.019
20	9.719	12.933
22.5	12.22	16.148

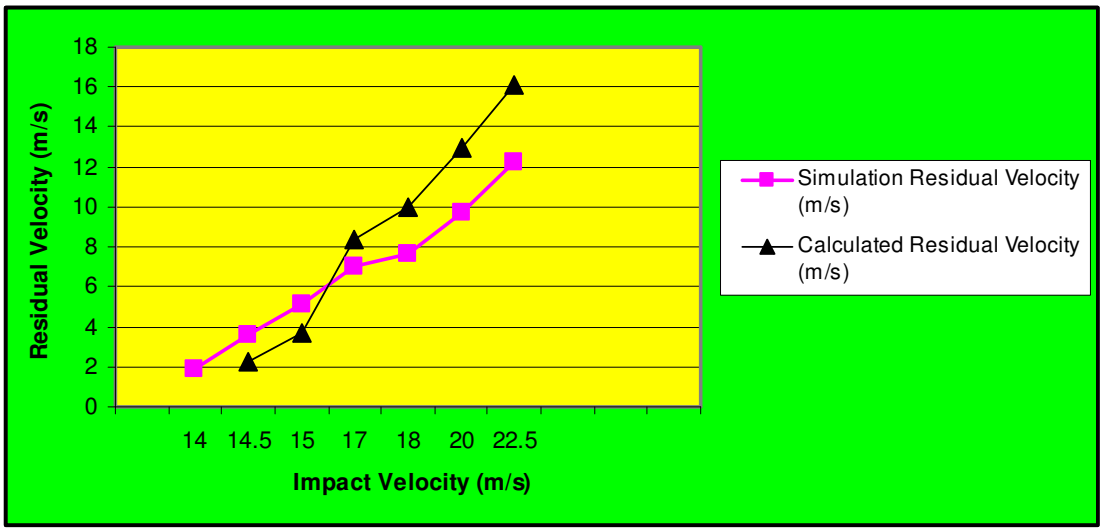

Figure 122: Graphical Representation of Residual Velocity Comparison

Note that, since the calculated limit velocity was 14.5 m/s, there was no residual velocity at 14 m/s for the "calculated" column (see Table 20).

As seen in Figure 122, as the impact velocities increase, the data lines intersect. Despite this, the distributions of the data between the two formulations of residual velocities match fairly well. Any differences in these values are possibly attributable to the inherent differences between the pine wood simulated target substrate and the plywood target in the equation based example.

Since the equations developed in this dissertation are tailored for an isotropic material, the simulation model is likewise created to be isentropic. In other words, the modeled targets are a single layer of pine wood. The pine was selected due to the similarities between pine properties and standard plywood properties. In reality plywood is a multi-layered cross-ply, uni-directional fiber reinforced composite or an anisotropic material. Although the one-layer pine wood modeled proved to be adequate for these impact dynamics applications, as seen in the Figure 22 graph, there is a need for further, more realistic, composite finite element modeling before more complicated situations are addressed.

The primary reason for conducting a finite element analysis of the principles contained in this dissertation was to add credibility to the herein developed equations. Not only did this effort lend good credibility to the premise of this study, but it also resulted in a much better understanding of the failure mechanisms that take place during the type of impacts under study. Localized deflection characteristics of the target were revealed, target scabbing (release of target material debris) was identified, and interesting phenomena associated with energy absorption was uncovered. All of these revelations will prove most useful as this study progresses to the next level. Based on the modeling accomplished during this study, more sophisticated models can evolve that include other materials such as steel and concrete, composite target substrates, variable projectile artifacts.

CHAPTER 8

RECOMMENDATIONS AND CONCLUSIONS

Clarification and Disclaimers

As mentioned earlier in this paper, tornadoes represent a phenomenon that continues to elude explanation. The wind field in and surrounding a tornado, though generally understood, still holds many secrets. At any one point in and around a tornado, winds can be multi-directional (including vertical components), velocities can vary considerably within a very small area, and debris can further complicate the environment and add to the damage potential. There is no all-inclusive definition of absolute safety. Even the most impenetrable shelter is vulnerable to failure. One would assume that an underground reinforced concrete shelter would provide assured protection in the event of a tornado; however, this in not always the case. Doswell illustrates one such failure during the tornado outbreak on 3 May 1999. [55] In describing the weaknesses of the doors usually installed onto underground tornado shelters, he recounts that during this violent tornado, the door to an underground concrete shelter failed and an airborne clothes dryer entered the shelter. Luckily, there were no occupants in this shelter.

Considering these statements, this study does not attempt to instruct methodology resulting in absolute safety of reinforced residences. Ultimately, survival during exposure to a powerful tornado is often a matter of chance. The primary purpose of this thesis is to offer illustrations, examples, and suggestions to increase the odds of survival. The very low probability of being involved in a tornado should not discourage preparedness. Inaction regarding tornado preparedness is foolish at best. While it is highly unlikely that any individual will ever experience a tornado strike, if such an event does occur, maximizing the odds of survival is essential.

The original intent of this discussion included the development of storm room construction procedures that would result in some level of protection in storm rooms taking under consideration the added benefits of various external wall surfaces; however, this endeavor required modification. The thought pattern included the premise that debris has to pass through the exterior wall (not considering the weak points inherent with doors and windows) prior to reaching the safe room; therefore, allowing a cutback in safe room wall construction. However, since a direct strike to a residence by a particularly strong tornado would destroy the outside home envelope, any suggestions related to the minimization of storm room walls for tornadoes expected to result in damage greater than EF2 are no longer considered. By definition, EF3 and above damage characteristics include the failure of all outside walls. Again, the goal is to increase one's odds of survival.

Figure 123 illustrates the characteristics of tornado damage referenced to the location in path of the storm. As expected, the most severe damage will occur near to the center of the vortex; however, much damage can be expected adjacent to and surrounding the funnel itself. Debris often travels great distances; therefore, very severe damage can occur quite a distance from the tornado.

Figure 123: Tornado Wind Regimes
[10]

Despite this fact, the argument stands that any additional barriers between the destructive winds and the individual augments the level of protection. There are likely instances where a single layer of ¾" plywood could theoretically increase the level of protection to the point of adequacy, but this is probably the exception rather than the rule. The following sections include suggestions, based on the findings described in the previous chapters regarding the increase of the odds of survival when a tornado event occurs.

Standard Homebuilding Techniques

Contemporary residential construction practices usually fall under the jurisdiction of local building codes. It is common practice by builders to meet these codes in a minimal fashion. Furthermore, in rural areas, either building codes do not apply or enforcement is questionable. Homebuilders are in the business of profit. Adding costs to the construction project to protect against an event that is likely to occur once every thousand years typically escapes the business plan. This does not infer that all builders work in this manner. There are exceptions including builders who include and highlight storm resistance as a standard feature. (See figure 124)

Figure 124: According to Texas Law, This Home Requires an Engineer to Oversee

The typical building practices used today for new home construction result in weaknesses in terms of wind resistance. As described in many studies, the load path defines the structural integrity of "stick-built" homes. [10, 12, 59, 110, and 129] This

load path includes the attachment of the roof structure (rafters) to the ceiling structure (joists), the ceiling joists to the stud walls, the stud walls to the baseplate, and the baseplate to the foundation. (See figure 125) This transmits the weight loads from the roof into the ground. From a gravity viewpoint, this method is more than adequate. However, with the introduction of wind, the forces are no longer only from top to bottom. Wind induces lateral forces, which puts these members into a tensile and shear environment, rather than a predominately-compressive situation. In extreme winds and tornadoes, forces are tremendous, especially with the addition of upward components.

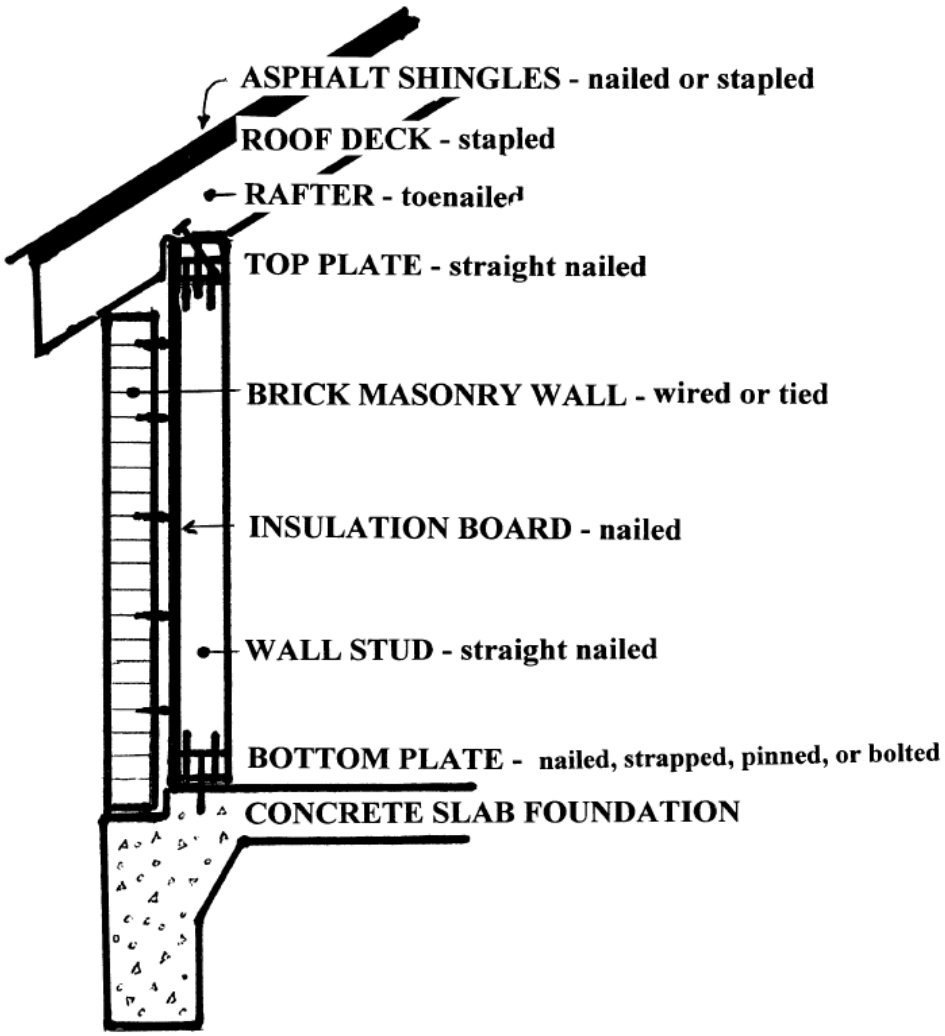

Figure 125: Graphical Representation of Typical Load Path
[13]

The attachments of these constituents to each other represent the biggest weaknesses with this method of construction. In many instances, the bottom plate attachment to the slab is via compressed-air driven concrete nails. This allows the bottom plate to resist lateral movement, but any uplift protection is minimal. Correspondingly, the stud and bottom plate attachment occurs while the wall section is lying on its side. Nails driven into the bottom of the bottom plate and into the ends of the studs define this attachment. Again, this resists lateral loads, but the walls structure is susceptible to uplift forces. Similar methods describe the attachment of the top plate of the stud walls to the ceiling joists and rafters. Repeating, this methodology allows gravity to hold everything together, but provides minimal protection against wind loads.

The techniques involved in home construction today differ from home building specifics of past decades, as illustrated in many of the damage photographs from the 1948 McKinney tornado in Chapter 4.

In 1948, dimension lumber (such as 2 x 4s, 2 x 6s, etc.) were the actual size indicated. For example, a 2 x 4 was actually 2 inches by 4 inches (instead of 1 ½ inches x 3 ½ inches). This additional material resulted in homes that were more rigid than the homes today. Real wood siding typically covered the exterior walls. Usually tongue-and-groove features allowed this siding to interconnect and result in a home less vulnerable to lateral forces. Additionally, this was before the wide use of sheetrock; therefore, solid wood slats covered the interior walls and the inside of the exterior walls. Tack-on wallpaper covered these interior wall surfaces. This resulted in a stud wall, not just the exterior walls, but also the interior walls had 2 x 4 inch studs sandwiched between wood slats on both sides. Today, the outside sheathing of the 1 ½ inch by 3 ½ inch stud walls is insulation board, and the inside and all interior walls are sandwiched with sheetrock – neither of which provides much in the way of rigidity or penetration resistance.

The deficiencies of homes built in decades past are many. As mentioned above the structures proved to exhibit strength, the inferior attachment of the homes to the foundations resulted in many structural failures during tornados and other high

wind events. Figure 126 illustrates this deficiency. Note that the overall structure of the home is intact. There is even a noticeable lack of debris impact damage. This did not prevent the wind from rolling the home off its foundation.

Figure 126: Home with Inferior Connection to Foundation

New Home Construction Recommendations

Despite the fact that the primary concentration of this study involves the hardening of existing homes against tornado debris penetration, new home construction suggestions are included because in this phase of construction, the most successful resistance techniques are cost effective.

The time to plan for optimal tornado resistant is during the home design. The earlier that tornado protection becomes a constituent of the design decision tree, the least expensive and more successful this endeavor will become. As explained in the chapter on storm damage surveys, load path weaknesses are the primary structural home failure mechanisms. Secondary, but not less important are penetration failures.

As indicated in many debris impact studies and from the results of this thesis, it becomes obvious that one of the best designs for exterior wall surfaces in terms of structural integrity and penetration prevention involve reinforced concrete. If finances allow, the optimal aboveground tornado resistant home would utilize reinforced concrete: possibly insulated concrete forms (ICFs). While many manufacturers supply these products, Poly-Steel provides an excellent good source of information. [129]

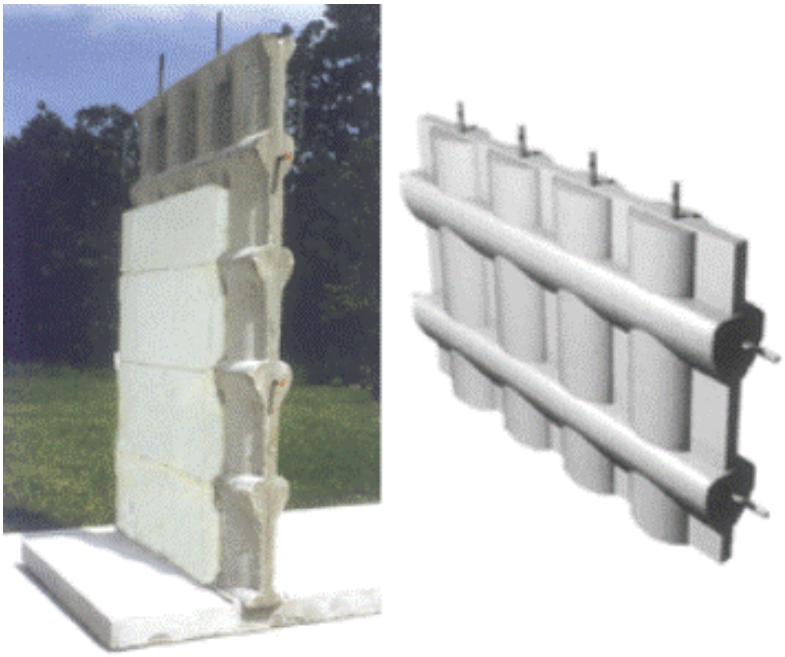

Figure 127: Cross-section of an ICF Wall
[101]

Figure 127 shows a cutaway of a typical Poly-Steel wall with the insulated foam partially removed for clarity, and with the foam removed entirely. This wall construction is included in the Texas Tech impact testing described in previous chapters. [19] The construction manual that accompanies the forms provides detailed instructions for insuring that the interface between the walls and the foundation insures a fundamentally strong attachment. Actually, the manual includes directions for the entire construction project in explicit detail. Even a concrete roof system (though the spans are limited) is available from this company. Unfortunately, these

measures would prove most difficult for existing homes and businesses. Polysteel also offers a complete storm room option for new construction, which is detached from the principle residence.

This method of building construction offers superior tornado resistance, as well as, other advantages. Homes constructed in this manner are more energy efficient, more fire resistant, quieter, bulletproof, and require less maintenance. If allowed by the local building code, a home constructed using insulated concrete forms with an additional interior storm room could be the closest thing to absolute tornado protection available in an aboveground option. According to Poly-steel, a home constructed in this manner would result in a cost increase of approximately 15% over that of typical construction practices.

For the design of a new wood frame residence that provides a superior resistance to wind forces, the use of metal connectors minimizes the failure possibilities via connection failures along the load path. By attaching the individual members of the load path structure to each other utilizing these connectors, the weak links in the load path become less susceptible to wind failure. Eliminating the weaknesses in the framing connections provides the most bang-for-the-buck in terms of tornado resistance versus cost. Figure 128 illustrates a cross section showing the appropriate use of metal connectors.

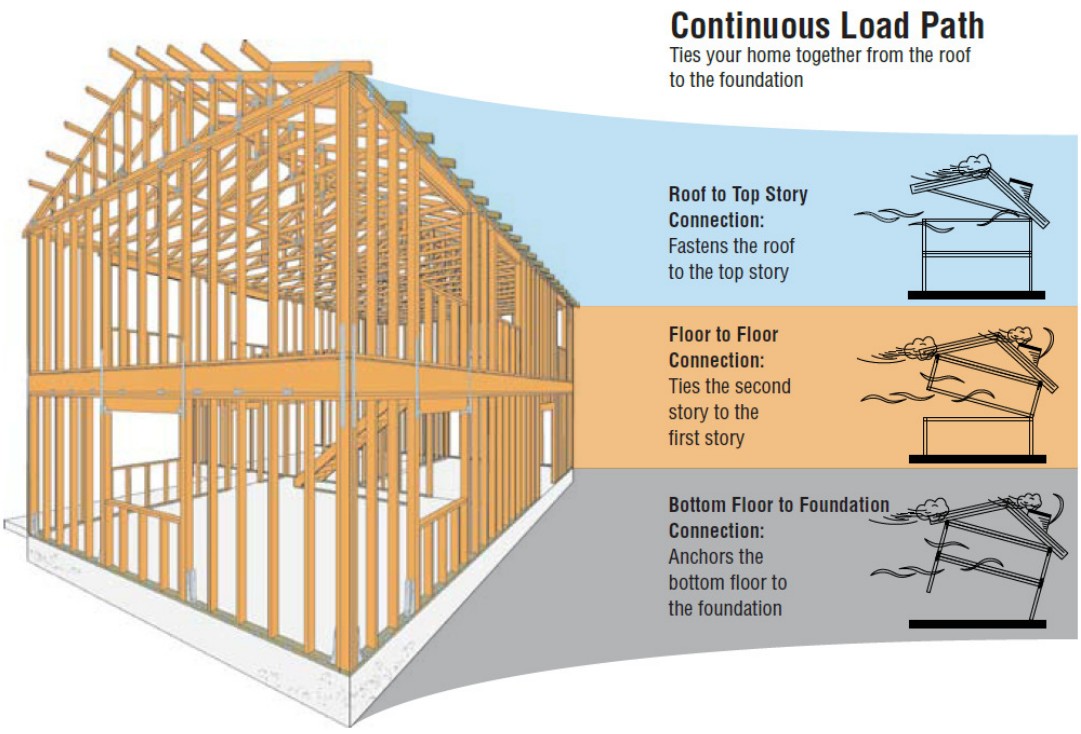

Figure 128: Typical Metal Wood Frame Connections
[109]

While the adoption of the insulated concrete insulated forms greatly increases the penetration hazard, the metal connector methodology does nothing to prevent penetration of flying debris. The initial design of a home designed to be tornado resistant should account for this weakness in penetration resistance. As seen in the previous chapter, brick exteriors offer some resistance to typical debris, but not enough to prevent danger inside of the residence. The addition of steel or plywood barriers around the entire house would be an appropriate added measure of protection, but at substantial costs.

The most tornado-resistant aboveground residence structure should consist of ICF exterior walls and roof plus the inclusion of an ICF interior safe room. If properly constructed, a home of this nature would approach near-absolute protection. In the absence of this or a similar methodology, it is unlikely that a wood frame residence would survive a direct strike from a violent tornado. Winds approaching 200 mph would render most homes unsafe as shelters, even with the hardening techniques

discussed in this paper. However, as mentioned throughout this study, the goal is not absolute protection, but increasing the odds of survival.

6.4 Existing Home Recommendations

Since the majority of homes in the United States already exist, it is important to address these residences in terms of tornado resistance. The equations and subsequent data described earlier in Chapters 5 and 6 provide validation for the recommendations contained herein. Prior to discussing storm room specifics, note the following general comments regarding storm room construction.

If possible, all storm room construction should be unattached to the existing home structure. It is preferable to build a second wall inside of an existing interior room to prevent the safe room from becoming susceptible to structural failure if the rest of the home fails. This is also true of the ceiling structure. If this is not possible to achieve or proves too expensive, an alternate design includes modifying the existing safe room walls in the following manner. Remove the sheetrock from the interior of the safe room. Add supplemental attachments from the bottom plate to the foundation. This will almost certainly be the use of compressed air driven concrete nails. Next, attach an extra stud and an extra joist to each stud and joist that already exists. Use metal connectors to reinforce the connection between all members of the safe room frame: studs to bottom plate, studs to top plate, and top plate to ceiling joists. This will greatly improve the structural integrity of the safe room, and provide the necessary framing strength to support the added plywood.

The attachment of the plywood to the framing is critical. Use wood screws that penetrate the plywood and enter the framing by a couple of inches or more. Keep in mind that with each subsequent layer of plywood used, a longer screw is required. The screw spacing is no further than 6 inches between screws. Furthermore, with the addition of each layer of plywood, a layer of quality wood glue is included between the plywood sheets. The idea is to create a solid “wall” of plywood, not just adjacent sheets. Provisions are also necessary for electrical outlets, lights, and air conditioning vents.

The recommendations mentioned above are not the result of testing or analyses, but represent best construction practices.

The weakest link in a storm room is the door. On all suggested storm room configurations, a door that meets the characteristics of the latest revision of the FEMA storm room document is required. See Figure 129.

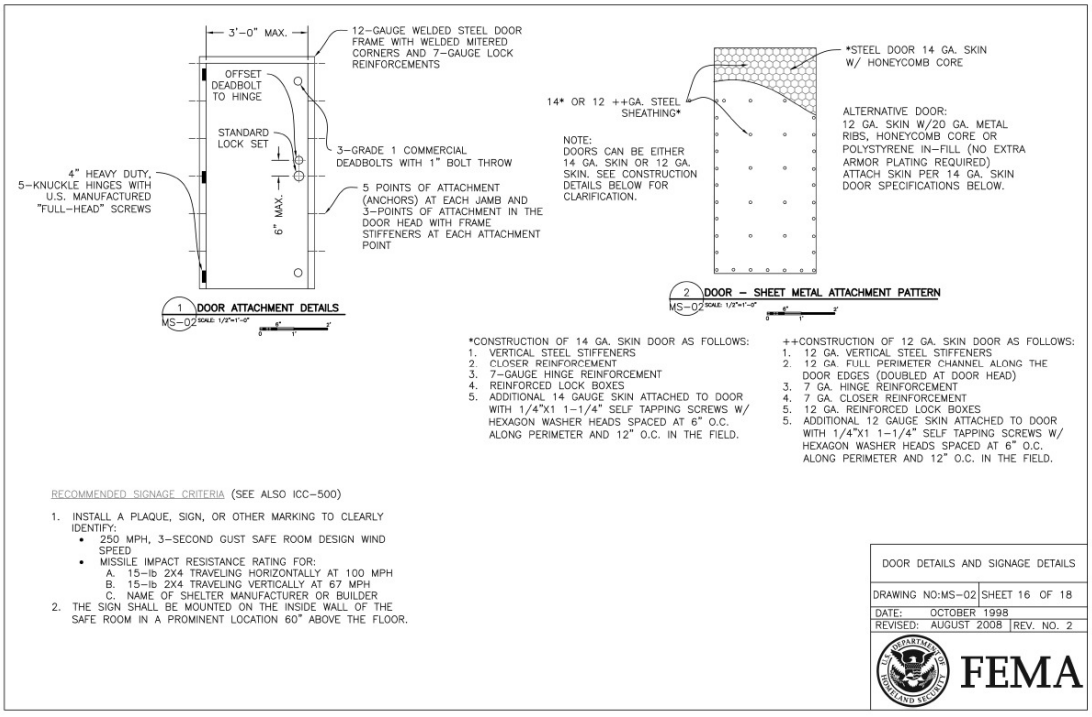

Figure 129: FEMA Shelter Door Requirements
[10]

EF0 level damage estimates wind speeds between 65 and 85 miles per hour. This translates to a top-end projectile speed of 68 mph for walls and 45 mph for ceilings. The design characteristics for a storm room capable of protection against debris penetration consist of two sheets of plywood on the ceiling and four sheets of plywood on the walls. Again, if a safe room is capable of providing EF0 level protection, this would provide protection from 53 8% of all tornadoes expected to occur.

At wind speeds in this lower category, the exterior home walls provide an added level of protection. In the case of a brick veneer exterior, chapter six defines the residual speed of a 15 lb. 2 x 4 after penetrating a wall consisting of brick, ¾" plywood, and ⅝" sheetrock to be 4.6 mph. Though not recommended that a reduction in the number of plywood sheets to repel this velocity of debris is appropriate, this provides a comfortable margin of safety. (All EF category photographs courtesy of [59])

Figure 130: EF0 Example

EF1 level damage estimates wind speeds between 86 and 110 miles per hour. This translates to a top-end projectile speed of 77 mph for walls and 51 mph for ceilings. The design characteristics for a storm room capable of protection against debris penetration consist of three sheets of plywood on the ceiling and five sheets of plywood on the walls. In addition to providing protection from EF1 damage levels, protection from EF0 is also included. This option would provide protection from 76.1% of all tornadoes expected to occur.

At the top end of this wind category, the exterior home walls start to experience some level of damage. If the exterior is brick veneer, chapter six defines the residual speed of a 15 lb. 2 x 4 after penetrating a wall consisting of brick, ¾" plywood, and ⅝" sheetrock to be 10.7 mph. This is not the case if exterior damage occurs or if the debris strikes a vulnerable portion of the exterior such as doors and windows. For this reason, the debris resistance of the exterior of the home is not considered. As with the EF0 level of protection, the exterior resistance acts as a margin of safety.

Figure 131: EF1 Example

EF2 level damage estimates wind speeds between 111 and 135 miles per hour. This translates to a top-end projectile speed of 83 mph for walls and 55 mph for ceilings. The design characteristics for a storm room capable of protection against debris penetration are the same as EF1: three sheets of plywood on the ceiling and five sheets of plywood on the walls. In addition to providing protection from EF2 damage levels, protection from EF1 and EF2 is also included. This option would provide protection from 88% of all tornadoes expected to occur. This means that by adding three sheets of plywood to the ceiling and five sheets of plywood to the walls of the storm room only 12% of tornadoes could produce debris that would penetrate this room.

However, at the top end of this wind category, the exterior home walls start to experience a greater level of damage. If the exterior is brick veneer and it survives initial impact, chapter six defines the residual speed of a 15 lb. 2 x 4 after penetrating a wall consisting of brick, ¾" plywood, and ⅝" sheetrock to be 13.5 mph. This must not cause optimism. At this level of storm, exterior damage is very possible, and roof damage is likely. With this degree of wind forces acting on the exterior, the penetration resistance of the exterior walls is questionable.

Considerable: Roof structures are damaged, mobile homes are destroyed, debris becomes airborne (missiles are generated), large trees are snapped or uprooted.

Figure 132: EF2 Example

EF3 level damage estimates wind speeds between 136 and 165 miles per hour. This translates to a top-end projectile speed of 87 mph for walls and 58 mph for ceilings. The design characteristics for a storm room capable of protection against debris penetration include three sheets of plywood on the ceiling and six sheets of plywood on the walls. This option would provide protection from debris penetration for 95% of all tornadoes expected to occur. This means that by adding three sheets of plywood to the ceiling and six sheets of plywood to the walls of the storm room only 5% of tornadoes could produce debris that would penetrate this room.

At this level of intensity, the tornado is very potent. The exterior walls begin to fail completely and offer no protection. Additionally, the outside walls become a major source of debris. At this point, the exterior of the home translates from a margin of safety to a liability.

Severe: Roofs and some walls are torn from structures, some small buildings are destroyed, non-reinforced masonry buildings are destroyed, most trees in forest are uprooted.

Figure 133: EF3 Example

EF4 level damage estimates wind speeds between 166 and 200 miles per hour. This translates to a top-end projectile speed of 90 mph for walls and 60 mph for ceilings. The design characteristics for a storm room capable of protection against debris penetration include four sheets of plywood on the ceiling and six sheets of

plywood on the walls. This option would provide protection from debris penetration for 98.3% of all tornadoes expected to occur. This means that by adding four sheets of plywood to the ceiling and six sheets of plywood to the walls of the storm room only 1.7% of tornadoes could produce debris that would penetrate this room.

However, at this level of intensity, the tornado is extremely violent. The exterior walls would all fail and produce a tremendous debris cloud. This home would then contribute to the damage to the next home, and so on. It is questionable whether the safe room would survive this level of intensity. As mentioned before, the goal is to increase the odds of survival. If this tornado strikes a home with no reinforced area for the inhabitants, serious injury or death is likely.

Figure 134: EF4 Example

EF5 level damage estimates wind speeds in excess of 200 miles per hour. This translates to a top-end projectile speed of 100 mph for walls and 67 mph for ceilings. The design characteristics for a storm room capable of protection against debris penetration include four sheets of plywood on the ceiling and seven sheets of plywood on the walls. The damage from this level of tornado is incomprehensible. No shelter above ground would guarantee survival if struck directly by these wind forces and dense debris cloud. Even underground shelters are no guarantee against phenomena of this magnitude. Fortunately, these are very rare, only 1.7% of all tornadoes fall into this category.

At this level of intensity, the tornado is indescribable. The exterior and interior walls would all fail and be blown some distance away. If the safe room survived this level of force, it would likely be by chance rather than by design. The calculation of the debris penetration characteristics of this safe room represents an exercise in

optimism. However, if the safe room did survive the structural destruction, the walls described would protect the inhabitants from debris impact.

Incredible: Strong frame houses are lifted from foundations, reinforced concrete structures are damaged, automobile-sized missiles become airborne, trees are completely debarked.

Figure 135: EF5 Example

Mobile Home Recommendations

The tornado resistance of mobile homes is minimal at best. Figure 136 illustrates the comparison of tornado related deaths for the period from 1995 until 2005 based on the location of the victims.

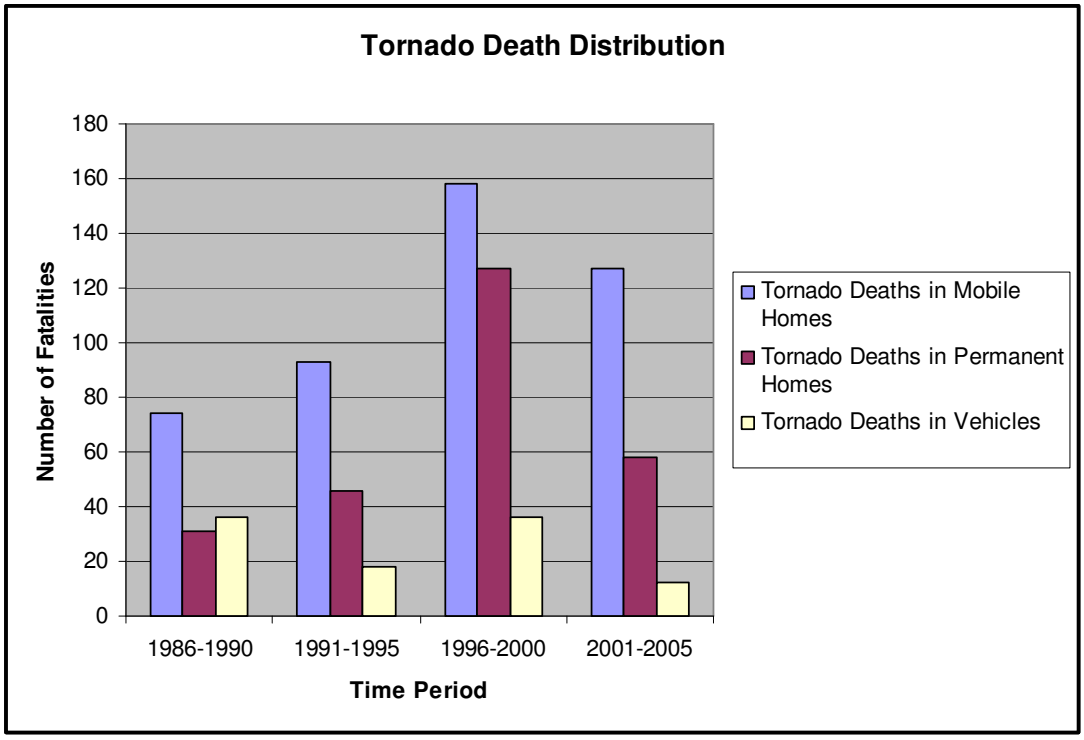

Figure 136: Tornado Death Distributions
[130]

As this chart indicates, the largest percentage of tornado related deaths occurred in mobile homes, and this trend seems to be continuing.

A good example of a comparison between permanent home and mobile home susceptibility resulted from three tornadoes that crossed central Florida on February 2, 2007. There were two hundred and eighty seven homes in the paths of these tornadoes. Figure 137 compares the level of damage to mobile homes versus permanent homes during this event. [131]

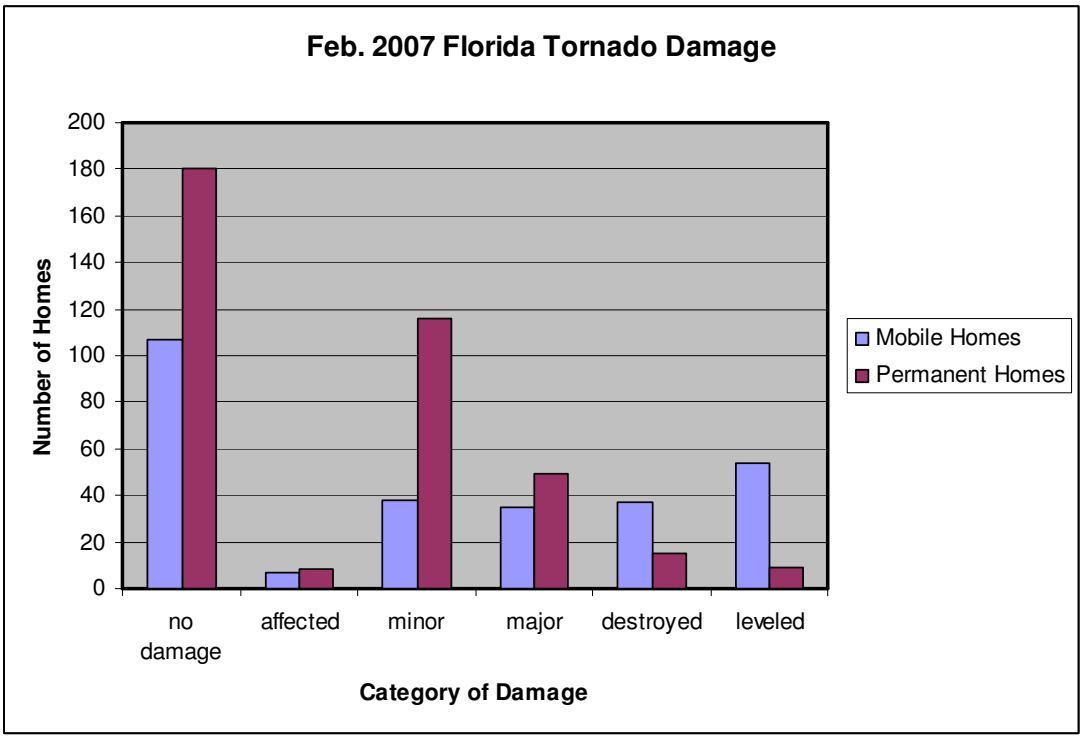

Figure 137: Florida Tornado Damage
[131]

Of the three surveys conducted for this thesis, one concentrated on a destroyed mobile home park in Lone Grove, Oklahoma. Chapter 4 describes many of the details of this survey, but it was a very sobering experience due to the vast devastation and loss of life. Figure 138 is one of many photographs taken during this survey. As this illustrates, the destruction of mobile homes during a tornado is often devastating.

Figure 138: Mangled Mobile Home Frame

Throughout this study, the mantra "increase the odds of survival" occurs. In the case of mobile homes during tornadoes, the only method to increase the odds of survival is evacuation. Despite improvements in the construction of mobile homes over the past few years, tornado resistance yet is unachieved. Some advances exist in terms of regulations for the construction of mobile homes [131], but these are not adequate to protect from tornadoes.

Anchoring the mobile home to the earth via tie-downs is ineffective for many reasons. One reason is the failure to use the factory installed tie-down provisions. Figure 139 shows a factory-installed tie-down still unused. Even when tie-down straps are property installed, the force of tornadic winds often shears the straps, pull the anchors from the ground, or destroy the connecting hardware. Tie-down straps are useful in conditions of strong winds, but not the extreme winds associated with tornadoes.

Another disadvantage of mobile homes involves the space underneath. This allows wind to get under the structure; therefore, the home often rolls or becomes airborne like any other vehicle.

Unlike new permanent home construction, hardening a new mobile home against the forces of tornadoes is impossible. Even a lesser intensity tornado can have a devastating effect on a mobile home.

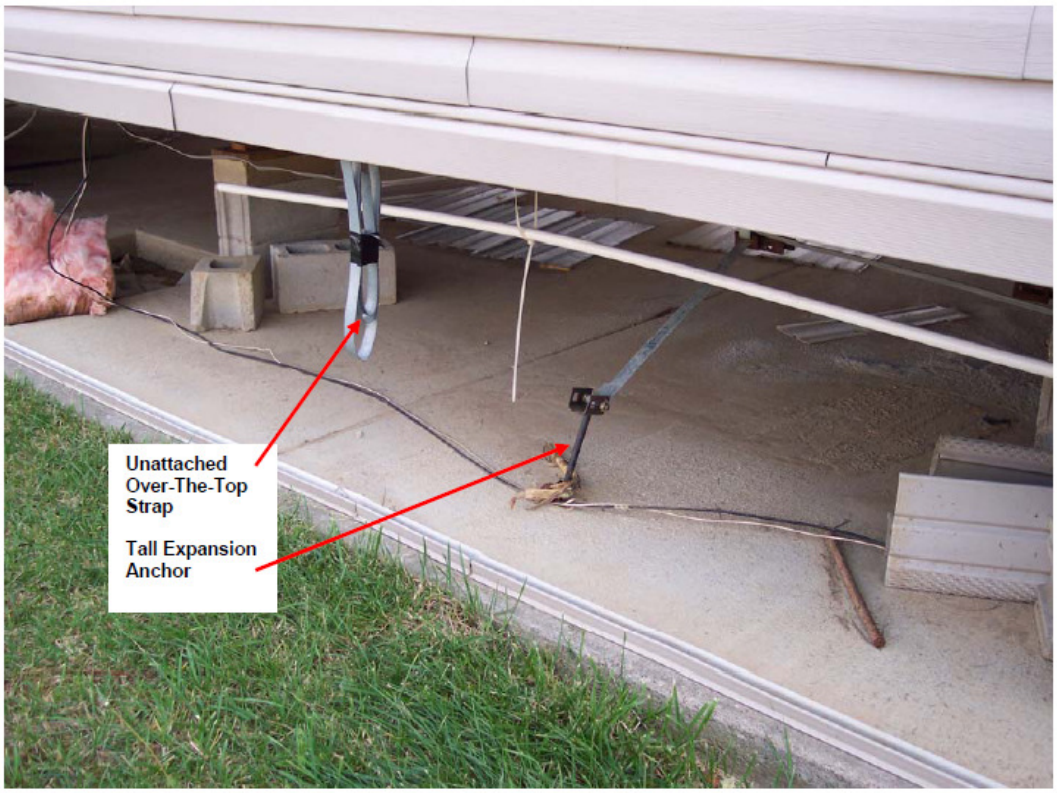

Figure 139: Even When Used - Tie-Downs Offer Little Protection
[132]

Much of this study has focused on the prevention of debris penetration. In the case of a mobile home, debris penetration is very dangerous. The exterior walls are similar to the exterior walls of a non-masonry permanent home; however, strengthening an existing mobile home against debris impact is almost impossible. This is primarily because most mobile homes do not have interior rooms. As shown in Figures 140 and 141, most rooms in a mobile home, even a doublewide unit, are located on an exterior wall. Given the construction techniques used on mobile home walls, penetration is unavoidable.

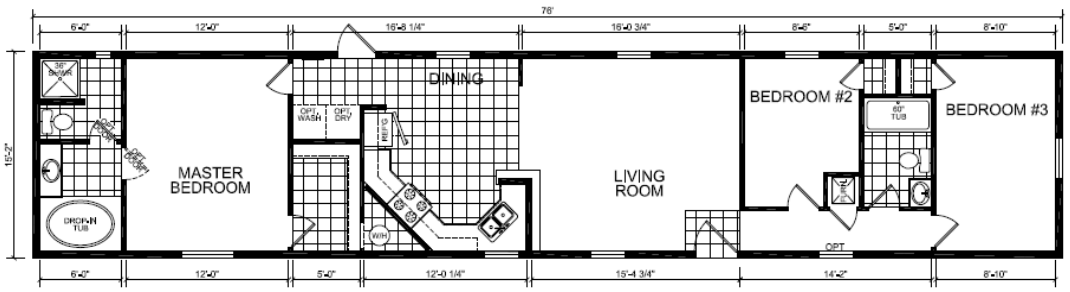

Figure 140: Typical Single-Wide Mobile Home Floor Plan

[133]

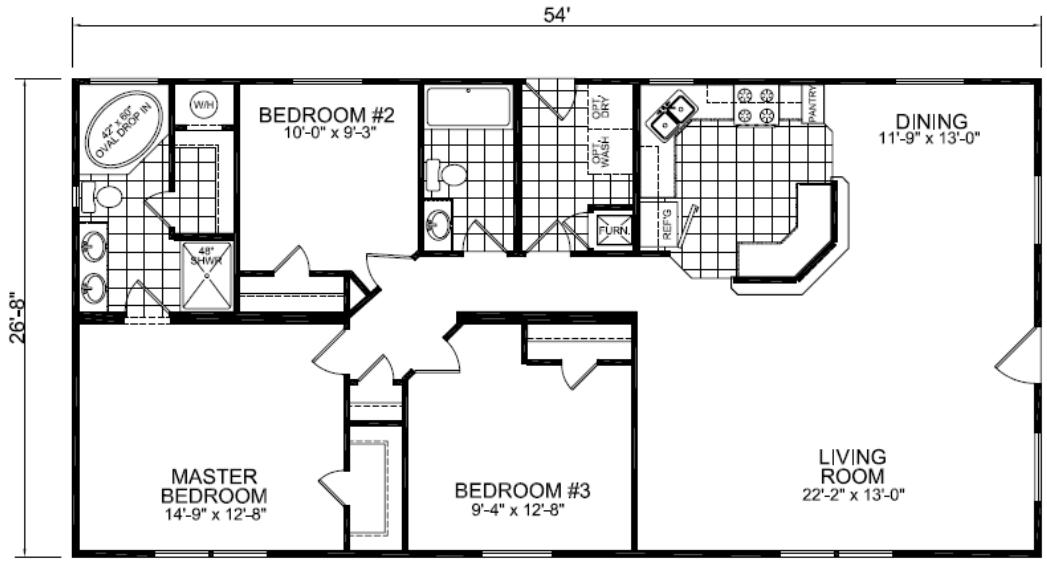

Figure 141: Typical Double-Wide Mobile Home Floor Plan
[133]

By reviewing the studies of mobile home/tornado interaction, it is most evident that mobile homes evacuation is appropriate in the event of a high wind episode. [134 135] This is often possible due to the advanced warnings that now occur. Much improvement exists since the first tornado forecast in 1948. [136]

In the past, tornado protection took the form of underground concrete structures. While these offered relative safety from tornadoes, they were dangerous in several ways. The foremost danger involved the location: external to the home. In the

past, warnings were not as timely as today; therefore, the trip to the "cellar" involved going out into the storm to get to safety, of spending hours and hours in the shelter waiting on the storm. Additionally, the doors to these shelters consisted of wood, sometimes covered with thin sheet metal. The doors provided no protection. There are modern underground shelters available today, but they are expensive, and certainly not moveable.

In regards to mobile home residents, two of the primary reasons for living in such a structure is either financial or the ability to be mobile. Since hardening a mobile home to withstand even a minimal tornado is impossible, and a detached shelter is expensive and permanent, the mobile home resident's choices are limited.

The only recommendation to mobile home residents is to seek shelter elsewhere. Future research should focus on a methodology to increase the odds of mobile home residents via the design of an inexpensive mobile tornado shelter. Such a concept is illustrated in the Appendix.

Conclusions/Contributions

Throughout this text, it has been demonstrated that the wind characteristics in and near tornadoes are largely undefined, but considerably intense. Winds that approach 300 mph from various directions, with rotational and upward vectors, wreak unimaginable destruction on structures and humans alike. Clouds of debris strike homes and people with devastating results. Environments of this magnitude are not defensible in a financially sound manner. Homes built to offer absolute safety from these conditions do not exist; however, the death tolls are often surprisingly low in comparison to the damage. This review demonstrates that increasing ones odds of survival is appropriate and successful given the limitations of money and shelter availability.

New home construction can provide protection from the majority of wind extremes likely to be experienced. Existing home modifications allow inexpensive options for hardening a home against tornado environments, to some degree. Mobile homes are simply death traps during tornadoes, despite any efforts to the contrary.

Corresponding to the objectives listed in chapter 1, listed below are the contributions of this research:

- By using a concept map tool, a new transdisciplinary collaborative framework has been developed to integrate research from diverse disciplines to solve complex problems related to tornadoes.

- A comprehensive review of tornado causation factors and behaviors helped to understand the wind fields associated with tornadoes and how these factors affect homes. By reviewing the most recent tornado science knowledge, the ability to develop alternate safety techniques was reinforced.

- The use of damage assessment surveys allowed for an understanding of the results of tornado and structure interaction. The forensic study of a far removed tornado proved that events in the past are useful for providing comparisons of the tornado-structure interaction for different historical building techniques.

- Analytical equations, in particular for composite wall systems, were developed for predicting the behavior of various wall surfaces when exposed to debris impact of various types. In addition to the equations, a finite element analysis was performed to simulate impact of this nature on plywood barriers. Equations and the Finite element modeling developed in this research are the main contributions of this study.

REFERENCES

[1] E.D. Fleharty, *Wild Animals and Settlers on the Great Plains*, University of Oklahoma Press, Norman, Oklahoma, 1995.

[2] G. Wise, *American Historical Explanations,* 2nd ed., University of Minnesota Press, Minneapolis, Minnesota, 1980

[3] A. B. C. Whipple, *Planet Earth-Weather*, Time-Life Books, Alexandria, Virginia, 1982.

[4] W.J. Burroughs, B. Crower, T. Robertson, E. Vallier-Talbot, and R. Whitaker, *The Nature Company Guide-Weather,* Time-Life Books, McMahons Point, Australia, 1996.

[5] NOAA, "2005 annual summaries," NOAA Department of Commerce, Ed.: National Climatic Data Center, 2006, pp. 36.

[6] T. P. Grazulis, *Significant tornadoes 1680-1991*. St. Johnsbury, VT., Environmental Films, 1993.

[7] S. A. Erickson, Brooks, H., "Lead time and time under tornado warnings: 1986-2004," in *23rd Conference on Severe Local Storms*. St. Louis, MO., 2006.

[8] J. E. Minor, "The tornado: An engineering-oriented perspective," *NOAA Technical Memorandum NWS SR-147*, NOAA Department of Commerce, 1993, pp. 196.

[9] C. Meade, "Strengthening research & development for wind hazard mitigation." Santa Monica, Ca.: RAND Corporation, 2004, pp. 10.

[10] FEMA320, "Taking shelter from the storm: Building a safe room for your home or small business," D. o. H. Security, 3rd ed: Federal Emergency Management Agency, 2008.

[11] T. P. Marshall, "Utilization of load/resistance statistics in a wind speed assessment," in *5th Annual Wind Engineering Conference*. Lubbock, TX, 1985.

[12] T. P. Marshall, W.F. Bunting, J.D. Weithorn, "Procedure for assessing wind damage to wood-framed residences," 2002.

[13] T. P. Marshall, "Tornado damage survey at Moore, Oklahoma," *Weather and Forecasting*, vol. 17, pp. 582-598, 2002.

[14] T. P. Marshall and M. Foster, "Damage survey and radar analysis of the forth worth and Arlington, TX tornadoes on March 28, 2000," Haag Engineering Co., Dallas, TX 2000.

[15] T. P. Marshall and J. R. McDonald, "An engineering analysis of the Grand Island, NE. Tornadoes," in *12th Conf. on Severe Local Storms*. San Antonio, TX, 1982.

[16] G. S. Forbes, H. B. Bluestein, "Tornadoes, tornadic thunderstorms, and photogrammetry: A review of the contributions by T.T. Fujita," *Bulletin of the American meteorological society*, vol. 82, pp. 73-96, 2001.

[17] ASCE, *Minimum design loads for buildings and other structures*, vol. ASCE/SEI 7-05: American Society of Civil Engineers, 2005.

[18] WSERC, "Debris impact testing at Texas Tech University," Texas Tech University, 2003.

[19] WSERC, "Construction materials threshold testing," Texas Tech University, 2004.

[20] WSERC, "Debris impact resistance of building assemblies," Texas Tech University, 2006.

[21] E. P. Chen, "Numerical simulation fo penetration of aluminum targets by spherical-nose steel rods," *Theoretical and Applied Fracture Mechanics*, vol. 22, pp. 159-164(6), 1995.

[22] R. P. Godwin, E.J. Chapyak, "Apparent target strength in long-rod penetration," *Int. J. Impact Engng.* , vol. 21, pp. 77-88, 1998.

[23] T. W. Wright, "A survey of penetration mechanics of long rods," in *Computational aspects of penetration mechanics*, J. Chandra, J. E. Flaherty, Ed. New York: Springer, pp. 85-106, 1983.

[24] T. S. Kuhn, *The structure of scientific revolutions*, 3rd ed. Chicago IL., University of Chicago Press, 1996.

[25] D. Tate, Nordlund, M., "Research methods for design theory," in *ASME 2001 Design Engineering Technical Conference and Computers and Information in Engineering Conference*. Pittsburgh, PA., 2001.

[26] D. Q. McInerny, *Being logical - a guide to good thinking*, Paperback ed. New York: Random House Trade Paperback, 2005.

[27] M. T. Bailey, "Do physicists use case studies? Thoughts on public administration research," *Public Administration Review*, vol. 52, pp. 47-54, 1992.

[28] T. P. Grazulis, *The tornado- nature's ultimate windstorm*. Norman, OK., University of Oklahoma Press, 2001.

[29] *The ATLAS net*, http://www.theatlasnet.org/?q=user/76/track, 2009.

[30] L. A. N. Amaral, Ottino, J.M., "Complex systems and networks: Challenges and opportunities for chemical and biological engineers," *Chemical Engineering Science*, vol. 59, pp. 1653-1666, 2004.

[31] T. Kollman, B. McPeak, C. Tosetto, R. Landis, T.J. Theodore, M. Solano, S. Gatchel, J. Carbone, "Practitioners approach to transdisciplinary engineering," Texas Tech, Lubbock, TX., 2008.

[32] B. McPeak and A. Ertas, "Eliminating disciplinary boundaries: A transdisciplinary approach to past tornado impact analysis." Lubbock, TX., Texas Tech University, 2008, pp. 30.

[33] A. Ertas, T. Maxwell, V. P. Rainey, and M. M. Tanik, "Transformation of higher education: The transdisciplinary approach in engineering," *IEEE Transaction on Education*, vol. 46, pp. 289-295, 2003.

[34] A. Ertas, Transdisciplinary comparison graphic. Lubbock, TX, personal communication, 2008.

[35] C. A. I. Doswell, "Severe convective storms - an overview," in *Severe convective storms*, C. A. I. Doswell, Ed. Boston: American Meteorological Society, pp. 1-26, 2001.

[36] T. Vasquez, *Weather forecasting handbook*, 5th ed. Garland, TX: Weather Graphics Technologies, 2002.

[37] C. A. Doswell III, "Severe convective storms," in *Meteorological monographs*, vol. 28, P. S. Ray, Ed. Boston: American Meteorological Society, 2001, pp. 561.

[38] C. A. I. Doswell, "The distinction between large scale & mesoscale contribution to severe convection: A case study," *Wea Forecasting*, vol. 2, pp. 3-16, 1987.

[39] S. Petterssen, *Introduction to meteorology*, 3rd ed. New York: McGraw-Hill, 1969.

[40] A. R. Moller, "Severe local storms forecasting," in *Severe convective storms*, C. A. Doswell III, Ed. Boston: American Meteorological Society, pp. 433-480, 2001.

[41] Thomson, "Thomson higher education," 2009, http://apollo.lsc.vsc.edu/classes/met130/notes/chapter11/cf_xsect.html

[42] R. H. Johnson, B.E. Mapes, "Mesoscale processes and severe convective weather," in *Severe convective storms*, C. A. Doswell III, Ed. Boston: American Meteorological Society, pp. 71-122, 2001.

[43] R. Davies-Jones, R.J. Trapp, H.B. Bluestein, "Tornadoes and tornadic storms," in *Severe convective storms*, C. A. Doswell III, Ed. Boston: American Meteorological Society, pp. 167-221, 2001.

[44] W. S. Lewellen, D.C. Lewellen, R.I. Sykes "Large-eddy simulation of a tornado's interaction with the surface," *Journal of the Atmospheric Sciences*, vol. 54, pp. 581-605, 1996.

[45] D. C. Lewellen, W.S. Lewellen, J. Xia, "The influence of a local swirl ratio on tornado intensification near the surface," *Journal of the Atmospheric Sciences*, vol. 57, pp. 527-544, 1999.

[46] W. F. Bunting, B.E. Smith, "A guide for conducting convective windstorm surveys," D. o. C. NOAA, 1993

[47] T. T. Fujita, "Proposed characterization of tornadoes and hurricanes by area and intensity," University of Chicago, Chicago, Satellite and Meteorology Research Paper Number 91, 1971.

[48] Wikipedia, Multi-vortex Dallas, TX tornado, http://en.wikipedia.org/wiki/Multiple_vortex_tornado

[49] W. H. J. Hoecker, "Wind speed and air flow patterns in the Dallas tornado of April 2, 1957," *Monthly Weather Review*, vol. 88, 1960.

[50] B. H. Fielder, R. Rotunno, "A theory for the maximum windspeeds in tornado-like vortices," *Journal of the Atmospheric Sciences*, vol. 43, pp. 2328-2340, 1986.

[51] D. Zrni'c, D.W. Burgess, L. Hennington, "Doppler spectra and estimated windspeed of a violent tornado," *Journal of Climate and Applied Meteorology*, vol. 24, pp. 1068-1081, 1985.

[52] H. Liu, *Wind engineering - a handbook for structural engineers*. Englewood Cliffs, NJ: Prentice-Hall, 1991.

[53] K. C. Mehta and J. M. Delahay, *Guide to the use of the wind load provisions of ASCE 7-02*. Reston, VA: American Society of Civil Engineers, 2004.

[54] P. Baker, meteorologist, national weather service Memphis, TN, personal communication, 2008

[55] C. A. I. Doswell, H.E. Brooks, "Lessons learned from the damage produced by the tornadoes of 3 may 1999," *Weather and Forecasting*, vol. 17, pp. 611-618, 2002.

[56] J. R. McDonald and T. P. Marshall, "Damage survey of the tornadoes near Altus, Oklahoma on may 11, 1982," Texas Tech University, Lubbock, Tx 1983.

[57] E. W. Scott, Photographs of the McKinney tornado damage, personal communication, 2007.

[58] *History of McKinney, TX*, http://www.mckinneytx.com/history/1948tornado.htm, 2008.

[59] FEMA342, "Midwest tornadoes of May 3, 1999," Federal Emergency Management Agency, 1999.

[60] B. Fraze, McKinney tornado survivor, personal communication, 2007

[61] H. Hall, McKinney tornado survivor, personal communication, 2007

[62] B. McPeak Sr., McKinney Tornado Survivor, personal communication, 2007

[63] A. Tolle, McKinney Tornado Survivor, personal communication, 2007

[64] *NOAA central library daily weather maps*, http://docs.lib.noaa.gov/rescue/dwm/data_rescue_daily_weather_maps.html, 2009.

[65] G. Woodall, Warning coordination meteorologist, nws, personal communication, 2008

[66] R. S. Hall, "Inside a Texas tornado," reprinted in *Weatherwise*, vol. 40, 1987.

[67] Collin-County, "Collin county death records," 2008, http://www.co.collin.tx.us/county_clerk/death/death.jsp

[68] B. Dennis, Department director of Jackson Madison county general hospital emergency dept, personal communication, 2008

[69] T. Ellsworth, *God in the whirlwind*. Nashville, TN: B&H Publishing Group, 2008.

[70] T. W. Wright, K.D. Frank, "Approaches to penetration problems," Ballistic Research Laboratory - Aberdeen Proving Ground, Maryland 1988.

[71] D. Baraff, "Analytical methods for dynamic simulation of non-penetrating rigid bodies," *ACM SIGGRAPH Computer Graphics*, vol. 23, pp. 223-232, 1989.

[72] "Materials response to ultra-high loading rates," Washington: National Materials Advisory Board 1980.

[73] L. Anand, "Constitutive equations for hot working of metals," *Int. J. Plas.*, vol. 1, pp. 213-232, 1985.

[74] D. J. Bammann, "An internal variable model of viscoplasticity," *Int. J. Engng. Sci.*, vol. 22, pp. 1041-1053, 1984.

[75] D. R. Curran, L. Seaman, D.A. Shockey, "Dynamic failure of solids," *Phys. Repts.*, vol. 147, pp. 253-388, 1987.

[76] J. A. Zukas, G.H. Jonas, K.D. Kimsey, T.M. Sherrick, "Three dimensional impact simulation: Resources and results," in *Computer analysis of large scale structures*, K. C. Park, R.F. Jones, Ed. New York: ASME, pp. 35-68, 1981.

[77] V. V. Bashurov, G.V. Bebenin, A.G. Ioilev, "Numerical simulation of rod particles hypervelocity impact effectiveness at various attack angles," *RFNC-VNIIEF*.

[78] Z. Rosenberg, E. Dekel, "Material similarities in long-rod penetration mechanics," *International J. of Impact Engng.*, vol. 25, pp. 361-372, 2001.

[79] C. Forsell, T.C. Gasser, P. Gudmundsson, G. Dohr, "Numerical simulation of failure of ventricular tissue due to deep penetration," in *8th World Congress Computational Mechanics (WCCM8) 5th European Congress on Computational Methods in Applied Sciences and Engineering (ECCOMAS)*, Venice, Italy, 2008.

[80] O. A. Shergold, N.A. Fleck, "Mechanics of deep penetration of soft solids with application to the injection and wounding of skin," *Proc. Royl. Soc. Lond.*, vol. 460, pp. 3037-3058, 2004.

[81] T. C. Gasser, G.A. Holzapfel, "Modeling dissection propagation in soft biological tissues," *Eur. J. Mech.*, vol. 25, pp. 617-633, 2006.

[82] M. N. Khan, G. Joseph, Y. Khaykin, K.M. Ziada, B.L. Wilkoff, "Delayed lead perforation: A disturbing trend," *Pacing and Clin, Electrophysiol.*, vol. 28, pp. 251-253, 2005.

[83] V. A. Kovtunenko, "Numerical simulation of the non-linear crack problem with non-penetration," *Mathematical Methods in the Applied Sciences*, vol. 27, pp. 163-179, 2004.

[84] H. Xicheng, C. Yuze, Z. Weizou, Z. Fangui, L. Yonggang, Z. Jianshi, "An analysis of rht parameters in 2d numerical simulation of concrete penetration with composite projectiles," *International Journal of Modern Physics B*, vol. 22, pp. 1291-1296, 2008

[85] Wikipedia, Multi-vortex Dallas, TX tornado, http://en.wikipedia.org/wiki/Multiple_vortex_tornado

[86] M. J. Forrestal, S.J. Hanchak, "Penetration limit velocity for ogive-nose projectiles and limestone targets," *J. Appl. Mech.*, vol. 69, pp. 853-854, 2002.

[87] V. P. Alekseevski, "Penetration of a rod into a target at high velocity," *Combustion Explosion and Shock Waves*, vol. 2, pp. 63-66, 1966.

[88] A. Tate, "A theory for the deceleration of long rods after impact," *J. Mech. Phys. Solids*, vol. 15, pp. 387-399, 1967.

[89] G. Luttwak, Z. Rosenberg, Y. Kivity, "Long rod penetration in oblique impact," in *American Physical Society topical group on shock compression of condensed matter*, 1996, pp. 1127-1130.

[90] G. C. Bessette, D.L. Littlefield, "Analysis of transverse loading in long-rod penetrators by oblique plates," in *10th American Physical Society topical conference on shock compression of condensed matter*, 1998, pp. 937-940.

[91] V. F. Nesterenko, S.S. Indrakanti, S. Brar, Y. Gu, "Long rod penetration test of hot isostatically pressed ti-based targets," in *Shock Compression of Condensed Matter-1999*, 1999, pp. 419-422.

[92] F. Malaise, J.Y. Tranchet, F. Collombet, "Effects of a dynamic confinement on the penetration resistance of ceramics against long rods," in *Shock Compression of Condensed Matter-1999*, 1999, pp. 1121-1124.

[93] K. Daneshjou, A. Kockakinejad, M. Rahimzadeh, "Numerical study of long-rod penetration depth in semi-infinite targets in electromagnetic launchers," *IEEE Transactions on Magnetics*, vol. 41, pp. 375-379, 2005.

[94] F. Huang, Z. Lei, S. Lian, "Investigation on ballistic performance of armor ceramics against long-rod penetration," *Metallurgical and Materials Transactions A.*, vol. 38, pp. 2891-2895, 2007.

[95] S. Rolc, J. Buchar, Z. Akstein, "On the protection capability of the flying plate against long-rod penetrators," *International Journal of Modern Physics B*, vol. 22, pp. 1285-1290, 2008.

[96] E. Wlodarczyk, M. Magier, "Dynamics of the rear part of a long-rod penetrator's core during firing," *Shock Waves*, vol. 18, pp. 401-409, 2008.

[97] F. I. Grace, "Long-rod penetration into targets of finite thickness at normal impact," *Int. J. Impact Engineering*, vol. 16, pp. 419-433, 1995.

[98] F. I. Grace, "Ballistic limit velocity for long rods from ordinance velocity through hypervelocity impact," *International J. of Impact Engng.*, vol. 23, pp. 295-306, 1999.

[99] S. B. Segletes, W.P. Walters, "Extensions to the exact solution of the long-rod penetration/erosion equations," *International J. of Impact Engng.*, vol. 28, pp. 363-376, 2003.

[100] F. I. Grace, "Nonsteady penetration of long rods into semi-infinite targets," *International J. of Impact Engng.*, vol. 14, pp. 303-314, 1993.

[101] C. E. Anderson, J.S. Wilbeck, J.S. Elder, "Long-rod penetration into highly oblique, water-filled targets," *International J. of Impact Engng.*, vol. 23, pp. 1-12, 1999.

[102] D. L. Orphal, R.R. Franzen, "Penetration of confined silicon carbide targets by tungsten long rods at impact velocities from 1.5 to 4.6 km/s," *International J. of Impact Engng.*, vol. 19, pp. 1-13, 1997.

[103] Y. N. Bukharev, V.A. Morovov, M.I. Khaimovich, I.N. Shutova, "Criteria for modeling the penetration by long rods impacting a semi-infinite target at a high velocity," *Combustion, Explosion, and Shock Waves*, vol. 28, pp. 419-423, 1992.

[104] J. D. Walker, C.E. Anderson, "A time-dependent model for long-rod penetration," *International J. of Impact Engng.*, vol. 16, pp. 19-48, 1995.

[105] S. B. Segletes, W.P. Walters, "Efficient solution of the long-rod penetration equations of alekseevski-tate," Army Research Lab Aberdeen Proving Ground, MD., 2002.

[106] W. J. Bruchey, "Fragment penetration modeling of anthropometric ballistic mannequins," in *24th International Symposium on Ballistics*, 2008.

[107] W. J. Bruchey, A. Tank, "Fragment penetration modeling," unpublished report, 2007.

[108] W. J. Bruchey, personal communication, 2009

[109] *Strong-Tie High wind resistant construction*, http://www.strongtie.com/ftp/catalogs/c-hw09/C-HW09.pdf, 2009.

[110] FEMA361, "Design and construction for community safe rooms," U. S. D. o. H. Security, 2nd ed: Federal Emergency Management Agency 2008.

[111] *The encyclopedia of wood*: Skyhorse Publishing, 2007.

[112] APA, "Panel design specification," The Engineered Wood Association, Tacoma, WA, 2008.

[113] Foamular Insulating Sheathing, Owens Corning product data sheet, www.owenscorning.com

[114] Gypsum Association, “Gypsum board typical mechanical and physical properties”, GA-235-05, Washington, D.C. 2005, www.gypsum.org

[115] Strength of Brick, website: http://chestofbooks.com/architecture/Building-Construction-2/Strength-Of-Bricks-Continued.html.

[116] C. E. Anderson, S.R. Bodner, "The status of ballistic impact modeling," *Int. J. Impact Engng. (submitted)*, 1987.

[117] R. L. Woodward, M.E. De Morton, "Penetration of targets by flat-ended projectiles," *Int. J. Mech. Sci.*, vol. 18, pp. 119-127, 1976.

[118] A. K. Kar, "Loading time history for tornado-generated missiles," *Nuclear Engineering and Design*, vol. 51, pp. 487-493, 1979.

[119] R. R. Carter, *Wind-generated missile impact on composite wall systems*, Texas Tech, master's thesis, 998.

[120] *Home design website*, www.homeplans.com, 2009.

[121] A. P. Christoforou, "Impact dynamics and damage in composite structures," *Composite Structures*, vol. 52, pp. 181-188, 2001.

[122] E. Fuoss, P.V. Straznicky, C. Poon, "Effects of stacking sequence on the impact resistance in composite laminates: Part 2: Prediction method," *Composite Structures*, vol. 41, pp. 177-186, 1998.

[123] J. M. McDonald, "Impact resistance of common building materials," *Journal of Wind Engineering and Industrial Aerodynamics*, vol. 36, pp. 717-724, 1990.

[124] S. R. Institute, "Schematic of behavior of metals." San Antonio, TX., 2007.

[125] *Penetration into ductile and brittle materials*, http://www.cs.chalmers.se/Conf/ECM198/standard/Abstracts/Materials/mark1.pdf

[126] J. V. J. Ramsdell and J. P. Rishel, "Tornado climatology of the contiguous united states," Pacific Northwest National Laboratory, Richland, WA., 2007.

[127] Y. J. Park and M. Reich, "Probabilistic wind/tornado/missile analyses for hazard and fragility evaluations," Brookhaven National Laboratory, Upton, NY.

[128] E. Oberg, F.D. Jones, H.L. Horton, and H.H. Ryffel, *Machinery's Handbook*, 25th ed., Industrial Press Inc., New York, 1996

[129] *Insulated concrete forms*, http://www.polysteel.com/, 2009.

[130] W. Ashley, "Spatial and temporal analysis of tornado fatalities in the United States: 1880-2005", *Weather and Forecasting*, vol. 22, pp. 1214-1228, 2007

[131] K. M. Simmons and D. Sutter, "Manufactured home building regulations and the February 2, 2007 Florida tornadoes," *Natural Hazards*, vol. 46, pp. 415-425, 2008.

[132] L. J. Tanner and J. E. Waller, "Tornado report Evansville, In. November 6, 2005 focus on eastbrook mobile home park," U.S. Department of Commerce, 70NANB8H0059, 2006.

[133] *Mobile homes sales*, http://www.factoryexpodirect.com/, 2009.

[134] H. Brooks, “Mobile home tornado fatalities: some observations, report for NOAA/ERL/National severe storms laboratory, Norman, OK., 1997

[135] S. Brown, P. Archer, E. Kruger and S. Mallone, “Tornado-related deaths and injuries in Oklahoma due to the 3 May 1999 tornado”, report for the Injury Prevention Center, Oklahoma State Dept of Health, 2002

[136] E. J. Fawbush and R. C. Miller, "An empirical method of forecasting tornado development," *Bulletin of the American meteorological society*, vol. 32, pp. 1-9, 1951.

APPENDIX

Conceptual Portable Concrete Tornado Shelter

This dissertation does not represent a product design document; however, the following concept might result in further refinement and provide an alternative for mobile home, and even permanent home, residents.

The three major requirements of such a shelter are:

- Provide safety in the event of a tornado
- Be inexpensive in relation to other alternatives
- Be moveable
-

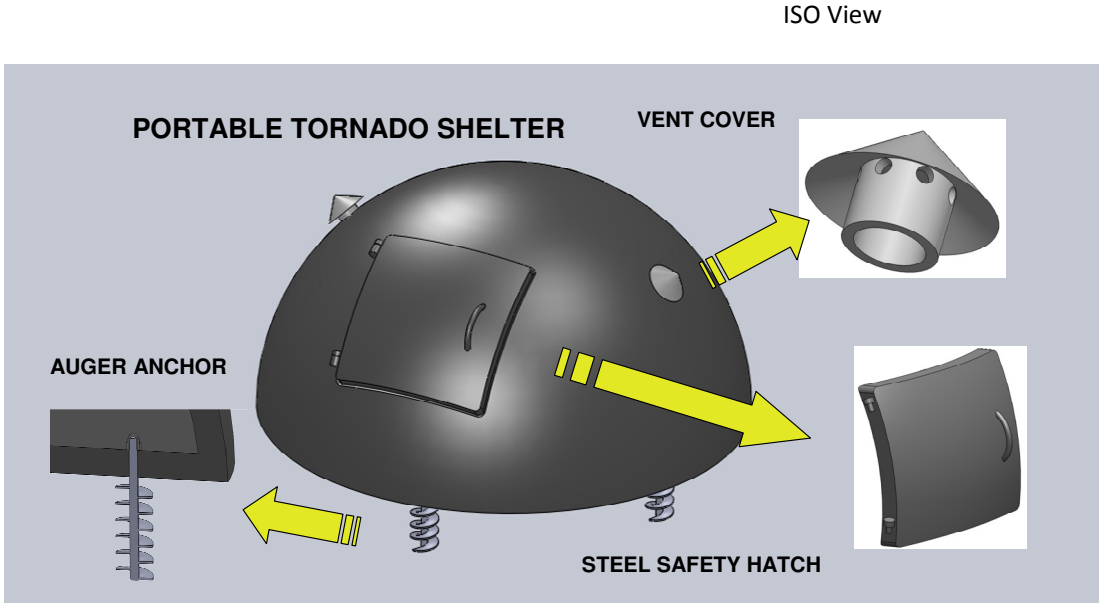

Figure 142: Portable Tornado Shelter Concept

Figures 142 through 146 illustrate a conceptual model of such a shelter. The construction is 4 inch thick concrete, reinforced with ½ inch rebar on a 6 x 6 inch gird. The shape is a semi-sphere with an inside radius of 42 inches. The outside profile minimizes uplift pressures due the fact there are no "surface changes". Additionally, the circular profile does not provide any flat surfaces, thus reducing the possibilities of a debris strike normal to the surface. There is a 30 x 30 inch opening for a steel doorframe and steel door with three hinges on one side, and a deadbolt on the other three sides. Two vents (with steel inserts) allow fresh air and prevent pressure build up inside the unit. Anchoring to the ground utilizes four auger anchors, such as those shown in Figure 147.

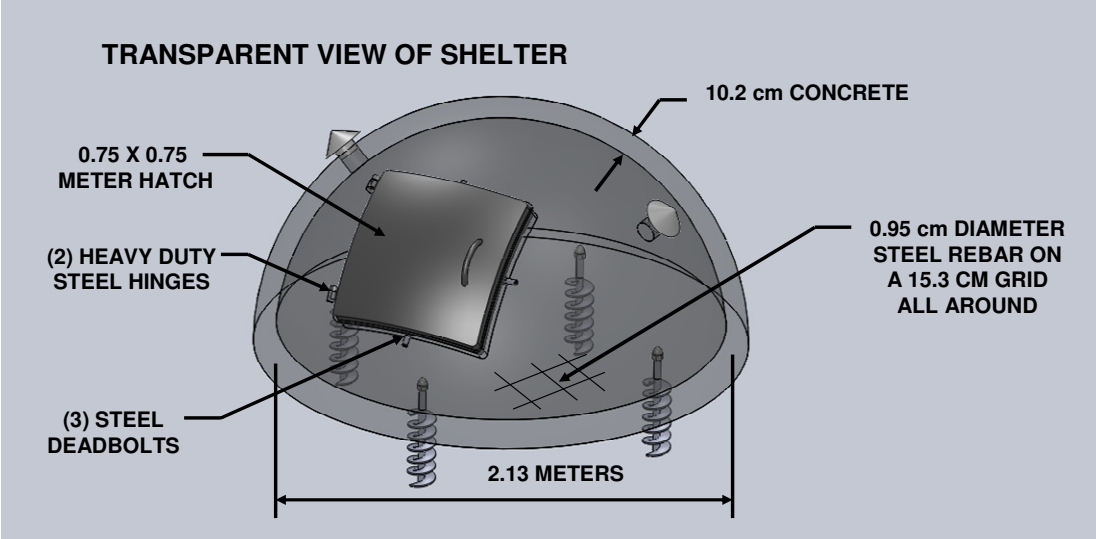

Figure 143: Transparent View of Shelter

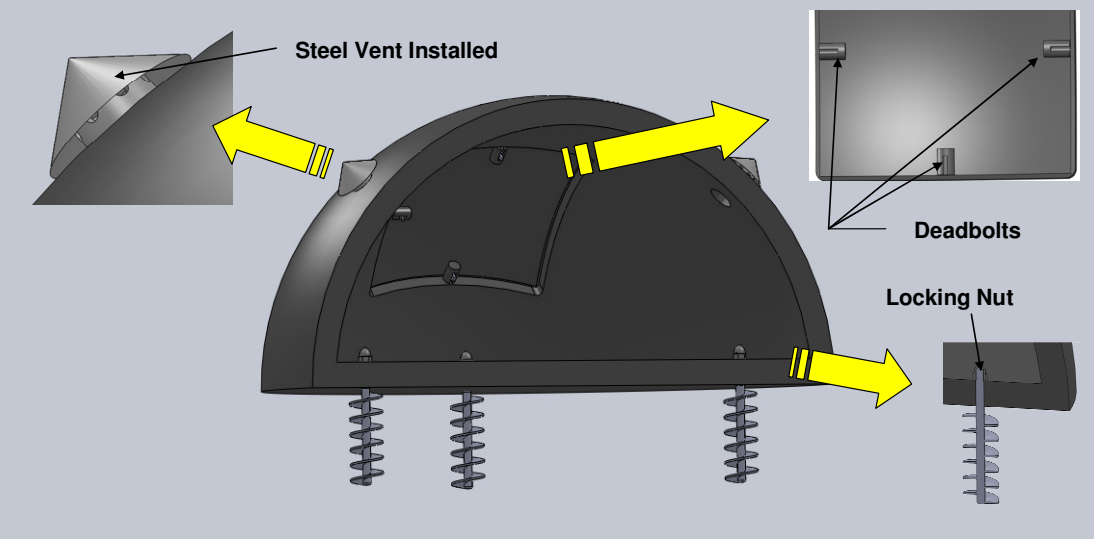

Figure 144: Cross-Sectional View of Shelter

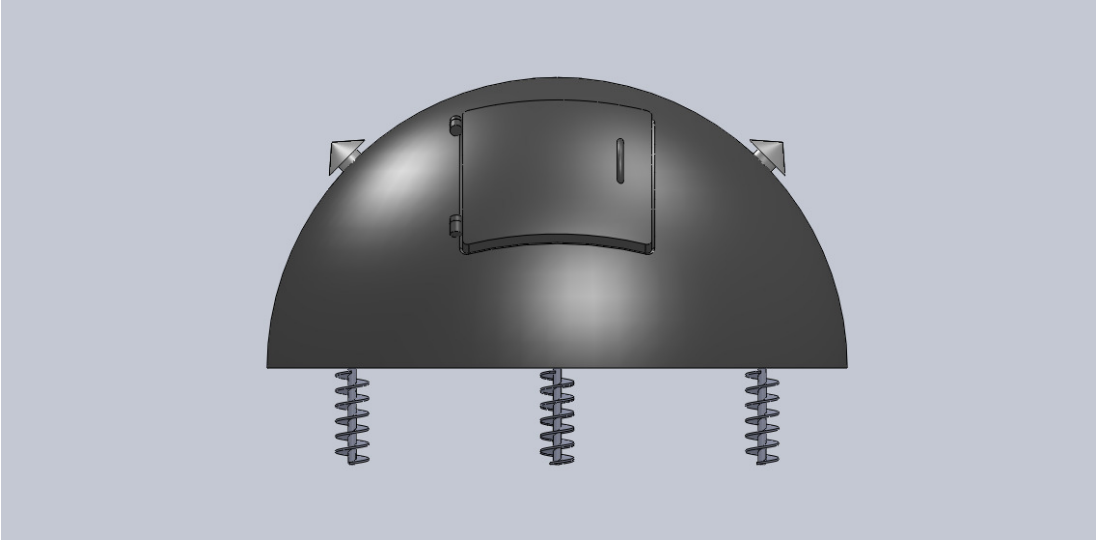

Figure 145: Front View of Shelter

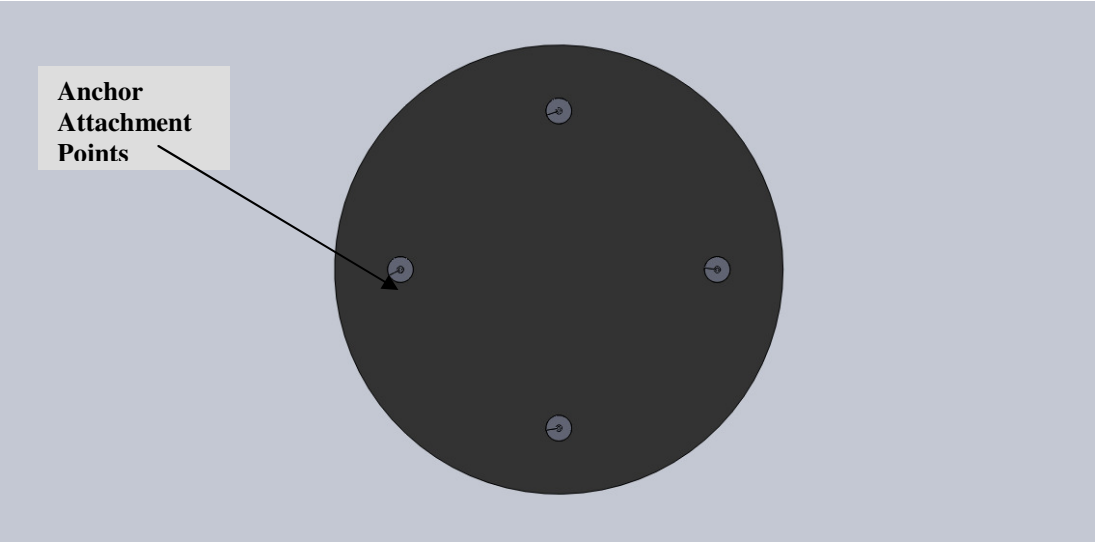

Figure 146: Bottom View of Shelter

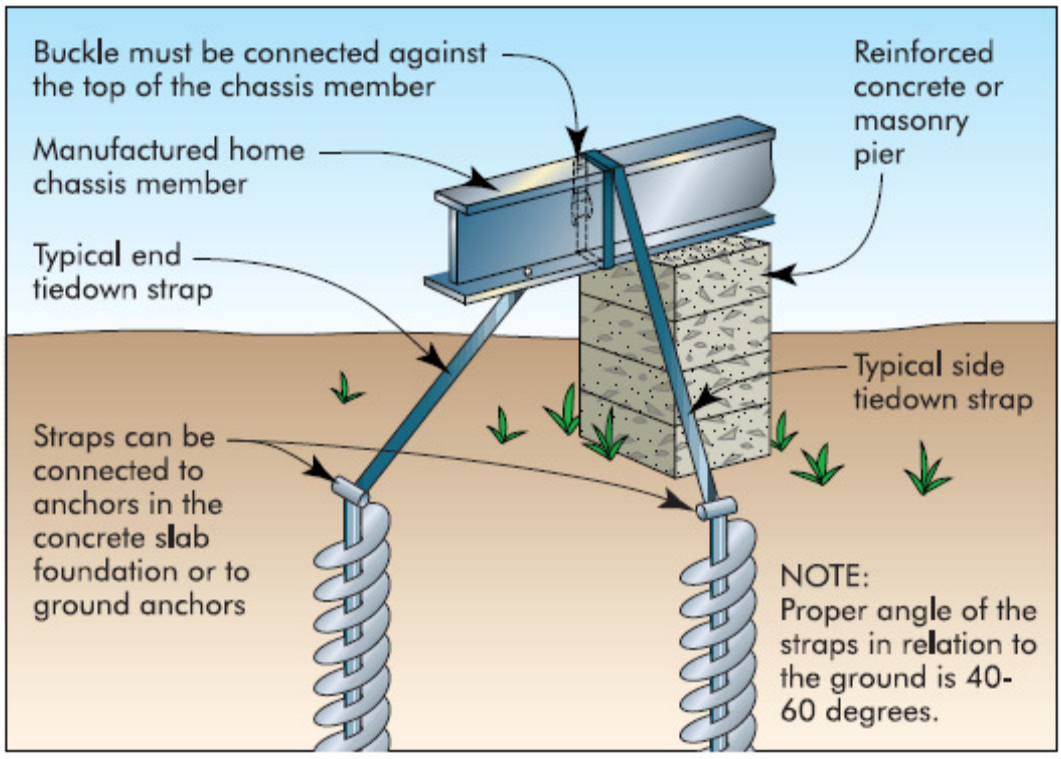

Figure 147: Typical Use of Auger Anchors

Such a unit would provide a no-frills enclosure for protection during a tornado. There is no room to stand or move about; however, most tornado events occur quickly. It could be located very near to the door of the home to minimize the exposure to the outside conditions.